

---

A Fundamental Study of Model Fuel Conversion Reactions in Sub and  
Supercritical Water

By

Russell P. Lachance

Lieutenant Colonel, United States Army

B.S., United States Military Academy, West Point, 1985

M.S., Chemical Engineering, Massachusetts Institute of Technology, 1995

Submitted to the Department of Chemical Engineering  
in partial fulfillment of the requirements for the degree of

DOCTOR OF PHILOSOPHY IN CHEMICAL ENGINEERING

at the


MASSACHUSETTS INSTITUTE OF TECHNOLOGY

June, 2005

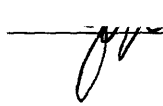
[September 2005]

© Massachusetts Institute of Technology 2005  
All Rights Reserved

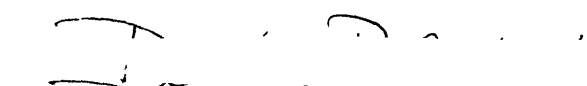
Signature of Author:

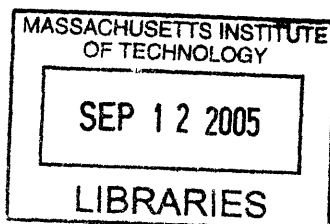
  
Department of Chemical Engineering  
June 30, 2005

Certified by:

  
Professor Jefferson W. Tester  
Thesis Supervisor

Accepted by:

  
Professor Daniel Blankschtein  
Professor of Chemical Engineering  
Chairman, Committee for Graduate Students



ARCHIVES

vol. 1

---

# A Fundamental Study of Model Fuel Conversion Reactions in Sub and Supercritical Water

By

Russell P. Lachance

Submitted to the Department of Chemical Engineering on June 30, 2005 in partial fulfillment of the requirements for the degree of Doctor of Philosophy in Chemical Engineering

## ABSTRACT

Model reactants under hydrothermal conditions were examined to improve our understanding of chemical transformations in this high temperature and pressure environment. Results have a direct impact on present and future hydrothermal fuel conversion research for a range of fossil-based and bio-mass based feed stocks. Methane was chosen as a model compound and two different approaches were taken to examine its conversion in supercritical water. Catalytic reformation of methane was studied experimentally while partial oxidation of methane was studied through the application of a previously developed detailed chemical kinetic model that was analyzed and refined specifically for this study. Glucose and glycine were also chosen as model compounds to study related conversion pathways experimentally under hydrothermal conditions for biomass-based feed stocks.

An experimental study of the catalytic reformation of methane in supercritical water (SCW) was completed that explored the use of carefully chosen catalysts under a variety of conditions and measured the conversion of methane and yields of various products. Eight metal catalysts were selected based on a review of previous catalysis experiments in hydrothermal conditions and those thought to be active for methane reforming. The range of conditions studied included 350 – 630°C, 150 – 400 bar, 0.01 – 2 wt% methane, 10 seconds to 72 minutes residence time, and with and without catalyst present. Four different experimental reactor designs were employed; a packed bed reactor, a continuous stirred tank reactor and two different batch reactor designs. A variety of techniques for reducing the metal catalysts and keeping them active in SCW were examined.

Despite the range of conditions studied here, significant conversion of methane was never achieved. The most encouraging result was the relatively low yield of CO<sub>2</sub> (2.19% of the product gas volume) in the experiments employing 1% Ru/TiO<sub>2</sub> catalyst pellets. An analysis of each catalyst before and after exposure to SCW revealed significant degradation which helped to explain the low methane conversions. Based on this analysis and our experimental results, the most promising active metal identified was ruthenium, and the most promising support was titania (rutile) with some promise for zirconia and activated carbon. Although active for steam reforming and other hydrothermal catalyst applications, the nickel and platinum catalysts examined in this study showed signs of rapid degradation and deactivation and yielded little conversion of methane.

---

In a previous study, researchers claimed to produce hydrogen from methane in SCW in the presence of alkali salts. Experiments with alkali salts in SCW were investigated here to further examine this claim. Our experiments with alkali salts revealed the importance of corrosion in the evolution of hydrogen from this media. Comparable amounts of hydrogen were produced from argon-alkali-SCW mixtures and from methane-argon-alkali-SCW mixtures suggesting that a significant amount of hydrogen in SCW reaction effluents can be attributed to water oxidizing the metal reactor material and not from hydrocarbon sources. Additional SCW alkali salt experiments in the same Hastelloy C-276 reactor eventually revealed an increasing catalytic conversion of methane, further emphasizing the likely importance of progressive metal corrosion. In the Hastelloy C-276 reactor, corrosion was confirmed by the presence of metal particulates and measurable amounts of dissolved nickel and chromium from the reactor metal alloy in the effluent. Comparable experiments in a gold-plated reactor still showed evidence of hydrogen generation from metal oxidation, but did not show evidence of corrosion.

A detailed chemical kinetic model (DCKM) for single carbon species (C1) was refined and analyzed to support an examination of the effects of experimental conditions on methanol selectivity and methane conversion for the partial oxidation (POX) of methane in SCW. Although a formal sensitivity analysis was not performed on this model, a study of several key reactions and rates from literature resulted in good agreement of model predictions with reliable C1 SCW oxidation experimental data. SCW methane POX predictions from the refined model were then compared with POX experimental data. Disagreements between the model and the data were discussed along with a detailed critique of experimental issues associated with all previous SCW methane POX experimental studies. A reaction path analysis was developed from the DCKM which helped to elucidate the fate of methane and methanol in this environment and to identify a set of promising conditions to maximize methanol selectivity.

Upon detailed analysis of both experimental and modeling results, the maximum methanol selectivity of about 80 % and maximum methane conversion of about 1 % occurs at low temperatures ( $\sim 400^\circ\text{C}$ ), medium to high pressure ( $P > 300$  bar), and high methane concentration ( $[\text{CH}_4]_0 > 50\text{mM}$ ) with fuel-rich conditions at medium to high methane to oxygen ratios of  $[\text{CH}_4]_0/[\text{O}_2]_0 > 10$ . The experimental results may have achieved less than the maximum possible methanol selectivity due to issues such as inadequate mixing and wall effects. The modeling results may also be under-predicting methanol selectivity due to inadequate inclusion of non-ideal PVTN effects and solvent effects. However, the current model predictions and experimental results both substantiate our concern that SCW methane POX may fall short of the goal of greater than 70 % methanol selectivity and 15% methane conversion. Nevertheless, other sets of experimental conditions that may show more promise have not been fully explored experimentally. In particular, the use of stable, selective catalysts, or inert wall material, or partial oxidation in the presence of hydrothermal flames have not been thoroughly analyzed here, and may improve the limited success discovered in this study.

Glucose, glycine and glucose-glycine mixtures were studied as a model Maillard reaction system in a hydrothermal environment to explore a range of conditions that might alter the formation of undesired Maillard-type polymeric products. These polymeric products reduce the yield of biomass-derived fuels and complicate the separation and processing steps of biomass-to-fuel applications. Initial experiments were performed to study the individual hydrothermal

---

degradation pathways of glycine and glucose and how those pathways change when the model compounds are mixed. Despite varying pH, time and temperature, we did not observe significant changes in the proposed Maillard mechanism, but product chromatograms did show possible development of alternate pathways particularly with furfural-type compounds.

Glycine alone was found to be largely refractory (only 0 – 33% conversion) in our hydrothermal conditions from 50 to 300°C at 55 – 110 bar and 4 – 67 minutes residence time while glucose alone was quite reactive. In most conditions studied here, glucose conversion was greater than 85%, but moderate glucose conversions were achieved in a new, short residence time plug flow reactor (e.g., conversion of 35 % was measured after 7.3 seconds at 200°C and 55 bar). The degradation of glucose-glycine mixtures was studied at times of 7 seconds and 6 minutes at pH 2 and pH 5 and over a range of temperatures from 100 – 300°C. Near complete conversion of both reactants was observed in almost all conditions. Several liquid phase products were identified and analyzed, but total organic carbon (TOC) and carbon-hydrogen-nitrogen (CHN) analysis showed that significant reacted carbon is still unaccounted for.

Thesis Supervisor:

Jefferson W. Tester

Herman P. Meissner Professor of Chemical Engineering



## Dedication

To the men and women who have served our country in Operation Iraqi Freedom. Please know that those soldiers did not decide to go to war. That decision was made for them. Nevertheless, they volunteered to endure incredible physical and mental hardships because they have an overwhelming sense of duty. May God bless them!

---

## Acknowledgements

My fondest memories of MIT will most certainly be the people who helped me survive this ordeal! At the risk of missing someone, I would like to especially recognize the following people.

God: Although I am not a particularly religious man, there is not doubt in my mind that God has blessed my life with many things. If you knew how this thesis came to be, you too would be convinced that someone is watching out for me. Thank you, God!

Family: My wife, Lisa, and my children, Zachary, Hannah, Chelsea, and Austin, have made enormous sacrifices throughout my Army career to support me unconditionally. I'm not sure how I could ever repay them, but I'd better start now if I hope repay what I owe them before I'm 70!

U.S. Army: The Army and my leaders in the Army have molded me for 20 years and have given me opportunities not found in any other job or any other place in the world. It just doesn't get any better than this!

Professor Tester: A close second to God himself, Professor Tester's influence is the main reason for completing this thesis on time. You cannot find a more understanding, supportive, and patient graduate student advisor who truly cares about his students. I hope I grow up to be just like him!

Thesis committee: Professors Green, Trout and Swallow were also extremely supportive throughout this unique thesis. I certainly appreciated the dedication of their time and commitment to help me, especially Professor Swallow who went so far as to personally analyze some of my samples.

Gwen Wilcox: As Tester Group "Mom", Gwen has bent over backward to help all of us during the past two years. Thank you for "dropping what you were doing" to help me countless times!!

Tester Group Members, Past and Present: I'm not sure how our lab group work environment compares with others, but my fellow lab mates made me look forward to coming to work each day. And that's saying a lot given our challenging setting of frustrating reactors in a window-less basement lab! Thank you for all that you've taught me, for sacrificing your time to help me and for making research fun! Although every Tester Group member bent over backwards to help me, Jason Ploeger and Andy Peterson should essentially be co-authors on this thesis (you'll see their names throughout Chapters 5 and 6). Thanks to Jason and Andy for being so important in helping me finish on time.

UROP Platoon: Lots of helping hands went into completing this research, and most of those hands belonged to several very dedicated UROPs who worked with me. Laura, Chris, George, Sam, Steph, and Adam. Thank you for helping me finish on time!

PSI Collaborators: A special thanks to Dr. Freddie Vogel and his co-workers who donated three catalysts for this work, and who greatly improved my working knowledge of catalysis in hydrothermal media.

The Ying Group: A special thanks to Steve Weiss, Pemakorn Pitukmanorom, and Hong He who helped with my countless catalyst questions and with BET and XRD support.

Johnson Matthey & Degussa: Thank you for supporting this research with donated catalysts.

CMSE: Thank you to Libby Shaw and Joe Adario who helped with XPS and XRD analysis respectively. This work made use of the Shared Experimental Facilities supported by the MRSEC Program of the National Science Foundation under award number DMR 02-13282

Dr. Andreas Matzakos: As Shell's representative for our project, you were always supportive even though our results were never "home run" material. Thank you for your support and positive attitude.

Dr. Terry Adams: As SEER's representative for our project, you went beyond your supervisory role and provided valuable guidance to steer our project in the right direction. Thank you for all your help and support.

Funding Sources: Obviously nothing would get done without someone paying the bills, so a special thank you to the U.S. Army for my funding and to the ARO, Shell and SEER for funding the materials and services of this research.

---

## Table of Contents

<b>1 Introduction and Background .....</b>	<b>19</b>
<i>1.1 Properties of sub and Supercritical Water .....</i>	<i>19</i>
1.1.1 High Temperature Water as a Solvent .....	19
1.1.2 High Temperature Water as a Fluid.....	25
1.1.3 High Temperature Water as a Reactant .....	26
1.1.4 Summary of HTW Characteristics.....	28
<i>1.2 Hydrothermal Waste to Fuels Research.....</i>	<i>29</i>
1.2.1 Biomass to Fuels Research in Supercritical Water .....	30
1.2.2 Sub-critical Water Biomass to Fuels Research .....	31
<i>1.3 Model Compound and Reaction Condition Selection.....</i>	<i>34</i>
1.3.1 Methane as a Model Compound .....	35
1.3.2 Glucose and Glycine as Model Compounds .....	37
<i>1.4 References.....</i>	<i>37</i>
<b>2 Research Goal, Objectives and Approach .....</b>	<b>43</b>
<b>3 Experimental Procedures and Techniques .....</b>	<b>45</b>
<i>3.1 Description of the Small Scale SCW PFR System .....</i>	<i>45</i>
3.1.1 Feed Preparation and Pressurization Stage .....	45
3.1.2 Preheating System .....	49
3.1.3 Reactor System .....	49
3.1.4 Letdown System and Sample Collection .....	52
3.1.5 Reactor Operation and Data Collection .....	53
3.1.6 Reactor system issues .....	54
<i>3.2 Description of SCW CSTR system .....</i>	<i>56</i>
3.2.1 Feed Preparation and Pressurization Stage .....	56
3.2.2 Preheating System .....	58
3.2.3 Reactor System .....	59
3.2.4 Letdown System and Sample Collection .....	60
3.2.5 Reactor Operation and Data Collection .....	60
3.2.6 CSTR Reactor Design and Operating Issues: .....	61
<i>3.3 Description of SCW Batch Reactor tube system.....</i>	<i>63</i>
3.3.1 Detailed Reactor System Description .....	63
3.3.2 Reactor Operation and Data Collection .....	65
3.3.3 Tube Batch Reactor Design and Operating Issues:.....	67
<i>3.4 Description of sub and SCW batch direct inject system .....</i>	<i>69</i>
3.4.1 Feed Preparation and Injection .....	70
3.4.2 Batch Reactors, Measurements, and Controls .....	71
3.4.3 Post-Reactor Quench and Sample Collection .....	73
3.4.4 Reactor Operation.....	74
3.4.5 Direct Inject Batch Reactor Design and Operational Issues: .....	77
<i>3.5 Analytical Methods and Analysis.....</i>	<i>78</i>
3.5.1 Feed & Product Analysis .....	79
3.5.2 Data and Error Analysis.....	80
<i>3.6 References.....</i>	<i>84</i>
<b>4 Catalytic Reformation of Methane in SCW .....</b>	<b>86</b>

---

4.1 Motivation and Introduction.....	86
4.1.1 Equilibrium Constraints for Methane SCW Reforming .....	88
4.1.2 Previous SCW Reforming Studies.....	90
4.2 Catalyst Choice for SCW.....	94
4.2.1 Previous SCWO Catalyst Studies.....	94
4.2.2 Previous Hydrothermal Catalyst Studies .....	94
4.2.3 Commercial Steam Reforming Catalyst Compositions and Reducing Techniques .....	99
4.2.4 Selected Catalysts .....	102
4.3 Heterogeneous Catalysis Results.....	103
4.3.1 Results of CSTR & PBR Experiments .....	104
4.3.2 Results of Tube Batch Reactor Experiments .....	107
4.3.3 Results of Direct Inject Batch Reactor Experiments .....	108
4.4 SCW Effects on Heterogeneous Catalysts .....	109
4.4.1 Commercial Nickel Catalysts: .....	110
4.4.2 Platinum Catalysts: .....	114
4.4.3 Ruthenium Catalyst: .....	118
4.4.4 Summary of Catalyst Analysis: .....	120
4.5 Homogeneous Catalysis Results.....	122
4.6 Conclusions.....	127
4.7 References.....	128
<b>5 SCW POX of Methane – An Elementary Reaction Modeling Study.....</b>	<b>133</b>
5.1 Introduction.....	133
5.1.1 Background on Direct Partial Oxidation of Methane .....	133
5.1.2 Previous SCW Methane POX Studies .....	135
5.2 C-1 Elementary Reaction Model Development & Refinement.....	143
5.2.1 Typical Approach to SCWO Detailed Chemical Kinetic Modeling.....	143
5.2.2 Previous SCWO Methane Kinetic Models .....	146
5.2.3 Development of Current MIT C-1 DCKM.....	148
5.2.4 Assessment and Refinement of Current MIT C1 DCKM.....	153
5.3 A Detailed Chemical Kinetic Modeling Analysis of Methane POX in SCW.....	163
5.3.1 Model Prediction of SCW methane POX experimental data.....	163
5.3.2 Reaction Path Analysis.....	165
5.3.3 Model Predictions over a Range of Conditions .....	169
5.4 Conclusions.....	174
5.5 References.....	175
<b>6 Model Maillard Reaction under Hydrothermal Conditions .....</b>	<b>180</b>
6.1 Motivation and Introduction.....	180
6.1.1 The Maillard Reaction .....	180
6.1.2 Influencing the Maillard Reaction .....	181
6.2 Previous Glucose-Glycine Studies.....	183
6.2.1 Glycine in sub and supercritical water.....	184
6.2.2 Glucose in sub and supercritical water .....	185
6.2.3 Glucose and Glycine Mixtures in sub and supercritical water.....	190
6.3 Initial Experimental Results from Glucose/Glycine Degradation Studies.....	191
6.3.1 Initial degradation results: Glycine.....	193
6.3.2 Initial degradation results: Glucose .....	194

---

6.3.3 Kinetics of degradation: Glucose and Glycine Mixtures .....	195
6.4 <i>Product Identification</i> .....	196
6.4.1 Analytical Techniques .....	196
6.4.2 Product Identification: Glycine.....	202
6.4.3 Product Identification: Glucose .....	204
6.4.4 Product Identification: Glucose-Glycine Mixtures .....	206
6.5 <i>Summary and Recommendations</i> .....	212
6.6 <i>References</i> .....	213
<b>7 Summary and Conclusions .....</b>	<b>217</b>
7.1 <i>Catalytic Reformation of Methane</i> .....	217
7.2 <i>SCW POX of Methane – An Elementary Reaction Modeling Study</i> .....	219
7.3 <i>Model Maillard Reaction under Hydrothermal Conditions</i> .....	220
<b>8 Recommendations.....</b>	<b>222</b>
8.1 <i>Experimental system Improvements:</i> .....	222
8.1.1 PFR System: .....	222
8.1.2 CSTR System: .....	224
8.1.3 Batch Direct Inject System: .....	225
8.2 <i>Catalytic Reformation of Methane in SCW</i> .....	226
8.3 <i>SCW POX of Methane – An Elementary Reaction Modeling Study</i> .....	228
8.3.1 C1 SCW DCKM:.....	229
8.3.2 Future SCW POX of Methane Experiments:.....	230
8.4 <i>Model Maillard Reaction Chemistry under Hydrothermal Conditions</i> .....	231
8.5 <i>References</i> .....	232
<b>A Appendix A.....</b>	<b>233</b>
<b>B Appendix B.....</b>	<b>238</b>
<b>C Appendix C – Experimental Data .....</b>	<b>247</b>
C.1 <i>Catalytic Reformation of Methane in SCW: CSTR Experiments</i> .....	247
C.2 <i>Catalytic Reformation of Methane in SCW: Batch Tube Experiments</i> .....	248
C.3 <i>Catalytic Reformation of Methane in SCW: Direct Inject Batch Experiments with Metal Catalysts</i> 249	
C.4 <i>Catalytic Reformation of Methane in SCW: Direct Inject Batch Experiments with Alkali Salts</i> .....	250
<b>D Appendix D – Catalyst Analysis Data .....</b>	<b>251</b>
D.1 <i>XRD Results</i> .....	251
D.2 <i>XPS Results</i> .....	259
D.3 <i>BET Surface Area Measurements</i> .....	267

---

## List of Figures

Figure 1.1 Solvation Properties of Pure Water at 250 bar. Properties shown are density and the dielectric constant, $\epsilon$ (Fernandez, 1997) – NIST Steam Table program) and the ionic dissociation constant, $\log K_w$ (Marshall and Franck, 1981).....	20
Figure 1.2 Critical Curves of Several Binary Aqueous Systems. The left side of each curve (hash mark side) represents a two-phase region while the right side of each curve represents complete miscibility in a single supercritical fluid phase (Hirth and Franck, 1993).....	22
Figure 1.3 Apparent first order rate constant for methylene chloride hydrolysis in HTW. (Salvatierra, Taylor et al., 1999). FMH stands for Fells and Moelwyn-Hughes correlation.....	23
Figure 1.4 Apparent first order rate constant for water gas shift reaction in SCW as a function of water concentration. (Rice, 1998).....	24
Figure 1.5 General Flow Diagram for Changing World Technology's TDP Plant. Adapted from (Roberts, Williams <i>et al.</i> , 2004).....	33
Figure 3.1 Small-Scale Plug Flow Reactor System. ....	46
Figure 3.2 Schematic Cross Section of the Packed Bed Reactor. ....	51
Figure 3.3 Continuous Stirred Tank Reactor System. ....	57
Figure 3.4 Evidence of Temperature Gradient in the CSTR Reactor during Heatup.....	62
Figure 3.5 Hydrothermal Batch Tube System. ....	64
Figure 3.6 Typical Tube Batch Reactor Temperature profile during Heatup and Quench.....	67
Figure 3.7 Sub and Supercritical Water Direct Injection Batch system.....	70
Figure 3.8 Medium Pressure Cross Batch Cell for Catalyst Studies.....	72
Figure 3.9 Medium Pressure Batch Cell for Alkali Salt Studies.....	73
Figure 3.10 Reactor Temperature and Pressure Traces for the Medium Pressure Cross Batch Cell for Catalyst Studies.....	76
Figure 4.1 Equilibrium Conversion of Methane and Product Yield: Conventional Steam versus SCW Reforming Conditions. Chart A = equilibrium conversion of methane. In this chart, solid lines represent conversion values corresponding to different initial conditions of $[H_2O]_0/[CH_4]_0$ and pressure (commercial reforming conditions = $[H_2O]_0/[CH_4]_0 = 3$ , 25 bar). Chart B = equilibrium $H_2$ and CO	

yields. In this chart, solid lines represent H<sub>2</sub> yields and dashed lines represent CO yields corresponding to different initial conditions of [H<sub>2</sub>O]<sub>0</sub>/[CH<sub>4</sub>]<sub>0</sub> and pressure. In both charts, SCW conditions correspond with [H<sub>2</sub>O]<sub>0</sub>/[CH<sub>4</sub>]<sub>0</sub> = 1000 (diamonds), 100 (squares), 10 (triangles) and 250 bar while commercial reforming conditions = [H<sub>2</sub>O]<sub>0</sub>/[CH<sub>4</sub>]<sub>0</sub> = 3 (circles), 25 bar.....89

- Figure 4.2 Experimentally determined gas compositions from nine experiments. (15 min, 650°C, ~600 bar (Expt 7 was 380 bar)) (Kruse and Dinjus, 2003).....91
- Figure 4.3 Equilibrium of Nickel Reduction in the Presence of H<sub>2</sub>O and H<sub>2</sub>. (Rostrup-Neilsen, J.R. 1984) ..101
- Figure 4.4 STEM Analysis of KATALCO 57-7 Catalyst before and after exposure to SCW for 11 hours, 400–500°C, 245 bar. ....111
- Figure 4.5 XRD Analysis of KATALCO 57-7 Catalyst before and after exposure to SCW for 11 hours, 400–500°C, 245 bar. ....112
- Figure 4.6: XPS Analysis of C11-PR Commercial Reforming catalyst before and after exposure to SCW for 37.5 hours, 400–500°C, 245 bar. The red trace corresponds to the catalyst sample before exposure to supercritical water. The blue and green traces are two different samples after experiments in SCW. Comparison of these traces confirms significant loss of nickel, calcium and magnesium from the surface. ....114
- Figure 4.7: XRD analysis of 5% Pt/Al<sub>2</sub>O<sub>3</sub> catalyst powder before and after exposure to SCW for 1.3 hours, 550°C, 370 bar. ....115
- Figure 4.8: XRD analysis of 10% Pt/activated carbon catalyst powder before and after exposure to SCW for 0.5 hours, 600°C, 265 bar.....118
- Figure 4.9: XRD analysis of 1% Ru/TiO<sub>2</sub> catalyst pellets before and after exposure to SCW for 0.7 hrs, 600°C, 300 bar. ....119
- Figure 4.10: Hydrogen Yield from Alkali-SCW mix: Argon versus Methane-Argon mix. Yellow-hashed bars = Argon only gas feed. Green solid bars = 10% CH<sub>4</sub> in Argon gas feed. Data are from the same Hastelloy reactor, two experiments per day, successive days in order from bottom to top of y axis. One KOH experiment in gold-plated reactor displayed at top. Reaction Conditions: 600°C, 275-300 bar, 15 minutes, initial loading of gas 300psig (corresponds to [H<sub>2</sub>O]<sub>0</sub>/[CH<sub>4</sub>]<sub>0</sub> ~140 molar basis) salt 1 wt%....123



- 
- Figure 4.11: Chromium and Nickel Ions in Liquid Phase from Alkali-SCW experiments: Argon versus Methane-Argon mix. Yellow hashed bars = Argon only gas feed. Green solid bars = 10% CH<sub>4</sub> in Argon gas feed. Data are from the same Hastelloy reactor, two experiments per day, successive days in order from bottom to top of y axis. Reaction Conditions: 600°C, 275-300 bar, 15 minutes, initial loading of gas 300psig (corresponds to [H<sub>2</sub>O]<sub>0</sub>/[CH<sub>4</sub>]<sub>0</sub> ~140 molar basis), salt 1 wt%. Results are semi-quantitative only due to limited sample size.....124**
- Figure 5.1 Methanol Selectivity as a function of methane conversion – most promising gas phase data. (Foulds and Gray, 1995).....135**
- Figure 5.2 Prediction of CO SCW Oxidation Data - Sullivan Model versus Ploeger Refinements. Charts on the left depict Sullivan model predictions. Charts on the right depict Ploeger model predictions. Top row plots are stoichiometric CO/O<sub>2</sub> ratio, middle row plots are fuel rich, and bottom row plots are fuel lean. All data was taken at 560°C, 245 bar.....155**
- Figure 5.3 H<sup>•</sup> Radical Rate of Production (ROP) from Reaction CO + OH<sup>•</sup> = CO<sub>2</sub> + H<sup>•</sup>: Original Sullivan Model versus modified C1 Mechanism from this study.....156**
- Figure 5.4 Prediction of CO Oxidation Data Sullivan Model versus Ploeger Refinements: Senosiain Rate reduced 1 OOM. Charts on the left depict Sullivan model predictions. Charts on the right depict Ploeger model predictions after adjusting the Senosiain rate down 1 OOM. Top row plots are stoichiometric CO/O<sub>2</sub> ratio, middle row plots are fuel rich, and bottom row plots are fuel lean. All data was taken at 560°C, 245 bar. ....159**
- Figure 5.5 Comparison of H<sub>2</sub>O<sub>2</sub> + OH<sup>•</sup> rate constants found in various SCWO Detailed Chemical Kinetic Models (DCKMs). Rate chosen by Ploeger is one taken from the DCKM of Rice & Croiset (2001).....162**
- Figure 5.6 Major Species Selectivity Comparison of Methane SCW POX Data with DCKM Predictions. Experimental conditions are 400°C, 250 bar, [CH<sub>4</sub>]<sub>0</sub> = 0.384M, [O<sub>2</sub>]<sub>0</sub> = 0.012M. Lee and Foster data are points, Ploeger-adjusted Sullivan model predictions are lines. (Lee and Foster (1996)). ....164**
- Figure 5.7 Dominant Pathways from Methane to Methanol in SCW. Conditions: T=400°C, P=250bar, [CH<sub>4</sub>]<sub>0</sub> = 0.3M, [O<sub>2</sub>]<sub>0</sub> = 0.009M. Each arrow corresponds to an important elementary reaction in our mechanism, and the percentage values near each arrow give a relative contribution for that reaction's role in total consumption of the reactant species.....167**

---

Figure 5.8 Comparison of Methanol Formation and Decomposition Rate Constants. Rate Constant used in Savage et al (2000) model displayed for comparison. ....	168
Figure 5.9 Methanol selectivity versus time for different initial oxygen/methane ratios-varying oxygen. $P = 245$ bar, $[CH_4]_0 = 1$ mM, $T = 400^\circ C$ . ....	170
Figure 5.10 Methanol selectivity versus time for different initial methane/oxygen ratios – varying methane. $P = 245$ bar, $[O_2]_0 = 1$ mM, $T = 400^\circ C$ . ....	172
Figure 5.11 Maximum methanol selectivity and methane conversion versus pressure. Methane conversion is value at same time as highest methanol selectivity. $T = 400^\circ C$ , $[CH_4]_0 = 1$ mM, $[O_2]_0 = 0.1$ mM. ....	173
Figure 6.1. Mechanism of Maillard reaction commonly cited from Hodge (1953). ....	182
Figure 6.2. Reaction network for glucose destruction. Adapted from (Kabyemela, Adschiri et al. (1997)), Antal et al (1990), and Srokol et al (2004). ....	186
Figure 6.3. Assumed First Order Arrhenius Plot of Glucose Degradation Data. Values for activation energies displayed next to linear fits. PFR and CSTR data from this study. Data from Amin et al, Bobletter and Pape, and Kabyemela et al from Kabyemela <i>et al.</i> , 1997. Xiang <i>et al</i> data from Xiang <i>et al</i> , 2004. ....	195
Figure 6.4 Compounds Identified in Liquid Effluent of Glucose and Glycine Hydrothermal Experiments..	201
Figure 6.5. HPLC Chromatogram of Glycine Degradation products. $T=250^\circ C$ , $P=800$ psig, 1000ppm glycine, 12.6 min residence time, $pH = 2.0$ . UV detection at 210 nm. ....	203
Figure 6.6. HPLC Chromatogram of Glucose Degradation products. $T=250^\circ C$ , $P=800$ psig (55 bar), 1000 ppm glucose, 6.3 min residence time in the CSTR reactor system, $pH = 5.0$ . UV detection at 210 nm. ....	205
Figure 6.7. HPLC Chromatogram of Glucose Degradation products. $T=150-250^\circ C$ , $P=800$ psig (55 bar), 1000 ppm glucose, 7 sec residence time in the PFR reactor system, $pH = 5.0$ . UV detection at 210 nm. ....	206
Figure 6.8. HPLC Chromatogram of Glucose-Glycine Degradation products. $T=250^\circ C$ , $P=800$ psig (55 bar), 1000 ppm glucose, 500 ppm glycine, 6.3 min residence time in the CSTR reactor system, $pH = 2.0$ and 5.0. UV detection at 210 nm. ....	208
Figure 6.9. HPLC Chromatogram of Glucose-Glycine Degradation products. $T=250^\circ C$ , $P=800$ psig (55 bar), 1000 ppm glucose, 500 ppm glycine, 6.3 min residence time in the CSTR reactor system, $pH = 2.0$ and 5.0. UV detection at 290 nm. ....	209

---

Figure 6.10 HPLC Chromatogram of Glucose-Glycine Degradation products. T=200-300°C, P=800 psig (55 bar), 1000 ppm glucose, 500 ppm glycine, 7 sec residence time in the PFR reactor system, pH = 5.0. UV detection at 290 nm. Glucose degradation shown for comparison.....	211
Figure 6.11 HPLC Chromatogram of Glucose-Glycine Degradation products. T=200-300°C, P=800 psig (55 bar), 1000 ppm glucose, 500 ppm glycine, 7 sec residence time in PFR reactor system, pH = 5.0. UV detection at 210 nm. ....	211
Figure D.1 XRD Results of KATALCO 57-7 pellets before and after exposure to SCW (11 hrs, 400-500°C, 245 bar). ....	251
Figure D.2 XRD Results of C11-PR pellets before and after exposure to SCW (37.5 hrs, 400-500°C, 245 bar; shorter exposure time saw similar results).....	252
Figure D.3 XRD Results of 5% Pt/Al <sub>2</sub> O <sub>3</sub> powder before and after exposure to SCW (1.3 hrs, 550°C, 370 bar). ....	253
Figure D.4 XRD Results of 0.5% Pt/Al <sub>2</sub> O <sub>3</sub> pellets before and after exposure to SCW (0.5 hrs, 600°C, 420 bar). ....	254
Figure D.5 XRD Results of 1% Pt/ZrO <sub>2</sub> powder before and after exposure to SCW (0.5 hrs, 600°C, 245 bar). ....	255
Figure D.6 XRD Results of 1% Pt/5% CeO/ ZrO <sub>2</sub> powder before and after exposure to SCW (2.3 hrs, 600°C, 270 bar). ....	256
Figure D.7 XRD Results of 10% Pt/activated carbon powder before and after exposure to SCW (0.5 hrs, 600°C, 265 bar).....	257
Figure D.8 XRD Results of 1% Ru/TiO <sub>2</sub> pellets before and after exposure to SCW (0.7 hrs, 600°C, 300 bar). ....	258
Figure D.9 XPS Results of KATALCO 57-7 pellets before and after exposure to SCW (11 hrs, 400-500°C, 245 bar). ....	259
Figure D.10 XPS Results of C11-PR pellets before and after exposure to SCW (37.5 hrs, 400-500°C, 245 bar; shorter exposure time saw similar results).....	260
Figure D.11 XPS Results of 5% Pt/Al <sub>2</sub> O <sub>3</sub> powder before and after exposure to SCW (1.3 hrs, 550°C, 370 bar). ....	261

---

<b>Figure D.12 XPS Results of 0.5% Pt/Al<sub>2</sub>O<sub>3</sub> pellets before and after exposure to SCW (0.5 hrs, 600°C, 420 bar)</b>	
.....	<b>262</b>
<b>Figure D.13 XPS Results of 1% Pt/ZrO<sub>2</sub> powder before and after exposure to SCW (0.5 hrs, 600°C, 245 bar).</b>	
.....	<b>263</b>
<b>Figure D.14 XPS Results of 1% Pt/5% CeO/ ZrO<sub>2</sub> powder before and after exposure to SCW (2.3 hrs, 600°C, 270 bar).</b>	
.....	<b>264</b>
<b>Figure D.15 XPS Results of 10% Pt/activated carbon powder before and after exposure to SCW (0.5 hrs, 600°C, 265 bar).</b>	
.....	<b>265</b>
<b>Figure D.16 XPS Results of 1% Ru/TiO<sub>2</sub> pellets before and after exposure to SCW (0.7 hrs, 600°C, 300 bar).</b>	
.....	<b>266</b>

---

## List of Tables

Table 1.1. Select Transport Properties of Pure Water at Various Conditions. Viscosity, thermal conductivity and heat capacity from (Fernandez, 1997) – NIST Steam Table program. Diffusivity from (Kubo, 2000).	25
Table 1.2 Operating Conditions of Select Current Hydrothermal Research Programs.	30
Table 4.1 Process conditions for various reforming product streams (Myers, 2000). Water-gas shift step is not considered for these conditions.	86
Table 4.2 Operating Conditions of Select Oxygen-Free Hydrothermal Catalyst Research Programs. (Tomita and Oshima, 2004; Davda, 2003; Minowa and Ogi, 1998; Elliott, 2004; Osada, Sato <i>et al.</i> , 2004; Vogel, 2002; Watanabe, Osada <i>et al.</i> , 2003; Park and Tomiyasu, 2003; Antal, 2000)	96
Table 4.3 Most Promising Catalyst Choices for SCW Reforming of Methane based on Previous Hydrothermal Catalyst Studies. Supporting and conflicting studies are listed by lead author of cited references. (Tomita and Oshima, 2004; Davda, 2003; Minowa and Ogi, 1998; Elliott, 2004; Osada, Sato <i>et al.</i> , 2004; Vogel, 2002; Watanabe, Osada <i>et al.</i> , 2003; Park and Tomiyasu, 2003; Antal, 2000; Ding, Frisch <i>et al.</i> , 1996; Frisch <i>et al.</i> , 1995)	99
Table 4.4 Experimental Conditions for CSTR and PBR Experiments. More details on experimental conditions can be found in Appendix C.	104
Table 4.5 Experimental Conditions for Tube Batch Experiments. More details on experimental conditions can be found in Appendix C.	107
Table 4.6 Experimental Conditions for Direct Inject Batch Experiments. More details on experimental conditions can be found in Appendix C.	109
Table 4.7 Summary of Catalyst Evaluation. (+) indicated a positive evaluation. (+/-) indicates a neutral evaluation based on conflicting or inconclusive results. (-) indicates a negative evaluation.	121
Table 4.8 Most Promising Catalyst and Support Choices for SCW Reforming of Methane based on this study. (+) indicated a positive evaluation. (+/-) indicates a neutral evaluation based on conflicting or inconclusive results. (-) indicates a negative evaluation.	121
Table 5.1. Conditions and Details of Previous Methane SCW POX Studies and Resulting Conversions and Selectivities	136

---

<b>Table 5.2. A Comparison of Current SCWO Methane Elementary Reaction Models .....</b>	<b>147</b>
<b>Table 5.3: Updated Thermodynamic values to Sullivan-Ploeger Model.....</b>	<b>151</b>
<b>Table 5.4: Updated Reactions to Sullivan-Ploeger Model.....</b>	<b>153</b>
<b>Table 6.1. Glucose degradation products observed in various studies. Studies and their conditions are given at the bottom of the table.....</b>	<b>188</b>
<b>Table 6.2. Results obtained in preliminary experiments on glucose and glycine. CSTR experiments had residence times of 3-67 min while PFR experiments had 10 sec residence times. Initial concentrations for glycine and glucose ranged from 100 – 2000 ppm.....</b>	<b>192</b>
<b>Table 6.3. Summary of Compounds Tested as Possible Liquid Phase Products. Retention times correspond to an Interaction ORH-801 organic acid column heated to 60°C, 0.01N H<sub>2</sub>SO<sub>4</sub> mobile phase, 0.7 mL/min flow rate. ....</b>	<b>199</b>
<b>Table 6.4. Semi-quantitative results of TOC and CHN analysis for select glucose, glycine and glucose-glycine experiments.....</b>	<b>200</b>
<b>Table C.1 Experimental Data for CSTR Experiments: SCW Reforming of Methane. Additional experiments using various reducing methods are omitted because steady state conditions were never achieved.....</b>	<b>247</b>
<b>Table C.2 Experimental Data for Tube Batch Experiments: SCW Reforming of Methane. Additional control experiments and experiments with possible leaks are omitted. (a) calculated pressure – pressure was not measured due to installation of a high temperature valve.....</b>	<b>248</b>
<b>Table C.3 Experimental Data for Direct Inject Batch Experiments: SCW Reforming of Methane with Metal Catalysts. Additional control experiments and experiments with possible leaks are omitted.....</b>	<b>249</b>
<b>Table C.4 Experimental Data for Direct Inject Batch Experiments: SCW Reforming of Methane with Alkali Salts. ....</b>	<b>250</b>
<b>Table D.1 BET Results for all Metal Catalysts. ....</b>	<b>267</b>

---

# 1 Introduction and Background

Several researchers have attempted to exploit the attractive properties of high pressure, high temperature water as a clean and effective means to convert current low-grade fuel and waste streams into useful products. Motivated by a growing global interest in renewable fuels, many of these studies focus on converting biomass or waste-biomass into fuels. In support of this effort, the research presented here centers around gaining a more thorough understanding of model fuel conversion reactions under hydrothermal conditions, both below and above water's critical point at 374°C and 221 bar. In this chapter, sub-critical (subCW) and supercritical water (SCW) are discussed as alluring media for fuel conversion. Examples of hydrothermal biomass conversion research are presented to help define the goals and objectives of this thesis. This chapter concludes with a section on model compound and reaction condition selection.

## 1.1 PROPERTIES OF SUB AND SUPERCRITICAL WATER

Among hundreds of journal articles on high pressure, high temperature water (HTW) research, there are four recent review papers that provide a detailed overview of the uniqueness of chemistry in a hydrothermal environment (Watanabe, 2004; Akiya and Savage, 2002; Broll, 1999; Savage, Gopalan *et al.*, 1995). Here we review their comments on the properties of sub and supercritical water and describe how those properties might be advantageous to fuel conversion processes.

### 1.1.1 High Temperature Water as a Solvent

The solvent properties of high temperature water (HTW) drastically change in the vicinity of water's critical point at 374°C, and 221 bar which can be easily seen in a plot of density, dielectric constant and ionic dissociation constant versus temperature along a

supercritical isobar (Figure 1.1). As you probably first learned in grade school, room temperature water is a highly polar solvent which readily dissolves polar solutes and ionic salts. These properties correspond with a relatively high dielectric constant ( $\epsilon = 79$  @  $25^\circ\text{C}$ ) and an ionic dissociation constant,  $K_w$ , of  $10^{-14}$  ( $K_w \equiv [a_{H^+}][a_{OH^-}]$ ). However, as you heat water at a constant supercritical pressure of 250 bar, its dielectric constant drops dramatically

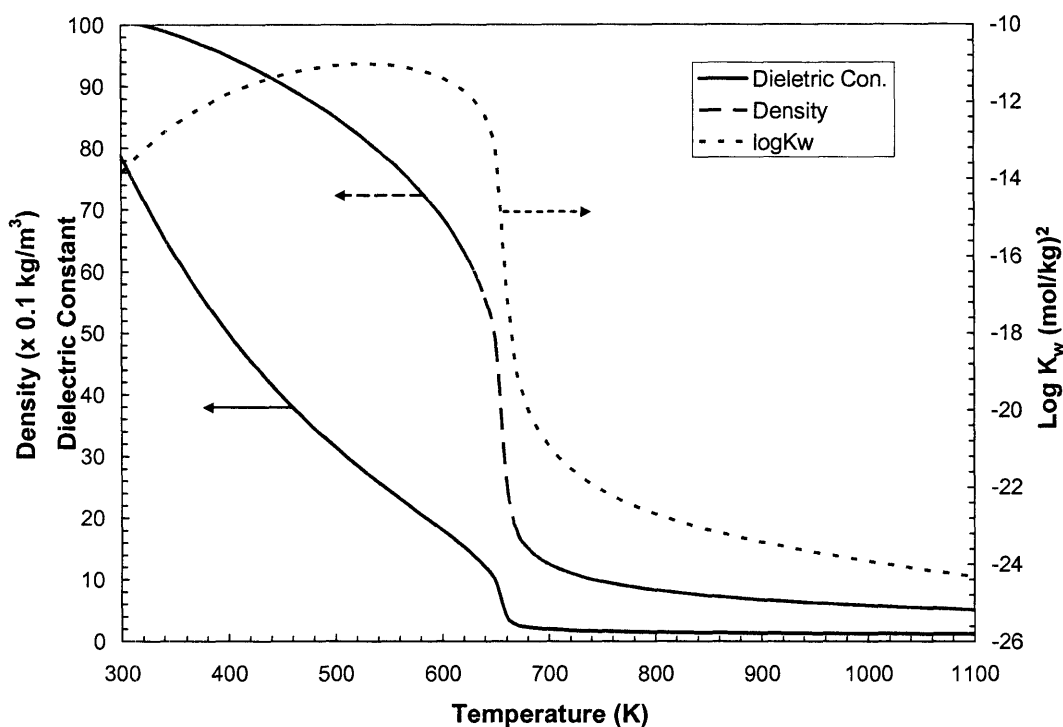


**Figure 1.1 Solvation Properties of Pure Water at 250 bar.** Properties shown are density and the dielectric constant,  $\epsilon$  (Fernandez, 1997) – NIST Steam Table program) and the ionic dissociation constant,  $\log K_w$  (Marshall and Franck, 1981).

reaching a value almost two orders of magnitude lower than room temperature water, while its dissociation constant first increases two orders of magnitude then drops precipitously at temperatures above the critical point. The striking changes in these and other properties result in supercritical water acquiring the characteristics of a non-polar solvent in which organic



substances and gases are readily dissolved and ionic compounds no longer dissociate yielding very low solubilities. Additionally, water's solvation properties at these high temperatures and pressures are strongly correlated to density and are therefore highly tunable in the near critical region by changing temperature and pressure. For example, at 400°C values for  $K_w$  can range from  $10^{-19}$  to  $10^{-11}$  and values for  $\epsilon$  can range from 2 to 12 when adjusting density by a factor of 3 by simply increasing pressure from 250 to 500 bar.

The structural characteristics of high temperature water explain the variability of its solvent properties. Although hydrogen bonding is still present in high temperature water, its prevalence varies greatly. For example, water at 400°C and  $\sim 0.5 \text{ g/cm}^3$  retains 30-45% of the hydrogen bonds that exist at ambient conditions whereas water at 500°C and  $\sim 0.1 \text{ g/cm}^3$  retains only 10 – 14% (Akiya and Savage, 2002). Knowledge of these structural characteristics helps explain the change in solubility of gases in water. As depicted in Figure 1.2, gases such as  $\text{O}_2$  and  $\text{CH}_4$ , that are fairly immiscible in ambient liquid water become completely soluble in supercritical water. Effective separation of product gases in a high temperature water process is therefore readily achieved by changing pressure or temperature.

However, it is these same structural characteristics of high temperature water that may also pose disadvantages to its use as a solvent for fuel conversion processes. Some studies have discussed a “cage-effect” evidenced by the long-range correlation of water molecules around solute molecules in SCW (Watanabe, 2004; Kremer, 1999; Ederer, 1999; Savage, Gopalan *et al.*, 1995). While these solvent cages may increase initial reaction rates with increased solvent-solute collisions locally, they also inhibit diffusion of reactants and products thereby reducing overall reaction rates in SCW. In those cases where free radicals are formed from uni-molecular

decomposition reactions, the nascent products may be likely to recombine before they can migrate from the solvent cage via diffusion.

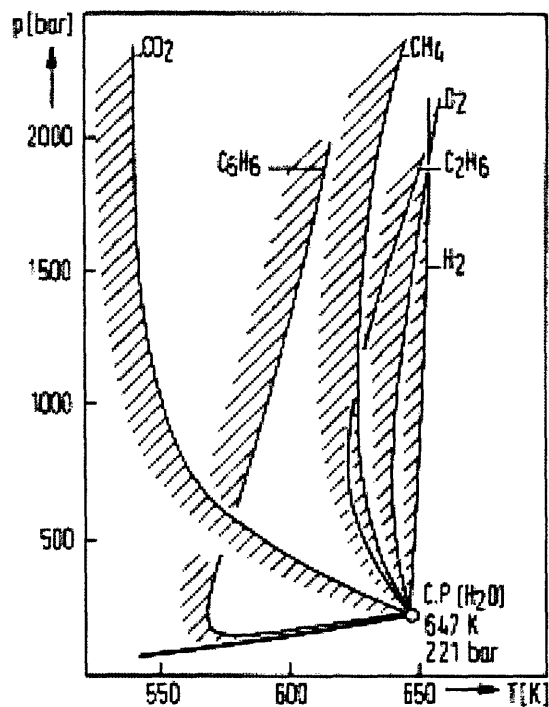


**Figure 1.2 Critical Curves of Several Binary Aqueous Systems.** The left side of each curve (hash mark side) represents a two-phase region while the right side of each curve represents complete miscibility in a single supercritical fluid phase (Hirth and Franck, 1993).

Solution phase reaction kinetics have been shown to be affected by the preferential solvation of reactants, transition states and/or products (Laidler, 1987) and HTW seems to display this same trait. Although HTW may be advantageous in dissolving non-polar reactants and products, it may actually slow reactions which proceed through more polar transition states. Our group at MIT reported on the solvent effects of methylene chloride hydrolysis in sub and supercritical water (Marrone, Arias *et al.*, 1998 and Salvatierra, Taylor *et al.*, 1999). In this study, a greater extent of hydrolysis under sub-critical temperatures and little hydrolysis under

supercritical conditions was observed. The authors applied a Kirkwood analysis to their data which showed an excellent correlation with changing solvent properties (see Figure 1.3). A similar result was found in another MIT study on methyl tert-butyl ether (MTBE) hydrolysis (Taylor, Pacheco *et al.*, 2002). Since we can tune the properties of HTW with changes in density, we should expect to find a range

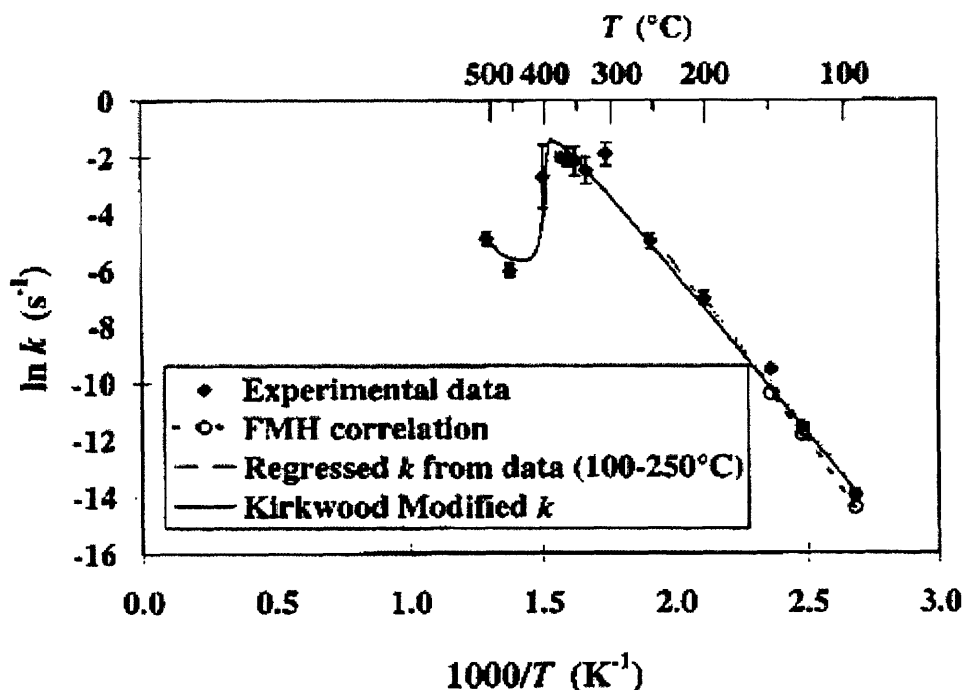


**Figure 1.3** Apparent first order rate constant for methylene chloride hydrolysis in HTW. (Salvatierra, Taylor *et al.*, 1999). FMH stands for Fells and Moelwyn-Hughes correlation.

of densities where solution-dependent rates improve. Such is the case with the water-gas shift reaction ( $\text{CO} + \text{H}_2\text{O} \rightleftharpoons \text{CO}_2 + \text{H}_2$ ) in HTW where the rate constant increases with increasing water density as shown in Figure 1.4 (Melius, Bergan *et al.*, 1990 and Rice, 1998).

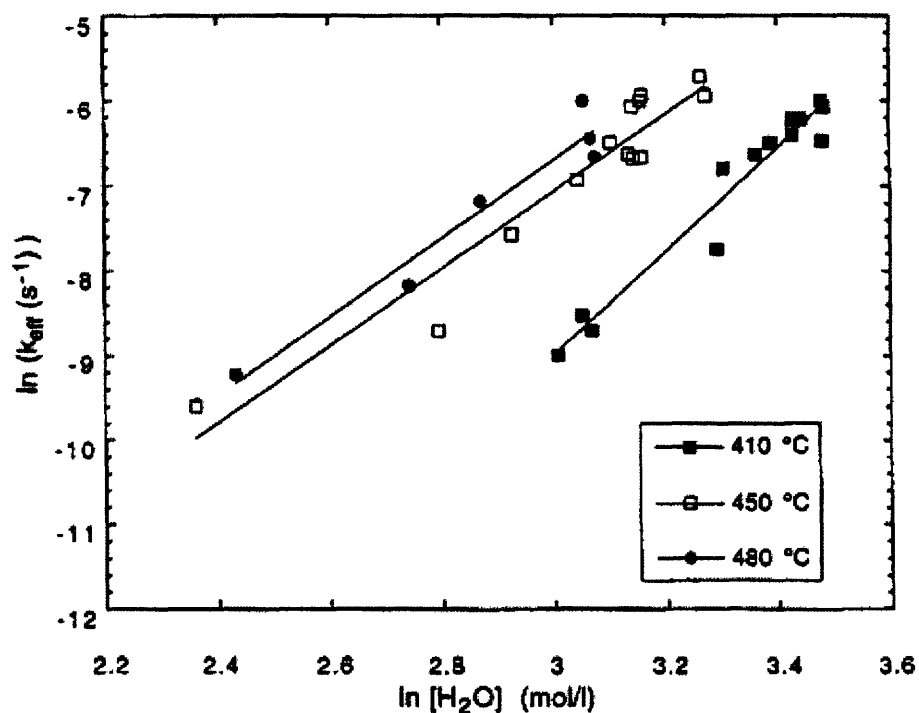


**Figure 1.4** Apparent first order rate constant for water gas shift reaction in SCW as a function of water concentration. (Rice, 1998).

The range of conditions of HTW allows for a variety of feasible chemical reaction pathways. Following the trend for the ionic dissociation constant of water, reactions can proceed via ionic pathways in liquid water and high pressure SCW while radical pathways dominate in steam and less dense SCW. Both types of reactions proceed in competition around the critical point of water. Therefore, a key challenge to using HTW as a medium for fuel conversion reactions is to carefully choose temperature and pressure conditions that will allow reactants to be miscible and yet promote the particular chemistry and kinetics to optimize useful fuel products.

### 1.1.2 High Temperature Water as a Fluid

In addition to its appealing properties as a solvent, HTW can be an ideal fluid with a range of attractive transport characteristics. Table 1.1 lists a range of possible values for dynamic viscosity, thermal conductivity, heat capacity and diffusivity of pure water at various conditions. At moderate SCW temperatures and densities (e.g., 400°C, 0.17 g/mL), dynamic viscosity is only one tenth to one twentieth of the value for ambient water which leads to an increase in the overall rate of reactions, especially heterogeneously catalyzed reactions that are limited by mass transfer to and from active centers. Reduced viscosity leads to increased diffusivity which is clearly displayed in the values in Table 1.1. Even at relatively high densities (at 500°C and 75 MPa,  $\rho \sim 0.5 \text{ g/cm}^3$ ) the self-diffusivity of SCW is almost two orders of magnitude higher than ambient water. As a result, one would expect diffusion-limited reactions in the liquid phase to occur more rapidly in SCW even at high densities.

**Table 1.1. Select Transport Properties of Pure Water at Various Conditions.** Viscosity, thermal conductivity and heat capacity from (Fernandez, 1997) – NIST Steam Table program. Diffusivity from (Kubo, 2000).

	Liquid Water ( $T < 100^\circ\text{C}$ , various $P$ )	Sub-critical Water ( $T < 374^\circ\text{C}$ , $P > P_{sat}$ )	Supercritical Water ( $T > 374^\circ\text{C}$ , $P > 221 \text{ bar}$ )	Gas ( $T > 100^\circ\text{C}$ , $P < P_{sat}$ )
Dynamic Viscosity (Pa·s)	$10^{-3}$	$10^{-4}$	$10^{-4} - 10^{-5}$	$10^{-5}$
Thermal Conductivity (W/m·K)	0.6	0.3 – 0.7	0.1 – 0.5	0.03 – 0.09
Heat Capacity, $C_p$ (kJ/kg K)	4	4 - 15	3 - 15	2
Diffusivity ( $\text{m}^2/\text{s}$ )	$10^{-8} - 10^{-9}$	$10^{-7} - 10^{-8}$	$10^{-6} - 10^{-7}$	$10^{-4} - 10^{-5}$

---

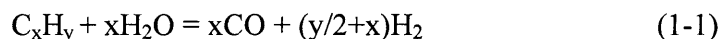
Because subcritical liquid and supercritical water are more efficient heat transfer media than steam, they may prove advantageous in several reaction schemes including partial oxidation reactions which often produce problematic hot spots in gas phase processing. Values for the thermal conductivity of pressurized liquid and supercritical water range from a factor of three to ten times higher than gaseous water (Broll, 1999). Near-critical HTW and SCW can have large variations in heat capacity as seen in Table 1.1. HTW can also participate in dominantly unimolecular elementary reactions as an effective, intermolecular energy transfer agent and collision partner thereby effecting overall reaction rates (Holgate and Tester, 1994; Steeper, Rice *et al.*, 1996).

HTW contains the best of both gas phase and liquid phase transport properties. With a careful selection of temperature and pressure conditions, one can achieve the reduced viscosity and increased diffusivity levels of a gas with the higher thermal conductivity, heat capacity and density of a liquid. SCW has the added benefit of eliminating two-phase transport issues associated with gas and liquid reactions that slow reaction rates.

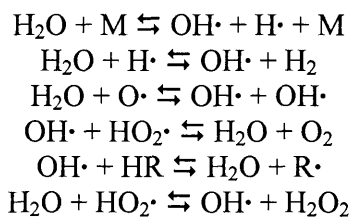
### *1.1.3 High Temperature Water as a Reactant*

High temperature water is not an inert solvent or fluid. Water molecules may participate in several types of reactions including hydrolysis and hydration, hydrogen donating reactions and free radical oxidation chemistry. Hydrolysis reactions involve bond breaking by water with several useful applications like processing waste polymeric materials such as plastics (Fang and Kozinski, 2001). Although most alkanes are resistant to hydrolysis without catalyst, hydrocarbons with heteroatoms or unsaturated bonds are susceptible to hydrolytic degradation. A complete description of fuel conversion reaction pathways in HTW should include hydrolysis routes (Akiya and Savage, 2002).

Experimental studies have concluded that water donates hydrogen atoms in HTW reactions (Kruse, 1996). This added hydrogen can participate in chain-terminating free-radical reactions ultimately reducing the formation of higher molecular weight species. The absence or suppression of char, tar and coke formation during the HTW pyrolysis of various hydrocarbons provides direct experimental evidence of this phenomena ((Lawson and Klein, 1985) and (Watanabe, 1998)). Water can also produce hydrogen through two well-known hydrolysis reactions; hydrocarbon reforming (Reaction 1-1) and water gas shift (Reaction 1-2):



Oxidation in SCW is thought to proceed through free radical pathways where water molecules play integral roles in generating and maintaining a pool of key reactive species. Examples of important elementary reactions which involve water are included in several detailed chemical kinetics models for supercritical water oxidation (SCWO) (Holgate and Tester, 1994; Brock and Savage, 1995; DiNaro, Howard *et al.*, 2000; Sullivan, 2004) and are listed below.



M indicates any third-body collision partner which is water in most cases. Water is thought to be a very effective collision partner which often results in conversion rates being dependent on water density or concentration (Helling and Tester, 1987; Steeper, Rice *et al.*, 1996). With an increased understanding of free radical oxidation processes in SCW, reactions previously thought to be restricted to the gas phase at high temperature and lower pressures can now be carried out at lower temperatures and higher pressures with different and appealing results.

#### 1.1.4 Summary of HTW Characteristics

The HTW environment is best summarized by the following bullets:

- Improved solubilities of organic and gaseous reactants and products
- Adjustment of the reaction medium density with changes in temperature and pressure may alter reaction rates and selectivities
- Tunable solvent that can promote both free radical reactions and ionic reactions
- Elimination of interphase transport restrictions on reaction rates at supercritical conditions
- Use of the solvent to facilitate both reaction and separation processes
- Improved transport properties: gas-like viscosities and liquid-like densities, thermal conductivities and heat capacities
- Source of hydrogen

Careful consideration of these particular characteristics allows one to easily conclude HTW's suitability as an effective fuel conversion processing medium. An example of this assessment can be taken from (Dinjus, 2004). In this article the authors list several advantages of hydrothermal gasification over traditional gasification including higher thermal efficiency, one-step production of a high pressure, hydrogen-rich gas with low CO content, suppression of soot and tar formation, separation of heteroatoms (S,N, and halogens) with the aqueous effluent thus avoiding expensive gas cleaning processes, and ease of CO<sub>2</sub> separation due to its high solubility in water under high pressure.

For those fuel conversion processes which use metal catalysts, supercritical water reaction media enjoy several added benefits including reduced coke formation and improved mass and heat transport. Hirth and Franck (1993) performed several experiments in hydrothermal flames which demonstrated a ten-fold decrease in soot formation in supercritical water. Supercritical water also improves mass transfer with its liquid-like densities and gas-like viscosities. Its higher thermal conductivity over gas phase conductivities enhances heat transfer in this medium (Baiker, 1999). Reduction of soot and improved mass and heat transfer will



---

prolong the life of heterogeneous catalysts, adding to the list of reasons to consider supercritical water media in catalytic fuel conversion reactions.

A critical evaluation of fuel conversion reactions in HTW should also consider potential drawbacks. As mentioned earlier, the “cage effect” phenomena of this dense solvent may hinder reaction rates and reduce selectivities to higher molecular weight species like longer chain hydrocarbon fuels. The ability to precipitate inorganic salts under supercritical water conditions may lead to accelerated corrosion of reactor walls and may contaminate or poison heterogeneous catalysts. The highly reactive HTW environment may cause more rapid degradation of common heterogeneous catalysts and make it more difficult to create stable, higher molecular weight fuels that will not further react. Consideration of these and other drawbacks provide context and help focus research into the potential applications of hydrothermal processes for biomass waste-to-fuel conversion.

## **1.2 HYDROTHERMAL WASTE TO FUELS RESEARCH**

The research presented in this thesis is focused on improved understanding of both natural gas and biomass conversion in hydrothermal environments. With respect to biomass, a good starting point is a review paper by Savage, Gopalan *et al.*, (1995) which represents a useful summary of initial research on the conversion and treatment of biomass in hydrothermal sub- and supercritical media. Here we present a few examples of current research programs that focus on studying the advantageous properties of HTW in waste-to-fuels applications. Table 1.2 depicts the conditions explored by several representative research groups.

**Table 1.2 Operating Conditions of Select Current Hydrothermal Research Programs.** FZT = Forschungszentrum, Karlsruhe, Germany; PSI = Paul Scherrer Institut, Villigen, Switzerland; PNNL = Pacific Northwest National Laboratory; CWT = Changing World Technologies, Inc. (Antal, 2000; Kruse, 2005; Vogel, 2002; Elliott, 2004; Davda, 2003; Roberts, Williams *et al.*, 2004)

Principal Investigators	Type Feed	Feed wt %	<i>T</i> (C)	<i>P</i> bar	Objective
Antal, U. of Hawaii	wet biomass, sewage, glucose	<22	600-650	345	Gasification, H <sub>2</sub> rich gas
Kruse & Dinjus, FZT, Karlsruhe	glucose, cellulose, plants, meats	1-5	500-700	300-500	Gasification, H <sub>2</sub> rich gas
Vogel, PSI	woody biomass, sewage, model biomass mixture	10-30	350 - 450	250 - 350	Gasification, CH <sub>4</sub> rich gas
Elliott, PNNL	wet biomass, manure, grains,	1-8	250-360	>220	Gasification, CH <sub>4</sub> rich gas
Dumesic, U. of Wisconsin	ethylene glycol	2-10	210-265	25-51	Gasification, H <sub>2</sub> rich gas & alkane formation
Appel, CWT	wet biomass, real wastes	40-50	200-300	40	Liquid fuels and fuel gas

### 1.2.1 Biomass to Fuels Research in Supercritical Water

For the past two decades, Professor Michael Antal has maintained a biomass conversion research program at the University of Hawaii. Some of his group's work has focused on the gasification of model biomass compounds such as glucose under supercritical water conditions to produce a hydrogen-rich product gas. Using activated carbon as a catalyst, Antal and co-workers achieved large gas yields (>2 L/g) with a high content of hydrogen (57%) but their experiments were plagued by plugging due to char from the biomass vapors and corrosion of nickel alloy reactors (Antal, 2000; Xu, 1998; Xu, 1996; Yu, 1993).

Drs. Andrea Kruse and Eckhard Dinjus at the Institut für Technische Chemie, Forschungszentrum Karlsruhe in Germany have developed a hydrothermal biomass research program centered on the fundamental aspects of reactions in supercritical water. Experimenting

with real biomass waste and model compounds such as glucose and glycine, these researchers varied several parameters to investigate affects on gas yields of targets gases like hydrogen and methane. They found that hydrogen yield was maximized at high temperatures, pressures and with the addition of alkali salts like KOH and  $K_2CO_3$ . Problems reported from these experiments include the observation of corrosion and low gas yields after conversion of the protein-containing biomass (Kruse, 2005; Dinjus, 2004; Kruse and Dinjus, 2003; Sinagju, 2003).

The Paul Scherrer Institut (PSI) in Villigen, Switzerland has established a hydrothermal biomass conversion research program focused on the gasification of wet biomass feedstocks to a methane-rich fuel gas. Since methane is the target product, researchers at PSI have concentrated on lower temperature conditions ( $\sim 400^\circ C$  & 300 bar) to exploit equilibrium predictions and the use of catalysts like Raney nickel to improve the kinetics. Experiments at PSI have shown >99% gasification of a 10 wt % woody biomass to a fuel gas containing almost 50% by volume methane from a batch reactor after 98 minutes of holding time. Future plans for this PSI program are to examine long term stability of their Raney nickel catalysts, and experiment using a continuous flow design with salt separation integration into that design (Vogel, 2002; Waldner, 2004; Vogel, 2005).

### *1.2.2 Sub-critical Water Biomass to Fuels Research*

Several researchers have achieved encouraging results for biomass conversion at sub-critical water conditions. Dr. Douglas C. Elliott and co-workers at Pacific Northwest National Laboratory, Washington have examined catalytic gasification of wet biomass for almost two decades. Their latest research involves a bench scale unit as well as a mobile unit, the MSRS (mobile scaled-up reactor system) which incorporates tubular fixed bed reactors filled with a patented ruthenium catalyst they have optimized for hydrothermal environments (Elliott, 2004).

---

In almost all experiments nominally at 350°C, 220 bar and 1 hour residence time, PNNL achieved near complete gasification of various biomass feeds producing a fuel gas with greater than 50% by volume methane and low hydrogen and CO content. Issues discovered in this work include plugging of the catalyst bed from the precipitation of biomass components. These precipitates also contaminated the catalyst and added to catalyst deactivation (Elliott and Sealock, 1998; Elliott and Sealock, 1998; Elliott, Werpy *et al.*, 2001; Elliott, 2004; Elliott, 1997).

Researchers at the University of Wisconsin, in Professor James A. Dumesic's group, have recently reported encouraging results on catalytic aqueous phase reforming (APR) of biomass-derived oxygenates like ethylene glycol. Operating at 225-265°C, 25 – 51 bar and using a variety of catalysts such as tin-promoted Raney nickel and silica supported metal catalysts, Dumesic and co-workers were able to achieve 50 – 100% conversion to a hydrogen rich gas phase. In a separate set of experiments, they observed significant yields of alkanes from the oxygenate, sorbitol, by aqueous phase reforming over a bi-functional metal-solid acid catalyst. Although these initial results were very encouraging, further tests should include a wider range of more challenging feeds which more closely simulate real biomass feed stocks. (Davda and Dumesic, 2003; Davda, 2003; Huber, Shabaker *et al.*, 2003; Huber, Cortright *et al.*, 2004; Shabaker, Huber *et al.*, 2004).

Changing World Technologies (CWT) is one of the first companies to create a commercial plant which exploits the hydrothermal environment as part of an innovative technology to convert animal food wastes to useful products. Their process, called the Thermal Depolymerization Process (TDP), follows a general flow sheet depicted in Figure 1.5 (see (Adams, Appel *et al.*, 2004; Roberts, Williams *et al.*, 2004 for further details). The process has three main stages. In the first stage the food processing waste is mechanically converted into a

slurry, pressurized to about 40 bar or a pressure high enough to maintain a liquid mixture, and then fed to a reactor where it is heated to 200 to 300°C. A series of separation steps comprise the second stage where the solids are separated and the liquid is flashed to separate water. The final step is where the non-aqueous phase is further processed by heat treatment in a second stage reactor (around 500°C) to crack the 1<sup>st</sup> stage oil into lighter hydrocarbon fractions and carbon. Recovered from the first stage are a solid phase (minerals) and liquid phase (containing nitrogen); both products are possible fertilizers. Fuel gas, carbon and diesel oil are produced from the second stage reactor. The fuel gas is used for the internal heat needs of the plant. The fertilizers, carbon and diesel oil are marketable products. The oil is dominated by straight hydrocarbons with a chain length between 15 and 20, at the light/medium end of conventional diesel oil (Adams, Appel *et al.*, 2004; Roberts, Williams *et al.*, 2004).

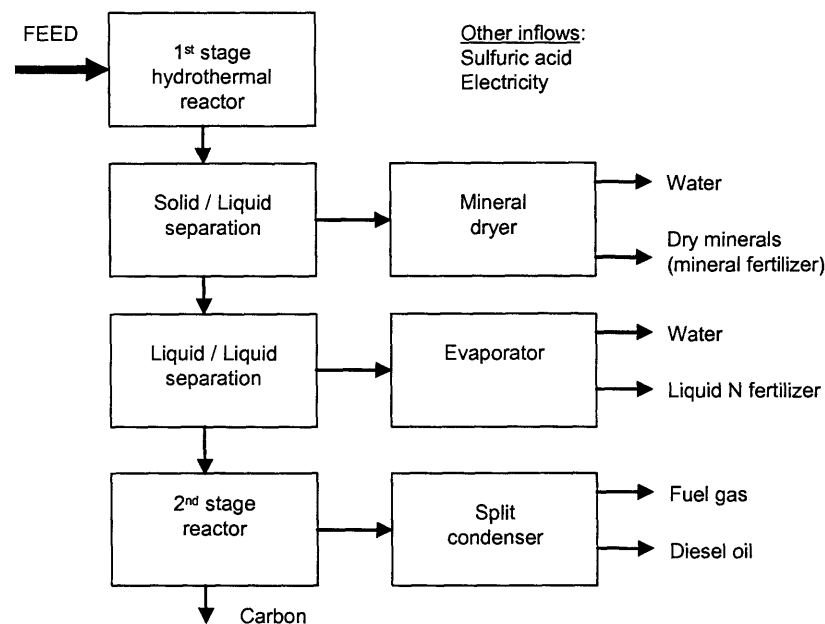


**Figure 1.5 General Flow Diagram for Changing World Technology's TDP Plant.** Adapted from (Roberts, Williams *et al.*, 2004)

CWT's TDP Plant offers an extraordinary option for converting waste feedstocks into useful products, perhaps the most attractive product being a clean, toxin-free renewable source of fertilizer, energy and other useful products. Plants like these offer partial solutions to many problems plaguing our world today such as solid waste disposal problems, shrinking landfill capacities, and the spread of diseases like Mad Cow Disease associated with animal wastes. Although CWT's first commercial plant at Carthage, Missouri is fully operational and realizing very encouraging results, there are several issues that should be addressed with additional hydrothermal research. For example, feed stocks high in carbohydrates and proteins have formed undesirable nitrogenous polymer side products which reduce yields of saleable products and clog components of their system.

### **1.3 MODEL COMPOUND AND REACTION CONDITION SELECTION**

In the previous section, we discussed examples of current hydrothermal biomass waste to fuels research and briefly mentioned issues and unanswered research questions in this field. Those issues ranged from imperfect gas yields and catalyst stability concerns for supercritical water processes to the formation of undesirable side products in sub-critical water processes. To improve our fundamental knowledge of reactions in hydrothermal environments and to help address issues already identified in this field of research, we have chosen to more closely investigate the fate of select model compounds under well defined hydrothermal conditions. Methane was chosen as a model compound for study at supercritical water conditions while glucose and glycine were selected for study at sub-critical water conditions.

### 1.3.1 Methane as a Model Compound

The choice of methane as a model compound was an easy one. In addition to being the target product of many hydrothermal biomass gasification processes, methane is bound to be a major degradation product of every organic feed material. While methane has been the subject of many supercritical water oxidation and partial oxidation studies, few have studied the fate of methane under oxygen-free hydrothermal conditions (Webley and Tester, 1991; Hirth and Franck, 1993; Kruse and Dinjus, 2003). A more thorough understanding of the fate of methane under hydrothermal conditions is critically important to achieve the goal of producing a hydrogen-rich, carbon monoxide-free product gas from biomass. Improved insight into this reaction environment may also enable us to explore a set of conditions where we might be able to convert methane to a liquid fuel possibly through a one-step process.

The study of methane in a high temperature, high pressure water environment may also help address a related concern of stranded gas utilization. Many global natural gas reserves are un-useable because of their remote location or poor quality, and, as a consequence, significant amounts simply go to waste. For example, in 2002, some oil companies reported flaring over 25% of their non-piped gas output (Golombeck, 2003). Apart from wasting its energy content, the practice of flaring is a significant contributor to greenhouse gas emissions. Globally, the earth may have twice as much natural gas than liquid petroleum resources (5400 versus 2600  $\times 10^{15}$  kJ), and yet the world currently produces twice as much liquid petroleum as gas (Tester, Drake *et al.*, 2005).

The question then is: why aren't we consuming our vast stores of methane instead of oil and why are we wasting it? While there are several factors that have limited methane use as a fuel, the efficient use of methane has several challenges. The first challenge is harvesting and

---

transporting the gas. Significant quantities of methane are labeled by the industry as “stranded gas”; stranded due to contamination by significant amounts of H<sub>2</sub>S or CO<sub>2</sub> or stranded due to remote locations away from end users. Other substantial sources of methane are equally troublesome to recover including gas fields associated with oil fields. Once harvested, methane must be efficiently transported over long distances by ship to end users, mostly in the form of liquefied natural gas (LNG), requiring refrigeration to liquefy the gas or by chemical conversion (Gas-to-Liquid technology (GTL), both processes being energy intensive. An additional complication to handling methane is fugitive emissions from pipelines and well leaks which significantly contribute to greenhouse gas emissions. Methane is 20-30 times stronger than CO<sub>2</sub> as a greenhouse gas so the impact of methane leaks must be carefully considered by proponents of increased methane fuel use (Tester, Drake *et al.*, 2005).

Supercritical water presents several attractive features for potential use as a methane conversion medium. In addition to possibly exploiting the fluid properties mentioned in Section 1.1 in a potential surface conversion process, the temperature and pressure conditions of many of the earth’s natural gas fields lend themselves to considering in-situ conversion strategies at hydrothermal or supercritical water conditions. Although conditions vary widely, some existing gas fields naturally sustain high pressures and relatively high temperatures. For example, geopressurized gas fields in the Gulf Coast area of the U.S. typically have temperatures ranging from 150 – 300 °C and pressures from 270 – 400 bar (Milora and Tester, 1976). With the addition of heat from a hydrothermal flame or an exothermic oxidation reaction, one could transform fluids contained in deep gas wells or reservoirs into homogeneous supercritical water mixtures ready for *in-situ* methane conversion.



### 1.3.2 Glucose and Glycine as Model Compounds

Glucose was chosen as a model for carbohydrates and glycine was chosen as a model for amino acids which are the building blocks of proteins. Sub-critical water conditions were chosen to more thoroughly investigate the chemical interaction of these compounds with each other and with water of importance to the formation of undesired side products during the hydrothermal processing of biomass feed stocks. Glucose has been the subject of many hydrothermal research studies (a comprehensive list of references on hydrothermal glucose studies is presented in Kruse *et al.*, (2005). Fewer studies have been performed with glycine as a model compound under hydrothermal conditions. A key objective of many earlier glycine studies in hydrothermal media has been to probe its role in “origin of life” related research particularly under the conditions of deep sea vents (50 – 400°C, 150 – 400 bar) (Alargov, Deguchi *et al.*, 2002; Islam, Kaneko *et al.*, 2003). Only one previous study was found which explores the model mixture of glucose and glycine under hydrothermal conditions (Inoue, Noguchi *et al.*, 2004). Therefore, additional research is warranted to investigate these model compounds and their well defined mixtures in order to quantify the range of parameters which affect degradation kinetics, reaction pathways and product distributions.

## 1.4 REFERENCES

- Adams, T. N., B. S. Appel, et al. (2004). "Converting Turkey Offal into Bio-derived Hydrocarbon Oil with the CWT Thermal Process". *Power-Gen Renewable Energy Conference*, Las Vegas, Nevada.
- Akiya, N. and P. E. Savage (2002). "Roles of Water for Chemical Reactions in High-Temperature Water." *Chem. Rev.* **102**: 2725-2750.

- 
- Alargov, D. K., S. Deguchi, et al. (2002). "Reaction Behaviors of Glycine under Super- and Subcritical Water Conditions." *Origins of Life and Evolution of the Biosphere* **32**: 1-12.
- Antal, M. J., Jr.; Allen, S.G.; Schulman, D.; Xu, X.; Divilio, R.J. (2000). "Biomass Gasification in Supercritical Water." *Ind. Eng. Chem. Res.* **39**(11): 4040-4053.
- Baiker, A. (1999). "Supercritical Fluids in Heterogeneous Catalysis." *Chem. Rev.* **99**: 453-473.
- Brock, E. E. and P. E. Savage (1995). "Detailed chemical kinetics model for supercritical water oxidation of C<sub>1</sub> compounds and H<sub>2</sub>." *American Institute of Chemical Engineers Journal* **41**(8): 1874-1888.
- Broll, D. K., C.; Kramer, A.; Krammer, P.; Richter, T.; Jung, M.; Vogel, H.; Zehner, P. (1999). "Chemistry in Supercritical Water." *Angew. Chem. Int. Ed.* **38**: 2998-3014.
- Davda, R. R. and J. A. Dumesic (2003). "Catalytic Reforming of Oxygenated Hydrocarbons for Hydrogen with Low Levels of Carbon Monoxide." *Angew. Chem. Int. Ed.* **42**: 4068-4071.
- Davda, R. R. S., J.W.; Huber, G.W.; Cortright, R.D.; Dumesic, J.A. (2003). "Aqueous-phase reforming of ethylene glycol on silica-supported metal catalysts." *Appl Catal B-Environ* **43**: 13-26.
- DiNaro, J., J. Howard, et al. (2000). "Elementary reaction mechanism for benzene oxidation in supercritical water." *J Phys Chem A* **104**(45): 10576-10586.
- Dinjus, E. K., A. (2004). "Hot compressed water - a suitable and sustainable solvent and reaction medium?" *J. Phys.: Condensed Matter* **16**: 1161-1169.
- Ederer, H. J. K., A.; Mas, C.; Ebert, K.H.; (1999). "Modelling of the pyrolysis of tert-butylbenzene in supercritical water." *J Supercritical Fluids* **15**: 191-204.
- Elliott, D. C., L. J. Sealock, Jr., et al. (1997) "Method for the catalytic conversion of organic materials into a product gas" USA, Patent #5616154.
- Elliott, D. C. and L. J. Sealock, Jr. (1998) "Improved catalyst formulations for use in wet biomass gasification: ruthenium stabilized nickel metal" USA, Patent #5814112.

- 
- Elliott, D. C. and L. J. Sealock, Jr. (1998) "Nickel/ruthenium catalyst and method for aqueous phase reactions" USA, Patent #5814112.
- Elliott, D. C., T. A. Werpy, et al. (2001) "Ruthenium on rutile catalyst, catalytic system, and method for aqueous phase hydrogenations" USA, Patent #6235797.
- Elliott, D. C. N., G.C.; Hart, T.R.; Butner, R.S.; Zacher, A.H.; Engelhard, M.H.; Young, J.S.; McCready, D.E. (2004). "Chemical Processing in High-Pressure Aqueous Environments. 7. Process Development for Catalytic Gasification of Wet Biomass Feedstocks." *Ind. Eng. Chem. Res.* **43**: 1999-2004.
- Fang, Z. and J. A. Kozinski (2001). "A Comparative Study of Polystyrene Decomposition in Supercritical Water and Air Environments Using Diamond Anvil Cell." *Journal of Applied Polymer Science* **81**: 3565-3577.
- Fernandez, D. P. A. R. H. G., E.W. Lemmon, J.M.H. Levelt Sengers, and R.C. Williams (1997). "A Formulation of the Static Permittivity of Water and Steam at Temperatures 238 to 873 K at Pressures up to 1200 MPa, Including Derivatives and Debye-Hückel Coefficients." *J. Phys. Chem. Ref. Data* **26**: 1125.
- Golombeck, M. (2003). MIT-Shell Mini-symposium. R. P. Lachance. Cambridge, MA.
- Helling, R. K. and J. W. Tester (1987). "Oxidation kinetics of carbon monoxide in supercritical water." *Energy Fuels* **1**: 417-726.
- Hirth, T. and E. U. Franck (1993). "Oxidation and Hydrothermolysis of Hydrocarbons in Supercritical Water at High Pressures." *Ber. Bunsenges. Phys. Chem.* **97**(9): 1091-1098.
- Holgate, H. R. and J. W. Tester (1994). "Oxidation of hydrogen and carbon monoxide in sub- and supercritical water: reaction kinetics, pathways, and water-density effects. 2. elementary reaction rate modeling." *J. Phys. Chem.* **98**(3): 810-822.
- Huber, G., R. D. Cortright, et al. (2004). "Renewable Alkanes by Aqueous-Phase Reforming of Biomass-Derived Oxygenates." *Angew. Chem. Int. Ed.* **43**: 1549-1551.
- Huber, G., J. W. Shabaker, et al. (2003). "Raney Ni-Sn catalyst for H<sub>2</sub> production from biomass-derived hydrocarbons." *Science* **300**: 2075-2077.

- Inoue, S., M. Noguchi, et al. (2004). "Organic Compounds Formed by Thermochemical Degradation of Glucose-Glycine Melanoidins Using Hot Compressed Water." *J. of Chemical Engineering of Japan* **37**(7): 915-919.
- Islam, M. N., T. Kaneko, et al. (2003). "Reaction of Amino Acids in a Supercritical Water-Flow Reactor Simulating Submarine Hydrothermal Systems." *Bull. Chem. Soc. Jpn.* **76**: 1171-1178.
- Kremer, M. J. C., K.A.; DiPippo, M.M.; Feng, J.; Chateasuneuf, J.E.; Brennecke, J.F.; (1999). "Laser Flash Photolysis Investigation of the Triplet-Triplet Annihilation of Anthracene in Supercritical Water." *J Phys Chem A* **103**: 6591-6598.
- Kruse, A. and E. Dinjus (2003). "Hydrogen from Methane in Supercritical Water." *Angewandte Che. Int. Ed.* **42**(8): 909-911.
- Kruse, A. E., K.H. (1996). "Chemical reactions in supercritical water - 1. Pyrolysis of tert-butylbenzene." *Ber. Bunsenges. Phys. Chem.* **100**: 80-83.
- Kruse, A. K., A.; Schwarzkopf, V.; Gamard, C.; Henningsen, T. (2005). "Influence of Proteins on the Hydrothermal Gasification and Liquefaction of Biomass. 1. Comparison of Different Feedstocks." *Ind. Eng. Chem. Res.* **44**: 3013-3020.
- Kubo, Y. (2000). "Molecular Dynamics and Self-Diffusion in Supercritical Water." Masters, *Chemical Engineering* MIT, Cambridge, MA
- Laidler, K. J. (1987). Chemical Kinetics. New York, Harper Collins.
- Lawson, J. R. and M. T. Klein (1985). "Influence of water on guaiacol pyrolysis." *Ind. Eng. Chem. Fundam.* **24**: 203-208.
- Marrone, P. A., T. A. Arias, et al. (1998). "Solvation effects on kinetics of methylene chloride reactions in sub and supercritical water: theory, experiment, and ab initio calculations." *J. Phys. Chem. A.* **102**: 7013-7028.
- Marshall, W. L. and E. U. Franck (1981). "Ion product of water substance, 0-1000 °C, 1-10,000 bars. New international formulation and its background." *Journal of Physical Chemistry Reference Data* **10**(2): 295-304.

- 
- Melius, C. F., N. E. Bergan, et al. (1990). "Effects of water on combustion kinetics at high pressure". *Twenty-Third Symposium (International) on Combustion*, Orleans, France.
- Milora, S. L. and J. W. Tester (1976). Geothermal Energy as a Source of Electric Power. Cambridge, MA, MIT Press.
- Rice, S. F. S., R.R.; Aiken, J.D. (1998). "Water Density Effects on Homogeneous Water-Gas Shift Reaction Kinetics." *J. Phys. Chem. A* **102**: 2673-2678.
- Roberts, M., J. Williams, et al. (2004). "Animal Waste to Marketable Products". *Natural Gas Technologies Conference*, Phoenix, Arizona.
- Salvatierra, D., J. D. Taylor, et al. (1999). "Kinetic study of hydrolysis of methylene chloride from 100 to 500 degrees C." *Ind. Eng. Chem. Res.* **38**(11): 4169-4174.
- Savage, P. E., S. Gopalan, et al. (1995). "Reactions at Supercritical Conditions: Applications and Fundamentals." *AICHE J.* **41**(7): 1723-1778.
- Shabaker, J. W., G. Huber, et al. (2004). "Aqueous-phase reforming of oxygenated hydrocarbons over Sn-modified Ni catalysts." *Journal of Catalysis* **222**: 180-191.
- Sinagju, A. K., A.; Schwarzkopf, V. (2003). "Formation and degradation pathways of intermediates formed in the hydrolysis of glucose as a model substance for wet biomass in a tubular reactor." *Chemie Ingenieur Technik* **75**(9): 1351-1355.
- Steeper, R. R., S. F. Rice, et al. (1996). "Kinetics measurements of methane oxidation in supercritical water." *J. Phys. Chem.* **100**(1): 184-9.
- Sullivan, P. A. P., Jason M.; Green, William H.; Tester, Jefferson W. (2004). "Elementary reaction rate model for MPA oxidation in supercritical water." *Physical Chemistry Chemical Physics* **6**(17): 4310-4320.
- Taylor, J. D., F. A. Pacheco, et al. (2002). "Multiscale reaction pathway analysis of methyl tert-butyl ether hydrolysis under hydrothermal conditions." *Ind. Eng. Chem. Res.* **41**(1): 1-8.
- Tester, J. W., E. M. Drake, et al. (2005). Sustainable Energy - Choosign Among Options. Cambridge, MA, MIT.

- 
- Vogel, F. (2005). Discussion of PSI Hydrothermal Research with R. Lachance. Villigen, Switzerland.
- Vogel, F. and Hildebrand, F. (2002). "Catalytic Hydrothermal Gasification of Woody Biomass at High Feed Concentrations." *Chem. Eng. Trans.* **2**: 771.
- Waldner, M. H. and Vogel, Frederic (2004). "Catalytic Hydrothermal Gasification of Woody Biomass". *2nd World Conference on Biomass for Energy, Industry and Climate Protection*, Rome, Italy.
- Watanabe, M. H., H.; Sawamoto, S.; Adschiri, T.; Arai, K. (1998). "Polyethylene conversion in supercritical water." *J. Supercrit. Fluid* **13**: 247-252.
- Watanabe, M. S., T; Inomata, H.; Smith, R.L., Jr; Arai, K.; Kruse, A.; Dinjus, E (2004). "Chemical Reactions of C1 Compounds in Near-Critical and Supercritical Water." *Chem Rev* **104**: 5803-5821.
- Webley, P. A. and J. W. Tester (1991). "Fundamental Kinetics of Methane Oxidation in Supercritical Water." *Energy and Fuels* **5**(3): 411-419.
- Wellig, B. (2003). "Transpiring Wall Reactor for Supercritical Water Oxidation." PhD Thesis, Swiss Federal Institute of Technology Zurich, Zurich
- Xu, X. A., M.J., Jr. (1998). "Gasification of sewage sludge and other biomass for hydrogen production in supercritical water." *Environmental Progress* **17**(4): 215-220.
- Xu, X. M., Yukihiro; Stenberg, Jonny; Antal, Michael Jerry, Jr. (1996). "Carbon-Catalyzed Gasification of Organic Feedstocks in Supercritical Water." *Industrial & Engineering Chemistry Research* **35**(8): 2522-2530.
- Yu, D. e. a. (1993). "Hydrogen Production by Steam Reforming Glucose in Supercritical Water." *Energy and Fuels* **7**: 574-577.

---

## 2 Research Goal, Objectives and Approach

**Overall Goal:** The overall goal of this research is to gain a more thorough understanding of model fuel conversion reactions in sub and supercritical water to support energy related processes in hydrothermal media. To achieve this goal, our research focused on three primary objectives briefly described below. The approach for each objective was built on previous hydrothermal research efforts here at MIT and elsewhere. Both experimental and modeling components were explored in order to quantitatively characterize the fate of three selected model compounds, methane, glycine and glucose, in these complex environments.

**Objective 1: Experimentally Examine Catalyzed Reformation of Methane in Supercritical Water:** Methane is a key by-product, desired or undesired, in the hydrothermal conversion of biomass and other organic feedstocks. However, due to its extremely refractory nature, methane is difficult to further convert under hydrothermal conditions ( $T = 350\text{-}700^\circ\text{C}$ ,  $P = 50 - 500$  bar) without the use of a catalyst. By examining a wide range of pressure/density, temperature, and catalyst conditions, we plan to experimentally determine the most promising conditions to convert methane in SCW. Several high temperature, high pressure reactor systems will be used to provide flexibility for study at a variety of conditions. A detailed analysis of the effects of SCW on several different heterogeneous catalysts used in this study will also be included.

**Objective 2: Examine Partial Oxidation (POX) of Methane in Supercritical Water through Refinement and Analysis of a Detailed Chemical Kinetic Model:** One strategy that has some promise for methane conversion is the selective homogeneous partial oxidation (POX) of methane to methanol in supercritical water ( $T > 374^\circ\text{C}$ ,  $P > 220$  bar). Although previous studies of methane SCW POX have had mixed results, mechanistic

---

understanding is incomplete. We hope to predict SCW conditions that will maximize methanol yields by employing a representative detailed kinetic model for methane SCWO. After refining an existing C1 elementary reaction model, a detailed modeling analysis of the reaction pathways will be implemented to maximize methanol yield and results will be compared with experimental findings reported in the literature.

**Objective 3: Determine kinetics and reaction pathways for a Model Maillard**

**Reaction in Hydrothermal Conditions:** A detailed experimental investigation will be conducted to determine degradation kinetics and possible reaction pathways of a model Maillard Reaction between glucose and glycine under variety of hydrothermal conditions. By systematically varying key parameters including temperature, residence time, pH, and initial concentrations we will define a set of conditions that minimize undesired polymeric by-products.



### **3 Experimental Procedures and Techniques**

In this research, experiments were performed using four different reactor systems; a small-scale plug-flow reactor system (PFR), a continuously-stirred tank reactor system (CSTR) and two different batch reactor designs. The CSTR and PFR were modifications of existing reactor systems in our research group while the batch reactor systems were designed, built and tested during this study. This chapter includes detailed descriptions of each reactor design, issues associated with each design, typical experimental procedures and analytical methods employed.

#### **3.1 DESCRIPTION OF THE SMALL SCALE SCW PFR SYSTEM**

A brief description of our small-scale PFR system follows including comments highlighting modifications made for this study. A diagram of the system as used in the present experiments is shown in Figure 3.1. A complete description of this version of the PFR system can be found in Phenix (1998) and DiNaro (1999).

##### *3.1.1 Feed Preparation and Pressurization Stage*

The PFR system was capable of separately feeding two different types of oxidant and organic feeds. The oxidant feed could be either hydrogen peroxide from a 4 liter high density polyethylene (HDPE) reservoir or dissolved oxygen from a 3 liter high pressure stainless steel saturator cylinder. The organic feed could be either an aqueous organic solution from a 5 liter plastic-coated glass vessel or dissolved gas solution from a 3 liter high pressure stainless steel saturator cylinder. The organic saturator delivery technique was used for all methane PFR experiments.

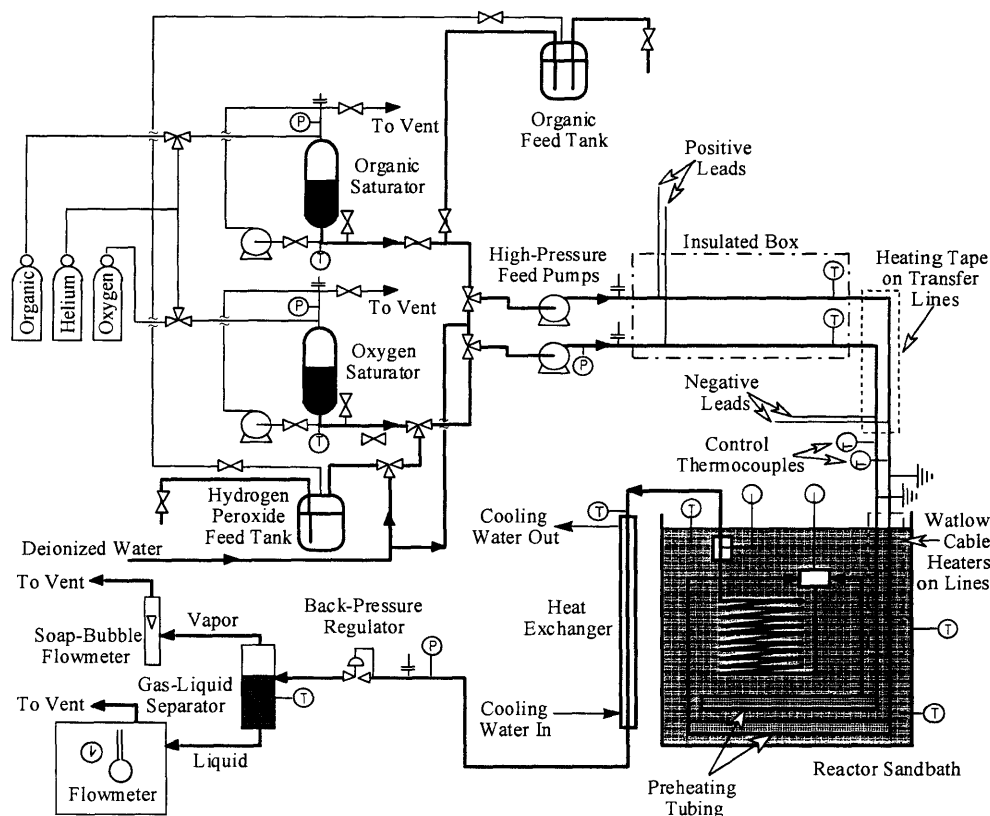


**Figure 3.1 Small-Scale Plug Flow Reactor System.**

A large reservoir was used as a feed tank for holding deionized water. All reactor feed solutions were made with deionized water from a Barnstead Nanopure-A water purification system. After loading the water feed tank, the deionized water was degassed with ~15 psig helium for over 10 minutes to remove most of the residual oxygen from the water. During this study, the system was modified by installing additional tubing so each high pressure saturator could be loaded with degassed, deionized water from the large water feed tank, significantly reducing dissolved oxygen in all feed solutions. The water reservoir was connected by stainless steel tubing to three-way valves that were located before two feed pumps on both the organic and oxidant feed lines. These valves allowed for pump feeds to be switched from water feed, used

during heat-up and cool-down operations, to organic and oxidant solutions once experimental conditions were achieved. The water feed tank also delivered water through the oxidant feed pump during all hydrolysis experiments (reaction of the organic in the absence of oxygen).

To prepare the methane feed solution, approximately 2.5L of deionized, degassed water was first added to the organic saturator. The head space of the saturator was then purged of other gases by filling with ~ 100 psig (~8 bar) methane and venting 10 minutes later; this fill and vent step was repeated three times before loading the saturator to the desired pressure. Once pressurized, the contents of the saturator were recirculated via a positive displacement pump (LDC Analytical, minipump model 2396) over a period of at least 12 hours (usually overnight) until equilibrium was achieved. The pressure of CH<sub>4</sub> needed was back-calculated from the desired aqueous concentration by Henry's Law:

$$\phi_i P_i = x_i K(T, P) \quad (3-1)$$

where  $P_i$  is the partial pressure of methane in the vapor phase (assumed to be pure methane),  $\phi_i$  is the methane fugacity coefficient in the vapor phase,  $x_i$  is the aqueous liquid phase mole fraction of methane,  $T$  is the temperature,  $P$  is the total pressure and  $K(T, P)$  is the Henry's Law constant for methane in H<sub>2</sub>O. Values for  $\phi_i$ , which are not unity due to the high methane pressures required (~150 – 1500 psig) (~11 – 104 bar), were determined using the Peng-Robinson equation of state with parameters for methane taken from (Reid, Prausnitz *et al.*, 1977). Values for  $K$  at ambient temperature were calculated from a correlation from (Rettich, Battino *et al.*, 1982). To correct for high pressure, the following relation was used:

$$\left( \frac{\partial \ln K(T, P)}{\partial P} \right)_T = \frac{\bar{V}_i^\infty}{RT} \quad (3-2)$$

where  $\bar{V}_i^\infty$  is the partial molar volume of methane at infinite dilution and  $R$  is the gas constant.

Integrating Equation 3-2 and referencing to ambient pressure  $P_o$  results in the following equation for  $K$ :

$$K(T_o, P) = K(T_o, P_o) \exp \left[ \frac{\bar{V}_i^\infty}{RT} (P - P_o) \right] \quad (3-3)$$

Values for  $\bar{V}_i^\infty$  for methane in H<sub>2</sub>O were derived from the correlation of (Rettich, Battino *et al.*, 1982). The accuracy of these equations for calculating the gaseous organic feed concentrations has been verified through control experiments conducted during this study and during a previous study using an earlier version of the same PFR system (Webley, 1989).

The oxidant and organic streams were pressurized and fed separately by two high pressure Rainin SD-200 HPLC pumps. Each pump had a maximum pressure of 4600 psig (318 bar) at a maximum flow rate of 25 mL/min. Equipped with pulse-dampening pressure modules, this feed system achieved essentially pulse-less flow confirmed by monitoring the pressure indicators on each pump, an additional pressure gage on the upstream side of the oxidant feed line and the main pressure transducer on the downstream effluent line. Actual flow rates were slightly higher than flow rate settings at each pump. As a result, each pump was calibrated creating calibration curves that are functions of pump setpoint, total system pressure and suction-side pressure. The resulting calibration equations were used to determine flow rate contribution by each separate feed pump in the design of experiments and data analysis. An additional discussion of pump calibration is presented in Section 3.1.6.

### *3.1.2 Preheating System*

The two separate, pressurized feed streams were preheated in a 9.5m long Direct Ohmic Heating (DOH) system described in detail in Phenix (1998). After the DOH system, each feed stream had a small section of tubing (~ 2 ft; ~0.6m) that was actively heated with heat tape and cable heaters to prevent heat loss. Following this small section of tubing, each feed stream passed through an additional 5.2m of coiled preheater tubing in the same fluidized sandbath as the reactor, thus ensuring that the feeds entered the reactor at the desired temperature. All tubing in the preheating system was 1/16" (1.59mm) O.D. HC-276 Hastelloy, chosen for its corrosion resistance properties. This extensive preheating system greatly improved heat transfer to the PFR feed streams compared to earlier designs.

### *3.1.3 Reactor System*

The entire reactor was submerged in a Techne FB-08 fluidized sandbath rated to 700°C. During each experiment, the isothermality of the reactor was evaluated by comparing readings from 5 different thermocouples: one in the reactor mixing cross, one in the reactor exit tee, two measuring the temperature of the fluidized sand at the top and bottom of the sandbath and the sandbath's thermocouple for temperature control. With proper fluidization and preheating, the measured temperatures of all five thermocouples were within 3°C of each other.

Before entering the reactor, the organic and oxidant feed streams were mixed in a specially modified 1/8-in.(3.18mm) HC-276 cross from High Pressure Equipment. To improve mixing, Phenix (1998) had the feed streams enter the cross at 90° from each other and pass through small diameter inserts in the cross, increasing their inlet velocities. The reactor itself was a 1/4" O.D x 0.0067-in. I.D. 4.71m coiled Inconel 625 tubing with an internal volume of

10.71 cm<sup>3</sup>. After the reactor exit tee, a 26-cm length of tubing above the fluidized sand connected the reactor to the heat exchanger. Although this tubing was insulated, it was confirmed to be non-isothermal as evidenced by a 50 to 150°C temperature drop from the reactor to the end of this riser. Since reaction did not occur at appreciable rates in the entire riser, we only included half of its volume in our residence time calculations. The reactor total volume including fittings and half of the riser was taken to be 11.23 cm<sup>3</sup> with a 2-3% uncertainty due to the riser volume assumption.

To ensure plug flow conditions, flow rates in the reactor were always maintained in the turbulent or transition regime (i.e., Reynolds number > 2100). This particular coiled reactor was previously evaluated several times (Webley, 1989; Holgate, 1993; and most recently Phenix, 1998) using the criteria established by Cutler, Antal *et al.* (1988). Based on Phenix's recent evaluation, it was determined that residence times had to be restricted to 2 – 14 seconds to ensure proper fluid dynamics mixing in the reactor.

To conduct catalyst experiments in the plug flow reactor system, a packed bed reactor was constructed similar to the reactor described in Webley (1989) and Holgate (1991) and shown in Figure 3.2. The reactor was a U-shaped Inconel 625 tube, 1.429 cm OD x 0.912 cm ID x 61.67 cm long. The outer diameter of the bend is 10.3 cm. The packing, void fraction and free volume depended on the choice of catalyst, but each type of catalyst was held in place by two, 10µm Hastelloy C276 fritted disks. The pressure drop across the catalyst bed was measured in the PFR system and was not detectable within the sensitivity of our pressure gages. More details are provided on packing and void volume in Chapter 4.

To properly reduce metal catalysts prior to any experiment, the PFR system was modified to allow a hydrogen-helium mixed gaseous feed to flow through one of the feed lines, through

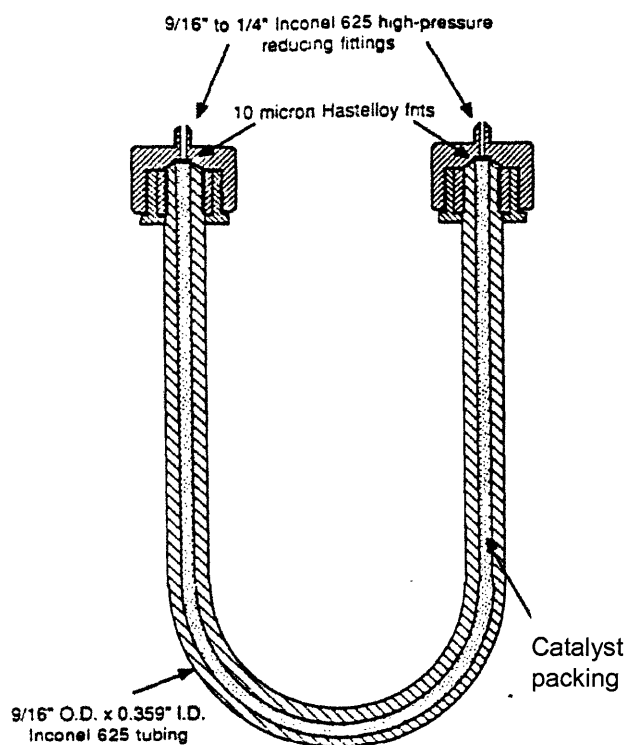


**Figure 3.2 Schematic Cross Section of the Packed Bed Reactor.**

the packed bed at temperature and out the gas effluent line to an exhaust hood. The hydrogen-helium gaseous feed line consisted of tubing from pure  $H_2$  and He cylinders through separate flowmeters (Matheson R7630 series) to manually control flow rates and into a valve connected to the oxidant feed line. To prevent unintentional mixing of a  $H_2$  stream with an oxidant stream, both lines were flushed several times with deionized water and helium and any oxidant feed was removed from the system during these experiments. Prior to any catalyst experiment, this hydrogen-helium mix (nominally 10%  $H_2$  in He) would be fed during system heat-up rather than

water to avoid catalyst deactivation due to the oxidizing environment of SCW. After at least four hours of reducing the catalyst in H<sub>2</sub>, the H<sub>2</sub>-He valve would be closed, the feeds would be switched to methane-water and water streams, the system pressurized, and the experiment would begin after the normal one hour waiting period to achieve steady state conditions.

#### *3.1.4 Letdown System and Sample Collection*

Upon exiting the reactor exit tee and riser section, the reaction effluent is rapidly quenched in a water-cooled, countercurrent shell-and-tube heat exchanger. Downstream of the heat exchanger was a pressure transducer from which the main system pressure was read. This pressure reading was compared to three other pressure readings; one from an upstream pressure gauge on the oxidant line as well as the pressure indicators on each feed pump. Typically, all pressure readings were the same within the accuracy of all instruments, but if significant pressure drops occurred they usually indicated clogged filters, lines or malfunctioning pump heads which were fixed immediately.

After passing through a 7 $\mu$ m in-line filter, the effluent is then reduced to ambient pressure upon passing through a spring-loaded, manual pressure regulator. At this point, the effluent has formed two phases. A glass-bead filled gas-liquid separator splits the vapor and liquid streams. The gaseous effluent exits out of the top of the separator past a septa sampling port, through a soap-bubble flowmeter and into an exhaust hood. The liquid effluent passes through an s-shaped tube from the bottom of the separator and drips into a waste line to a waste jug. Gas flow rates are measured by timing the rise of a soap bubble in this calibrated glass flow meter, while liquid flow rates are measured by observing the time it takes to fill a 25 or 50mL volumetric flask. Gaseous effluent samples were taken with a gas tight 200 $\mu$ l syringe from the



---

septa sampling port above the gas-liquid separator. Liquid samples were simply collected from the liquid line in between flow rate measurements.

### 3.1.5 Reactor Operation and Data Collection

The day prior to every experiment, a saturated methane feed was prepared in the high pressure organic saturator according to the description provided in Section 3.1.1. Each experiment started with system pressurization and heating while flowing deionized degassed water from the main water feed tank. For oxidation experiments, the H<sub>2</sub>O<sub>2</sub> feed solution was prepared while the system was heating. After loading the H<sub>2</sub>O<sub>2</sub> feed vessel, samples were taken for analysis from an on-line valve before the start of the first experiment and again at the end of the day. Once the desired temperature had been reached, the pump flowrates were set to achieve the appropriate residence time, and the pump feeds were switched from the water feed to organic and oxidant feeds. Once this switch-over occurred, one hour was allowed to achieve steady state conditions.

Once steady state was achieved, a typical experiment lasted approximately one hour; one experiment being defined as a session of data collection at a single temperature, pressure, residence time, and initial organic and oxidant feed concentration. During this hour, three to six liquid and gas effluent samples were collected and analyzed. Gas samples were immediately injected onto three different gas chromatography instruments, and liquid samples were loaded into 2 mL vials and placed in an autosampler tray for later analysis. In between sampling sessions, gas and liquid flowrates were measured totaling at least six measurements in an hour-long experiment. With every flowrate measurement, the system pressure was recorded from the pressure transducer and the organic saturator pressure was recorded a Bourdon tube dial gauge. Pump pressures and feed pressures were also recorded at this time to examine system pressure

drop. Temperatures readings from thermocouple measurements were logged to a computer automatically every ten seconds using HOTMUX software from DCC Corporation. After obtaining at least three consistent gas-phase concentrations, the feed pump flow rates were changed to achieve a new residence time condition. An additional hour was allowed to achieve steady state at this new condition. For each set of conditions, the ambient temperature and pressure were also recorded to calculate the Henry's law coefficients required to determine aqueous phase solubility of the gas phase compounds.

### 3.1.6 Reactor system issues

As experiments were performed, several reactor system operating issues were identified that adversely affected the results. Here we present a short discussion of important issues with recommendations for resolving them in future experiments.

- **Negative methane conversions:** In some experiments, methane conversion was calculated to be slightly negative ( $< -5\%$ ) indicating that effluent methane concentrations were measured to be higher than calculated inlet concentrations. A review of data from a previous methane study on an earlier version of the PFR system (Webley 1989) did not reveal a similar issue. There may be several factors which contribute to this issue like accuracy of the saturator pressure gauge which reads initial methane saturator pressure, but our troubleshooting points to erroneous pump calibrations as a major contributing factor. The pumps on the present PFR system are completely different than the pumps used on Webley's PFR system. By recalibrating the newer pumps, we were able to improve our carbon balance agreement, but a more extensive methane balance study is recommended before embarking on the next extensive study using a gaseous reactant feed.

- 
- ***DOH operation:*** Our experiments suffered through several issues with failures of the DOH preheating system. Most of the failures involved water leaks which may have resulted from too much current passing through the DOH tubing and weakening the tube walls. This issue was compounded when a loss of pressure from the leak caused the DOH to overheat and on one occasion, a 40 amp fuse was blown in the power control box. To alleviate this problem, we made sure to attach the DOH leads to 1/16" fittings with more metal mass than the previous technique of trying to connect the leads to the thin-walled tubing. Also, future experimentalists using the PFR system should consider redesigning the power control to the DOH where more careful selection of fuses may prevent serious tube or circuit damage.
  - ***Catalyst deactivation prior to experiment:*** As discussed in Section 3.1.3, the PFR system was altered to reduce the catalyst in the packed bed reactor during heat-up and prior to any experiment by flowing a H<sub>2</sub>-He stream over it. However, the present design could not prevent exposure of the reduced catalyst to hot sub and supercritical water as feed streams were changed over and the system was pressurized. This shortcoming in the current design may have caused significant catalyst deactivation prior to the start of any experiment. To minimize this problem, the PFR system should be further altered in one of two ways:
    - Build a high pressure gaseous feed system that will allow the simultaneous feed of a high concentration reducing gas, keeping the metal catalyst active while the system achieves the proper supercritical water conditions.
    - Allow the simultaneous flow of an appropriate labile feed (e.g., methanol or hexane) that will itself crack or reform, producing sufficient quantities of

hydrogen which should keep the catalyst active during pressurization and heat-up.

Both suggestions should help to keep a catalyst active at the start of a SCW experiment, but care must be taken to properly differentiate products of co-fed reducing streams from products from the reaction of interest.

## **3.2 DESCRIPTION OF SCW CSTR SYSTEM**

To explore longer residence times and a variety of catalyst reducing techniques, this study employed the use of the our Continuous-Stirred Tank Reactor (CSTR) System designed and built by Philip Marrone and described in detail in his doctoral thesis (Marrone, 1998). A brief description of the CSTR is provided in the following sections. A diagram of the system as used in the present experiments is illustrated in Figure 3.3.

### *3.2.1 Feed Preparation and Pressurization Stage*

Similar to the PFR system, the current CSTR system is designed to feed organic and oxidant separately or flow deionized (DI), degassed water through those same feed lines during pressurization and pre-heating. As in the PFR system design, the oxidant feed could be a hydrogen peroxide solution or a saturated oxygen solution, but unlike the PFR system design, the primary method for delivering the pure organic reactant was to feed it directly into the reactor without preheating via a syringe pump (Isco, Model 100DM). However, the syringe pump method would not work for methane delivery due to size and flow control constraints, so we made slight modifications to the CSTR design to accommodate methane as a reactant. Since our primary focus was methane hydrolysis or reformation and not oxidation, we converted the

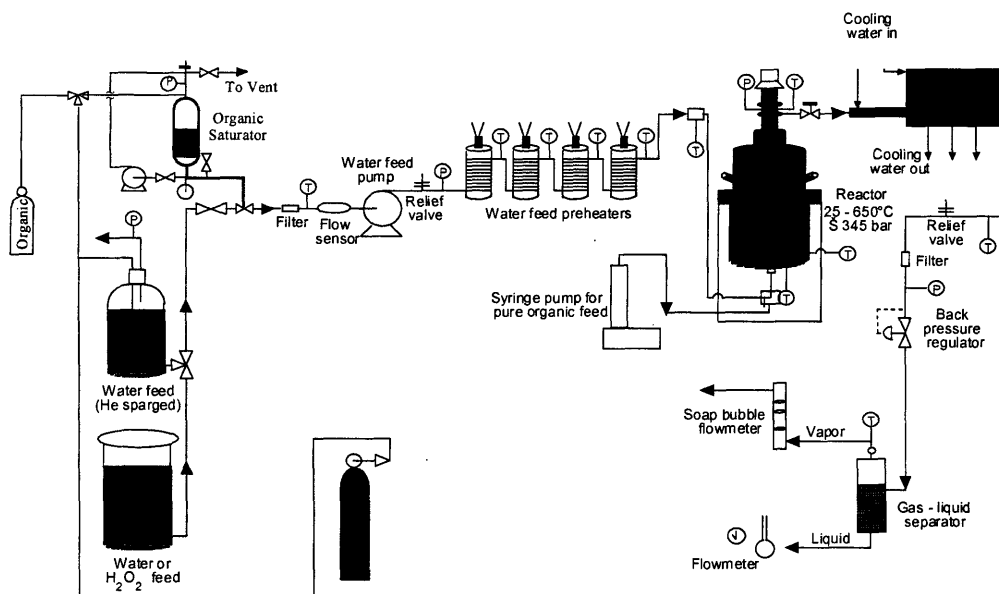


**Figure 3.3 Continuous Stirred Tank Reactor System.**

oxygen saturator to a methane saturator and used the syringe pump to co-feed labile compounds to help reduce the metal catalysts in the reactor. Naturally, these modifications eliminated current oxidant feed methods, but alternate hydrogen peroxide feed designs could be constructed either using the same syringe pump and a separate pre-heating system or through a separate pump and pre-heating system entering the reactor through a separate feed port.

The CSTR methane feed solution was prepared in the same manner as the PFR methane feed solution with minor differences. The organic saturator for the CSTR was a 15 L vessel (Hoke, model 8HD4G) instead of the 2 L saturator used for the PFR and it was filled with 12 L (not 2.5 L) of deionized, degassed water after modifications similar to those made to the PFR were made to the CSTR to fill the saturator from the main water feed tank. The larger saturator was used in the CSTR system to enable longer run times with faster flow rates. The same procedure was followed to fill and vent the saturator headspace three times before loading the

saturator to the desired pressure. The entire contents of the saturator were recirculated overnight using a much larger pump than the PFR recirculation pump (100 mL/min flow versus 10 mL/min flow).

The water or methane-water stream is pressurized and fed by a Rainin Dynamax (model SD-1) HPLC-type pump. It delivers pulseless flow up to a maximum of 200 mL/min and a maximum pressure of 6000 psig (415 bar). Pulseless flow and pressure drop in this system were constantly evaluated by taking pressure readings from four different indicators: the digital pressure indicator on the feed pump, an analog pressure gauge on line just after the feed pump, an analog pressure gauge on the reactor and a pressure transducer on line after the heat exchanger. DI water is typically fed to the system during pre-heating and pressurization and during cool-down operations.

### *3.2.2 Preheating System*

To accommodate the higher flow rates, the CSTR preheating system has a different design than the PFR system. The CSTR preheater section consists of four, 2000 W Watlow Firerod cartridge heaters, each housed in a bored out copper rod, around which is wrapped 6.1 m of 1/8" Hastelloy C-276 tubing. The heaters are wired in parallel and thermocouples after each heater allow monitoring of the fluid temperature increase. After the last firerod preheater, the heated feed passes through an a ~2 m long section of tubing, that is actively heated with heat tape and wrapped with insulation, before it combines with the pure, unheated syringe pump feed in a mixing cross just below the bottom inlet port of the reactor.

### 3.2.3 Reactor System

The reactor itself is an AE Closure Stirred Reactor from Autoclave Engineers, Inc with an approximate working volume of 500 mL. Made of the high nickel alloy, Inconel 625, the reactor is rated to 650°C and 345 bar. The stirring mechanism for the reactor is an AE MagneDrive unit which magnetically drives a solid Inconel 625 shaft upon which is mounted a variety of impellers. For the catalyst experiments in this study, a Hastelloy C276 basket was also mounted on the stirring rod to suspend the catalyst as in a Carberry, gradient-less type of reactor. The basket is about 1.5” in (3.8 cm) diameter and 2” (5.1 cm) long with a “cross-like” design of four rectangular sections. The center portion of each section is covered in a porous 50 x 50 x 0.009 wire mesh to allow access of the fluid to the catalyst particles. The reactor is heated by three, 120 V ceramic band heaters wired in parallel and controlled by the same controller and relay design as the preheaters.

The reactor vessel was custom designed to be as versatile as possible and, accordingly, it has a total of ten access ports which can be arranged in a variety of ways. In Marrone’s original experiments, the pure organic feed entered the reactor through a side port, but a subsequent CFD modeling study of flows in the CSTR suggested this configuration may result in feed by-passing (Zhou, Krishnana *et al.*, 2000). Accordingly, the present configuration has both the syringe pump and HPLC pump feeds combining in a mixing tee and entering the reactor from the center bottom port. Five ports accommodate thermocouples for temperature measurements at different places in the reactor; one in an off-center port in the bottom, three in side ports and one in a thermowell at the top of the reactor. Two other ports at the top of the reactor accommodate the effluent exit and a tube to a rupture disk and a pressure gauge.

### 3.2.4 Letdown System and Sample Collection

Upon exiting the reactor through a top access port, the reaction effluent is first rapidly quenched with a shell and tube heat exchanger then completely cooled to ambient temperature as it passes through 6.1m of coiled tubing submersed in a 64 L stainless steel water cooling tank. From this point on, the remainder of the CSTR system is nearly identical to the PFR system including an in-line filter, pressure transducer, back pressure regulator, and gas-liquid separator complete with gas and liquid sampling ports. The major differences are longer tubing due to geometric constraints and a larger gas-liquid separator due to larger flow rates.

### 3.2.5 Reactor Operation and Data Collection

The major tasks for the PFR reactor operation were the same for the CSTR reactor operation in terms of preparation of the saturator feed the day prior to an experiment, the pressurization and heat-up of the system, time allowed to achieve steady state conditions, and sampling and data collection sequences. A major modification of the CSTR system for this study was the installment of a data acquisition system to more closely monitor a variety of temperature measurements. The new data acquisition system consisted of an Omega Engineering DAS16 A/D board connected to an Omega Engineering PCI-DAS08 computer card installed in a Gateway 2000 P5-60 computer. With the use of Data Logger software installed as Microsoft Excel macros, we were able to simultaneously monitor and record four different preheating temperatures and all five reactor temperatures.

The operating procedure for the CSTR differed from the PFR in the particular steps involving liquid organic feed and mixing. Before starting the flow of the liquid organic feed, the syringe pump was rinsed and flushed with DI water and rinsed and flushed with the liquid



organic feed to remove any residual water, feed and air. The reservoir inside the syringe pump was then pressurized to a value approximately 20 bar higher than the system pressure. The pump was then switched to a constant flow mode, the desired flow rate was entered and the pump was started. At this time, mixing in the CSTR was begun by starting the cooling water to the magnets of the stirrer and setting the rotational speed of the MagneDrive shaft (as measured by the tachometer) to the intended value.

### *3.2.6 CSTR Reactor Design and Operating Issues:*

As with the PFR system, the CSTR system has several issues which lead to less than ideal conditions. Some of those issues are discussed below and possible solutions are presented.

- ***Residence Time Distribution:*** A residence time distribution (RTD) study was never performed on the CSTR system. Although Marrone's early work using the CSTR suggest that well-stirred conditions can be achieved in this reactor (Marrone, 1998), the best way to be sure of this fact is if the signature ideal mixing exponential decay profile is observed in RTD experimental measurements. An RTD analysis is critical for future kinetic studies using the CSTR.
- ***Temperature Gradient at Supercritical Water Conditions:*** With the help of the newly installed temperature data acquisition system, a significant temperature gradient in the reactor itself was identified and examined. As seen in Figure 3.4, the five thermocouples in the reactor media are in fairly good agreement until the temperature rises above the critical temperature (374°C), and the disparity gets worse when the stirring rod begins to stir at 500 rpm. Upon stirring, the bottom temperature rises ~ 10°C higher than the temperature at the 4 o'clock thermocouple and ~ 20°C higher than the other thermocouples, creating a significant gradient where the top of

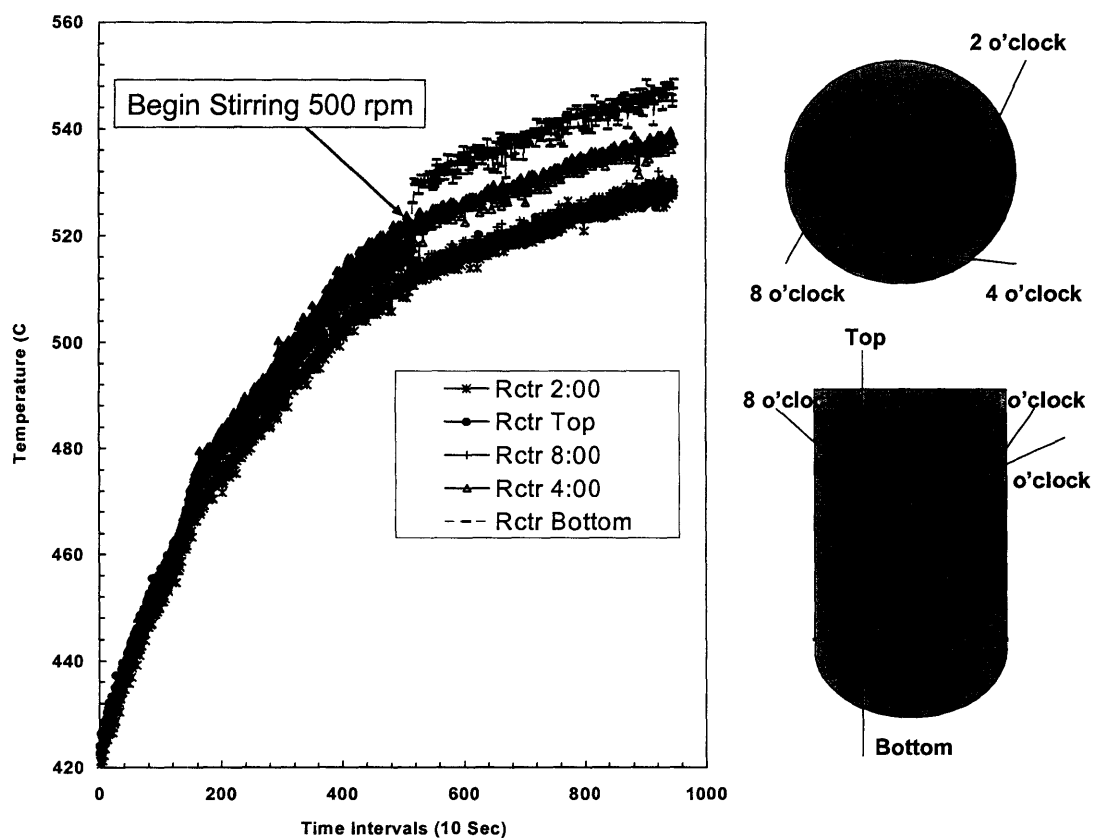


**Figure 3.4 Evidence of Temperature Gradient in the CSTR Reactor during Heatup.**

the reactor is much colder than the bottom. This gradient is most likely the result of the requirement to flow cooling water past the magnets of the MagneDrive unit which is close to the top of the reactor. The gradient is worse as the density of the reacting media becomes less dense in supercritical conditions. Several attempts to alleviate the gradient were explored including improved insulation, additional reactor-top heating with heating tape, additional baffles in the reactor, using different impellers and additional impellers and changing stirring rod speed, but no significant

improvement was achieved. A representative from Autoclave Engineers finally suggested installing more powerful additional cartridge heaters in the main nut at the top of the reactor to actively heat the cooler section. Time did not allow us to follow through with this suggestion, but the next CSTR experimentalist should explore the idea to help alleviate the current non-isothermal conditions at SCW conditions.

- **Potential multi-phase flow conditions:** In the current design, a pure organic feed is delivered by a syringe pump directly into the reactor, which, under most circumstances, immediately turns into a single phase reacting medium. However, the quenched reactor effluent may form multiple liquid and solid phases which are not handled very well in the current CSTR system design. One example of this issue was the complications observed when feeding hexane as a reducing agent during some catalyst experiments. Any unreacted hexane and other insoluble organics caused erratic flow, poor separation, and possible pooling in some dead-volume zones of the reactor system. The current CSTR should be modified to properly separate multiple liquid effluents and reduce possible pooling sites for these multi-phase effluents.

### **3.3 DESCRIPTION OF SCW BATCH REACTOR TUBE SYSTEM**

#### *3.3.1 Detailed Reactor System Description*

To examine higher concentrations and longer residence times, a hydrothermal batch tube system was designed, built and tested during this study. The design was very similar to that found in (Kruse and Dinjus, 2003); the major difference being the use of a fluidized sand bath (Technique 4D) in place of an oven for heating and the testing of different reactor sizes and fittings.

A simplified view of the design is shown in Figure 3.5. The left side of Figure 3.5 depicts the loading and sampling section which supported gas loading and venting before an experiment, vacuum evacuation prior to sampling, and gas sampling after an experiment. The right side of Figure 3.5 depicts the reactor section which allows for pressure measurement via a high pressure transducer and two temperature measurements, one in the reactor tube itself and one above the reactor at a high pressure cross outside of the sandbath during an experiment. Valves and quick disconnect fittings were installed to allow for detachment and lowering of the reactor into the sandbath and detachment of the gas sampling cylinder for ease of sampling by injections into remote gas chromatography instruments. The entire batch tube system was suspended by a UNISTRUT support system built in the same safety enclosure as the CSTR system. This reactor support system included roller attachments which aided the lowering and raising of the reactor into the sandbath and into a water quench bath at the end of each experiment.

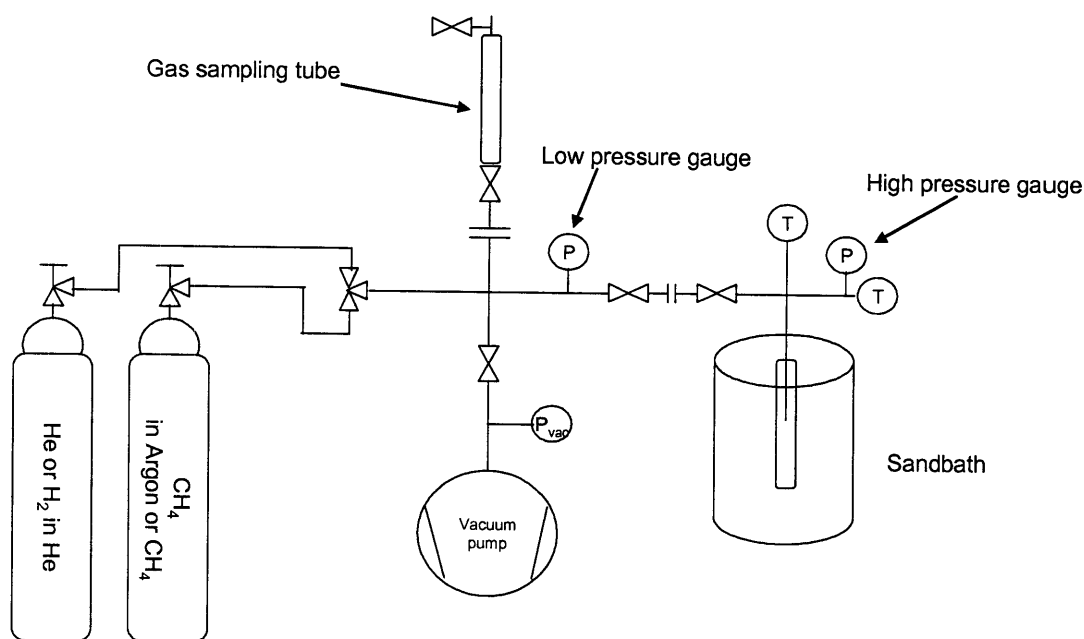


**Figure 3.5 Hydrothermal Batch Tube System.**

Several batch reactors were constructed and tested in this system. The reactors were thick walled SS316, Hastelloy or Inconel tubes with outer diameters ranging from 1/4" to 3/4". The height of each reactor was constrained by the minimum working depth of the sand bath (~5"). The bottom of each reactor was a Swagelok type end-cap compression fitting. Attempts were made to use Swagelok fittings for the top reactor fittings, but they were quick to fail after repeated openings. High Pressure Equipment (HIP) type coned-and-threaded reducing union fittings were more reliable under these severe conditions of temperature cycling at high pressure in fine fluidized sand.

### *3.3.2 Reactor Operation and Data Collection*

A typical experimental procedure for the tube batch system began with reducing the loaded catalyst. After loading a desired weight of catalyst into the tube batch cell, the reactor was sealed, repeatedly filled and vented with 10% H<sub>2</sub> in He, loaded to approximately 60 psig with the H<sub>2</sub>-He mix and lowered into a preheated sandbath. The catalyst was reduced at the desired reaction temperature (typically 600°C) for at least 2 hours and then quenched in the water quench tank. The reactor was then opened and charged with a measured amount of deionized, degassed water that would result in the desired supercritical pressure upon constant volume heating. The reactor system was then repeatedly loaded and vented with pure methane or a 10% methane in argon mix (argon was used as an inert gas to more accurately determine moles of loaded and sampled gas phases). After at least three iterations of loading and venting feed gas, the reactor was loaded with the reactant gas to a specified pressure, measured with a low pressure transducer (Omega PX203-300A5V connected to Omega digital meter DP25B-E). The reactor was then removed from the loading system and lowered into the preheated sand bath.

Four temperature measurements were continuously monitored during each reaction; one thermocouple was in the sandbath thermowell, one thermocouple was in the fluidized sand at approximately half-depth, one thermocouple was placed inside the reactor at approximately half depth and one thermocouple was inside a high pressure cross above the level of the sand. All thermocouples were read with the same data acquisition system used for CSTR temperature measurements. A plot of typical reactor temperature profile during heatup and quench is displayed in Figure 3.6. Due to a variety of issues like leaks and reactor replacements, thermocouple positions were altered for a few experiments, but a similar reactor temperature profile could be expected since virtually the same procedure was followed for each tube batch experiment.

After the reactor system was quenched sufficiently, it was reattached to the sampling/loading system which was then evacuated with a Welch Duoseal vacuum pump. Once the sampling cylinder was sufficient evacuated ( $\sim 250$  mtorr based on a vacuum gauge reading), the reactor system valve was opened and the product gas phase was allowed to equilibrate in the entire system for approximately five minutes. The sampling system pressure was then recorded with the low pressure transducer, and the cylinder was then detached and brought over to the gas chromatography instruments for sampling by repeated syringe injections.

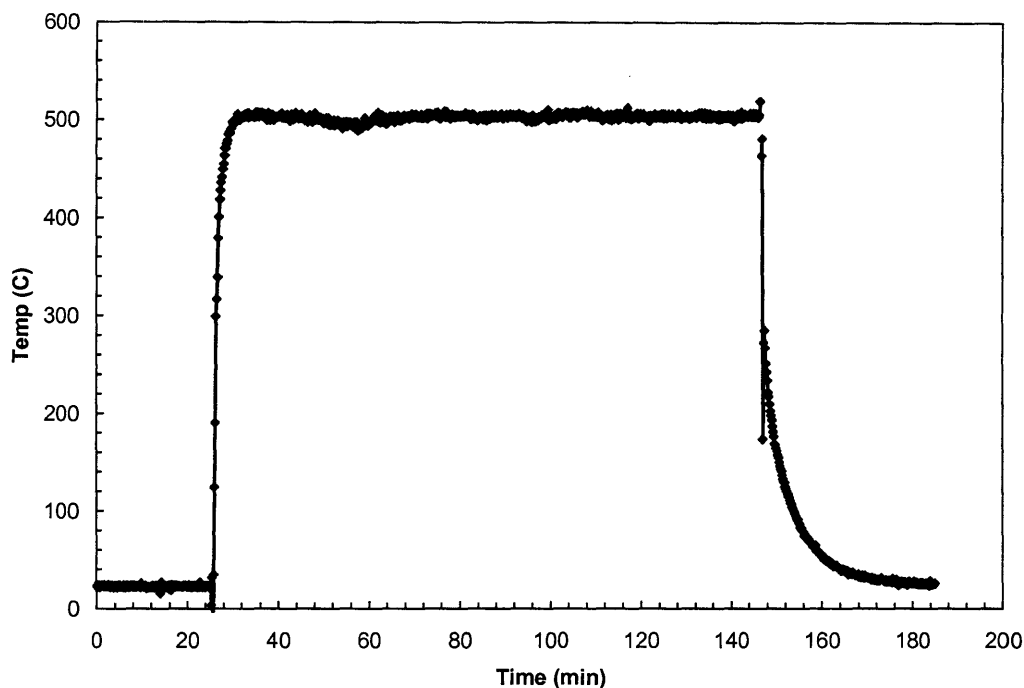


**Figure 3.6 Typical Tube Batch Reactor Temperature profile during Heatup and Quench.**

### 3.3.3 Tube Batch Reactor Design and Operating Issues:

Although useful as an apparatus to quickly screen various catalysts in the presence of SCW and gaseous reactants, the current design of this tube batch system had several shortcomings which limited the usefulness of the data. Some of those issues are discussed below.

- **Unheated Reactor Dead Volume:** As Kruse and Dinjus (2003) admitted, this particular design must include a significant amount of volume in the reactor system tubing and fittings above the level of the sand in the bath to allow for gas loading and sampling and pressure measurements. An attempt was made to make this “cold” volume small relative to the “hot” reactor volume, but dead volume areas like the

---

well in the pressure transducer still contributed a significant “cold” volume. For example, in one design arrangement, the cold volume was measured to be  $3.90 \pm 0.02$  mL while the hot reactor volume was measured to be  $9.16 \pm 0.03$  mL. In this cold volume it is difficult to determine the actual temperature and phase behavior during the reaction. Below the critical temperature of the mixture, methane and certainly a methane-argon mixture will form a second, dense gas phase above the hot supercritical phase complicating mass transfer between phases and concentration calculations (Shmonov, Sadus *et al.*, 1993)). This considerable unreacted gas volume significantly dilutes product gases, and severely effects the accuracy of any results. For some experiments, a high temperature valve was installed just above the reactor and closed during the experiment thereby eliminating most of the cold volume. However, installation of this valve presents other issues like the inability to measure reactor pressure during the experiment and a smaller product gas that must expand to fill the larger loading and sampling volume.

- **Failure of high pressure fittings:** The set of tube batch experiments were plagued by leaks due to failure of both compression and coned-and-threaded fittings. It is reasonable to expect such problems due to the harsh, shock-like conditions these fittings experienced due to rapid temperature and pressure cycling with the presence of small particles of fluidized sand complicating fitting threads and seals. Swagelok compression fittings failed more frequently than HIP coned-and-threaded fittings, but typically, Swagelok fittings could not be repaired while HIP fittings were usually repaired by sanding smooth the seal area between the coned tube and the tapered female fitting. It was the failure of a Swagelok compression fitting while at high



temperature and pressure that convinced us to design and build a different type of batch reactor system. Careful selection of HIP-only fittings and less severe temperature and pressure cycling may reduce failures, but the advantages and disadvantages of this batch tube design should be weighed against other designs like the one described in Section 3.4 before one embarks on major modifications.

In addition to the issues mentioned above, batch reactors are inherently poor choices for kinetic studies with heterogeneous catalysts mostly due to their unsteady state nature (Delannay, 1984). Nevertheless, this simple design did facilitate meaningful screening studies, narrowing our focus in identifying the best catalyst candidate.

### **3.4 DESCRIPTION OF SUB AND SCW BATCH DIRECT INJECT SYSTEM**

To address some of the problems with the tube batch system, a new direct-inject batch system was designed, built, tested and employed as part of this study. The design was based on similar heat-up, injection and quenching principles as a recent design in our lab (Taylor, Steinfeld *et al.*, 2001), but major modifications had to be made to accommodate gaseous feeds, catalyst loading and reducing, and proper sampling of gases. Figure 3.7 is an illustration of the system and a brief description follows.

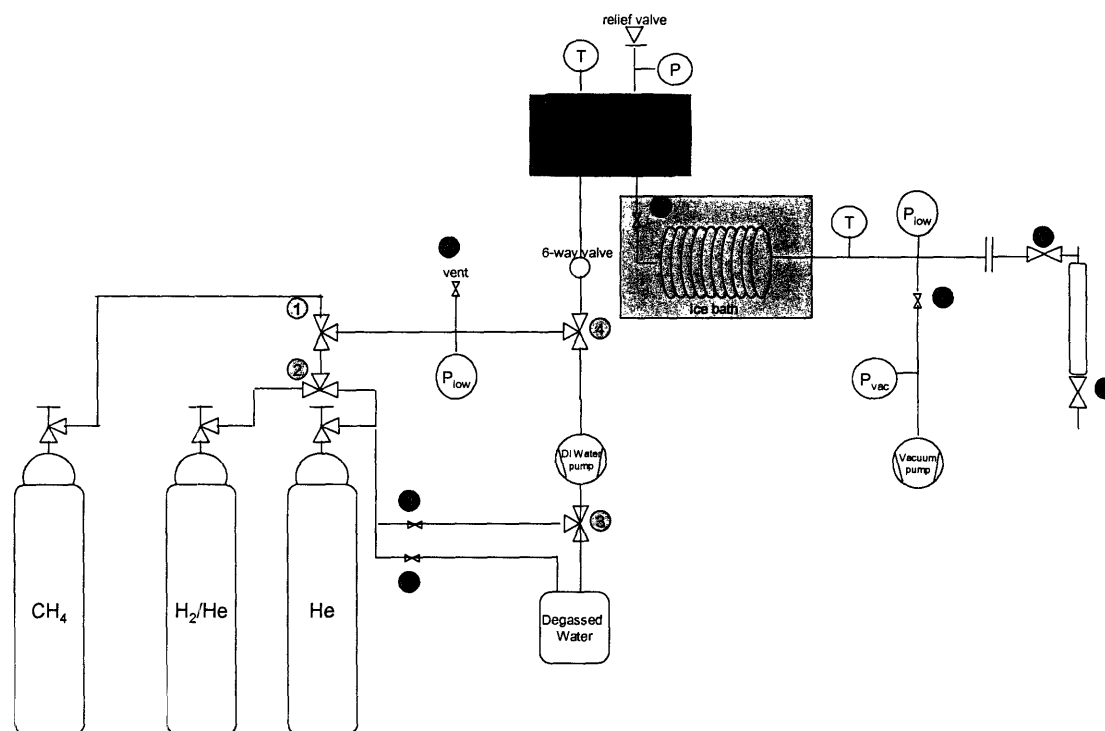


**Figure 3.7 Sub and Supercritical Water Direct Injection Batch system**

### *3.4.1 Feed Preparation and Injection*

The water used for this reactor was deionized water from the lab's Barnstead Nanopure-A system that was further degassed by boiling over a hot plate for at least one hour. A small helium head pressure was then applied to the water feed tank which forced the water through tubing coiled in an ice bath into the inlet of an Eldex, single piston, high pressure metering pump (Model #B-100-S). The pump was always set for the largest piston stroke which corresponded to a flowrate of approximately 7.5 mL/min against a system pressure of 3500 psig (242 bar). Additional feed lines and valves leading up to the reactor provided the flexibility to purge the

lines and the reactor with pure helium, reduce the catalyst in place with a H<sub>2</sub>/He mix or feed pure CH<sub>4</sub> or a CH<sub>4</sub>/Ar mix to the reactor or sample loop. Valves also allowed gas lines to be vented and prevented the reaction media from back-flowing to the pump or feed lines.

The ability to direct-inject a reactant was provided by a 6 port, two-position Valco valve (P/N C6UW) installed immediately upstream from the reactor. With this valve in the “load” position, reactant could be loaded into a sample loop of precise volume while the water feed passed directly through to the reactor. When the two position valve was switched to the “inject” position, the water feed was redirected through the sample loop to push its contents into the main reactor vessel. A 100 μL sample loop was used to inject alkali salt solution for experiments without metal catalysts, and a 5 mL sample loop was used to inject compressed methane or methane-argon mixtures for metal catalyst experiments. The procedure to direct-inject a gas involved loading the 5 mL sample loop with a specific pressure of gas (measured by a low pressure transducer (Omega PX203-300A5V)), then compressing that gas with deionized, degassed water from an HIP pressure generator (P/N 37-6-30) to a pressure greater than 2000 psig (139 bar) to reduce large pressure fluctuations that would occur upon injection and to ensure all the gas was displaced into the reactor.

### 3.4.2 Batch Reactors, Measurements, and Controls

Two different main reactor vessels were employed in our direct-inject batch system; one small internal volume cell (~ 8 mL) to accommodate small samples of donated catalysts and one larger volume cell (~ 13 mL) for the alkali salt studies. The small internal volume cell was constructed out of an HIP 316SS medium pressure cross (P/N# 21-LF9) with reducing union fittings to attach small inner diameter 1/16” stainless steel tubing for inlet and outlet lines.

Figure 3.8 is a schematic of this batch cell. Small amounts of catalyst were held in the center of

this cross with three 10  $\mu\text{m}$  Hastelloy frits at the bottoms of the inlet, outlet and pressure line fittings, leaving the fourth fitting open to allow a 1/16" (1.59 mm) Inconel sheathed Type K thermocouple to measure temperature (T) in the center of the cross. The pressure line fitting was connected to a Dynisco Pressure Transducer (P/N G832-000-7.5M) capable of reading pressures up to 7500 psig (518 bar) and to a pressure relief valve (Nupro P/N SS-4R3A-F).

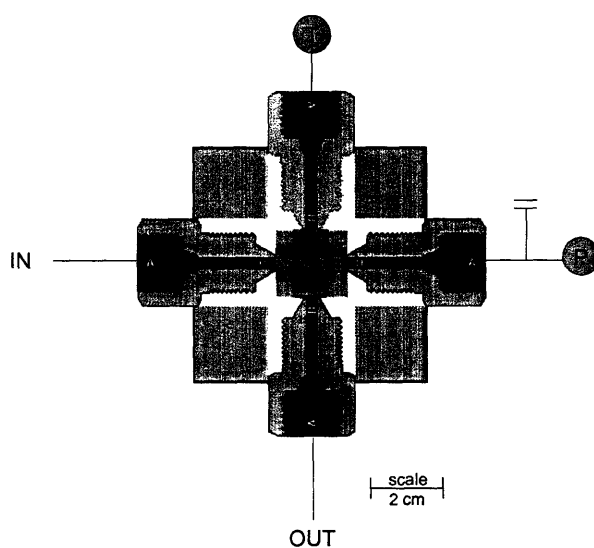


**Figure 3.8 Medium Pressure Cross Batch Cell for Catalyst Studies**

As shown in Figure 3.9, the larger volume batch reactor was constructed out of two HIP Hastelloy C-276 medium pressure tees (P/N 20-23LF9) on either end of a Hastelloy C-276 coned and threaded nipple (P/N 20-LM9-4) with reducing union fittings to attach 1/16" (1.59 mm) tubing for inlet and outlet lines. As in the smaller volume batch cell, a Type K thermocouple was installed with its tip in the center of the nipple to record reaction temperature and the small pressure transducer was connected to the pressure fitting. Both reactors were fairly easily removed and reconnected to the inlet and outlet lines of the reactor system.

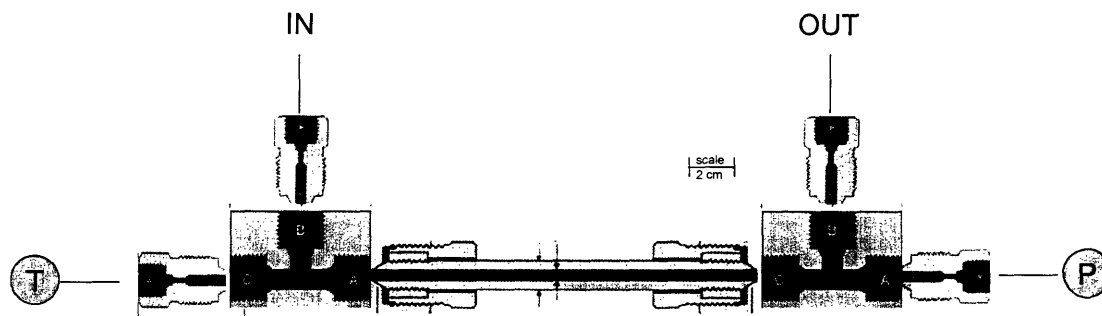


**Figure 3.9** Medium Pressure Batch Cell for Alkali Salt Studies

Both reactors were heated by six strip heaters (Omega P/N NSA\_711) with a maximum power output of 125 W each at 110 VAC. The strip heaters were placed evenly around each reactor and held in place by two metal straps. For the cross batch cell, three strip heaters were placed evenly on the large flat surface on top and three evenly spaced on the large flat surface on the bottom. For the larger cell, three strip heaters were placed on one tee (2 on top and 1 on the bottom) and three were placed on the other tee (1 on top and 2 on the bottom). Each reactor was then carefully surrounded by at least two layers of insulation to minimize heat loss. An Omega PID controller (P/N CN9000A) controlled the temperature based on the thermocouple measurement. The controller output was converted to on/off control by a solid state relay (Omega P/N SSR240DC45). The voltage to the strip heaters was then reduced manually using a potentiometer (Cole-Parmer P/N P-02604-00), typically set at 40% of maximum power output for our supercritical experiments.

### 3.4.3 *Post-Reactor Quench and Sample Collection*

A high temperature HIP valve (P/N 15-11AF1 with grafoil packing) was placed in an ice-water bath immediately after the reactor. Following this valve was a coil of 1/16" (1.59 mm)

stainless steel tubing (~3 feet (~1 m) long) placed in the ice-water bath to serve as a heat exchanger, rapidly quenching the reactor contents when the outlet valve was opened. Complete recovery of low pressure product gases was found to be difficult with this small ID tubing as a quench, so a crude cold trap consisting of an HIP cross oriented vertically replaced the coiled tube in the ice-water bath. This trap allowed water to condense in the larger volume of the cross and enabling the downstream tubing to pass product gases to the sample cylinder. The temperature of the quenched reactor effluent was monitored downstream of the ice-water bath for both heat exchange designs and it never exceeded 27°C. The sample collection system was virtually the same as the sample collection system for the tube batch design. It consisted of a second low pressure transducer to measure the pressure of the product gases, a vacuum pump with vacuum gauge to evacuate the lines prior to sample collection and a high pressure sample cylinder attached with a quick disconnect and outfitted with valves and a septa sampling port.

#### 3.4.4 Reactor Operation

Each experimental day began with degassing deionized water by boiling it and then purging reactor system lines with degassed and deionized water to remove air and other possible contaminants. For metal catalyst experiments, the catalyst was weighed, loaded and the reactor pressure-tested the day prior to an experiment. Once the lines were purged, the reactor was heated in increments of 200°C until the desired temperature (normally 600°C) was reached. During heating any loaded metal catalyst was reduced by a low flow of a 10% H<sub>2</sub>/He mix and continued to be reduced for approximately 2 hours longer at reaction temperature. For experiments without metal catalyst, the reactor was filled with a small amount of argon to reduce contamination and improve the behavior of controlled heating.

The two different sets of experiments, metal catalysts and alkali salt, followed different procedures once the reactor was at the desired temperature. For the metal catalyst experiments, the reactant gas was loaded into the 5 mL sample loop in the 6 port valve, its pressure was measured, then the gas was compressed in the sample loop with the pressure generator to a pressure greater than 2000 psig (139 bar). Prior to any injection, the reactor was purged of all hydrogen reducing gas by loading, venting and flowing pure helium. The reactor was then loaded with ~300 psig (27 bar) of a helium bath gas to provide sufficient pressure for product gas capturing after quenching. The injection sequence began by pumping several “clicks” or piston strokes of water to approximately half the desired pressure, then the two position valve was switched to “inject” directing the water feed through the sample loop displacing the reactant gas into the reactor until the desired pressure is reached. Immediately after injection, the two-position valve was switched back to “load” and the inlet feed valve was closed.

For the alkali salt experiments, the reactant gas was loaded into the heated reactor just prior to injection of water and salt solution. The reactant gas initial pressure was recorded and the injection sequence began immediately. First, purified water was pumped into the reactor to approximately half the desired pressure. Then, the two position valve was switched from “load” to “inject” to water was further pumped to displace a previously loaded salt solution from a 100  $\mu$ L sample loop until the desired pressure was reached. For all experiments, pressures and temperatures were recorded using Natural Instruments Virtual Bench data acquisition software through a National Instruments BNC panel. A plot of typical reactor temperature profile during injection and quench is displayed in Figure 3.10. Notice that the reactor temperature initially drops significantly ( $\sim 150^{\circ}\text{C}$ ) upon injection of room temperature water, but returns fairly rapidly (within  $\sim 1$  minute) to the original target temperature.

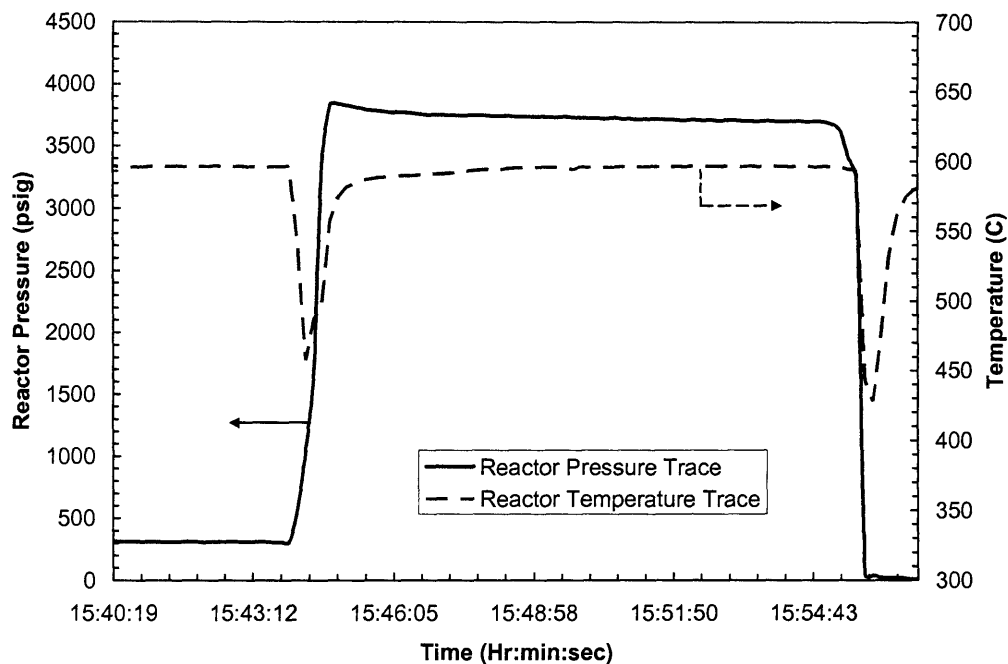


**Figure 3.10 Reactor Temperature and Pressure Traces for the Medium Pressure Cross Batch Cell for Catalyst Studies**

Experimental sampling was essentially the same for both sets of experiments. Prior to reaching the desired residence time, the sample system was evacuated by a vacuum pump for at least ten minutes. After reaching the desired residence time, the high temperature outlet valve was opened, allowing the contents of the reactor to expand and quench, eventually filling the entire sampling system. In a few cases where product gas pressure was low, a small amount of helium was flowed through the reactor and quench lines in an attempt to recover more product. The sampling system was allowed to equilibrate for at least five minutes, then the sample pressure was recorded by a second low pressure transducer and the sample cylinder was detached



and brought over to the GCs for gas analysis. For those experiments where we collected a measurable amount of liquid product at the bottom of the sample cylinder, the pH of that product was determined with pH strips. In the alkali salt experiments, the liquid sample in the cold trap was weighed, pH was determined to within 0.3 pH units with pH color strips, and collected in a small sample vial for further analysis. Metal catalyst experiments consumed an entire day with time required to reduce the catalyst, but two alkali salt experiments were performed each day, with the reactor being flushed with purified water and argon in between each experiment.

#### *3.4.5 Direct Inject Batch Reactor Design and Operational Issues:*

The direct inject batch reactor system appears to be an improvement over the tube batch reactor system, but it is not without some shortcomings. Some of those issues are discussed below.

- ***Failure of high pressure fittings:*** Although not as catastrophic as the tube batch reactor failures, the reactors made from HIP fittings also suffered from leaks. Leaks were mostly found after 1/16" (1.59 mm) compression fittings but occasionally the larger 9/16" (14.28 mm) fittings would leak through weep holes in the cross or tee. Failure of 1/16" (1.59 mm) fittings were difficult to repair by retightening, but failed 9/16" (14.28 mm) fittings were easily repaired by re-tightening or removing, sanding the sealing surface and re-tightening. A few SS316 fittings also seized in the crosses used, but the use of an anti-seize compound (Swagelok Silver Goop) eliminated that problem. Leaks associated with failed fittings were most likely caused by severe temperature and pressure cycling upon injection of cold water into the hot reactor or upon quenching by rapid expansion.

Although it would be difficult to avoid some degree of cycling to achieve well-defined

conditions, compression fittings should be avoided in problem areas like inlet and outlet fittings and in some cases welding the smaller fittings in place should be considered.

- ***Incomplete recovery of the gas effluent:*** Particularly during metal catalyst experiments with the smaller volume batch cell, complete recovery of the gas effluent was difficult. At times, the failure to recover all the gas could be traced to possible leaks in the system, but even with controlled tests under hot conditions, it was difficult to recover all of an inert gas like argon. Cold tests were generally successful, and detailed troubleshooting eliminated possible issues like pressure drop across catalyst beds and leaks past the outlet and vacuum valves. Control tests pointed to two possible major contributors to low gas recovery: small, difficult-to-detect leaks past the pressure relief valve and improper condensing and gas-liquid separation of the reactor effluent during quenching. After removing the pressure relief valve and installed a crude cold trap to collect condensed water, recovery of gas products vastly improved. Nevertheless, a more detailed series of tests should be performed to optimize the gas sampling procedure.

### **3.5 ANALYTICAL METHODS AND ANALYSIS**

Product analysis and data analysis were performed using methods similar to those of previous studies (Sullivan, 2003; Dinero, 1998; Phenix, 1998). A general discussion of product and data analysis is presented below while analysis unique to a particular study, like the product identification procedures for the Model Maillard reaction study, are presented in the chapter presenting the results of that study.

### 3.5.1 Feed & Product Analysis

Proven analytical procedures previously developed in our lab were employed for all gas phase and liquid phase products.

- **Liquid Phase Analysis:** Gas chromatography (GC) with flame ionization detection (FID) was used to identify and quantify liquid reactants and products. Methanol was analyzed using helium as the carrier gas on a 30m x 530  $\mu\text{m}$  x 1  $\mu\text{m}$  DB-WAX column (J & W Scientific) on an HP 6890 GC. Hexane, hexene and their degradation products were analyzed using a helium carrier gas on a 30m x 530  $\mu\text{m}$  x 5  $\mu\text{m}$  DB-1 column (J & W Scientific) on an HP5890 GC. Both GCs were equipped with autosamplers, used splitless injections and each column was preceded by 5 m of a Restek Hydroguard retention column to handle aqueous samples.
- **Hydrogen Peroxide Analysis:** Aqueous hydrogen peroxide concentrations were measured by a ceric ion titration method found in the users manual for the Hach Digital Titrator (Model # 16900-01). During this titration, a  $\text{H}_2\text{O}_2$  sample is titrated with tetravalent cerium ion, a strong oxidant, in the presence of a ferroin indicator. After the  $\text{H}_2\text{O}_2$  is completely oxidized, the cerium ion then oxidizes the indicator, causing a color change from bright orange to light blue. The concentration of  $\text{H}_2\text{O}_2$  is proportional to the amount of the cerium titrant used. On the day of an oxidation experiment, this titration was performed in triplicate on before and after samples of the hydrogen peroxide feed solution. These six measurements determined the average  $\text{H}_2\text{O}_2$  concentration and its standard deviation from which the  $\text{O}_2$  concentration and standard deviation was calculated for that experiment.

- **Gas Phase Analysis:** To analyze the gas effluent, four separate GCs were employed. For the light gases, such as O<sub>2</sub>, N<sub>2</sub>, CO, CO<sub>2</sub>, and CH<sub>4</sub>, an HP 6890 GC was used with a thermal conductivity detector (TCD) and helium as the carrier gas. Two columns were used in series with an air-actuated switching valve in order to separate all of the analytes well. The first column was a 60/80 mesh Carboxen 100 column which separated the carbon containing gases. The follow-on column was the 60/80 mesh Molsieve 5A column which separated the O<sub>2</sub> and N<sub>2</sub>. A second GC was used to analyze light hydrocarbons in the gas phase, such as methane and ethylene. This method employed a 5890 GC equipped with an FID detector and helium carrier gas. The column used was a bonded PLOT column developed by Astec that can separate hydrocarbons up to C-10. Hydrogen and helium gases were separated and quantified using a third instrument, another HP 5890 series GC with a TCD detector. This GC uses the same column phases as the light gas HP 5890 GC with TCD detector, but nitrogen is used as the carrier gas to allow for analysis of helium and hydrogen. Previous researchers developed all three GC methods, but modifications had to be made to accommodate the higher concentrations of hydrocarbon gases and improve separations. A new, fourth GC method was developed to analyze for argon. Argon is difficult to separate from oxygen in most GC columns and methods, so a specially designed column was employed, an Alltech CTR 3 concentric two-packing column (P/N # 8725), using a helium carrier gas and a TCD on a third HP 5890 GC.

### 3.5.2 Data and Error Analysis

Although reliable kinetic parameters could not be derived from experiments in this study, the recorded experimental and analytical measurements were still used to analyze the resulting

changes in global conversions and product spectra when experimental conditions were changed. A detailed discussion of the approach used for data and error analysis calculations in this thesis was reported earlier by Sullivan (2003), thus only a brief summary is provided below.

In general, a variety of measurements were periodically recorded during every experiment in an elaborate Microsoft Excel spreadsheet developed to specifically for data analysis of our plug flow system. Those measurements included reactor temperature and pressure, ambient temperature and pressure, batch reactor holding times, vapor and liquid flowrates for flow reactors and gas loading and sampling pressures for batch reactors. Using the analytical chemistry methods described earlier, ambient feed and product concentrations were determined. Concentrations at reactor conditions were derived from these measured parameters and conversion, product yield, and carbon balance could also be determined. Uncertainties were calculated and propagated by assuming the errors on the measured values were independent and random and using the differential method. Reproducibility errors of each instrument and the precision error from multiple measurements of each parameter were used to determine the uncertainties of all measured quantities. These are discussed below:

- **Reactor Concentrations:** For the flow reactors, reactor concentration calculations required values for ambient concentrations, ambient volumetric flow rates, and ambient and hydrothermal water densities respectively ( $\rho_{amb}$ ,  $\rho_{scw}$ ) calculated at *in situ* conditions from the NIST property correlation for water (Haar, Gallagher *et al.*, 1984). Generic equations for reactor concentration calculations are given in Equation (3-4) for initial concentrations in the PFR,  $[X]_{o,scw}$ , and in Equation (3-5) for effluent concentrations,  $[X]_{scw}$ :

$$[X]_{o,SCW} = \frac{[X]_{o,amb} F_X \rho_{scw}}{F_{total} \rho_{amb}} \quad (3-4)$$

$$[X]_{SCW} = \frac{[X]_{amb} \rho_{scw}}{\rho_{amb}} \quad (3-5)$$

where  $F_{total}$  is a measured effluent volumetric flow rate while  $F_X$  is a feed species flowrate determined by pump calibration in the case of methane or by subtracting the methane flow rate from the total flowrate in the case of the oxidant. To calculate ambient concentrations for effluent gas-phase species, it is assumed that some of the gas is dissolved in the liquid phase in accordance with Henry's Law:

$$y_i \hat{\phi}_i(T, P, y_i) P = x_i K_{i, H_2O}(T, P) \quad (3-6)$$

where  $y_i$  is the gas-phase mole fraction of species  $i$ ,  $\hat{\phi}_i$  is the gas-phase fugacity coefficient (assumed to be one at ambient conditions),  $P$  is the pressure,  $x_i$  is the liquid-phase mole fraction and  $K$  is the Henry's Law coefficient for species  $i$  in water. Correlations for Henry's Law constants were taken from the literature and Sullivan (2003) lists all sources. The overall equation to calculate ambient concentrations of gaseous species is:

$$[X]_{amb} = \frac{(x_X F_L \rho_{L,amb} + y_X F_V \rho_{V,amb})}{F_L} \quad (3-7)$$

where  $\rho_{L,amb}$  and  $\rho_{V,amb}$  are ambient molar densities with the value for the vapor phase coming from the ideal gas equation.

- **Residence Time:** For the batch reactors, residence time was simply taken to be the batch holding time measured after the brief heat-up time and before quenching began (see Figures 3-6 and 3-10 for typical heat and quench profiles). The determination of residence time in the flow reactors had to include adjustments due to the less dense supercritical water environment. In this case, the reactor residence time was calculated

by dividing the reactor volume ( $V_{ctr}$ ) by the ambient volumetric flow rate,  $F_L$ , and multiplying by a ratio of SCW to ambient densities.

$$\tau = \frac{V_{ctr} \rho_{SCW}}{F_L \rho_{amb}} \quad (3-8)$$

- **Key Reaction Parameters:** Standard reaction parameters were calculated in accordance with the following equations:

- Conversion: 
$$X = \frac{[Methane]_o - [Methane]}{[Methane]_o} \times 100\%$$

- Product Yield: 
$$Y = \frac{[product]}{[Methane]_o} \times 100\%$$

- Carbon Balance: 
$$C_{bal} = \frac{[moles\ carbon\ in\ effluent]}{[Methane]_o} \times 100\%$$

Carbon balance was a particularly useful indicator as to the quality of the experimental data. Poor or inconsistent carbon balance results typically indicated that there may have been problems with reactor operations, analytical instruments and/or the presence of undetected products.

- **Confidence Intervals and Uncertainties:** Where possible, all calculated parameter values are reported with 95% or 99% confidence intervals. These confidence intervals were derived from uncertainty determinations for all measured parameters which are then propagated using differential techniques. Both precision error and reproducibility error were considered in determining parameter uncertainty. For those values calculated from calibrations, such as species effluent concentrations, the uncertainties in the calibration parameters were also included in the error propagation calculations.

---

### 3.6 REFERENCES

- Cutler, A. H., M. J. J. Antal, et al. (1988). "A critical evaluation of the plug-flow idealization of tubular-flow reactor data." *Ind. Eng. Chem. Res.* **27**(4): 691-697.
- Delannay, F., Ed. (1984). Characterization of Heterogeneous Catalysts. New York, Marcel Dekker, Inc.
- DiNaro, J. L. (1999). "Oxidation of Benzene in Supercritical Water: Experimental Measurements and Development of an Elementary Reaction Mechanism." PhD thesis, Chemical Engineering, Massachusetts Institute of Technology, Cambridge, MA
- Haar, L., J. S. Gallagher, et al. (1984). NBS/NRC Steam Tables. New York, Hemisphere Publishing Corp.
- Holgate, H. R. (1993). "Oxidation Chemistry and Kinetics in Supercritical Water: Hydrogen, Carbon Monoxide, and Glucose." thesis, Chemical Engineering, Massachusetts Institute of Technology, Cambridge, MA
- Kruse, A. and E. Dinjus (2003). "Hydrogen from Methane in Supercritical Water." *Angewandte Che. Int. Ed.* **42**(8): 909-911.
- Marrone, P. A. (1998). "Hydrolysis and Oxidation of Model Organic Compounds in Sub-and Supercritical Water: Reactor Design, Kinetics Measurements, and Modeling." PhD thesis, Chemical Engineering, Massachusetts Institute of Technology, Cambridge, MA
- Phenix, B. (1998). "Hydrothermal oxidation of simple organic compounds." PhD thesis, Chemical Engineering, Massachusetts Institute of Technology, Cambridge, MA
- Reid, R. C., J. M. Prausnitz, et al. (1977). The Properties of Gases and Liquids. New York, McGraw-Hill.
- Rettich, T. R., R. Battino, et al. (1982). "Solubility of gases in liquids. 15. High-precision determination of Henry's coefficients for carbon monoxide in water at 278 to 323K." *Berichte Bunsengesellschaft für Physiche Chemie* **86**: 1128-1132.
- Shmonov, Y., R. Sadus, et al. (1993). "High Pressure Phase Equilibria and Supercritical pVT Data of the Binary Water + Methane Mixture to 723 K and 200 MPa." *J. Phys. Chem.* **97**: 9054-9059.
- Sullivan, P. (2003). "Oxidation Kinetics of Methylphosphonic Acid in Supercritical Water: Experimental Measurements and Model Development." PhD thesis, Chemical Engineering, MIT, Cambridge, MA



- Taylor, J. D., J. I. Steinfeld, et al. (2001). "Experimental measurement of the rate of methyl tert-butyl ether hydrolysis in sub- and supercritical water." *Ind. Eng. Chem. Res.* **40**(1): 67-74.
- Webley, P. A. (1989). "Fundamental Oxidation Kinetics of Simple Compounds in Supercritical Water." PhD thesis, Chemical Engineering, Massachusetts Institute of Technology, Cambridge, MA
- Zhou, N., A. Krishnana, et al. (2000). "A computational model for supercritical water oxidation of organic toxic wastes." *Advances in Environmental Research* **4**: 79-95.

## 4 Catalytic Reforming of Methane in SCW

### 4.1 MOTIVATION AND INTRODUCTION

Catalytic steam reforming of methane, whose origins date back to the late 1800s (Rostrup-Nielsen, 1984), is by far the most applied method for methane conversion in commercial use today. The procedure converts methane into synthesis gas, or syngas, which is a mixture of hydrogen ( $H_2$ ) and carbon monoxide (CO). Syn gas can then be further converted into denser products such as methanol or higher molecular weight hydrocarbons via a Fischer-Tropsch process. The overall reaction stoichiometry of steam reforming is



This reaction is highly endothermic, with a standard enthalpy of reaction of  $\Delta H_{rxn}^o = 206$  kJ/mol (298K, 1 bar) (Rostrup-Nielsen, 1984). Based on LeChatelier's principle, the equilibrium conversion of methane to syn gas is favored at high temperatures and low pressures. Table 4-1 lists process conditions for industrial conversion of methane with steam reforming.

**Table 4.1 Process conditions for various reforming product streams** (Myers, 2000). Water-gas shift step is not considered for these conditions.

Desired Product	H <sub>2</sub> O/CH <sub>4</sub> Ratio	Temperature (°C)	Pressure (MPa)
Methanol Syn Gas	2.5 – 2.8	700 - 900	2 - 3
Hydrogen	4 – 5	800 - 900	1.5 - 3

In the presence of excess water, the steam reforming reaction is commonly coupled with the water-gas shift (WGS) reaction to form carbon dioxide (CO<sub>2</sub>) and additional hydrogen:



The WGS is exothermic, with a standard enthalpy of reaction of  $\Delta H_{rxn}^{\circ} = -41$  kJ/mol (298K, 1 bar) (Rostrup-Nielsen, 1984). The resulting system equilibrium is a trade-off between reforming favored at higher temperatures and WGS favored at lower temperatures. In practice, it is performed as a two-step process; the endothermic Reaction (4-1) is carried out at high temperature with nickel-based catalysts while the exothermic Reaction (4-2) is a second step carried out a lower temperature with iron or copper catalysts

The catalyst of choice for methane steam reforming incorporates nickel as the active metal arranged on a support in banks of vertical catalyst tubes heated by combusting natural gas to supply the endothermic reaction enthalpy for Reaction (4-1). There are several disadvantages to the current methane steam reforming conversion process. For example,

a. *Capital and energy expenses.* Because the costs of building and operating large scale reformers able to withstand high temperatures along with the inherent energy requirements to drive the reactions can be exorbitant, one need not wonder why it might be cheaper to flare remote gas rather than lose money converting it.

b. *Catalyst deactivation.* Coking (or carbon deposition) and sulfur fouling are common ailments in steam reforming with nickel-based catalysts. Industrial catalysts must be occasionally regenerated or replaced to ensure optimum catalytic activity for the process (Trimm, 1987).

c. *Expense of purification.* Reforming gas streams typically contain CH<sub>4</sub>, CO, CO<sub>2</sub>, H<sub>2</sub>, H<sub>2</sub>O, and other sulfur and higher hydrocarbon contaminants which require purification for end uses such as hydrogen fuel for fuel cells and syn gas for methanol production.

These disadvantages and the ultimate desire to develop a one-step process that can convert methane to higher alkanes, or to a liquid product such as methanol, or to a hydrogen-rich

gas free of carbon monoxide, constitute the driving force behind recent methane conversion research. The question we address in our research is whether we can apply a supercritical water process to efficiently convert methane?

#### *4.1.1 Equilibrium Constraints for Methane SCW Reforming*

The equilibrium conversion of methane in supercritical water was first explored to identify optimal conditions to study experimentally. The EQUIL module of CHEMKIN 3.7.1 was employed to carry out these calculations (Reynolds, 1986). This program incorporates only ideal gas assumptions, but based on our typical experimental conditions of dilute feeds and high temperatures, solvent compressibility and component fugacity coefficients approach unity and therefore, these assumptions are valid as a first approximation (see Section 5.2.1 for a complete discussion). The components of CH<sub>4</sub>, H<sub>2</sub>O, H<sub>2</sub>, CO and CO<sub>2</sub> were considered. Figure 4.1 shows the results of these calculations as methane conversion versus temperature on the left and hydrogen and carbon monoxide yield versus temperature on the right.

The comparison of conventional steam reforming conditions versus SCW reforming conditions in both Figure 4.1 charts is quite revealing. The conventional steam reforming results, where [H<sub>2</sub>O]<sub>0</sub>/[CH<sub>4</sub>]<sub>0</sub> = 3 and 25 bar pressure, agree with traditional processes where high temperatures are employed to achieve high methane conversions while achieving modest hydrogen yields and significant carbon monoxide yields. To operate under SCW conditions, one must employ much higher pressures, which, by examination of Reaction 5-1, should force the main steam reforming reaction towards reactants, thereby reducing methane conversion. The results corresponding to [H<sub>2</sub>O]<sub>0</sub>/[CH<sub>4</sub>]<sub>0</sub> = 10 and 250 bar pressure support this prediction of reduced conversion at higher pressure even though the concentration of water, a reactant in this system, was increased over three fold.

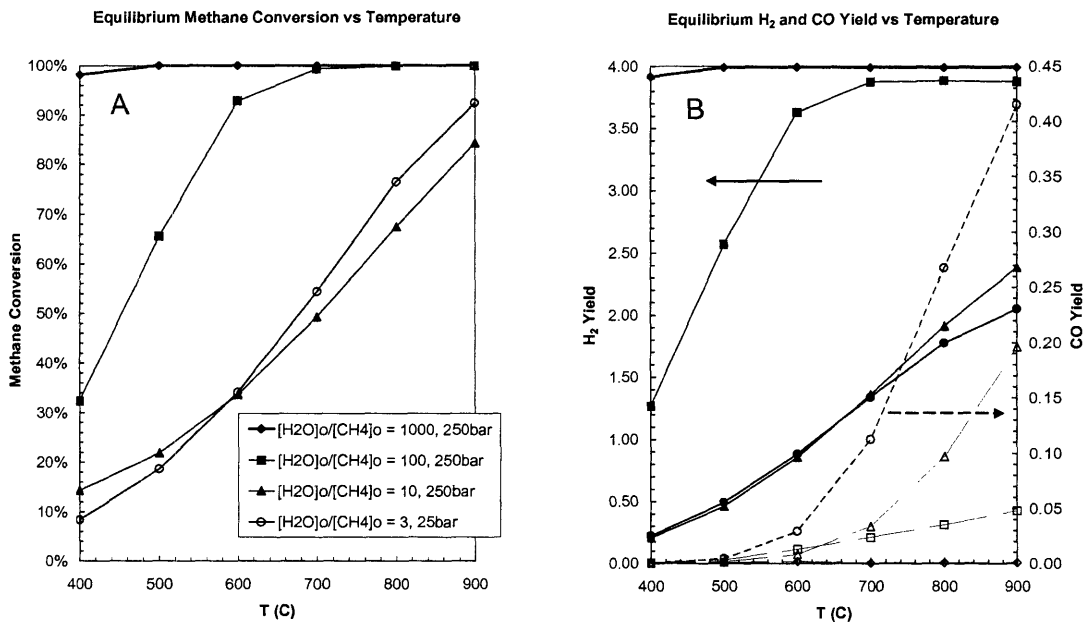


**Figure 4.1 Equilibrium Conversion of Methane and Product Yield: Conventional Steam versus SCW Reforming Conditions.** Chart A = equilibrium conversion of methane. In this chart, solid lines represent conversion values corresponding to different initial conditions of  $[\text{H}_2\text{O}]_0/[\text{CH}_4]_0$  and pressure (commercial reforming conditions =  $[\text{H}_2\text{O}]_0/[\text{CH}_4]_0 = 3, 25\text{bar}$ ). Chart B = equilibrium  $\text{H}_2$  and CO yields. In this chart, solid lines represent  $\text{H}_2$  yields and dashed lines represent CO yields corresponding to different initial conditions of  $[\text{H}_2\text{O}]_0/[\text{CH}_4]_0$  and pressure. In both charts, SCW conditions correspond with  $[\text{H}_2\text{O}]_0/[\text{CH}_4]_0 = 1000$  (diamonds), 100 (squares), 10 (triangles) and 250 bar while commercial reforming conditions =  $[\text{H}_2\text{O}]_0/[\text{CH}_4]_0 = 3$  (circles), 25 bar.

However, the equilibrium predictions for higher water concentrations, corresponding to typical dilute experimental conditions, are very encouraging, despite the discouraging effects of higher pressures on the steam reforming reaction. For the results corresponding to  $[\text{H}_2\text{O}]_0/[\text{CH}_4]_0 = 100$  and 1000 at 250 bar pressure, high methane conversion is achieved at much lower temperatures, producing a very rich hydrogen gas with trace amounts of CO. These predictions make perfect sense if you consider the role of water as a reactant in both Reactions 4-1 and 4-2. Excess water will drive both methane reforming (Reaction 4-1) and the water-gas shift (Reaction 4-2) towards products resulting in higher conversions of methane producing more hydrogen and carbon dioxide and little CO.

---

From this set of equilibrium calculations using ideal gas assumptions, methane reforming in SCW appears to be an attractive option, making it possible to achieve high conversions and hydrogen yields at much lower temperatures. It is reasonable to assume that separation costs would also be reduced since CO content is minimized and CO<sub>2</sub> is easily separated from the gas stream due to its high water solubility. The following sections discuss the results of previous studies of methane SCW reforming and the experimental results of the current study and our attempts to achieve these equilibrium predictions.

#### 4.1.2 Previous SCW Reforming Studies

As in the gas phase, methane reformation in SCW appears to be kinetically limited. Although the thermodynamics seem to indicate higher possible conversions and hydrogen yields, limited experimental results by three separate investigators confirm the refractory nature of methane in SCW without catalyst. Webley and Tester (1991) conducted two PFR experiments at 652°C and 246 bar with a dilute methane feed (~ 4.2 mM) and only residual oxygen normally dissolved in water (~  $7 \times 10^{-6}$  M), and they did not see any measurable conversion at 7.1 and 14.8 seconds. Hirth and Franck (1993) also conducted two separate experiments but at much longer times in a batch cell with much higher concentrations. At 600°C, 600 bar, 91 mol % water and 9 mol % methane, they recorded only 2.54% conversion at 60 minutes and 3.50% conversion at 120 minutes. The main products they identified were CO<sub>2</sub>, H<sub>2</sub> and C<sub>2</sub>H<sub>4</sub>, prompting them to propose a pyrolytic pathway to C<sub>2</sub>H<sub>4</sub> and a hydrolysis/reforming pathway to CO<sub>2</sub>. Lee and Foster (1996) were the last to report on the stability of methane in SCW. They conducted two laminar flow reactor experiments at 450°C and 250 bar, [CH<sub>4</sub>]<sub>0</sub> = 0.189 and 0.311 mM, and measured zero conversion after 78.2 and 84.1 seconds.

The preliminary results of the only catalytic SCW methane reforming study in the literature were recently released in a three-page paper by Kruse and Dinjus (2003) from Karlsruhe, Germany. In their study, the authors explored hydrogen generation in SCW in the presence of different catalysts (aqueous solutions of KOH,  $K_2CO_3$ , NaOH, KOH/Ni, a Raney Ni suspension, and Raney Ni/KOH). The conditions of their nine batch cell experiments were 650°C (1 experiment at 570°C), 330 – 680 bar, 15 minutes, and  $[H_2O]_0/[CH_4]_0 = 143$  with hydrogen yield results captured in Figure 4.2.

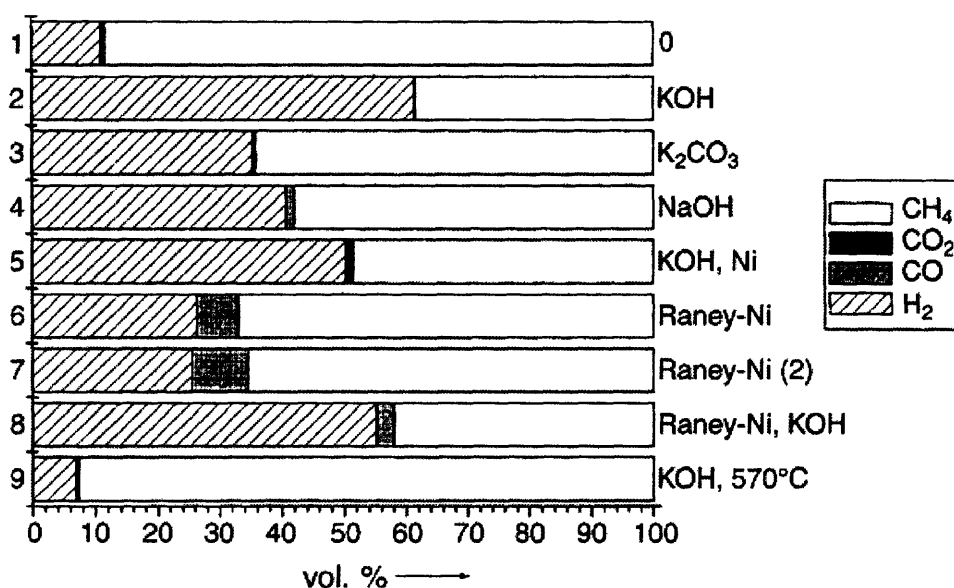


**Figure 4.2** Experimentally determined gas compositions from nine experiments. (15 min, 650°C, ~600 bar (Expt 7 was 380 bar)) (Kruse and Dinjus, 2003)

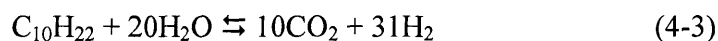
Experiment #1 (top row in Figure 4.2) qualitatively agrees with previous non-catalytic experiments of methane in SCW, that is very limited conversion after long times producing small amounts of  $H_2$  and  $CO_2$ . The experiments with alkali metal salts (Experiments 2-4 in Figure 4-2) show a significant increase in  $H_2$  yield. Kruse and Dinjus postulated that any  $CO_2$  formed may have been dissolved in the high pH aqueous phase as carbonates, thus explaining the small

amounts of CO<sub>2</sub> found in the gas phase. When nickel, in the form of nickel sheets and Raney nickel (Experiments 5 & 8 above), was added with the alkali salt catalysts, the gas phase showed similar hydrogen yields and a measurable amount of CO in the experiment with Raney Nickel. Two experiments with Raney nickel only (Experiments 6 & 7 above) resulted in lower hydrogen yields and significant CO yields. Kruse and Dinjus concluded that alkali metal salts catalyzed both the reforming reaction and the shift reaction (Reactions (4-1) and (4-2) above) while the nickel compounds only catalyzed the reforming reaction. The preliminary results of this recent Karlsruhe study are encouraging and provide a solid launching point for this study.

A literature search revealed three additional related SCW reforming studies with reactants other than methane and no catalysts. Two recent studies on methanol reforming in SCW were conducted at high temperatures, high feed concentrations and without catalysts. Boukis, Diem *et al.*, (2003) performed experiments at pressures of 250-450 bar, temperatures of 400-600°C and methanol feed concentrations of 5 – 64 wt% in an Inconel 625 tubular flow reactor. Their results showed conversions greater than 99% and high hydrogen yields (close to 80% gas vol) in less than one minute residence time. Pre-treating their reactor with 3 wt % hydrogen peroxide solution resulted in the highest conversions and lowest CO yields. Taylor, Herdman *et al.* (2003) conducted several reforming experiments with primarily methanol and also ethanol, ethylene glycol, acetone and diesel fuel in supercritical water from 550-700°C and 276 bar in an Inconel 625 tubular flow reactor. With methanol feed concentrations of 15-45 wt% and 3 – 6 seconds residence time, a gas stream was produced containing 70 vol% H<sub>2</sub>, 20 vol % CO<sub>2</sub> and small amounts of CH<sub>4</sub> and CO. Feeds of ethanol and ethylene glycol produced less hydrogen and more methane while feeds of acetone and diesel fuel resulted in reactor plugging and black deposits.



Pinkwart, Bayha *et al.* (2004) recently reported the results of hydrocarbon reformation in SCW in the presence of 4 different commercial steam reforming catalysts (1-45% wt% NiO, various Mg, K, Ca, Si binders on Al<sub>2</sub>O<sub>3</sub> supports). Their experiments included two different feeds, 10 vol % of n-decane and 2.5 – 20 vol % of diesel fuel, in a tubular flow reactor at 550°C and 250 bar. After 10 seconds residence time over a 32.4 wt % NiO catalyst, 80% of the n-decane feed was converted into a hydrogen-rich gas, yielding almost 4 moles of H<sub>2</sub> gas per mole of n-decane compared with 0.05 H<sub>2</sub> molar yield without catalyst. Although hydrogen yield was clearly higher with catalyst in almost all cases, the highest yield of 4 moles H<sub>2</sub>/mole of n-decane, or 13% yield, is well short of the stoichiometric goal of 31 moles of H<sub>2</sub> gas for complete reforming to CO<sub>2</sub>.



Reformation of diesel fuel required longer residence times to achieve the highest yields; for example, after 40 seconds, a hydrogen yield of 2 moles H<sub>2</sub>/mole diesel fuel was obtained with no evidence of coke formation. Unfortunately, Pinkwart *et al.* did not report any analysis of commercial catalyst stability and activity during these experiments.

Previous studies of hydrocarbon reforming in SCW confirm the refractory nature of methane, the labile nature of methanol, and offer promise of a possible catalytic conversion of methane and other hydrocarbons to a hydrogen-rich gas product. However, there is much more to learn about catalyst stability and choosing the best catalyst for reformation reactions in SCW. The following section describes the catalyst options best suited for SCW and details the catalysts selected for this study.

## 4.2 CATALYST CHOICE FOR SCW

### 4.2.1 Previous SCWO Catalyst Studies

Most of the catalyst investigations in SCW have focused on supercritical water oxidation (SCWO). There have been several SCWO catalyst studies prompting three review papers (Ding, Frisch *et al.*, 1996; Baiker, 1999; Savage, 2000) and a catalyst evaluation paper (Frisch, Li *et al.*, 1994). These papers identify several groups of catalytic materials that are suitable for reactions in SCW, and rule out several others due to their instability in this aggressive fluid environment. For example, the oxides of V, Cr, Ni, Cu, Zr, Ti, Al, Ce, Co, Fe, Mn, Ti, and Zn may be used as catalysts supported on Al, Hf, Zr, and Ti in SCW due to their hydrothermal stability and high melting points while low melting points preclude the use of the oxides of Ag, As, B, Cs, P, Re, and Se (Ding, Frisch *et al.*, 1996). Frisch found the best supports to be zirconia, titania,  $\alpha$ -alumina and hafnia while NiO exhibited crystalline growth and aggregation, and supported platinum catalysts deactivated over the course of 13 hours on stream (Frisch *et al.* 1995). Although these studies provide valuable information on catalyst suitability, those catalysts found to be suitable in a SCW oxidation environment may not be suitable for an oxygen-free SCW reformation environment.

### 4.2.2 Previous Hydrothermal Catalyst Studies

This section provides background on related catalyst studies in both sub-critical and supercritical water oxygen-free conditions that narrows our focus to the most promising catalyst combinations. As we alluded to in Section 1.2, most of the oxygen-free, hydrothermal studies using catalysts involve gasification of biomass or waste feedstocks under a wide range of conditions. Table 4.2 lists the operating conditions of the more recent studies, including

---

catalysts employed and observations related to catalyst activity and stability. In this table, the studies are listed in general order of increasing temperatures examined.

One of the most detailed and extensive studies of catalysts in oxygen-free sub-critical water environments are those of Dumesic and Elliot. Professor James A. Dumesic and co-workers at the University of Wisconsin have published several articles on catalytic aqueous phase reforming (APR) of biomass-derived oxygenates like ethylene glycol. Operating at 225-265°C, 25 – 51 bar and feed concentrations of 2-10 wt%, they have studied the activity and stability of a variety of catalysts such as tin-promoted Raney nickel and silica supported metal catalysts. Their studies indicated that tin-promoted catalysts and silica-supported platinum catalysts were the most stable and most active for reforming these oxygenate feeds (Davda and Dumesic, 2003; Davda, 2003; Huber, Shabaker *et al.*, 2003; Huber, Cortright *et al.*, 2004; Shabaker, Huber *et al.*, 2004).

Dr. Douglas C. Elliott and co-workers at Pacific Northwest National Laboratory, Washington have examined catalytic gasification of wet biomass for more than two decades. They have studied a variety of real biomass and biomass-simulant feeds at 250-360°C and pressures of 220 bar and less in the presence of numerous metal catalysts. One measure of the success of their work is the patents they have generated for developing stable and active catalysts

**Table 4.2 Operating Conditions of Select Oxygen-Free Hydrothermal Catalyst Research Programs.** (Tomita and Oshima, 2004; Davda, 2003; Minowa and Ogi, 1998; Elliott, 2004; Osada, Sato *et al.*, 2004; Vogel, 2002; Watanabe, Osada *et al.*, 2003; Park and Tomiyasu, 2003; Antal, 2000)

Principal Investigators	Type Feed	Feed wt %	T (C)	P bar	Catalyst	Catalyst Activity
Tomita and Oshima	propylene	3.6 – 30mM	100-420	216-314	MoO <sub>3</sub> /Al <sub>2</sub> O <sub>3</sub> , TiO <sub>2</sub>	TiO <sub>2</sub> best catalyst
Dumesic et al.	Ethylene glycol, glycerol, sorbitol	2-10%	210-265	25-51	Sn-Raney-Ni; Ni, Pd, Pt, Ru, Rh, Ir on SiO <sub>2</sub> ; Pt/Al <sub>2</sub> O <sub>3</sub> ; Ni/Al <sub>2</sub> O <sub>3</sub> , NiSn/Al <sub>2</sub> O <sub>3</sub>	Sn-Raney-Ni stable & = Pt/Al <sub>2</sub> O <sub>3</sub> ; Pt~Ni>Ru>Rh~Pd >Ir; Sn promoted improves stability & H <sub>2</sub> yield
Minowa and Ogi	cellulose	14%	200-250	30	Commercial Ni on Si/Al <sub>2</sub> O <sub>3</sub> /Mg	Magnesia highest activity, no spt lowest activity
Elliott et al.	Wet biomass, manure, grains,	1-8%	250-360	220>	Numerous Ni, Ru, Pt, Pd, catalysts	Best catalysts = Ru,Rh,Ni on a-Al <sub>2</sub> O <sub>3</sub> , ZrO <sub>2</sub> , TiO <sub>2</sub> , C
Osada et al.	Lignin, cellulose	4.7%	240-400	288	2wt% Ru/TiO <sub>2</sub> , 17-19wt% Ni on Al <sub>2</sub> O <sub>3</sub>	Ru/TiO <sub>2</sub> better than Ni/Al <sub>2</sub> O <sub>3</sub>
Vogel et al.	Woody biomass, sewage, model biomass mixture	10-30%	350 - 450	250 - 350	Ni, Ru/TiO <sub>2</sub> , Raney Ni, Pt/ZrO <sub>2</sub>	Raney Ni appears to be stable & active
Watanabe, M. et al.	formaldehyde	0.15-1.7 M	400	250-400	CeO <sub>2</sub> , ZrO <sub>2</sub> , MoO <sub>3</sub> , TiO <sub>2</sub>	CeO <sub>2</sub> , ZrO <sub>2</sub> promoted CH <sub>3</sub> OH; MoO <sub>3</sub> , TiO <sub>2</sub> promoted CO
Park and Tomiyasu	Napthlene, cellulose, & more	3.2%	450	440	RuO <sub>2</sub>	D <sub>2</sub> O oxidized Ru to make D <sub>2</sub>
Antal et al.	wet biomass, sewage, glucose	22 % >	600-650	220-345	Activated carbon	Deactivated after 4-6h, some C gasification

for this hydrothermal, near critical environment. After extensive experiments and catalyst analysis, Elliott and co-workers have identified the best possible catalysts for biomass gasification under sub-critical water conditions as those containing the metals Ru, Rh, or Ni on supports of  $\alpha$ -Al<sub>2</sub>O<sub>3</sub>, ZrO<sub>2</sub>, TiO<sub>2</sub>, or carbon (Elliott and Sealock, 1998; Elliott and Sealock, 1998; Elliott, Werpy *et al.*, 2001; Elliott, 2004; Elliott *et al.*, 1997).

Catalytic reforming at higher temperatures and pressures in supercritical water has been less studied. Professor Antal and co-workers at the University of Hawaii have been pioneers in this field with their studies of SCW biomass gasification over packed beds of various activated carbons. Typical operating conditions are high temperatures (600-650°C), supercritical pressures (220-345 bar) and concentrated feeds (22 wt % and below). The variety of activated carbons studied includes spruce wood charcoal, macadamia shell charcoal, coal activated carbon and coconut shell activated carbon. Although Antal and co-workers achieved complete gasification of their feeds to high hydrogen yields, they did experience deactivation of the carbon catalysts after several hours on stream. Gasification of the activated carbon itself was measured in one study, but the gas produced from the carbon catalysts was less than 3% of the gas produced from a concentrated glucose feed (1.2M) (Antal *et al.*, 2000; Xu *et al.*, 1996; Xu and Antal, 1998; Matsumura, Xu *et al.*, 1997; Antal, 1996).

Other studies using catalysts in oxygen-free supercritical water have been less extensive. Osada *et al.* (2004) reported on the successful gasification of cellulose type feeds using a ruthenium catalyst. Park and Tomiyasu (2003) also examined cellulose and other feeds over a ruthenium catalyst in SCW. Their work included an interesting set of experiments with D<sub>2</sub>O in lieu of H<sub>2</sub>O which resulted in the formation of CD<sub>4</sub> and D<sub>2</sub>. The authors postulated that the ruthenium catalyst may have been oxidized by the deuterized-water creating D<sub>2</sub> and methanation

reactions between CO, CO<sub>2</sub> and D<sub>2</sub> may be responsible for creating CD<sub>4</sub>. Watanabe *et al.* (2003) contributed one article on the conversion of formaldehyde in SCW in the presence of CeO<sub>2</sub>, ZrO<sub>2</sub>, MoO<sub>3</sub>, and TiO<sub>2</sub>. Unfortunately, the journal articles covering all of these studies do not include detailed information on long term catalyst stability and activity.

The remaining SCW catalyst study listed in Table 4.2 is that of The Paul Scherrer Institut (PSI) in Villigen, Switzerland. Dr. Vogel and co-workers at the PSI have recently established a hydrothermal biomass conversion research program focused on the catalytic gasification of wet biomass feedstocks to a methane-rich fuel gas. Since methane is the target product, the PSI study has concentrated on lower temperature conditions (~400°C and 300 bar) to exploit equilibrium predictions and the use of catalysts like Raney nickel to improve the kinetics. Experiments at PSI have shown >99% gasification of a 10 wt % woody biomass to a fuel gas containing almost 50% by volume methane from a batch reactor after 98 minutes of holding time. Vogel and co-workers have reported on the detailed analysis of the Raney Ni catalysts which indicate long term stability and activity (Vogel, 2002; Waldner, 2004; Vogel, 2005).

The discussion above on previous catalysts explored in sub and supercritical water is useful to help narrow the focus on choosing the most promising catalysts for methane reforming in supercritical water. The results of this discussion and analysis are summarized in Table 4-3 which identifies the active metal and support choices that seem to hold the most promise based on documented catalyst stability and activity. Some studies offer conflicting results on catalyst stability and activity, but these differences may be due to different experimental conditions (e.g., oxidation versus oxygen-free environment) or to measurement uncertainties. For completeness, both studies that support the catalyst choice and those that conflict with the catalyst choice are listed in Table 4-3. In those cases where the same author is listed as both supporting and

conflicting the catalyst material choice, that author published evidence of both activity and deactivation in SCW.

**Table 4.3 Most Promising Catalyst Choices for SCW Reforming of Methane based on Previous Hydrothermal Catalyst Studies.** Supporting and conflicting studies are listed by lead author of cited references. (Tomita and Oshima, 2004; Davda, 2003; Minowa and Ogi, 1998; Elliott, 2004; Osada, Sato *et al.*, 2004; Vogel, 2002; Watanabe, Osada *et al.*, 2003; Park and Tomiyasu, 2003; Antal, 2000; Ding, Frisch *et al.*, 1996; Frisch *et al.*, 1995)

Active Metal	Supporting Studies	Conflicting Studies
Ni	Elliott, Dumesic, Vogel, Ding, Minowa	Elliott, Frisch
Raney-Ni	Dumesic, Vogel	Vogel
Ru	Elliott, Dumesic, Osada, Vogel, Park	
Pt	Dumesic	Elliott, Frisch
Supports	Supporting Studies	Conflicting Studies
$\alpha$ -Al <sub>2</sub> O <sub>3</sub>	Elliott, Dumesic, Ding, Frisch	Frisch
TiO <sub>2</sub> (rutile)	Elliott, Tomita, Watanabe, Ding, Frisch	
ZrO <sub>2</sub> (monoclinic)	Elliott, Watanabe, Ding, Frisch	
Activated Carbon	Elliott, Antal	Antal

#### 4.2.3 Commercial Steam Reforming Catalyst Compositions and Reducing Techniques

While a SCW methane reforming catalyst must be stable under hydrothermal conditions, it must also display good activity for methane reactions. After decades of research on different catalysts for commercial methane steam reforming processes, the highest active metals identified were those of Group VIII in the periodic table (Rostrup-Nielsen, 1984; Golodets, 1983).

Therefore the best candidates for SCW catalysis of methane should be the Group VIII metals that are also stable in SCW like Ni and Ru (Choudhary, Aksoylu *et al.*, 2003).

Years of research and development have also been invested in identifying the best support compositions for commercial methane steam reforming processes. Although catalyst manufacturers use a variety of support compositions and configurations to optimize their performance, there are three common components to typical catalyst supports: base support material, binder additives and promoter additives. The most common base support material used in commercial steam reforming catalysts is  $\alpha$ -alumina, which happens to be a candidate material for SCW processes found in Table 4-3. Different binding materials may be added to the  $\alpha$ -alumina to add strength such as a calcium aluminate hydraulic cement, silica or magnesia. Unfortunately binding materials such as these may easily transform in supercritical water, causing the catalyst support to lose strength and integrity. Promoters like potassium and sodium may also be added to the support material to reduce carbon formation and polymerization, but these promoters may also transform, become mobile or dissolve into SCW thus degrading the catalyst (Twigg, 1989).

Active metals in steam reforming catalysts typically revert to their oxidized states and must be properly reduced to be active. Nickel can be particularly challenging to reduce in the presence of excess water. Figure 4.3 depicts the equilibrium of nickel reduction in the presence of water and hydrogen



An equilibrium analysis of Reaction (4-3) shows that NiO may be the favored form of nickel if water is in excess. The temperatures and  $\text{H}_2\text{O}/\text{H}_2$  ratios of our typical SCW experimental conditions clearly put us above the equilibrium line in Figure 4-3, favoring the



oxidized form of nickel. Although the equilibrium calculations that contributed to the line drawn in Figure 4-3 do not take into consideration other possible species or reactions or the effects of non-idealities, they do identify potential concerns for keeping nickel active in our system. For the best reducing techniques, we here again turn to the wealth of knowledge in the commercial steam reforming industry.

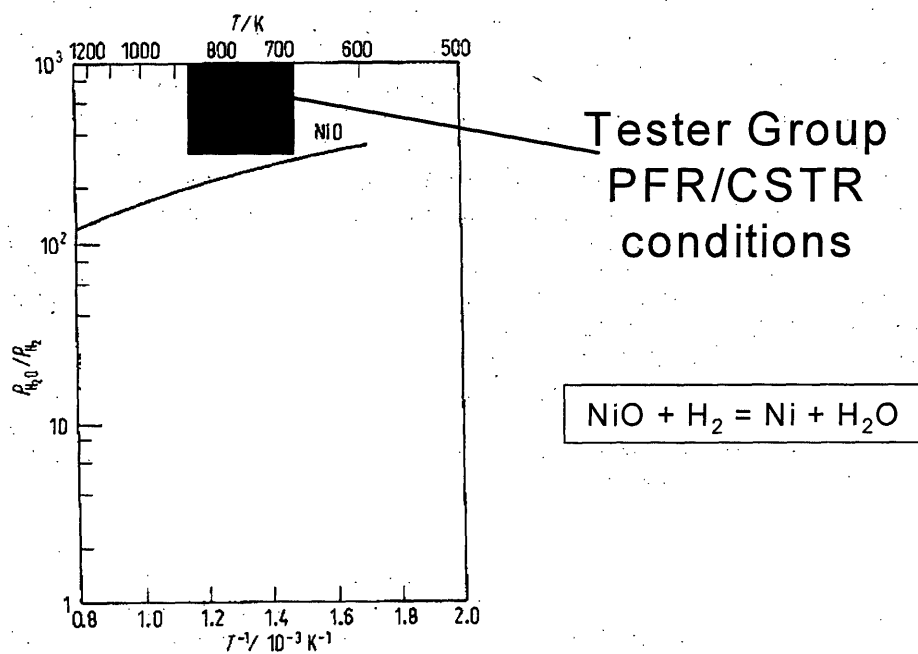


**Figure 4.3 Equilibrium of Nickel Reduction in the Presence of H<sub>2</sub>O and H<sub>2</sub>.** (Rostrup-Neilsen, J.R. 1984)

There are several techniques for reducing metal reforming catalysts. The most popular technique is using pure hydrogen or hydrogen diluted with steam (steam:hydrogen ratios ranging from 6-8:1) or inert gases. Temperatures and holding times vary, but typically reforming catalysts are reduced at ~ 600°C for 6-8 hours. Other reducing feed streams that produce hydrogen may be used including ammonia, methanol, natural gas and other hydrocarbons.

---

Temperatures and holding times for alternate feed streams also vary but they are typically chosen to produce similar steam:hydrogen ratios and reducing conditions (Twigg, 1989; Rostrup-Nielsen, 1975). To keep a nickel catalyst active, Rostrup-Nielsen (1975) recommends maintaining a steam:hydrogen ratio of 15 or lower depending on the interaction of active metal and support.

In summary, the comparison of stable active catalysts in SCW with the most active commercial steam reforming catalysts leads one to conclude that a nickel or ruthenium based catalyst on an  $\alpha$ -alumina support might be the most promising combination for SCW methane reforming. However, care must be taken to keep the nickel reduced and active, and avoid conditions which may lead to aggregation of the nickel. Also, careful consideration of the right mix of stable binding and promoting agents in the support may prolong the life of the SCW catalyst.

#### 4.2.4 Selected Catalysts

Based on the analysis and information presented above, the advice of several different collaborators, and the availability of resources, a variety of catalysts were chosen for this study.

- **Nickel Catalysts:** Nickel was a clear choice based on its history of success in commercial steam reforming applications and limited success in SCW applications. Due to their availability, we first conducted experiments with pure nickel wire and pure nickel pellets to examine the activity of un-supported nickel. We received donations of two different commercial reforming catalysts: Johnson Matthey donated 500 grams of KATALCO 57-7 catalyst (~18 wt % nickel oxide on CaO/Al<sub>2</sub>O<sub>3</sub> support) and Shell donated 2 kg of spent pre-reforming catalyst, C11-PR (>55% nickel on SiO/Al<sub>2</sub>O<sub>3</sub> support). These commercial

reforming catalysts were recommended for our applications since they were designed to handle more aggressive, pre-reforming conditions.

- **Platinum Catalysts:** Since platinum is reported to be less susceptible to deactivation by oxidation, several supported platinum catalysts were explored. Three off-the-shelf platinum catalysts were purchased; 5% platinum on alumina powder, 0.5% platinum on alumina pellets and 10% platinum on activated carbon. Alumina was a clear choice for a support, and powder and pellet forms were purchased to identify possible mass transfer issues in our reactors. Activated carbon as a support was chosen based on the success of Antal and Elliott (see Table 4-2). Also, Muradov (2001) achieved encouraging results for gas phase catalytic methane decomposition over elemental carbon. We received donations of 2 different proprietary catalysts from the Paul Scherrer Institut (PSI) who recommended these catalysts based on their work with catalytic gasification of biomass in hydrothermal environments: 1% Pt on  $ZrO_2$ , 1% Pt/5%  $CeO/ZrO_2$ .
- **Ruthenium Catalysts:** PSI also donated a small amount of their 1% Ru on  $TiO_2$  Degussa catalyst. Ru-based catalysts have enjoyed significant success at lower temperatures and pressures in sub-critical water applications, but they have not been extensively tested at the higher temperatures and pressures of methane SCW reforming (Davda, 2003; Elliott and Sealock, 1998; Park and Tomiyasu, 2003).

### 4.3 HETEROGENEOUS CATALYSIS RESULTS

In this study we examined the reformation of methane in supercritical water under a variety conditions to determine the most promising parameters for methane conversion. The range of conditions included 350 – 630°C, 150 – 400 bar, 0.01 – 2 wt% methane, 10 seconds to 72 minutes residence time, and with and without different catalysts. We employed 4 different

reactor designs in this study; a packed bed reactor (PBR), a continuous-stirred tank reactor (CSTR) and two different batch reactor designs. The CSTR and PBR were modifications of our existing reactor systems while the two batch reactors were designed, built and tested during this study. All reactors and experimental procedures are described in detail in Chapter 3 of this thesis. Corresponding experimental conditions and data are tabulated in Appendix C. This section describes the results of each set of experiments.

### 4.3.1 Results of CSTR & PBR Experiments

We performed 24 initial catalyst experiments on our modified high pressure, high temperature CSTR system and 3 experiments using a PBR in our plug-flow system. The conditions are summarized in the table below:

**Table 4.4 Experimental Conditions for CSTR and PBR Experiments.** More details on experimental conditions can be found in Appendix C.

Reactor	#/Type experiments	Type catalyst	Reducing techniques	$T$ (°C)	$P$ (bar)	$t$ (sec)	$[\text{CH}_4]_0$ (mM)
CSTR	24 hydrolysis-reforming	Ni pellets, Ni wire, KATALCO 57-7, C11-PR	hexane, methanol	409 - 593	136 - 254	60 - 248	0.6 - 5.0
PBR	3 reforming	KATALCO 57-7	10%-H <sub>2</sub> /He, 1-hexene	350 - 600	246	8 - 60	2.0 - 18.0

During this phase of the study, only nickel catalysts were available for experiments. No deliberate reducing procedures were employed for the first 14 experiments in the hope of observing measurable conversion without catalyst pretreatment, as was seen in the SCW reforming study of Pinkwart *et al.* (2004).

Despite the variety of conditions explored, methane conversions greater than 11% and hydrogen yields greater than 8% could not be achieved. The highest methane conversions did not correspond with any measurable carbon product (e.g., CO, CO<sub>2</sub>), leading us to believe small leaks, saturator or pump problems may have been responsible for the loss of methane. Only two experiments saw CO<sub>2</sub> in the effluent (both approximately 1% yield) and CO was never observed in any experiment. One experiment producing CO<sub>2</sub> was a high temperature nickel wire experiment where the small yield of CO<sub>2</sub> agrees with similar findings in the non-catalytic methane hydrolysis study of Hirth and Franck (1993). Our first experiment with a commercial nickel catalyst, KATALCO 57-7, also produced a small amount of CO<sub>2</sub>, but the CO<sub>2</sub> yield decreased over the one hour sampling period, leading us to believe that that catalyst may have been rapidly deactivating. Small amounts of hydrogen were observed in almost every experiment, but it may have been the result of SCW oxidizing the metal catalyst or the metal reactor walls.

Attempts were made to reduce the two commercial nickel catalysts with a hexane-SCW mix and with a methanol-SCW mix. These labile, hydrogen-producing organic compounds were fed separately from the methane feed both before methane was introduced and while methane was being fed in an attempt to keep the nickel catalyst active. A syringe pump was used to feed pure hexane and methanol to a mixing tee just below the CSTR where it combined with pre-heated SCW before entering the reactor containing the catalyst. Target concentrations were 2 – 20 mM flowing for more than two hours before methane was introduced.

Deliberately reducing the nickel catalysts did not improve the results. There was clear evidence that both hexane and methanol were reacting to form significant amounts of hydrogen, but that hydrogen yield would drastically decrease over the one hour sampling period after

introducing methane. Experiments with hexane as the reducing stream did not produce measurable amounts of CO<sub>2</sub>. Reducing with methanol did produce small yields of CO and CO<sub>2</sub>, that rapidly decreased after methane was introduced.

Three packed bed experiments were conducted to explore shorter residence times and possible mass transfer issues. KATALCO 57-7 commercial nickel catalyst pellets were loaded into a U-shaped tube reactor described in detail in Chapter 3. The void fraction of the packing was measured to be 0.77 such that the free volume in the packed tube was 28.24 mL. The nickel catalyst was reduced with a H<sub>2</sub>-He gas stream during heat-up and for more than three hours prior to the introduction of methane. The PBR/PFR system would not accommodate co-feed of hydrogen and methane, but one experiment was performed where a dilute 1-hexene solution was co-fed with methane as an alternate means of reducing the catalyst. Similar to the CSTR results, the PBR results showed no evidence of methane conversion, no measurable production of CO<sub>2</sub> and a decreasing yield of hydrogen after switching to a methane feed.

It is logical to conclude that our low conversions and yields were primarily due to the rapid deactivation of the nickel catalysts in our SCW environment. The fact that the active metal nickel readily oxidizes in SCW coupled with our flow reactor constraint of low initial methane concentrations may have created an environment where there was not enough generated hydrogen to keep a reduced catalyst active. Different techniques to reduce the catalyst failed to maintain measurable methane conversions, but those techniques were also limited in the amount of reducing hydrogen they could maintain. In an attempt to overcome possible issues related to low concentrations, a transition was made to a set of batch experiments which were not limited to saturator feed of methane solutions and short residence times.

### 4.3.2 Results of Tube Batch Reactor Experiments

We performed 21 catalytic reforming experiments using a new batch system for gaseous feeds. Separate experiments were conducted using two different commercial nickel catalysts, three different platinum catalysts and one experiment with 1wt% NaOH. The conditions are summarized in the table below with more details found in Appendix C. Metal catalysts were reduced with a 10% H<sub>2</sub>/He gas mixture for more than 2 hours at 600°C.

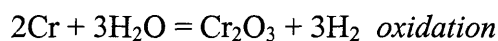
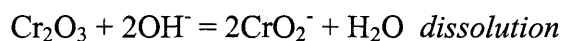
The hydrogen and carbon dioxide yields observed here were similar to our previous experiments. While most of the experiments produced small amounts of hydrogen, only four experiments produced measurable amounts of CO<sub>2</sub>, the largest amount being ~1% of the gas phase. It is interesting to note that all four experiments producing CO<sub>2</sub> used the 5% Pt/Al<sub>2</sub>O<sub>3</sub> catalyst pellets.

**Table 4.5 Experimental Conditions for Tube Batch Experiments.** More details on experimental conditions can be found in Appendix C.

Reactor	#/Type experiments	Type catalyst	Reducing techniques	<i>T</i> (°C)	<i>P</i> (bar)	<i>t</i> (min)	$\frac{[\text{H}_2\text{O}]_o}{[\text{CH}_4]_o}$
Tube Batch	21 hydrolysis-reforming	KATALCO 57-7, C11-PR, 5% Pt/Al <sub>2</sub> O <sub>3</sub> , 0.5% Pt/Al <sub>2</sub> O <sub>3</sub> , 1% Pt/ZrO <sub>2</sub> , 1.1wt% NaOH	10% H <sub>2</sub> /He	600	56 - 407	30 - 77	11 - 147

When a 1 wt % NaOH solution was used in lieu of pure water and metal catalysts, the highest hydrogen yield was achieved; 48% of the product gas phase. There was no evidence of any CO<sub>2</sub> formed, but it may have been dissolved as carbonate in the high pH liquid product.

However, there was significant evidence of corrosion of the 316SS reactor, evident by a cloudy effluent with visible particles. The metal particles responded to a magnet indicating the presence of NiO and the digestate of the particles formed a colored complex with thiocyanate indicating the presence of iron. The particles were filtered, dissolved with acid and analyzed for nickel and chromium. A semi-quantitative analysis revealed significant amounts of nickel and chromium in the effluent; ~ 10 and 5 ppm respectively. Since corrosion was observed, it is possible that hydrogen was produced not from methane, but from the interaction of SCW with the metal reactor walls. This alkali environment may be dissolving the protective metal oxide layer on the reactor walls, exposing fresh, temporarily reduced metal to SCW which quickly oxidizes that metal producing hydrogen according to the following example reactions (Kritzer *et al.*, 1999):



More on the topic of alkali salts in SCW is presented in Section 4.5.

To address some of the problems with the tube batch system (see Section 3.3 for details), a new direct-inject batch system was designed, built, tested and employed to test the remaining metal catalysts.

### 4.3.3 Results of Direct Inject Batch Reactor Experiments

We performed 12 catalytic reforming experiments using a direct inject batch system for gaseous feeds. Separate experiments were conducted using one commercial nickel catalyst, 2 different platinum catalysts and one ruthenium catalyst. The conditions are summarized in the table below with more details found in Appendix C. Metal catalysts were reduced by flowing a 10% H<sub>2</sub>/He gas mixture during heatup and more than 2 hours at 600°C.



This set of experiments revealed the two most promising catalysts: ruthenium on titania and platinum on activated carbon. The 1% Ru on TiO<sub>2</sub> produced the highest yield of CO<sub>2</sub> (2.2% of the product gas volume). A 10% Pt on activated carbon catalyst produced a smaller yield of CO<sub>2</sub> (0.89% of the product gas volume) but the liquid product had a low pH (~1.9) indicating significant dissolved CO<sub>2</sub>. Although these yields appear to be small, they were accompanied by large hydrogen yields (> 50% of the gas volume), and, as discussed in the next section, correlate with relative catalyst stability and activity based on detailed analysis of the catalysts themselves.

**Table 4.6 Experimental Conditions for Direct Inject Batch Experiments.** More details on experimental conditions can be found in Appendix C.

Reactor	#/Type experiments	Type catalyst	Reducing techniques	$T$ (°C)	$P$ (bar)	$t$ (min)	$\frac{[\text{H}_2\text{O}]_o}{[\text{CH}_4]_o}$
Direct Inject Batch	9 hydrolysis-reforming	KATALCO 57-7, 1% Ru/TiO <sub>2</sub> , 10% Pt/C, 1% Pt/CeO/ZrO <sub>2</sub>	10% H <sub>2</sub> /He	600	250 - 290	10 - 20	142 - 188

#### 4.4 SCW EFFECTS ON HETEROGENEOUS CATALYSTS

Several different instrumental techniques were used to analyze the effects of supercritical water (SCW) on all catalysts employed in this study. We used Scanning Transmission Electron Microscopy (STEM) to examine morphology changes, x-ray diffraction (XRD) to study crystallite composition and size changes, x-ray photoelectron spectroscopy (XPS) to examine chemical changes on surfaces, and the Brunauer-Emmett-Teller (BET) method to measure surface area changes. The results of these analyses were quite revealing and helped form a reasonable explanation for our limited conversion of methane in supercritical water. A complete set of XRD, XPS and BET analysis results can be found in Appendix D.

---

#### 4.4.1 Commercial Nickel Catalysts:

**KATALCO 57-7:** After exposure to SCW, the KATALCO 57-7 catalyst pellets drastically changed color, going from a dark grey to a light green color, giving us our first hint that the catalyst significantly transformed. STEM and XRD results for the KATALCO 57-7 catalyst also indicated significant chemical changes after exposure to SCW. Figure 4.4 displays one set of STEM results, depicting digital pictures of the pellets, micrographs of catalyst particles, and elemental analyses of points on the particles. The first row corresponds with the catalyst before exposure to SCW and the bottom row corresponds with after exposure to SCW. Although the micrographs do not indicate significant morphology changes, the elemental analysis indicates that nickel was not uniformly dispersed before catalyst use, but it was uniformly dispersed after SCW exposure. This may be due to partial dissolution and re-crystallization of the nickel or mobility of the nickel in the catalyst, both phenomena indicating an unstable catalyst.

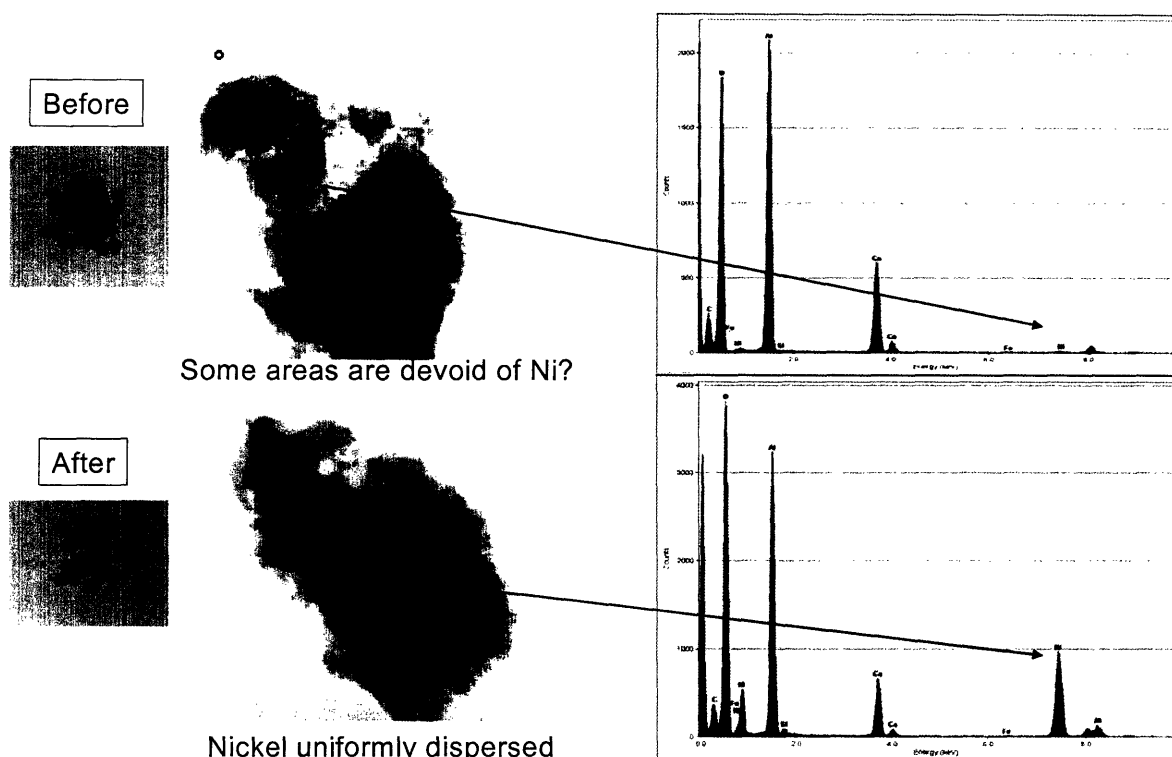


**Figure 4.4** STEM Analysis of KATALCO 57-7 Catalyst before and after exposure to SCW for 11 hours, 400–500°C, 245 bar.

XRD results for the KATALCO 57-7 catalyst are displayed in Figure 4.5. The disparity of the XRD patterns for the catalyst before and after exposure to SCW indicates a significant change. The two most significant, identifiable changes are the grain growth of the alumina and the calcium changes. In the after sample, the peaks associated with the alumina phase are much taller and more narrow indicating grain growth or aggregation. Calcium seems to form at least one new phase after exposure to SCW with the evolution of a new calcium hydroxide peak the near nine degree angle. There are several unidentified peaks in the after sample that could belong to other calcium-aluminum phases formed during this transformation. Nickel oxide is present before and after SCW exposure since the before sample was not reduced prior to XRD

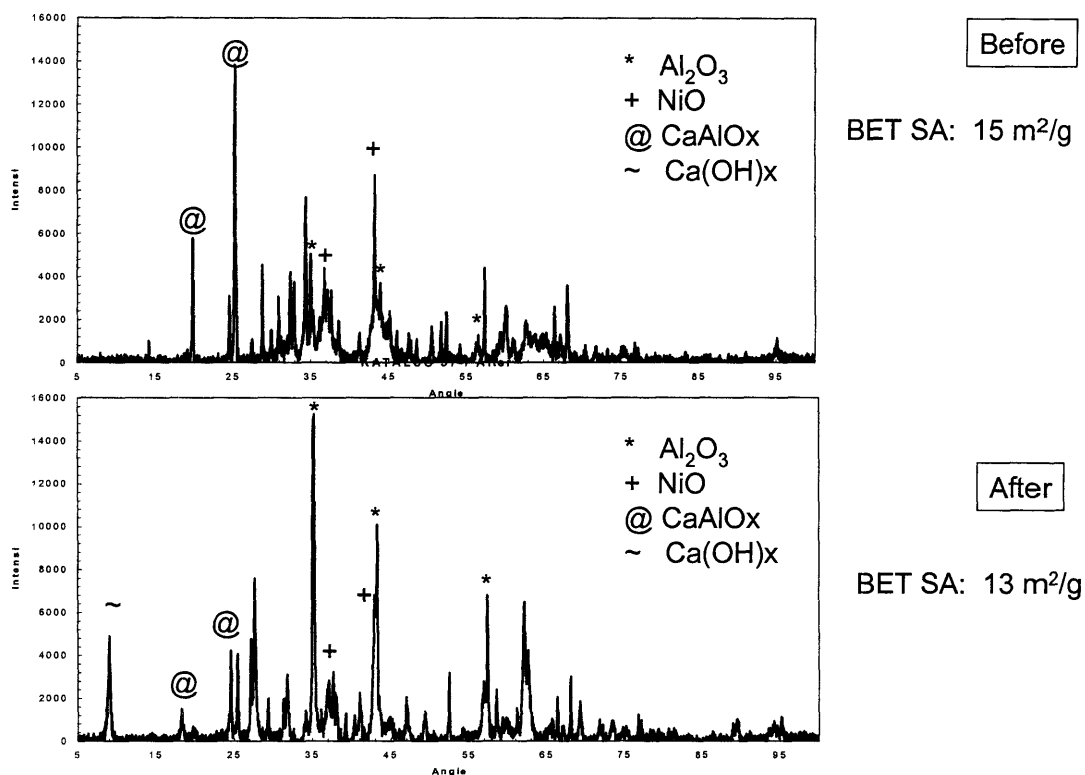


**Figure 4.5 XRD Analysis of KATALCO 57-7 Catalyst before and after exposure to SCW for 11 hours, 400–500°C, 245 bar.**

analysis. Nickel hydroxide may also be present in the after sample since  $\text{Ni(OH)}_2$  is a light green in color.

XPS and BET surface area measurements of the KATALCO catalyst did not indicate significant catalyst changes after SCW exposure. The KATALCO before and after XPS traces found in Appendix D are nearly identical, indicating that the elemental composition of the surfaces did not change significantly. Exact quantification of elemental composition with XPS was not possible due to low resolution scans. The BET surface area of the before sample was measured as  $15 \text{ m}^2/\text{g}$  and the after sample was  $13 \text{ m}^2/\text{g}$  indicating little change.

---

Although the XPS and BET analyses contradict the STEM and XRD analyses, the fact that the KATALCO catalyst was never really active for SCW methane reforming in any of our experiments supports our contention that the catalyst was severely degraded in this study.

**C11-PR:** All analyses performed on the C11-PR catalyst indicated drastic changes after exposure to SCW. The most graphic representation of these changes is the XPS plot in Figure 4.6. The XPS traces of two different samples after exposure to SCW are drastically different than the before trace, indicating significant loss of nickel, calcium and magnesium at the catalyst surface based on instrument sensitivity factors. Quantitative analysis of these XPS results indicated a loss of nickel from 33 wt % to 4 wt%, and losses of calcium from 4 and 8 wt% respectively to zero.

XRD and BET analyses found in Appendix D corroborate significant transformation of the C11-PR in SCW. XRD results show grain growth of the alumina and severe loss of nickel and silica. BET measurements indicated that C11-PR surface area decreased from 7 m<sup>2</sup>/g to 1 m<sup>2</sup>/g after SCW exposure. The loss of calcium, magnesium and silica correspond to a loss of the binding and promoting agents in this commercial steam reforming catalyst which was previously observed and discussed in Section 4.2.3. The compelling evidence here of C11-PR transformation in SCW supports its observed lack of activity to SCW methane reforming.

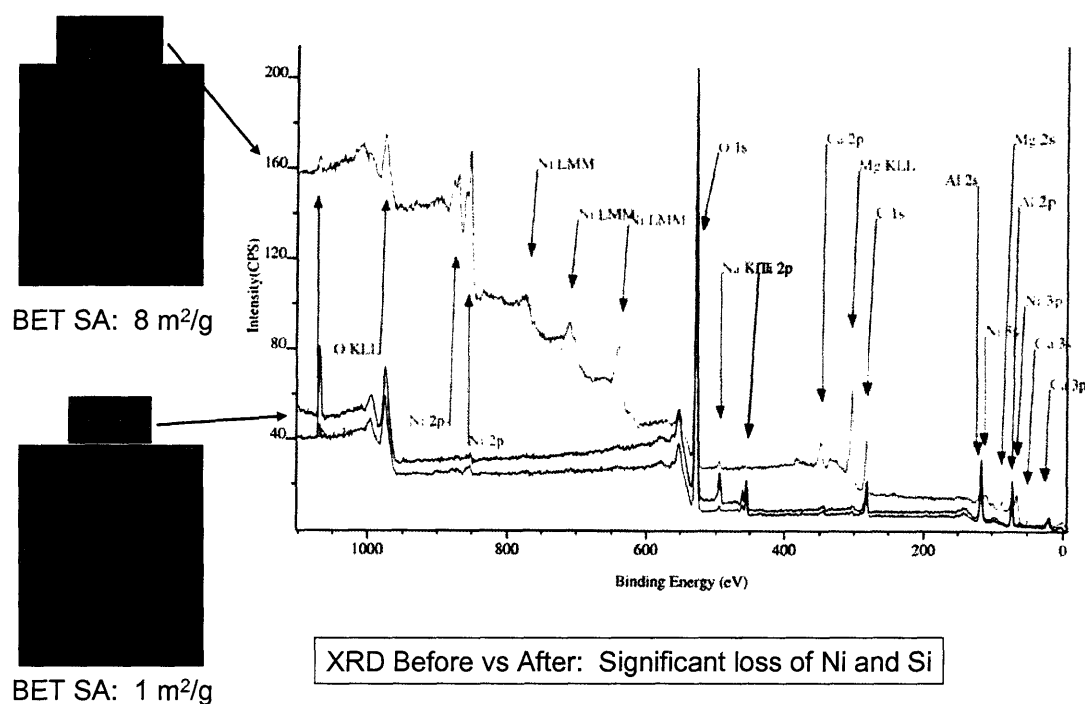
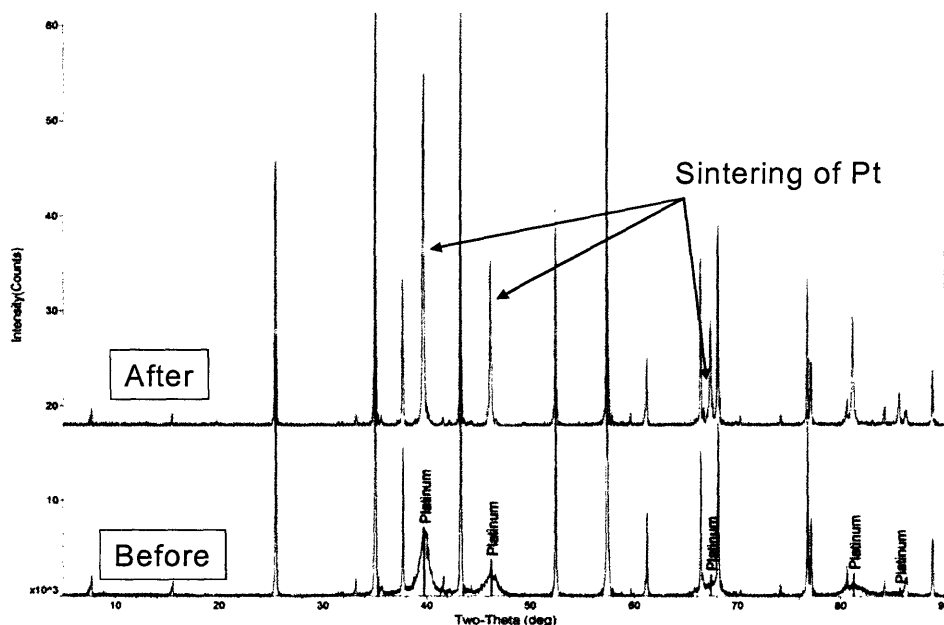


**Figure 4.6: XPS Analysis of C11-PR Commercial Reforming catalyst before and after exposure to SCW for 37.5 hours, 400–500°C, 245 bar.** The red trace corresponds to the catalyst sample before exposure to supercritical water. The blue and green traces are two different samples after experiments in SCW. Comparison of these traces confirms significant loss of nickel, calcium and magnesium from the surface.

#### 4.4.2 Platinum Catalysts:

**5% Pt/Al<sub>2</sub>O<sub>3</sub> Powder:** XRD analysis of the 5% Pt/Al<sub>2</sub>O<sub>3</sub> catalyst indicated significant aggregation of the platinum in SCW. Figure 4.7 displays the XRD traces for the 5% Pt/Al<sub>2</sub>O<sub>3</sub> catalyst before and after exposure to SCW. Although no changes are apparent in the peaks associated with the Al<sub>2</sub>O<sub>3</sub> support, the platinum peaks are much sharper in the after trace, indicating significant grain growth and aggregation. An estimate of the crystallite size calculated by the Scherrer formula gave a grain size of 630 nm and >10000 nm for the before and after samples respectively.

XPS and BET surface area measurements of the 5% Pt/Al<sub>2</sub>O<sub>3</sub> catalyst did not indicate significant catalyst changes after SCW exposure. The 5% Pt/Al<sub>2</sub>O<sub>3</sub> before and after XPS traces found in Appendix D are nearly identical, which only indicates the similar elemental composition at the catalyst surface and does not contradict the XRD finding of platinum grain growth. The BET surface area of the before sample was measured as 0.70 m<sup>2</sup>/g and the after sample was 0.37 m<sup>2</sup>/g. As expected, both measurements indicate extremely low surface areas for the alumina support, but we note that the BET results are at the limit of accuracy of the BET instrument. The analysis of the 5% Pt/Al<sub>2</sub>O<sub>3</sub> catalyst supports rapid deactivation due to platinum grain growth.



Other Pt sample - 0.5% Pt/Al<sub>2</sub>O<sub>3</sub> pellet: significant loss of SA & formation of PtO

**Figure 4.7:** XRD analysis of 5% Pt/Al<sub>2</sub>O<sub>3</sub> catalyst powder before and after exposure to SCW for 1.3 hours, 550°C, 370 bar.

**0.5% Pt/Al<sub>2</sub>O<sub>3</sub> Pellets:** XRD and BET analysis of the 0.5% Pt/Al<sub>2</sub>O<sub>3</sub> catalyst pellets indicated significant transformation in SCW. The XRD traces in Appendix D depict severe grain growth and possible formation of oxidized platinum, PtO. BET measurements of the catalyst surface area before and after exposure to SCW are drastically different; 96 versus 2 m<sup>2</sup>/g. As we saw earlier, XPS results for before and after samples were nearly identical, but that does not contradict the XRD and BET finding of significant grain growth and loss of surface area. As with the previous platinum on alumina catalyst, the analysis of the 0.5% Pt/Al<sub>2</sub>O<sub>3</sub> catalyst pellets supports rapid deactivation due to grain growth and possible transformation of the platinum's morphology.

**1% Pt/ZrO<sub>2</sub> Powder:** Only XRD and XPS analyses were performed on the 1% Pt/ZrO<sub>2</sub> catalyst powder due to limited quantities of this proprietary catalyst. Both XRD and XPS comparisons in Appendix D indicate limited transformation in SCW. Although XRD analysis was complicated by the overlap of the small platinum and large zirconia peaks, XRD of before and after samples looked nearly identical. Estimates of crystallite size by Scherrer's method corroborated limited change via grain growth; before samples were ~1140 nm and after samples were ~1710 nm. Although this analysis of the 1% Pt/ZrO<sub>2</sub> catalyst powder seems encouraging, it did not reveal much about the fate of platinum on this support and it does not explain its lack of activity to SCW reforming of methane.

**1% Pt/5% CeO/ZrO<sub>2</sub> Powder:** Like the other proprietary platinum catalyst examined, limited quantities of 1% Pt/5% CeO/ZrO<sub>2</sub> catalyst powder only permitted XRD and XPS analyses. Both XRD and XPS comparisons in Appendix D indicate limited transformation in SCW. XRD analysis of the platinum and cerium was complicated by large overlapping peaks for zirconia, and both samples seemed coarse with poor resolution of peak to background signal.



However, estimates of crystallite size by Scherrer's method corroborated limited change via grain growth; before samples were ~1070 nm and after samples were 1290 nm. XPS traces of before and after samples appear similar, the only difference being larger cerium and platinum peaks in the after sample. This may indicate diffusion of those metals to the surface while exposed to SCW. Unfortunately, these solid phase analysis results are not conclusive and do not offer any insight into the lack of activity of SCW reforming of methane with 1% Pt/5% CeO/ZrO<sub>2</sub> catalyst powder.

**10% Pt/Activated Carbon Powder:** XRD, XPS and BET analysis of the 10% Pt on activated carbon catalyst powder gave somewhat conflicting results. BET measurements of the before and after samples confirmed a high surface area powder that actually showed a slight increase in surface after SCW exposure; before sample surface area = 729 m<sup>2</sup>/g and after sample surface area = 795 m<sup>2</sup>/g. XPS traces for the before and after samples were very similar (see Appendix D) and did not indicate any significant change of surface elemental composition.

XRD traces of the before and after samples were also peculiar (see Figure 4.8 and Appendix D). Although the before sample XRD trace clearly confirmed the presence of platinum, the after sample XRD trace had platinum peaks that shifted by ~ 2 degrees indicated different lattice parameters for platinum. These corresponding peaks for platinum appeared significantly sharper in the after sample, indicating aggregation and grain growth. Estimates of crystallite size by Scherrer's method confirmed grain growth from ~790 nm before to ~1470 nm after SCW exposure.

Here again, the catalyst analysis is inconclusive, although it shows that activated carbon as a support did not change significantly, there are indications that the active metal platinum aggregated similar to the other platinum catalysts. The 10% Pt on activated carbon catalyst

powder appeared to have limited activity in SCW methane reforming experiments, but that activity may be short-lived if platinum aggregation continues after longer SCW exposure times.

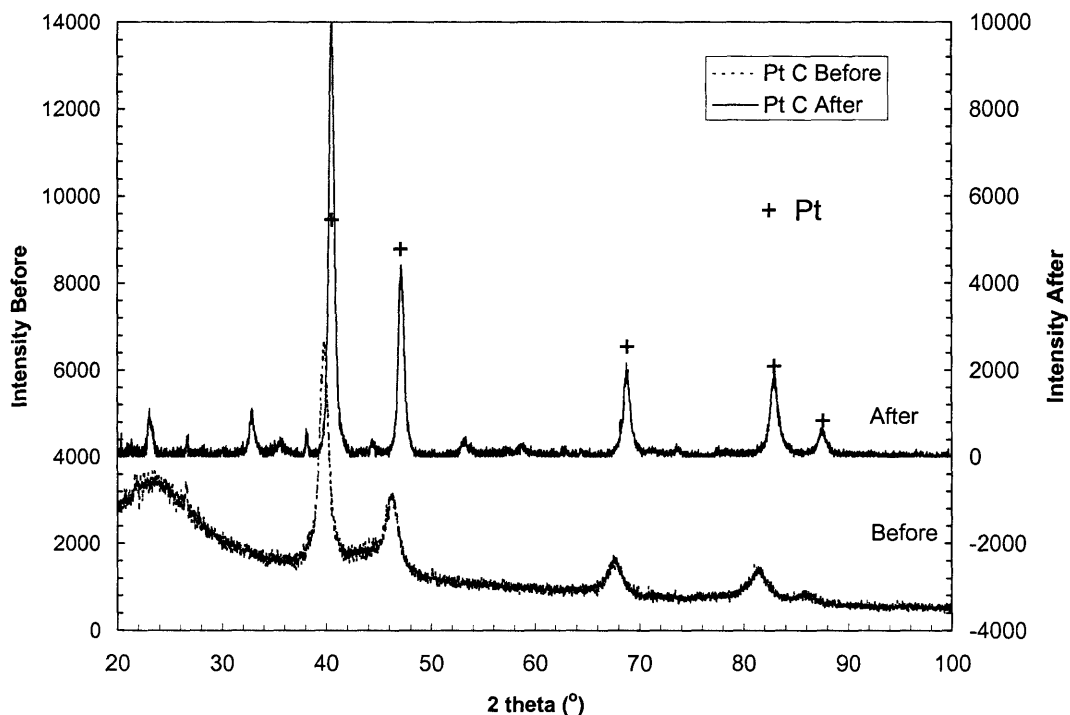
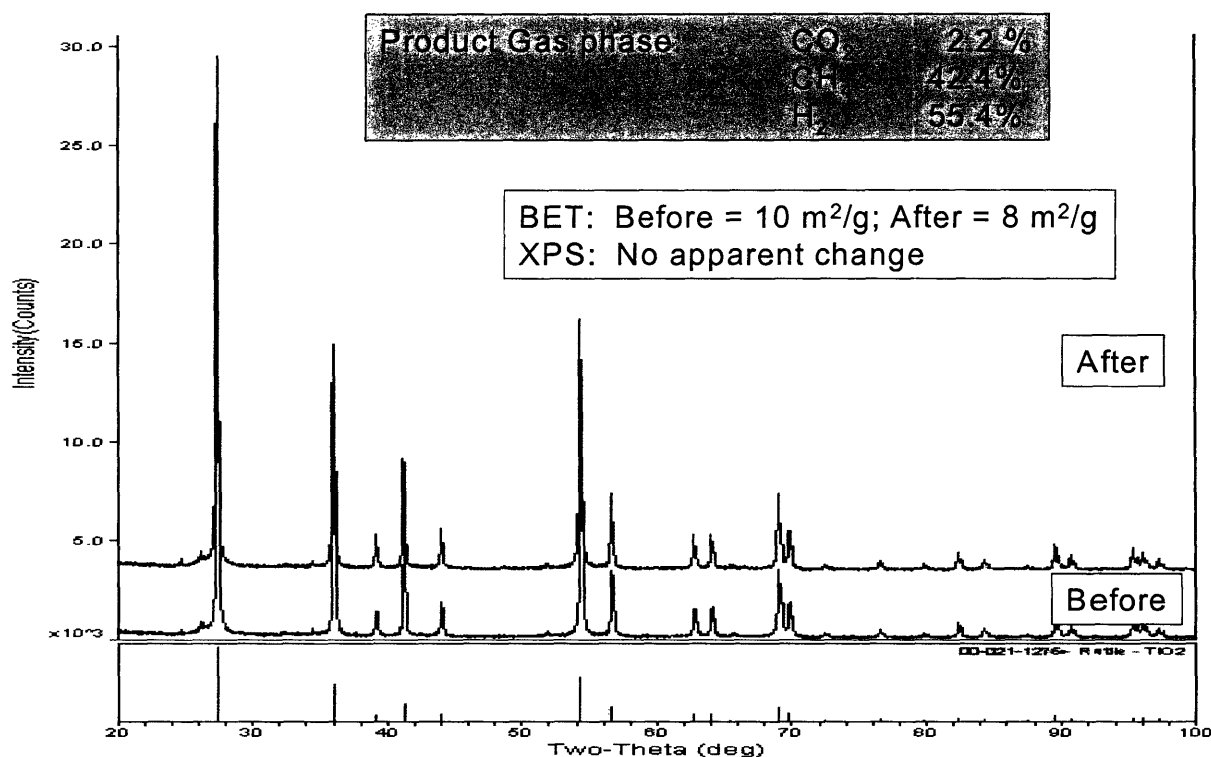


**Figure 4.8: XRD analysis of 10% Pt/activated carbon catalyst powder before and after exposure to SCW for 0.5 hours, 6000°C, 265 bar.**

#### 4.4.3 Ruthenium Catalyst:

**1% Ru/TiO<sub>2</sub> Pellets:** All analyses performed on the 1% Ru/TiO<sub>2</sub> catalyst pellets indicate very little transformation in SCW. The XRD traces of this catalyst before and after exposure to SCW are displayed in Figure 4-8. The XRD patterns are nearly identical, both displaying a high degree of crystallinity typical of the rutile phase of TiO<sub>2</sub>. Ruthenium appears to be oxidized in

both samples since minor peaks offer a better match to  $\text{RuO}_2$  than Ru metal. Unfortunately, XRD analysis of this small amount of ruthenium is complicated by the large, overlapping peaks of  $\text{TiO}_2$ , particularly near 28 and 54 degrees. An analysis was not performed on a pre-reduced



sample of this catalyst which may have revealed an oxidation of ruthenium in SCW.

**Figure 4.9: XRD analysis of 1% Ru/TiO<sub>2</sub> catalyst pellets before and after exposure to SCW for 0.7 hrs, 600°C, 300 bar.**

XPS and BET results also confirm that little change occurred with 1% Ru/TiO<sub>2</sub> pellets exposed to SCW. The BET surface area of this ruthenium catalyst before and after exposure to SCW was 9.74 and 7.58 m<sup>2</sup>/g respectively, indicating a small but measurable decrease. The XPS traces of the 1% Ru/TiO<sub>2</sub> pellets before and after SCW exposure were a nearly perfect match indicating no change of the elemental composition of the surface. The evidence here of catalyst

---

stability and its observed experimental activity to SCW reforming of methane make the ruthenium on titania combination the most promising catalyst of our study.

#### 4.4.4 Summary of Catalyst Analysis:

Table 4-4 summarizes the results of catalyst analysis for all metal catalysts used in this study and assigns an evaluation “grade” for their observed stability in SCW and activity for SCW reforming of methane. Further more extensive studies at longer SCW exposure times and more detailed analysis of fine chemical changes may alter these evaluations slightly, but they are in general agreement with previous catalyst studies under hydrothermal conditions, mostly at lower temperatures.

Table 4-5 provides an overall evaluation of various active metals and supports based on the results of this study. Results in Table 4.5 are, in part, consistent with those reported earlier in Table 4-3, which listed specific active metals and supports based on previous hydrothermal catalyst studies. The choice of ruthenium as the best active metal is fairly obvious based on its demonstrated activity and stability. Nickel and platinum were relatively inactive and showed signs of rapid aggregation and oxidation in SCW. Although titania and zirconia appeared to be stable in SCW, only titania was part of a metal-support combination that displayed activity to SCW reforming of methane.  $\alpha$ -alumina certainly showed signs of rapid degradation in SCW, but it may have been attributed to labile binders and promoters in the support that transformed in SCW destroying the integrity of the support. Activated carbon showed peculiar signs of transformation in SCW, but its past success at these conditions (see references to Professor Antal’s work (Antal, 1996)) and its association with some methane conversion in this study warrant a neutral evaluation here.

**Table 4.7 Summary of Catalyst Evaluation.** (+) indicated a positive evaluation. (+/-) indicates a neutral evaluation based on conflicting or inconclusive results. (-) indicates a negative evaluation.

Catalyst	XRD	XPS	BET	Overall Stability in SCW	Activity for SCW Reforming of Methane
KATALCO (18 wt% NiO on CaO/Al <sub>2</sub> O <sub>3</sub> spt) (Johnson Mathey)	(-)	(+)	(+)	(+/-)	(-)
C-11PR (~ 50 wt% NiO on Al <sub>2</sub> O <sub>3</sub> spt, Si) (Shell catalyst)	(-)	(-)	(-)	(-)	(-)
5% Pt/Al <sub>2</sub> O <sub>3</sub> powder (Alfa-Aesar)	(-)	(+)	(+/-)	(-)	(-)
0.5% Pt/Al <sub>2</sub> O <sub>3</sub> pellets (Alfa-Aesar)	(-)	(+)	(-)	(-)	(-)
1% Pt/ZrO <sub>2</sub> (proprietary)	(+)	(+)	N/A	(+)	(-)
1 % Pt/5% CeO/ZrO <sub>2</sub> (proprietary)	(+)	(+/-)	N/A	(~)	(-)
10% Pt/Activated Carbon (Alfa-Aesar)	(-)	(+)	(+)	(+/-)	(+)
1 % Ru/TiO <sub>2</sub> (Degussa)	(+)	(+)	(+)	(+)	(+)

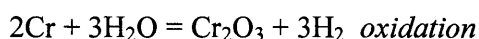
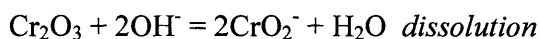
**Table 4.8 Most Promising Catalyst and Support Choices for SCW Reforming of Methane based on this study.** (+) indicated a positive evaluation. (+/-) indicates a neutral evaluation based on conflicting or inconclusive results. (-) indicates a negative evaluation.

Active Metal	Overall Grade Based on Stability and Activity in SCW
Ni	(-)
Ru	(+)
Pt	(-)
Supports	
$\alpha$ -Al <sub>2</sub> O <sub>3</sub>	(+/-)
TiO <sub>2</sub> (rutile)	(+)
ZrO <sub>2</sub> (monoclinic)	(+/-)
Activated Carbon	(+/-)

## 4.5 HOMOGENEOUS CATALYSIS RESULTS

As we discussed in Section 4.1.2, (Kruse and Dinjus, 2003) reported that one could achieve significant yields of hydrogen from reforming methane in SCW solutions of alkali salts. In an effort to reproduce their results, we achieved a similar hydrogen yield using a 1 wt% NaOH solution in a stainless steel tubular batch cell at 600°C, 245 bar and residence time of 30 minutes (48% by volume hydrogen gas yield). Kruse and Dinjus postulated a combination of two mechanisms; one where methane reformation is catalyzed by the reactor walls which may be activated due to corrosion and another mechanism where the alkali metal may be catalyzing the water gas shift through formation of a formate intermediate. We followed this initial experiment with a series of others to further explore these proposed mechanisms.

Using a direct injection batch cell design (see Section 3.4 for details), we conducted ten experiments in the same Hastelloy C-276 batch reactor to compare results of an inert gas (100% high purity argon) with alkali salt in supercritical water versus results when a methane-inert gas mix is loaded (10% methane in high purity argon). Figure 4.10 displays the results as gas volume yield of hydrogen after 15 minutes at 600°C and 275 – 300 bar. The fact that significant hydrogen is produced from an argon-alkali-SCW mix is readily explained if one considers the possible effects of general corrosion. This alkali environment may be dissolving the protective metal oxide layer on the reactor walls, exposing fresh, temporarily reduced metal to SCW which quickly oxidizes that metal producing hydrogen according to the following example reactions (Kritzer *et al.*, 1999):



Cloudy reactor effluents with particulates were observed which support the corrosion theory. We performed a semi-quantitative analysis of these reactor effluent samples using atomic absorption spectrometry and found measurable amounts of dissolved chromium and nickel ions ( $\sim 0.1 - 9$  ppm) (see Figure 4.11). The solid particulates responded to magnets. We dissolved the particulates with nitric acid and a thiocyanate spot test of the solution indicated the presence of iron. Also, the solution from the dissolved particulates qualitatively tested positive for chromium and nickel.

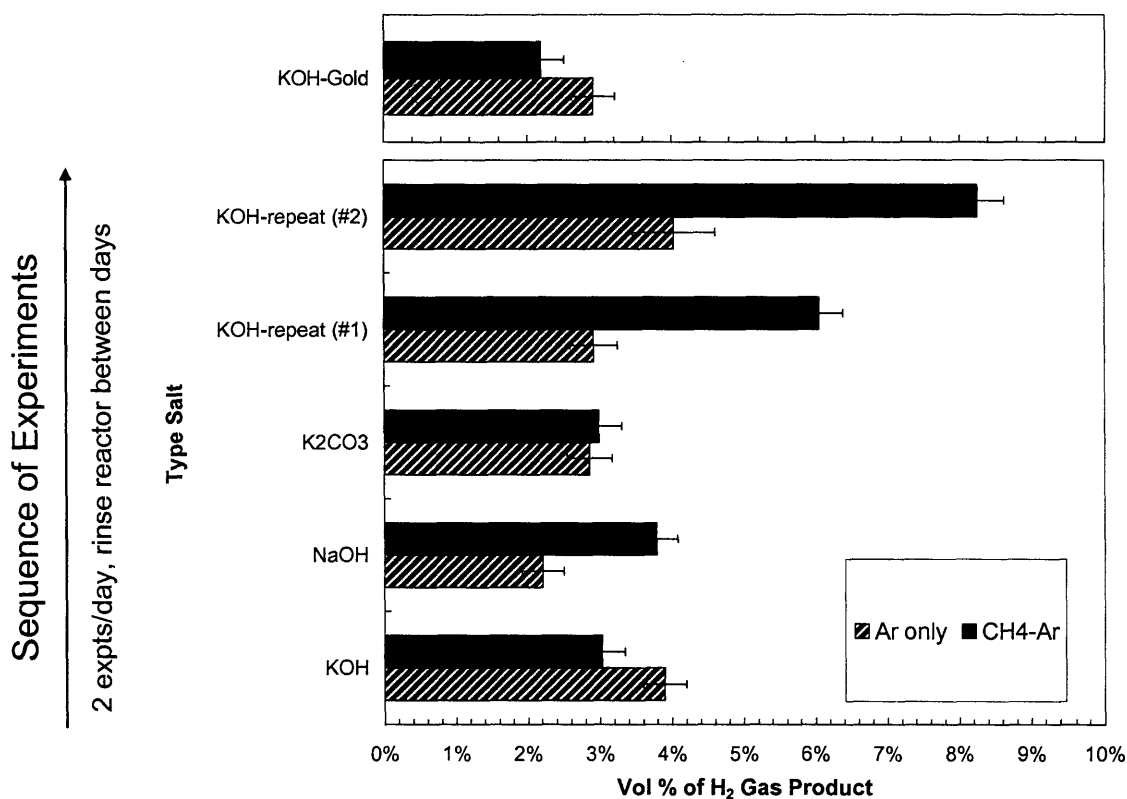


**Figure 4.10: Hydrogen Yield from Alkali-SCW mix: Argon versus Methane-Argon mix.** Yellow-hashed bars = Argon only gas feed. Green solid bars = 10% CH<sub>4</sub> in Argon gas feed. Data are from the same Hastelloy reactor, two experiments per day, successive days in order from bottom to top of y axis. One KOH experiment in gold-plated reactor displayed at top. Reaction Conditions: 600°C, 275-300 bar, 15 minutes, initial loading of gas 300psig (corresponds to [H<sub>2</sub>O]<sub>0</sub>/[CH<sub>4</sub>]<sub>0</sub> ~140 molar basis) salt 1 wt%.

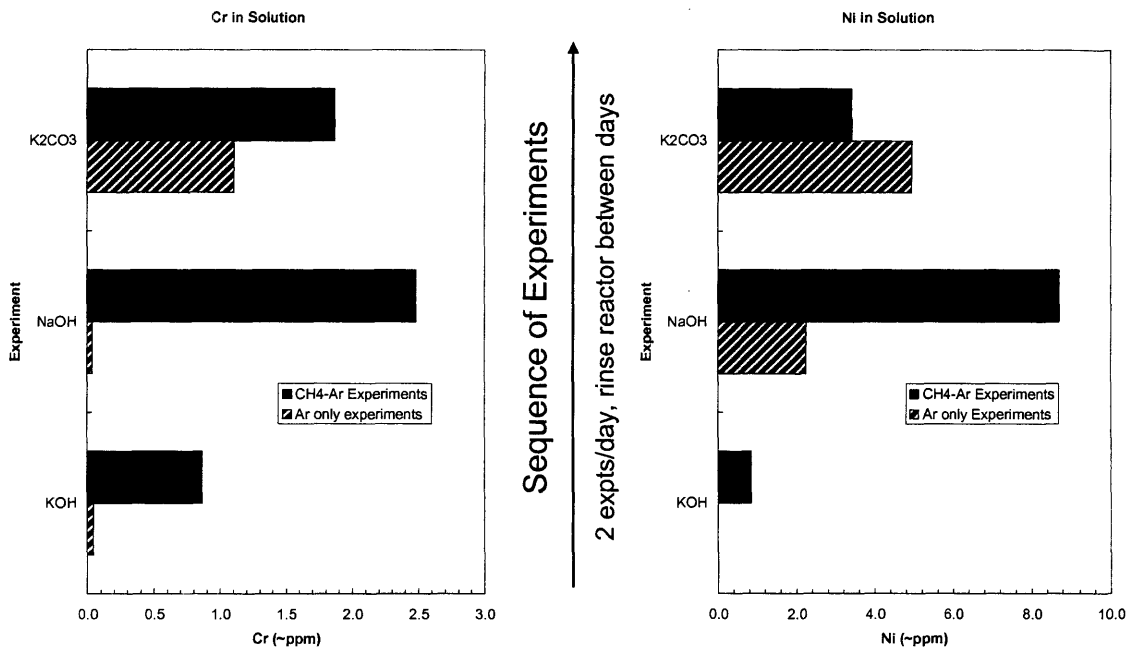


**Figure 4.11: Chromium and Nickel Ions in Liquid Phase from Alkali-SCW experiments: Argon versus Methane-Argon mix.** Yellow hashed bars = Argon only gas feed. Green solid bars = 10% CH<sub>4</sub> in Argon gas feed. Data are from the same Hastelloy reactor, two experiments per day, successive days in order from bottom to top of y axis. Reaction Conditions: 600°C, 275-300 bar, 15 minutes, initial loading of gas 300psig (corresponds to [H<sub>2</sub>O]<sub>0</sub>/[CH<sub>4</sub>]<sub>0</sub> ~140 molar basis), salt 1 wt%. Results are semi-quantitative only due to limited sample size.

Evidence of corrosion in this alkali-SCW nickel alloy reactor system can be found in previous studies. Under typical SCW conditions, alkali hydroxides do not dissociate and can form separate melt phases (Sue and Arai, 2004; and Ho, Palmer *et al.*, 2000). Gencheva has recently published several reports on the corrosion of nickel-based alloys in hydroxide melts (Tzvetkoff and Gencheva, 2003; Gencheva, Tzvetkoff *et al.*, 2005; Gencheva and Tzvetkoff, 2003). Although the conditions of these studies do not mirror SCW conditions, there have been



limited reports of similar alkali corrosion in SCW studies (Kritzer, Boukis *et al.*, 1999; Swallow, 2005; Sinag, Kruse *et al.*, 2004). In particular, Professor KC Swallow saw similar trends of chromium and nickel ions in the effluent at high pH conditions with Inconel 625 and Hastelloy reactors in SCW experiments at MODAR, Inc.

Results from experiments with the methane-argon gas feed warrant further discussion. In the first six experiments (two each using 1wt% KOH, NaOH and K<sub>2</sub>CO<sub>3</sub> salts), the hydrogen produced from a methane-argon mix is not significantly different than hydrogen that evolves with just argon as the gas feed. This result seems to indicate that methane continues to be refractory even in an alkali –SCW environment. The last four experiments were attempts at reproducing the first two experiments with a KOH feed. In the experiment labeled “KOH repeat #1”, we conducted the argon only experiment first and then the methane-argon experiment next in the same day, flushing the reactor with pure argon and cleaning our sampling system in between the experiments. In the experiment labeled “KOH repeat #2” we switched the order of the experiments, using the methane-argon feed first, then the argon only feed next in the same day. As one can see in Figure 4.10, these reproducibility runs resulted in roughly the same hydrogen yield for argon only feeds and sequentially more hydrogen for the methane argon feeds. The methane-argon feeds also produced very small, but measurable amounts of CO and CO<sub>2</sub> in the gas phase (~0.1 vol%). In all alkali experiments we expect to see most of the evolved CO<sub>2</sub> to be dissolved in the basic aqueous phase. One explanation for more hydrogen from methane-argon feeds is the possible increasing catalytic activity of the reactor walls as they are further exposed to more alkali salt environments with each experiment.

In an attempt to prevent the effects of corrosion and focus on other possible pathways with alkali-SCW mixtures, two experiments were conducted with a gold-plated version of the

same direct-inject batch reactor. The reactor was 316SS constructed of the same high pressure fittings with similar internal volumes, but it was plated with 300-400 micro-inches of pure nickel and then 30-50 micro-inches of pure gold by F.M. Callahan & Son, Inc. of Malden, MA. The method of nickel plating was electroless precipitation of nickel while the method of gold plating was the traditional electrochemical deposition with electrodes. Surprisingly, the hydrogen yield results were similar, but the effluents were clear with no visible particles possibly indicating the absence of aggressive corrosion. Hydrogen yield from the argon-alkali-SCW experiment was 2.91 % of the gas volume and 2.19% for the methane-argon-alkali-SCW experiment. These values are very similar, but slightly smaller than the results of our first experiment in the unplated Hastelloy reactor (see Figure 4.10) which may also indicate some oxidation of the new gold plating as part of a conditioning of the reactor. More experiments are warranted to more clearly discern the fate of gold in this environment and its influence, if any, on the SCW reforming of methane.

The results of this small study on alkali salts in SCW reactors call into question previous claims of alkali catalysis under these conditions. While our study does not refute the fact that increased conversion of hydrocarbons in SCW-alkali mixtures occurs, but it does identify the important role that aggressive corrosion plays in those results. There have been several studies which report a “catalytic” effect of alkali salts in sub-critical and supercritical water, and some of them report on observed corrosion, but none of them have focused on the importance that corrosion may play in this reaction medium (Kruse and Dinjus, 2005; Kruse, Meier *et al.*, 2000; Schmieder, Abeln *et al.*, 2000; Elliott and Sealock, 1983; Elliott, Sealock *et al.*, 1986). Although Kruse and Dinjus admit that activation of reactor walls may be an important part of a reaction pathway in this environment, they do not conclude that most of the hydrogen being measured

may be from the oxidation of the reactor metal alone, and not from methane at all. It is difficult to precisely measure methane conversion in these experiments due to the difficulty of quantifying feeds and products in these small batch cells. Since carbon dioxide may also partition into difficult-to-detect carbonates in the high pH aqueous product, it is extremely challenging to close the carbon balance for these experiments or measure methane conversion based on the evolution of carbon products. Using  $CD_4$  or  $D_2O$  in lieu of  $CH_4$  and  $H_2O$  might be an effective way of identifying the true source of hydrogen evolution in this complex environment.

#### 4.6 CONCLUSIONS

An experimental study of the catalytic reformation of methane in SCW was completed that explored the use of carefully chosen catalysts under a variety of conditions and measured the conversion of methane and yields of various products. Eight metal catalysts were selected based on a thorough review of previous catalysis experiments in hydrothermal conditions and those thought to be active for methane reforming. The range of conditions studied included 350 – 630°C, 150 – 400 bar, 0.01 – 2 wt% methane, 10 seconds to 72 minutes residence time, and with and without catalyst. Four different reactor designs were employed in this study; a PBR, a CSTR and two different batch reactor designs. A variety of techniques for reducing the metal catalysts and keeping them active in SCW were examined.

Despite the range of conditions studied here, significant conversion of methane was never achieved. The most encouraging sign of conversion was a relatively low yield of  $CO_2$  (2.19% of the product gas volume) in the experiments employing the 1% Ru/ $TiO_2$  catalyst pellets. A thorough analysis of each catalyst before and after exposure to SCW revealed significant

degradation and helped to explain low methane conversions. Based on this analysis and our experimental results, the most promising catalyst identified was 1% Ru/TiO<sub>2</sub>. Similarly, the most promising active metal was ruthenium, and the most promising supports were titania (rutile) with some promise for zirconia and activated carbon. Although active for steam reforming and other hydrothermal catalyst applications, the nickel and platinum catalysts used in this study showed signs of rapid degradation and deactivation.

Experiments with alkali salts in SCW revealed the importance of corrosion in the evolution of hydrogen from this media. Comparable amounts of hydrogen were produced from argon-alkali-SCW mixtures and from methane-argon-alkali-SCW mixtures suggesting that a significant amount of hydrogen in SCW reaction effluents can be attributed to oxidation of metal reactor material and not from hydrocarbon sources. Additional SCW alkali salt experiments in the same Hastelloy reactor revealed an increasing activation of methane, further emphasizing the likely importance of progressive corrosion. Comparable experiments in a gold-plated reactor still showed evidence of hydrogen generation from metal oxidation, but did not show evidence of corrosion.

#### 4.7 REFERENCES

- Antal, M. (1996) "Catalytic supercritical gasification of wet biomass" USA, Patent #WO9630464.
- Antal, M. J., Jr.; Allen, S.G.; Schulman, D.; Xu, X.; Divilio, R.J. (2000). "Biomass Gasification in Supercritical Water." *Ind. Eng. Chem. Res.* **39**(11): 4040-4053.
- Baiker, A. (1999). "Supercritical Fluids in Heterogeneous Catalysis." *Chem. Rev.* **99**: 453-473.
- Boukis, N., V. Diem, et al. (2003). "Methanol reforming in supercritical water." *Ind. Eng. Chem. Res.* **42**(4): 728-735.

- 
- Choudhary, T. V., E. Aksoylu, et al. (2003). "Nonoxidative Activation of Methane." *Catalysis Reviews* **45**(1): 151-203.
- Davda, R. R. and J. A. Dumesic (2003). "Catalytic Reforming of Oxygenated Hydrocarbons for Hydrogen with Low Levels of Carbon Monoxide." *Angew. Chem. Int. Ed.* **42**: 4068-4071.
- Davda, R. R. S., J.W.; Huber, G.W.; Cortright, R.D.; Dumesic, J.A. (2003). "Aqueous-phase reforming of ethylene glycol on silica-supported metal catalysts." *Appl Catal B-Environ* **43**: 13-26.
- Ding, Z. Y., M. A. Frisch, et al. (1996). "Catalytic Oxidation in Supercritical Water." *Ind. Eng. Chem. Res.* **35**: 3257-3279.
- Elliott, D. C. and L. J. Sealock, Jr. (1983). "Aqueous catalyst systems for the water-gas shift reaction. 1. comparative catalyst studies." *ind. Eng. Chem. Prod. Res. Dev.* **22**: 426-431.
- Elliott, D. C., L. J. Sealock, Jr., et al. (1997) "Method for the catalytic conversion of organic materials into a product gas" USA, Patent #5616154.
- Elliott, D. C. and L. J. Sealock, Jr. (1998) "Improved catalyst formulations for use in wet biomass gasification: ruthenium stabilized nickel metal" USA, Patent #5,814,112.
- Elliott, D. C., L. J. Sealock, Jr., et al. (1986). "Aqueous catalyst systems for the water-gas shift reaction. 3. continuous gas processing results." *ind. Eng. Chem. Prod. Res. Dev.* **25**: 541-549.
- Elliott, D. C., T. A. Werpy, et al. (2001) "Ruthenium on rutile catalyst, catalytic system, and method for aqueous phase hydrogenations" USA, Patent #6235797.
- Elliott, D. C. N., G.C.; Hart, T.R.; Butner, R.S.; Zacher, A.H.; Engelhard, M.H.; Young, J.S.; McCready, D.E. (2004). "Chemical Processing in High-Pressure Aqueous Environments. 7. Process Development for Catalytic Gasification of Wet Biomass Feedstocks." *Ind. Eng. Chem. Res.* **43**: 1999-2004.
- Frisch, M. A., L. Li, et al. (1994). "Catalyst evaluation: Supercritical water oxidation process". *49th Purdue Industrial Waste Conference*, Lewis Publishers.
- Gencheva, P. and T. Tzvetkoff (2003). "Corrosion and anodic oxidation of Ni and Ni-Cr alloy in NaOH melts." *Journal of the University of Chemical Technology and Metallurgy* **38**(3): 973-980.
- Gencheva, P., T. Tzvetkoff, et al. (2005). "Composition and conduction mechanism of the surface oxide film on Ni-based alloys in molten hydroxide." *Applied Surface Science* **241**: 459-470.

- Golodets, G. I. (1983). Heterogeneous Catalytic Reactions Involving Molecular Oxygen. Amsterdam, Elsevier.
- Hirth, T. and E. U. Franck (1993). "Oxidation and Hydrothermolysis of Hydrocarbons in Supercritical Water at High Pressures." *Ber. Bunsenges. Phys. Chem.* **97**(9): 1091-1098.
- Ho, P., D. Palmer, et al. (2000). "Conductivity measurements of dilute aqueous LiOH, NaOH and KOH solutions to high temperatures and pressures using a flow-through cell." *J. Phys. Chem. B* **104**: 12084-12089.
- Huber, G., R. D. Cortright, et al. (2004). "Renewable Alkanes by Aqueous-Phase Reforming of Biomass-Derived Oxygenates." *Angew. Chem. Int. Ed.* **43**: 1549-1551.
- Huber, G., J. W. Shabaker, et al. (2003). "Raney Ni-Sn catalyst for H<sub>2</sub> production from biomass-derived hydrocarbons." *Science* **300**: 2075-2077.
- Kritzer, P., N. Boukis, et al. (1999). "Factors controlling corrosion in high-temperature aqueous solutions: a contribution to the dissociation and solubility data influencing corrosion processes." *J. Supercrit. Fluid* **15**(3): 205-227.
- Kruse, A. and E. Dinjus (2003). "Hydrogen from Methane in Supercritical Water." *Angewandte Che. Int. Ed.* **42**(8): 909-911.
- Kruse, A. and E. Dinjus (2005). "Influence of salts during hydrothermal biomass gasification: the role of the catalysed water-gas shift reaction." *Z. Phys. Chem.* **219**: 341-366.
- Kruse, A., D. Meier, et al. (2000). "Gasification of pyrocatechol in supercritical water in the presence of potassium hydroxide." *Ind. Eng. Chem. Res.* **39**: 4842-4848.
- Lee, J. H. and N. R. Foster (1996). "Direct Partial Oxidation of Methane to Methanol in Supercritical Water." *The Journal of Supercritical Fluids* **9**: 99-105.
- Matsumura, Y., X. Xu, et al. (1997). "Gasification characteristics of an activated carbon in supercritical water." *Carbon* **35**(6): 819-824.
- Minowa, T. and T. Ogi (1998). "Hydrogen production from cellulose using a reduced nickel catalyst." *Catalysis Today* **45**: 411-416.
- Muradov, N. (2001). "Catalysis of methane decomposition over elemental carbon." *Catalysis Communications* **2**: 89-94.
- Myers, D. B. (2000). "Steam Reforming of Methane with Nickel Aluminate-Based Catalysts." Master of Science in Chemical Engineering thesis, Department of Chemical Engineering, MIT, Cambridge, MA.

- Osada, M., T. Sato, et al. (2004). "Low-temperature catalytic gasification of lignin and cellulose with a ruthenium catalyst in supercritical water." *Energy and Fuels* **18**: 327-333.
- Park, K. C. and H. Tomiyasu (2003). "Gasification reaction of organic compounds catalyzed by RuO<sub>2</sub> in supercritical water." *Chem. Commun.* **6**: 694-695.
- Pinkwart, K., T. Bayha, et al. (2004). "Gasification of diesel oil in supercritical water for fuel cells." *Journal of Power Sources* **136**: 211-214.
- Reynolds, W. C. (1986). *The Element Potential Method for Chemical Equilibrium Analysis: Implementation in the Interactive Program STANJAN*, Department of Mechanical Engineering, Stanford University.
- Rostrup-Nielsen, J. R. (1975). Steam Reforming Catalysts: An investigation of catalysts for tubular steam reforming of hydrocarbons. Copenhagen, Danish Technical Press, Inc.
- Rostrup-Nielsen, J. R. (1984). Catalytic Steam Reforming. New York, Springer-Verlag.
- Savage, P. E. (2000). "Heterogeneous catalysis in supercritical water." *Catalysis Today* **62**: 167-173.
- Schmieder, H., J. Abeln, et al. (2000). "Hydrothermal gasification of biomass and organic wastes." *J. of Supercritical Fluids* **17**: 145-153.
- Shabaker, J. W., G. Huber, et al. (2004). "Aqueous-phase reforming of oxygenated hydrocarbons over Sn-modified Ni catalysts." *Journal of Catalysis* **222**: 180-191.
- Sinag, A., A. Kruse, et al. (2004). "Influence of the heating rate and the type of catalyst on the formation of key intermediates and on the generation of gases during hydrolysis of glucose in supercritical water in a batch reactor." *Ind. Eng. Chem. Res.* **43**: 502-508.
- Sue, K. and K. Arai (2004). "Specific behavior of acid-base and neutralization reactions in supercritical water." *J. of Supercritical Fluids* **28**: 57-68.
- Swallow, K. C. (2005). Discussion of MODAR SCWO corrosion study. R. Lachance. Andover, Ma.
- Taylor, J., C. Herdman, et al. (2003). "Hydrogen production in a compact supercritical water reformer." *Int. J. Hydrogen Energy* **28**: 1171-1178.
- Tomita, K. and Y. Oshima (2004). "Enhancement of the catalytic activity by an ion product of sub- and supercritical water in the catalytic hydration of propylene with metal oxide." *Ind. Eng. Chem. Res.* **43**: 2345-2348.
- Trimm, D. L. (1987). "Methane Conversion". *Symposium on the Production of Fuels and Chemicals from Natural Gas*, Auckland, New Zealand, Elsevier.

- 
- Twigg, M. V., Ed. (1989). *Catalyst Handbook*. Frome, England, Wolfe Publishing Ltd.
- Tzvetkoff, T. and P. Gencheva (2003). "Mechanism of formation of corrosion layers on nickel and nickel-based alloys in melts containing oxyanions - a review." *Materials Chemistry and Physics* **82**: 897-904.
- Vogel, F. (2005). Discussion of PSI Hydrothermal Research. R. Lachance. Villigen.
- Vogel, F. H., F. (2002). "Catalytic Hydrothermal Gasification of Woody Biomass at High Feed Concentrations." *Chem. Eng. Trans.* **2**: 771.
- Waldner, M. H. V., Frederic (2004). "Catalytic Hydrothermal Gasification of Woody Biomass". *2nd World Conference on Biomass for Energy, Industry and Climate Protection*, Rome, Italy.
- Watanabe, M., M. Osada, et al. (2003). "Acidity and basicity of metal oxide catalysts for formaldehyde reaction in supercritical water at 673K." *Appl Catal A: General* **245**: 333-341.
- Webley, P. A. and J. W. Tester (1991). "Fundamental Kinetics of Methane Oxidation in Supercritical Water." *Energy and Fuels* **5**(3): 411-419.
- Xu, X. M., Yukihiko; Stenberg, Jonny; Antal, Michael Jerry, Jr. (1996). "Carbon-Catalyzed Gasification of Organic Feedstocks in Supercritical Water." *Industrial & Engineering Chemistry Research* **35**(8): 2522-2530.
- Xu, X. A., M.J., Jr. (1998). "Gasification of sewage sludge and other biomass for hydrogen production in supercritical water." *Environmental Progress* **17**(4): 215-220.

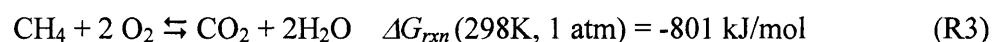
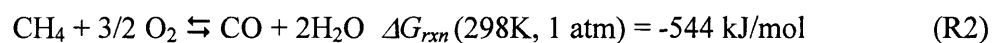
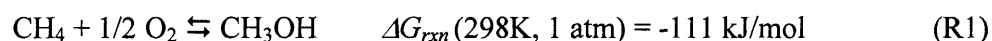


## 5 SCW POX of Methane – An Elementary Reaction Modeling Study

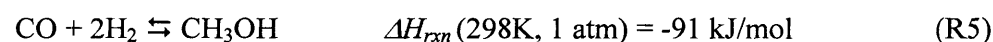
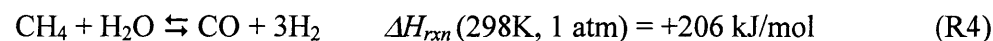
### 5.1 INTRODUCTION

#### 5.1.1 Background on Direct Partial Oxidation of Methane

Since its discovery in the earlier 1900s, the direct partial oxidation (POX) of methane to methanol has been studied extensively as an attractive potential industrial process to convert our vast stores of natural gas resources to more useful liquid fuels. However, high yields of methanol continue to be elusive. It is difficult to convert the more refractory methane faster than the further oxidation of the more labile methanol; as soon as you make methanol, it reacts away. The key reactions for the oxidation of methane indicate that while the formation of methanol is thermodynamically feasible, production of carbon monoxide and carbon dioxide are more favored:



The current commercial process for the conversion of methane to methanol has two main steps: initial conversion of methane to synthesis (syn) gas by catalytic steam reforming (R4) followed by catalytic conversion of the sny gas to methanol (R5).



This process suffers from complications due to detailed engineering steps, catalyst degradation issues for the nickel steam reforming catalysts and the copper-zinc-alumina syn gas-to-methanol catalysts, and inefficiencies from the indirect approach of oxidizing methane then reducing the CO product. Clearly a direct conversion of methane to methanol should have less complications and be more energetically efficient.

Gas-phase direct partial oxidation to methanol experiments were first conducted in the 1930s (Gesser, Hunter *et al.*, 1985). These earlier studies achieved a maximum methanol selectivity (defined as moles of product over moles of reactant consumed) of 54% at 3% conversion at elevated pressures (50 – 160 atm), moderate temperatures (300 - 450°C) and moderate times (1-100 min). More recent studies have observed methanol selectivities up to 80% and methane conversion up to 10% (Foulds and Gray, 1995) at similar conditions. Economic analysis reported by Foulds and Gray (1995) have demonstrated that, with methanol selectivity greater than 70% at 8-15% methane conversion, the direct partial oxidation conversion of methane would be able to compete with the current indirect method of methanol production from syngas derived by steam reforming methane. Although a few gas phase studies have approached this challenging commercial target (see Figure 5.1), often results have been difficult to reproduce and most studies fall well short of this goal (Zhang, He *et al.*, 2002). Several other research studies have examined alternate routes like catalytic partial oxidation of methane to methanol (Hall, Hargreaves *et al.*, 1995) and partial oxidation in plasma reactors (Nozaki, 2004) with similar results. In the early 1990s, controlled oxidation in supercritical water was first proposed as a possible approach to the daunting challenge of maximizing methanol yield in the presence of an oxidizing environment for methane. SCW researchers hypothesized that the unique chemistry and solvent properties of SCW may enhance methanol

yields at methane conversions higher than previously realized (i.e., > 15%). The section that follows presents the results of these studies.

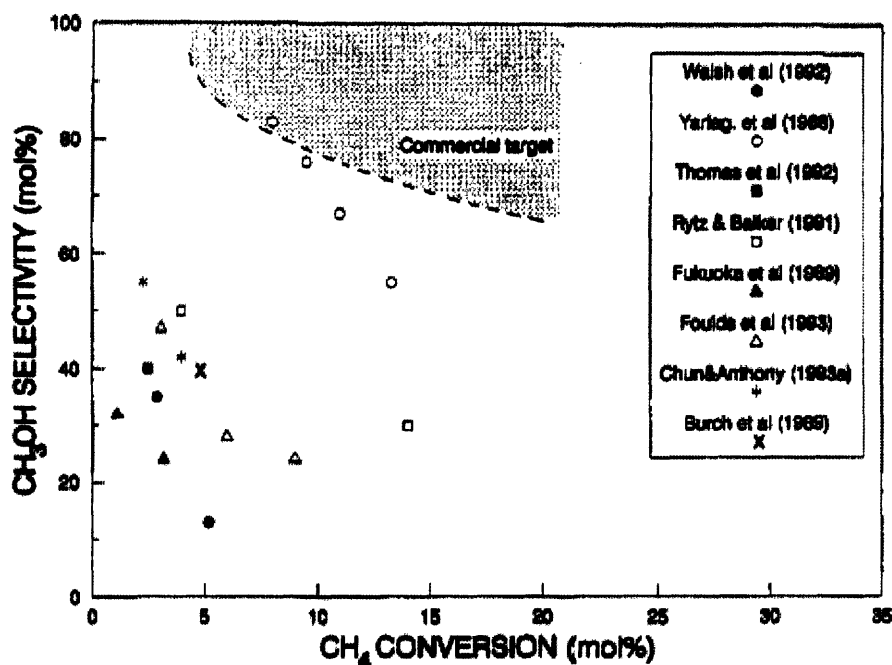


Figure 5.1 Methanol Selectivity as a function of methane conversion – most promising gas phase data. (Foulds and Gray, 1995)

### 5.1.2 Previous SCW Methane POX Studies

Seven previous studies of methane SCW POX (Hirth and Franck, 1993; Savage, Li *et al.*, 1994; Dixon and Abraham, 1992; Aki and Abraham, 1994; Lee and Foster, 1996; Broll, Kramer *et al.*, 2002; Sato, Watanabe *et al.*, 2003) were identified and reviewed. Table 5.1 outlines key operating conditions of these studies along with conversion and selectivity results. In general, these initial SCW POX studies resulted in similar conversions and selectivities to gas phase studies. Catalysts used in these studies had little influence in methanol selectivity. A closer examination of each of these studies reveals issues that may warrant further research of methane

Table 5.1. Conditions and Details of Previous Methane SCW POX Studies and Resulting Conversions and Selectivities

Investigators	[CH <sub>4</sub> ] (mM)	[O <sub>2</sub> ] (mM)	T (°C)	P (bar)	τ (sec)	Reactor type	Reactions Explored	X (%)	S <sub>MEOH</sub> (%)
Hirth & Franck, '93	30 mol %	0 - 30 mol %	380 - 440	300 - 1000	NR	Semi-batch, Ni alloy	~ 20 SCWO 2 SCW hydrolysis	NR	0 - 22
Dixon & Abraham, '92	94 - 627	8.7 - 5470	450	114 - 439	5 - 40 min	Batch, SS, 3/8" tube	14 catalytic SCW POX to CH <sub>3</sub> OH	7 - 30	~10 - 40
Savage et al, '94	690 - 3750	53 - 256	349 - 481	~245	1 - 9 min	Batch, SS & glass lined	39 SCW POX to CH <sub>3</sub> OH	0.01 - 5.86	4 - 75
Aki & Abraham, '94	0.5% CH <sub>4</sub> in N <sub>2</sub>	4.79e-3	400 - 475	241	13-31	Flow	Catalytic POX to CH <sub>3</sub> OH and HCOOH	2.3 - 17.8	0 - 1.7
Lee & Foster, '96	189 - 387	0 - 13.1	400 - 450	250	6.4 - 84.1	PFR, laminar	41 SCW POX to CH <sub>3</sub> OH	0 - 4.7	20 - 38
Broll et al, '02	0.1 - 4 mol %	0.1 - 2 mol %	375 - 500	220 - 350	0.5 - 60	Differential loop flow reactor	> 200 catalytic SCW POX to CH <sub>3</sub> OH	0 - 11	~10 - 60
Sato et al, '04	300	9	400	200 - 350	29 - 117	PFR, SS316	25 POX expts density effects	0.51 - 3	20 - 40

---

SCW POX to examine a wider range of temperature, pressure, concentration, and residence time conditions.

Hirth and Franck (1993) conducted several experiments with methane in supercritical water; two sets of those experiments explored methanol selectivity from SCW POX of methane. The first set employed a batch view cell operated in a semi-batch mode where methane and pure water were initially loaded (70% H<sub>2</sub>O/30% CH<sub>4</sub>), heated and pressurized, and pure oxygen was metered in at 1–5 mm<sup>3</sup>/s. Samples were drawn at different CH<sub>4</sub>/O<sub>2</sub> ratios corresponding to different times following the initiation of oxygen flow. Their results showed the highest methanol selectivity at the higher pressures and highest CH<sub>4</sub>/O<sub>2</sub> ratios;  $S_{MEOH} = 22\%$  at CH<sub>4</sub>/O<sub>2</sub> = 40, at 600 bar. The second set of experiments included the addition of cobalt chloride and cobalt acetate as possible homogeneous POX catalysts and platinum surfaces as a possible heterogeneous catalyst. No enhancement was observed with these additional ingredients.

It is difficult to properly assess the success or failure of the Hirth and Franck study due to the lack of reported data (e.g., no reported residence time, no reported conversion data). However, this semi-batch study was most likely plagued by issues associated with experiments in similar SCW batch equipment. Judging from the description of the experimental apparatus and procedures, improper mixing, non-isothermal dead volumes, and difficulty with phase separation during sampling of this high methane concentration mixture may have affected results. Hirth and Franck admitted in their paper that complete mixing, identified “by the gradual disappearance of a darkening of the reactor contents,” could take as long as one hour, which brings into question how long they waited to sample the reactor contents, particularly after injecting a small amount of oxygen, corresponding to high methane-oxygen ratios and high methanol selectivity. Other issues with the Hirth and Franck study include operating at 380°C

which is very close to the critical point of water at 374°C. In this near critical region it is often difficult to obtain reliable data. Specifying and maintaining isothermal conditions by apparently measuring temperature from only one thermocouple and operating at such high methane concentrations is also questionable.

Dixon and Abraham (1992) explored both gas phase and SCW POX of methane in the presence of  $\text{Cr}_2\text{O}_3$  as a catalyst in small stainless steel tube batch cells. Each 1.26 mL batch reactor was loaded with 0.8mg of the catalyst, 0.4g of water and a mixture of gases to reach 51.7 bar. The batch tubes were then lowered into a fluidized sand bath (heatup time ~ 1 minute) and quenched in a water bath after the desired reaction time. At a given reaction time, SCW POX methane conversions were much lower than gas phase conversions (approximately half as much), but no methanol was detected in any gas phase experiment. The highest methanol selectivity achieved was 40% at a methane conversion of 10% corresponding to a methanol yield of 4% (yield defined as moles of product over initial moles of reactant).

As with the semi-batch study of Hirth and Franck, the batch study of Dixon and Abraham may have suffered from similar challenges of SCW batch experiments. This article did not report on deliberate measures taken to ensure a well-mixed environment, which may have been an issue since it appears that the solid catalyst was sitting at the bottom of a vertical tube. Dixon and Abraham also operated with relatively high initial methane concentrations which may have caused issues maintaining isothermality and possibly contributing to phase separation in dead volume zones of the reactor. Additional issues with this study contribute to the difficulty of fully assessing the data. For example, Dixon and Abraham did not report on any experiments without catalyst to provide a comparison of the true effect of the catalyst nor did they report on characterizing the catalyst before or after their experiments leaving questions like catalyst

activity and stability unanswered. Also, this study used naphthalene as an internal standard for aqueous phase analysis and quantification which may have been problematic due to naphthalene's low solubility in water.

Savage *et al.* (1994) also explored SCW POX of methane in stainless steel tube batch cells, but did not employ any catalysts. They also examined results when using glass liners in their batch cells. Their experimental procedure was nearly identical to that of Dixon and Abraham, first loading the tubes, then heating them in a fluidized sand bath, then quenching them in water. The maximum conversion of CH<sub>4</sub> achieved was 6%, and methanol selectivity ranged from 4 – 75%, but high selectivity corresponded to extremely low conversions (0.04%). Experiments with glass-lined reactors resulted in higher methanol yields, but also higher methane conversions which kept methanol selectivity down to less than 15%.

As with the previous two SCW batch studies mentioned, the Savage *et al.* study had several issues which made data interpretation difficult. The tube batch cells and the procedure used in this study seemed to be similar to the cells and procedure used in the Dixon and Abraham study and most likely suffered from similar issues of limited mixing, possible phase separation and reactor dead volume zones. The reported low oxygen conversion figures indicated possible issues with mixing or sampling. The data table given by Savage *et al.* (1994) reported the highest oxygen conversion as 27.3% at the highest temperature of 481°C and longest residence time of 5 minutes. A 27.3% conversion is very low compared with other studies at similar conditions. Savage and co-workers report lower methane conversions than flow studies under similar conditions which may also be attributed to a lack of mixing or sampling issues.

Aki and Abraham (1994) were first to report the results of flow experiments on methane SCW POX. As with Abraham's earlier batch study, this work employed catalysts, Cr<sub>2</sub>O<sub>3</sub>/Al<sub>2</sub>O<sub>3</sub>

---

and MnO<sub>2</sub>/CeO, but the feed was a 0.5% CH<sub>4</sub> in nitrogen gas mixture along with oxygen dissolved in water at atmospheric pressure. Although higher methane conversions were achieved (maximum of 17.8% with MnO<sub>2</sub>/CeO), methanol selectivity suffered, peaking at 1.7% with Cr<sub>2</sub>O<sub>3</sub>/Al<sub>2</sub>O<sub>3</sub> at 475°C, 32.4s, and a O<sub>2</sub>/CH<sub>4</sub> ratio of 0.024. This study reported on the production of formic acid as well; achieving a maximum selectivity of 70% at a conversion of 6.7% over the MnO<sub>2</sub>/CeO catalyst. A thorough critique of the Aki & Abraham study could not be completed since we were not able to retrieve a copy of the entire manuscript.

Lee and Foster (1996) conducted a kinetic investigation of methane SCW POX to methanol in a Hastelloy C276, laminar flow reactor without catalyst. Although the main goal of this study was to determine a global kinetic rate expression for methane oxidation under oxygen deficient conditions, the authors also reported on the effects reaction parameters had on the selectivity of methanol. They found a maximum methanol selectivity of approximately 35% at methane conversions of 1-3% between 400 – 410°C, with selectivity decreasing as oxygen conversion increased.

The presentation of this study by Lee and Foster is very detailed, providing a complete description of their experimental apparatus, analysis of that apparatus and procedures employed. However, there still may have been issues associated with incomplete mixing due to laminar flow and high methane concentrations which may make data interpretation difficult. As Vogel *et al.* (2005) pointed out in a critique of a methanol study by Lee and Foster conducted in a similar apparatus to their methane work, the hydrodynamics of their laminar flow reactor may be responsible for results different than those achieved with experiments under turbulent, plug-flow conditions. Also, there may have been some issues with two-phase flow in the quench and sampling section of their apparatus which may have complicated their results.



Broll and co-workers (2002) conducted a very thorough methane SCW POX study, but their focus was on the effect of different catalysts. The catalysts they investigated were chips of Inconel 625, sheets of Cu, Ag/Cu alloy sheets (72% Ag), Ag sheets, Au-Ag alloy sheets (2.8% Ag) and Al<sub>2</sub>O<sub>3</sub> supported Ag catalyst. Cold, pure methane was fed via a booster while a hydrogen peroxide solution was preheated and decomposed to provide the oxygen. The two feeds mixed and reacted in a differential loop reactor with mixing from a jet-loop principle (Broll, Kramer *et al.*, 2001). In the experiments without catalyst, selectivity towards methanol was only high at very low conversion ( $S \sim 60\%$  at  $X < 1\%$ ). The presence of heterogeneous catalysts showed little influence on methane conversion and methanol selectivity; most often promoting total oxidation beyond intermediates products like methanol. However, reactor material like Inconel 625 was found to have a catalytic effect; the impact of which should be carefully considered in studies using similar reactor materials.

This report by Broll *et al.* is extremely thorough, providing sufficient detail to properly assess their data. The differential loop reactor described in this study is an intriguing approach to SCW experiments, but the authors should analyze this reactor design in more detail to fully characterize the jet mixing employed and investigate possible reactant by-passing of the catalyst to the reactor outlet. A lack of additional details on the activity and stability of the catalysts used prevents a proper analysis of choosing the best catalyst for SCW POX of methane. Broll and co-workers also operated with high methane concentrations, and, as discussed above with previous studies, there may have been two-phase flow issues particularly in the quench and sampling sections of their apparatus.

Sato *et al.* (2004) used a flow reactor to explore the effects of density on methane SCW POX. Using a preheated, aqueous hydrogen peroxide solution as a source of oxygen and a

---

methane-neon boosted gas feed (neon was used as an internal standard), the reactants were fed to a stainless steel coiled tube reactor in a molten sand bath. This study achieved results very similar to the earlier non-catalytic flow study by Lee and Foster; maximum conversion of 3% and a maximum selectivity of approximately 35%. Higher pressures corresponding to higher water densities resulted in higher methanol and formaldehyde yields, but both maximum yields were less than 1% of the methane feed.

In many ways, the study by Sato and co-workers is similar to that of Lee and Foster; accordingly, the critique of this study will be similar. Laminar flow and high methane concentrations may have resulted in incomplete mixing and two-phase down-stream flow and separation issues. Unlike Lee and Foster, Sato's group did examine a wide range of pressures and explored the density effect on product selectivity, but they only studied one set methane-oxygen ratio, limiting the usefulness of their results.

This brief review and critique of the previous SCW methane POX studies suggests that more extensive experimentation over a wider range of well-defined conditions still needs to be explored. Although earlier work achieved limited methanol selectivity at low methane conversions, the possible set of conditions that may attain more encouraging results with higher yields of methanol have not been identified. The approach we selected at this point was to perform a detailed examination of a valid SCW kinetic mechanism which will help to reveal that critical elementary steps in the production and destruction of methanol and to identify conditions which will maximize methanol selectivity and methane conversion.

## 5.2 C-1 ELEMENTARY REACTION MODEL DEVELOPMENT & REFINEMENT

In this section, we describe the typical approach to developing a SCW detailed chemical mechanism and provide an analysis of previous SCW C1 mechanisms. The key steps taken to develop the mechanism used in this study as well as the assessment and refinement of that mechanism are also identified. Finally we compare model results with existing SCW methane POX data, provide a reaction path analysis from the model, and predict the set of conditions that will maximize methanol selectivity and methane conversion.

### 5.2.1 Typical Approach to SCWO Detailed Chemical Kinetic Modeling

The most common approach to developing a Detailed Chemical Kinetic Model (DCKM) for a supercritical water oxidation (SCWO) process has three steps:

1. Choose an accepted gas-phase elementary reaction model along with accepted ideal-gas thermodynamic parameters for each possible species as a foundation. Because SCWO densities and concentrations are more gas-like than liquid-like, an accurate gas-phase combustion mechanism provides a reasonable starting point to model the radical reactions occurring during oxidation in SCW. There are many gas-phase, free-radical combustion mechanisms available in the literature which have been extensively scrutinized and are now widely accepted (Warnatz, 1984; Dagaut, Boettner *et al.*, 1990; Yetter, Dryer *et al.*, 1991).

2. Include species not typically found in combustion conditions. For example, high temperature, low pressure gas-phase combustion mechanisms generally do not include methyl peroxy compounds (e.g.,  $\text{CH}_3\text{OO}$ ,  $\text{CH}_3\text{OOH}$ ) or HOCO (a potentially stable intermediate in the conversion of CO to  $\text{CO}_2$ ) or methanol ( $\text{CH}_3\text{OH}$ ), but under the lower temperature, higher pressure conditions of SCWO, these species have a higher chance of survival.

3. Correct rate parameters for SCWO pressures and temperatures.

a. Pressure Dependence: The low pressures characteristic of most gas phase reactions have resulted in kinetic models with few pressure-dependent rate parameters. To more accurately reflect the pressure dependence of unimolecular reactions and chemically-activated bimolecular reactions, their gas-phase rate constants are adjusted for the high-pressure SCWO environment by techniques such as RRKM theory.

b. Non-ideal effects: The ideal gas assumption is typically accurate for combustion at low pressures and high temperatures, but supercritical water is a dense gas phase environment for which this assumption may not hold. A standard approach to modeling the non-ideal effects of the supercritical water environment is through the calculation of equilibrium constants and reverse reaction rate constants through microscopic reversibility using Equations (5-1) and (5-2) respectively.

$$K_c = \frac{K_a}{K_\phi} \left( \frac{P_{atm}}{ZRT} \right)^{\sum \nu_i} \quad (5-1)$$

$$k_r = \frac{k_f}{K_c} \quad (5-2)$$

where  $K_c$  is the equilibrium constant in concentration terms,  $K_a$  is the general equilibrium constant,  $K_\phi$  is the equilibrium term that collectively represents the fugacity coefficients of each species,  $P_{atm}$  is the standard state pressure employed to define the standard state fugacity,  $f^\circ$ ,  $Z$  is the compressibility factor and  $\nu_i$  is the stoichiometric coefficient for each reactant.  $K_a$  is defined as

$$K_a = \exp\left(\frac{-\Delta G^\circ}{RT}\right) = \exp\left(\frac{-\Delta H^\circ}{RT} + \frac{\Delta S^\circ}{R}\right) \quad (5-3)$$

and calculated for each elementary reaction from the ideal gas thermodynamic parameters input to the program to derive the enthalpy ( $\Delta H^\circ$ ), entropy ( $\Delta S^\circ$ ), free energy ( $\Delta G^\circ$ ) and heat capacity for each species. Typical reference standard state conditions for these parameters are 298K and 1 bar.

Nonidealities are captured in Equation (5-1) terms,  $K_\phi$  and  $Z$ . Typically  $K_\phi$  and  $Z$  are assumed to be one for our dilute, medium density conditions. Webley (1989) calculated values for some fugacity coefficients and the compressibility factor to test this assumption. He employed the high temperature, high pressure equation of state of (Christoforakos and Franck, 1986) which required the use of pure component and mixture parameters in standard mixing rules. These parameters were obtained by regression to  $PVT$  data of both pure compounds and binary mixtures. Webley found that for typical, dilute SCWO laboratory conditions above 450°C and 245 bar,  $Z$  ranged from 0.78 – 0.9 and fugacity coefficients approached one, carbon dioxide having the greatest deviation ranging from ~ 2.1 at 450°C down to ~ 1.5 at 700°C. Thus, though SCW is a dense fluid, it can be approximated as an ideal gas at SCW temperatures and densities. Furthermore, invoking ideal gas assumptions for calculations with DCKMs should not significantly affect the model predictions.

SCWO DCKMs have several limitations in addition to difficulties with highly non-ideal conditions. All models of this type employ rate constants and thermochemical values with inherent uncertainties, resulting in varying degrees of success in precisely predicting measured rates and concentration profiles. Current SCWO DCKMs do not accurately model solvent effects associated with SCW, nor do they model surface effects observed experimentally. However, they have been useful in validating and identifying important reaction intermediates and their reaction channels.

### 5.2.2 Previous SCWO Methane Kinetic Models

Although the three steps above are common for developers of SCWO kinetic models, a search of the literature revealed several different executions of these steps in previously developed SCWO methane DCKMs. Table 5-2 highlights four existing SCWO methane kinetic models (Webley and Tester, 1991; Dagaut, de Marcillac *et al.*, 1995; Alkam, Pai *et al.*, 1996; Brock, 1997). The models are listed in chronological order with the more recent models citing the earlier models in their articles. In each case, the investigators take a slightly different approach in developing an elementary reaction model for the SCWO of methane with encouraging results when compared with experimental data. To model non-ideal effects, three of the four models assume unity for all fugacity coefficients and calculate the compressibility factor for the supercritical water mixture by using a current version of the extended steam tables for pure water. The resulting error of this approach is likely to be small (~30%) relative to much higher uncertainty factors associated with many important rate constant values (Holgate, 1993a). Nevertheless, Alkam *et al.* (1996) took a different approach by estimating all fugacity coefficients and calculating the mixture compressibility factor rigorously through the Peng-Robinson Equation of State with appropriate mixing rules, all facilitated by the use of the CHEMKIN Real Gas software package (Schmitt, Butler *et al.*, 1993). Despite their attempt to account for PVT non-idealities, the Alkam model was about as successful as the others.

Table 5.2. A Comparison of Current SCWO Methane Elementary Reaction Models

		Characteristics					
		#of Species	# of Rxns	Non-ideal effects	Model Foundation	Compare w/ data	Major Differences
Investigators	Webley and Tester, '91	18	66	$\phi = 1$ ; Z from steam tables	Warnatz '84 combustion model	<ul style="list-style-type: none"> <li>• His own data;</li> <li>• model underpredicts conversion</li> </ul>	<ul style="list-style-type: none"> <li>• Pressure dependence of CO+OH</li> <li>• no HOCO</li> <li>• no CH<sub>3</sub>OO</li> </ul>
	Dagaut et al, '96	21	127	$\phi = 1$ ; Z from steam tables	Dagaut '90 combustion model	<ul style="list-style-type: none"> <li>• Compared to Webley CH<sub>4</sub> data.</li> <li>• Good agreement with conversion;</li> <li>• had trouble with fuel lean agreement</li> </ul>	<ul style="list-style-type: none"> <li>• CH<sub>3</sub>OO</li> <li>• No HOCO</li> <li>• Modified rate constants by factors</li> </ul>
	Alkam et al, '96	> 22 (incl. C2 species)	184 for $\leq$ CH <sub>3</sub> OH	$\phi ? 1$ ; $\phi$ & Z from PR EOS	Holgate & Tester H <sub>2</sub> -O <sub>2</sub> model and Norton & Dryer CH <sub>3</sub> OH model	<ul style="list-style-type: none"> <li>• Compared to Tester H<sub>2</sub> and CH<sub>3</sub>OH data data.</li> <li>• Good agreement with conversion</li> </ul>	<ul style="list-style-type: none"> <li>• CH<sub>3</sub>OO</li> <li>• No HOCO</li> <li>• Used CHEMKIN RG</li> <li>• Modified rate constants</li> </ul>
	Brock '97 PhD Thesis	22	150	$\phi = 1$ , Z from steam tables	Started from scratch; took rates from combustion reviews and literature	<ul style="list-style-type: none"> <li>• His own data &amp; Webley data</li> <li>• overpredicts oxidation rate</li> </ul>	<ul style="list-style-type: none"> <li>• Revised <math>\Delta H_f</math></li> <li>• updt HO<sub>2</sub> parameters</li> <li>• CH<sub>3</sub>OO</li> <li>• HOCO</li> </ul>

(Webley and Tester, 1991a); (Dagaut, de Marcillac *et al.*, 1995); (Alkam, Pai *et al.*, 1996); (Brock, 1997)

As highlighted in Table 5.2, each model also used different foundations, different species and incorporated pressure dependence differently. In spite of these differences, all models predicted available experimental data fairly well with one exception, the 1991 Webley and Tester model, which represented one of the earliest attempts at developing a SCWO elementary kinetic model. Our analysis of these four models suggests the following refinements for the development of future SCWO methane kinetic models:

- a. The difficulty in modeling the non-ideal effects of the SCWO environment does not necessarily result in more accurate models. In most cases, assuming  $K_\phi = 1$  and  $Z = 1$  is an appropriate first approximation (especially since  $Z \sim 0.9$  in most SCW conditions of interest).

b. Although the four different model foundations in Table 5.2 appear to have little effect on predictive accuracy, starting frameworks based on well documented and validated combustion models with the most recent rate parameters from literature is appropriate and will develop confidence by combustion researchers in interpretation of results generated.

c. Detailed chemical kinetic models for SCWO should include all possible species, including  $\text{CH}_3\text{OO}$ ,  $\text{CH}_3\text{OOH}$  and  $\text{HOCO}$  with their appropriate rate and thermodynamic parameters, and make all necessary pressure dependent corrections to accurately predict the complex free radical chemistry of the SCWO environment.

In this work, the conclusions above were applied in an effort to improve on previous SCWO methane modeling efforts.

### 5.2.3 Development of Current MIT C-1 DCKM

Since Webley's first attempt at developing detailed chemical kinetic models here at MIT, our group has continued to improve and expand on that work in developing other SCWO elementary mechanisms for hydrogen and carbon monoxide (Holgate and Tester, 1994b), benzene (DiNaro, Howard *et al.*, 2000) and most recently methyl phosphonic acid (MPA) (Sullivan, 2003). The foundation for the current MIT C-1 DCKM was the product of extensive research and development in our group by (Sullivan, 2003). Since 2003, an MIT Tester Group co-worker, Jason Ploeger, has further improved this foundation by adding additional reactions and parameters as these have come available in the literature (Ploeger, 2006). The model used in this study is principally the Sullivan-Ploeger model with minor refinements detailed in Section 5.2.4 below. The steps taken by Sullivan and Ploeger to develop this model are presented here for completeness; a more detailed discussion can be found in Sullivan's doctoral thesis (2003) and a recent paper from our group (Ploeger, P.A. *et al.*, 2005).



### 5.2.3.1 Leeds Combustion Mechanism

The foundation of our current SCWO methane elementary reaction model is commonly referred to as the “Leeds Methane Oxidation Mechanism.” The Leeds mechanism for methane is an extremely comprehensive, well-documented elementary reaction model consisting of 37 species and 351 irreversible reactions for the oxidation of methane under the standard combustion conditions of high temperature and low pressure. Although a complete description and analysis of this model can be found in a recent journal article (Hughes, Turanyi *et al.*, 2001), one of the most attractive features of the Leeds mechanism is the authors’ claim of being “always up-to-date.” The University of Leeds, UK plans on achieving this “up-to-date” goal by frequently re-examining this mechanism and continually posting updated versions on their web page at <http://www.chem.leeds.ac.uk/Combustion/Combustion.html>.

In addition to being current, comprehensive and accessible from the Internet in CHEMKIN format, the Leeds mechanism has several attractive features for use as a SCWO kinetic model foundation. All thermodynamic parameters, rate parameters and rate equations found in the Leeds mechanism are fully documented. This documentation facilitates further research of the most important reactions and parameters for a particular process requiring closer examination. The authors of the Leeds mechanism also went to great lengths to categorize the rate parameters and thermodynamic values of each species to provide the reader with a better sense of the accuracy of these figures. In some cases, the classification of rate parameters includes evaluations from the Commission of European Communities (CEC), a group of leading European kinetic investigators, which adds even more credibility to the values selected for these parameters.

Nevertheless, the Leeds mechanism has some weaknesses which must be considered when adapting this model to a SCWO process. Hughes *et al.* admittedly adjusted a few rate parameters to obtain better agreement with data, but those adjustments may be problematic and unnecessary for oxidation in SCW. As with all combustion models, the Leeds mechanism must be significantly adjusted to properly simulate the high density/high pressure, low temperature conditions of SCW. To compensate or avoid the inherent weaknesses of the Leeds Mechanism at SCW conditions, several modifications were made as detailed below.

#### 5.2.3.2 Modifications to the Leeds Mechanism

Following a procedure similar to that of previous developers of SCWO elementary reaction models, the Leeds mechanism was systematically modified to more accurately represent oxidation at SCW conditions. The resulting model is a combination of the thermodynamic values listed in Appendix A and reactions listed in Appendix B. A discussion of the modifications which led to our model is provided below.

#### *Species*

In general, SCWO conditions for methane do not support the generation of carbon atoms or some species containing two or more carbons so several species were not included in our modified Leeds mechanism. Sullivan added the species,  $\text{CH}_3\text{OO}$ ,  $\text{CH}_3\text{OOH}$ , and  $\text{CH}_3\text{OH}$ , which, as stated earlier, play a role in SCWO reactions but are too labile for standard high temperature, low pressure combustion conditions. Ploeger added several species to support his work with ethanol co-oxidation in SCW, including new C1 species which Sullivan did not include like,  $\text{HOCO}$  and  $\text{HCOOH}$ , and several C2 and higher species to support an ethanol mechanism.

### Thermodynamics

The Leeds mechanism draws most of its thermodynamic parameters from Alexander Burcat's Ideal Gas Thermochemical Database, found at <http://garfield.chem.elte.hu/Burcat/burcat.html>, which is updated frequently (Burcat, 2005). Consequently, most of the thermodynamic parameters found in Appendix A come from Burcat with a few exceptions. Naturally, thermodynamic parameters were added for the species added like CH<sub>3</sub>OO, CH<sub>3</sub>OOH, and CH<sub>3</sub>OH from Burcat. In addition to adding thermochemical parameters for C<sub>2</sub>< species, Ploeger adjusted the parameters of CH<sub>3</sub>OO and added parameters for three other C<sub>1</sub> species, HOCO, CH<sub>2</sub>OOH, and HCOOH; current values can be found in Table 5-3 (Ploeger, 2006). A complete listing of all species thermochemical parameters used in this study can be found in Appendix A.

**Table 5.3: Updated Thermodynamic values to Sullivan-Ploeger Model**

The  $\Delta H_f^\circ$  values are in kcal/mol,  $S^\circ$  and  $C_p^\circ$  are in cal/mol K for ideal gas state reference conditions at the temperatures shown in ( ) and 1.01 bar.

Compound	$\Delta H_f^\circ$ (298K)	$S^\circ$ (298K)	$C_p^\circ$ (300K)	$C_p^\circ$ (400K)	$C_p^\circ$ (500K)	$C_p^\circ$ (600K)	$C_p^\circ$ (800K)	$C_p^\circ$ (1000K)	$C_p^\circ$ (1500K)	Source
CH <sub>3</sub> OO	2.15	65.27	12.51	14.78	16.81	18.62	21.58	23.77	27.11	a
Additional C1 Species										
HOCO	-43.30	59.86	10.44	11.78	12.99	13.99	15.33	16.35	29.33	b
CH <sub>2</sub> OOH	33.34	59.54	13.56	16.00	18.24	20.16	22.99	24.98	39.06	c
HCOOH	-91.79	56.12	16.04	16.83	17.56	18.24	19.43	20.43	22.24	d

Sources: a) (Janoschek and Rossi, 2002), b) (Gardiner, Olson *et al.*, 1978) c) (Kaiser, Westbrook *et al.*, 1986) d) (Marinov, 1999)

### Reactions

Since several species were deleted in the first modification to the Leeds mechanism, all reactions involving those deleted species were removed. Similarly, several additional reactions were included to properly model the chemistry of added species. Sullivan modified the Leeds

mechanism by supplementing it with 20 reactions involving  $\text{CH}_3\text{OO}$  and  $\text{CH}_3\text{OOH}$  and 25 reactions for  $\text{CH}_3\text{OH}$ . These reactions are documented in the text file of the model. In general, methanol reactions were taken from the methanol mechanism of (Held and Dryer, 1998) and methylperoxy reactions were taken from (Tsang and Hampson, 1986). In addition to the  $\text{CH}_3\text{OO}$ ,  $\text{CH}_3\text{OOH}$  and  $\text{CH}_3\text{OH}$  reactions discussed above, there were several other one-carbon (C1) species reactions that were not in the Leeds mechanism but are commonly included in SCWO elementary reaction models. Accordingly, Sullivan included 38 additional C1 reactions from various sources. In addition to including several reactions to support C2 and higher species associated with ethanol oxidation, Ploeger also added several more methyl peroxy reactions and sub-mechanisms for  $\text{HCOOH}$  and  $\text{HOCO}$ . Table 5.4 depicts updated reactions in the Sullivan model while Appendix B contains the full list of reactions in the model used in this study along with their kinetic parameters.

The Leeds mechanism includes pressure dependence for only two reactions. As discussed earlier, modeling of the high pressure conditions of SCWO reactions requires a much more thorough consideration of pressure dependence in certain rate constants. Therefore, several additional pressure-dependent parameters were added to the model including two QRRK calculated rate constants from (DiNaro, Howard *et al.*, 2000). Appendix B and Table 5-4 depict pressure dependent reactions with a (+M) and include, when available, all parameters to determine high and low pressure rate constants as well as TROE centering constants and third-body collision efficiency values. Ploeger did not change the pressure dependence of any of Sullivan's original reactions, but some of the reactions he added to the mechanism reflected proper pressure dependence like Reaction #150,  $\text{CO} + \text{OH} (+\text{M}) \rightleftharpoons \text{HOCO} (+\text{M})$ .

**Table 5.4: Updated Reactions to Sullivan-Ploeger Model**

$E_a$  is in cal/mol in this table and  $A$  has units of  $s^{-1}$  or  $mol/(cm^3s)$ . For the pressure dependent rate constants (denoted with (+M)), the first line is the high-pressure rate constant ( $k_\infty$ ) and the second line is the low pressure rate constant ( $k_0$ ). When available, TROE constants are included to better estimate rate constants at intermediate pressures below the high-pressure limit. Also, third-body collision efficiencies are included for some pressure-dependent reactions as noted in the table. For pressure dependent rate constants with only +M, these are low pressure rate constants,  $k_0$ . Reaction #s correspond to Sullivan model/Ploeger model for “**ADJUSTED REACTIONS**” and Ploeger model found in Appendix B for “**NEW C1 REACTIONS**.”

No.	Reaction	$A$	$n$	$E_a$	Source
<b>ADJUSTED REACTIONS</b>					
8/33	$H_2O_2+OH = H_2O+HO_2$	2.40E+00	4.0	-2162	a
9	Deleted				
102/394	$CH_3OO+CH_3OO = CH_3O+CH_3O+O_2$	5.48E+10	0.0	-835	b
103/395	$CH_3OO+CH_3OO = CH_3OH+CH_2O+O_2$	2.19E+09	0.0	-3580	b
150/426	$CO+OH (+M) \Rightarrow H+CO_2 (+M)$	9.54E+04	2.0	-1484	c
	$k_\infty$	3.80E-137	51.93	-75965	
	TROE: 0.6 / 1.0E-15 / 1.0E-15				
<b>NEW C1 REACTIONS</b>					
411	$CH_3OO+HO_2 \Rightarrow CH_3O+OH+O_2$	1.00E+12	0	0	d
412	$CH_3OOH+OH \Rightarrow CH_2OOH+H_2O$	2.51E+13	0	1000	d
413	$CH_2OOH+H_2O \Rightarrow CH_3OOH+OH$	3.01E+13	0	32800	d
414	$CH_3OOH+CH_3O \Rightarrow CH_3OO+CH_3OH$	7.07E+11	0	4000	d
415	$CH_3OO+CH_3OH \Rightarrow CH_3OOH+CH_3O$	3.01E+13	0	32800	d
416	$CH_3OOH+CH_3O \Rightarrow CH_2OOH+CH_3OH$	7.07E+11	0	4000	d
417	$CH_2OOH+CH_3OH \Rightarrow CH_3OOH+CH_3O$	3.01E+13	0	32800	d
418	$HCOOH+HO_2=HOCO+H_2O_2$	2.40E+19	-2.2	14030	a
419	$HCOOH+OH=HOCO+H_2O$	1.85E+07	1.5	-962	a
420	$HCOOH+H=HOCO+H_2$	6.06E+13	-0.3	2988	a
421	$HCOOH+CH_3=HOCO+CH_4$	3.90E-07	5.8	2200	a
422	$HOCO+O_2=CO_2+HO_2$	8.73E+11	0	0	e
423	$HOCO+HO_2=CO_2+H_2O_2$	1.00E+12	0	0	e
424	$HOCO+CH_3OO=CO_2+CH_3OOH$	1.00E+12	0	0	e
425	$CO+OH(+M)=HOCO(+M)$	1.20E+07	1.8	-236	c
	$k_0$	7.24E+25	-3.85	1550	
	TROE: 0.6 / 1.0E-15 / 1.0E-15				

a) (Marinov, 1999); b) (Baulch, Cobos *et al.*, 1992); c) (Senosiain, Musgrave *et al.*, 2003); d) (Kaiser, Westbrook *et al.*, 1986); e) (Brock, Oshima *et al.*, 1996)

#### 5.2.4 Assessment and Refinement of Current MIT C1 DCKM

Although one can never prove a mechanism completely correct (Steinfeld, Francisco *et al.*, 1999), one can evaluate a mechanism’s merit by comparing its predictions to available experimental data. Before applying the current MIT C1 DCKM to examine methane SCW POX, an attempt was made to compare model predictions to existing SCWO data for CO oxidation.

The CO comparison was chosen over comparisons with compounds like methane or methanol because of past success in modeling the CO data set (Holgate and Tester, 1994b) and a lack of success in modeling methane or methanol data ((Webley and Tester, 1991; Savage, Yu *et al.*, 1998; Vogel, DiNaro Blanchard *et al.*, 2005). The calculations were performed using the AURORA module of CHEMKIN 3.7.1 (Meeks, Moffat *et al.*, 1996). The thermochemical values and mechanism depicted in Appendices A and B respectively were used in this module along with input files that reflected proper initial concentrations of CO, O<sub>2</sub> and the proper density of water according to values from expanded steam tables (Haar, Gallagher *et al.*, 1984).

To evaluate the recent updates made to the Sullivan model by Ploeger, both the Sullivan model and the updated model are compared with CO data in Figure 5.2. As one can clearly see in this figure, the updates by Ploeger have resulted in a model that overpredicts CO conversion under all conditions of stoichiometric, fuel rich and fuel lean oxygen ratios. On the other hand, the earlier version of the Sullivan model does a good job of predicting species profiles in all three conditions, particularly if you manually invoke an experimentally observed induction time of ~ 2.0 sec (Holgate and Tester, 1994a). A closer examination of radical rates of production from these two models reveals the source of the discrepancy.

Figure 5.3 compares H<sup>•</sup> radical rates of production (ROP) from the original Sullivan model and the updated, current model of Ploeger using the initial conditions of the Holgate stoichiometric 560°C data set ([CO]<sub>o</sub> = 1.02mM, [O<sub>2</sub>]<sub>o</sub> = 0.5mM, 246 bar). Here we have singled out the H<sup>•</sup> ROP from the reaction:



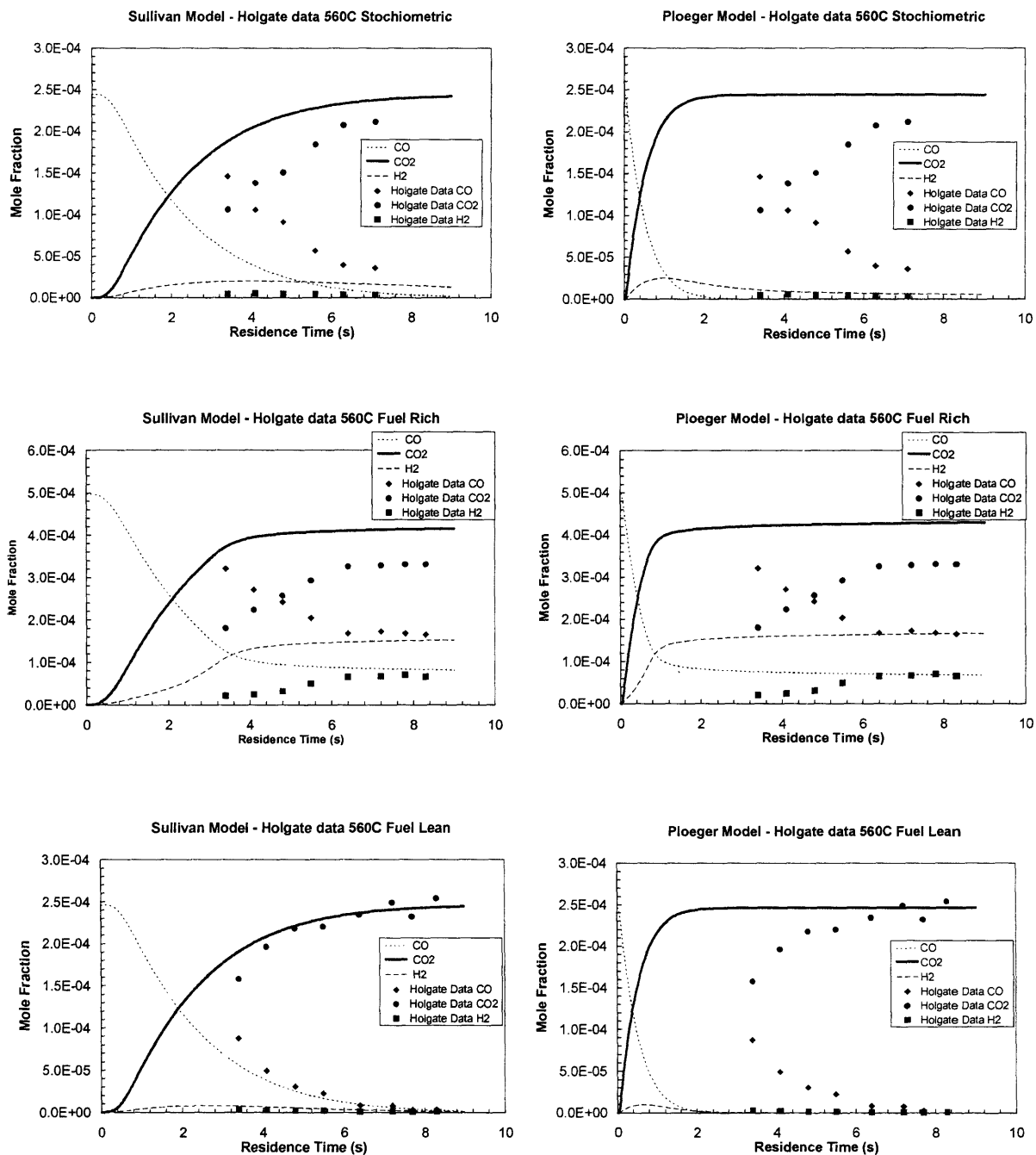
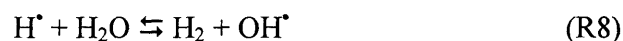


**Figure 5.2 Prediction of CO SCW Oxidation Data - Sullivan Model versus Ploeger Refinements.** Charts on the left depict Sullivan model predictions. Charts on the right depict Ploeger model predictions. Top row plots are stoichiometric CO/O<sub>2</sub> ratio, middle row plots are fuel rich, and bottom row plots are fuel lean. All data was taken at 560°C, 245 bar.

since Ploeger had changed the kinetic parameters for this reaction. With an initial  $H^\bullet$  ROP that is orders of magnitude faster than the original model, the updated Ploeger model is able to generate a pool of radicals more quickly, leading to an increased overall CO oxidation rate. In these SCWO mechanisms,  $H^\bullet$  radicals contribute to the propagation steps of other radicals via the following reactions:



The large disparity in rates for Reaction R6 is discussed below.

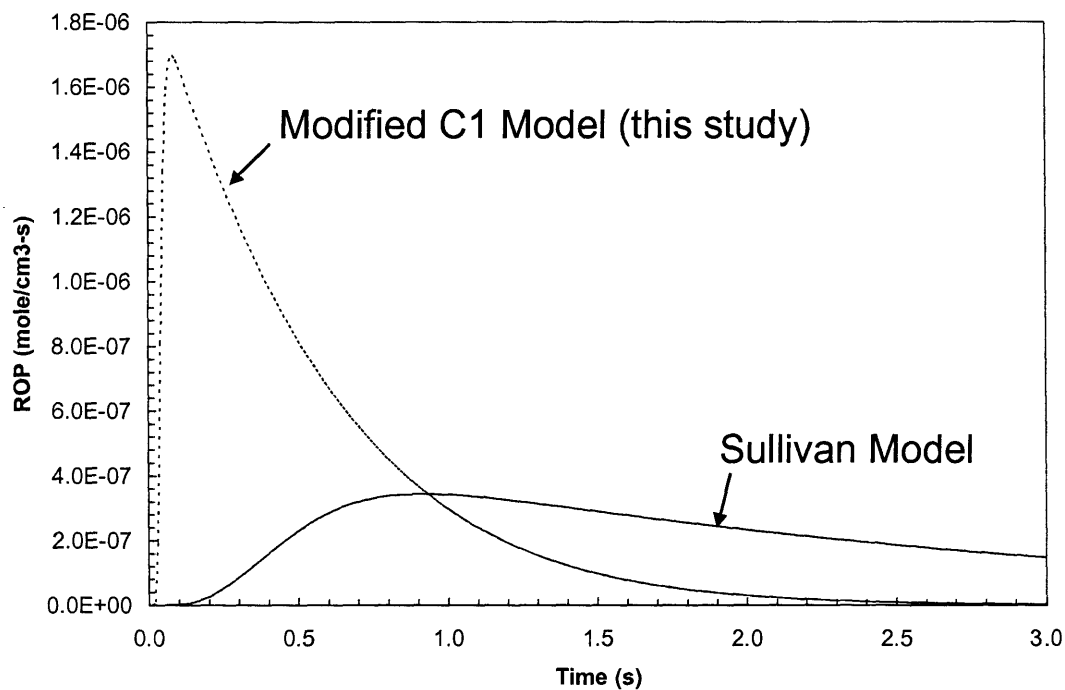


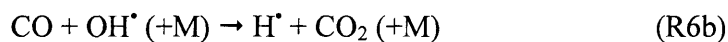
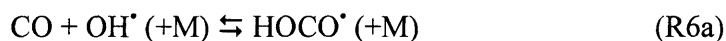
**Figure 5.3  $H^\bullet$  Radical Rate of Production (ROP) from Reaction  $CO + OH^\bullet = CO_2 + H^\bullet$ : Original Sullivan Model versus modified C1 Mechanism from this study**



#### 5.2.4.1 Selecting the “Best” CO Chemistry

Since 1964, it has been accepted that CO reacts with OH<sup>\*</sup> radicals at high pressure to form a collisionally-stabilized intermediate, HOCO<sup>\*</sup>, which can either return to CO + OH<sup>\*</sup> or decompose to H<sup>\*</sup> + CO<sub>2</sub> (Ung and Back, 1964). However, Sullivan (2003), like Holgate (1994), Dinero (2000) and others before her, chose to exclude the HOCO<sup>\*</sup> intermediate in SCWO elementary mechanisms due to the large amount of uncertainty in the reported thermochemical parameters of HOCO<sup>\*</sup> (Larson, Stewart *et al.*, 1988; Fulle, Hamann *et al.*, 1996; Ruscic and Litorja, 2000; Duncan and Miller, 2000). For the Sullivan Model, reaction R6 was taken from Holgate and Tester (1994b) who calculated an overall rate constant at  $P=246$  bar and  $T=400$  to  $600^{\circ}\text{C}$  from Larson *et al.* (1988). This reaction worked quite well for reproducing Holgate CO SCWO data as can be seen in Figure 5.2.

With the recent publication of a new potential energy surface for this system (Yu, Muckerman *et al.*, 2001) and the calculation of new rate parameters based on this surface (Senosiain, Musgrave *et al.*, 2003), Ploeger decided to update the Sullivan model treatment of the complex HOCO chemistry by breaking Reaction (R6) into the following two reactions:



The optimized parameters to properly reflect the temperature and pressure dependence of these two reactions were taken directly from Senosiain *et al.* (2003). Ploeger also added HOCO degradation and formation reactions (Reactions 418-424 in Table 5-5) found in the ethanol SCWO mechanism of Rice and Croiset (2001).

The sensitivity of the Ploeger model to each new HOCO and CO reaction was examined. The sensitivity analysis involved varying the pre-exponential rate parameters by an order of

magnitude and re-running the model using Holgate CO initial conditions. Although the adjustment of a rate by one order of magnitude may seem unreasonable, the uncertainties associated with various kinetic and thermochemical parameters may result in an order of magnitude difference in the reaction rate. For example, Senosiain did not publish uncertainty with his rate parameters for Reaction (R6b), but by making reasonable adjustments to his parameters, like a 20% decrease in the temperature exponent (2.02 down to 1.68), one can decrease the overall reaction rate by an order of magnitude. This kind of sensitivity analysis confirmed reaction (R6b), and not any of the other new reactions, to be the major contributor to the model's over-prediction of CO oxidation. The most surprising result came when the pre-exponential factor for Reaction (R6b) was lowered one order of magnitude (OOM) and the rest of the updated Ploeger model was kept the same. Figure 5.4 depicts the Ploeger model predictions with the Senosiain rate lowered one OOM versus the original Sullivan model predictions.

The updated Ploeger model with the reduced rate for reaction (R6b) is in excellent agreement with Holgate CO data over a wide range of fuel to oxygen ratios, performing notably better than the original Sullivan model at fuel rich conditions. The agreement also seems to hold if you invoke the experimentally observed induction time of ~ 2.0 sec (Holgate and Tester, 1994a). Prediction of additional CO oxidation data at other temperatures was also examined, and the adjusted Ploeger model performed equally well when compared with predictions from the original Sullivan model.

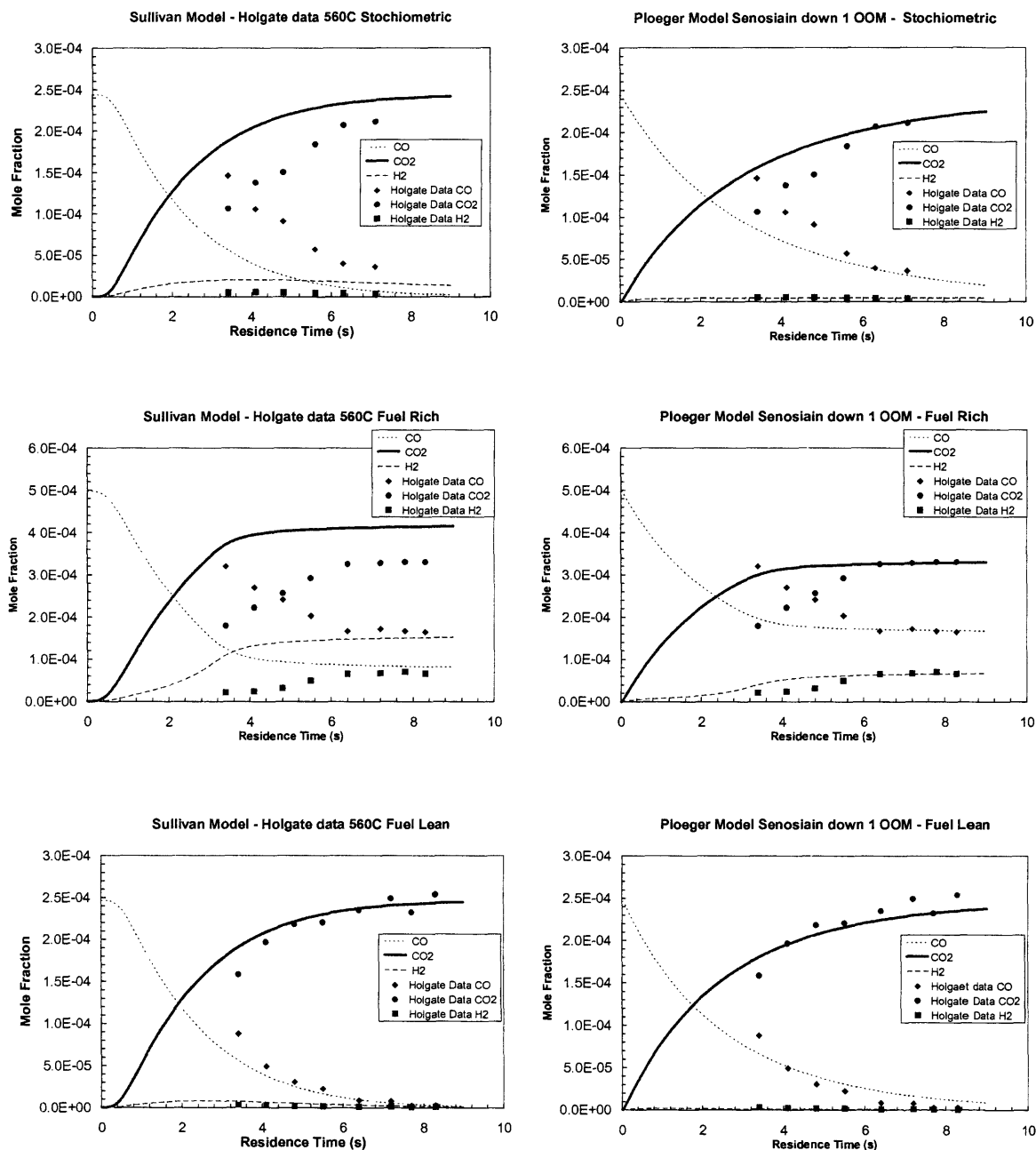


**Figure 5.4 Prediction of CO Oxidation Data Sullivan Model versus Ploeger Refinements: Senosiain Rate reduced 1 OOM.** Charts on the left depict Sullivan model predictions. Charts on the right depict Ploeger model predictions after adjusting the Senosiain rate down 1 OOM. Top row plots are stoichiometric CO/O<sub>2</sub> ratio, middle row plots are fuel rich, and bottom row plots are fuel lean. All data was taken at 560°C, 245 bar.

Issues associated with the proper treatment of HOCO<sup>\*</sup> chemistry in SCWO models are not unprecedented. (Brock, 1997), using an earlier version of HOCO<sup>\*</sup> chemistry, observed similar problems of “over-oxidation” that were corrected when he eliminated Reaction 422 (Table 5-4), HOCO<sup>\*</sup> + O<sub>2</sub>. Although making these kinds of adjustments to properly model HOCO<sup>\*</sup> chemistry is suspect at best, it certainly emphasizes the need to further and more thoroughly investigate HOCO<sup>\*</sup> chemistry in SCW. There are numerous examples of uncertainty in the gas phase study of HOCO<sup>\*</sup> chemistry such as Senosiain *et al.* (2003) admitting to changing a transition state energy by 40% to match data and Fulle *et al.* (1996) remarking on bath gas dependence and changes in activation energies. HOCO<sup>\*</sup> chemistry in SCW has yet to be studied experimentally or through modeling. A theoretical study of the effects of water on the HOCO<sup>\*</sup> system, similar to the studies by Akiya and Savage (1998) and Melius, Bergan *et al.* (1990) on formic acid decomposition in SCW, may reveal acceleration or inhibition of these elementary reactions. Nevertheless, for this SCW methane POX study, we decided to retain the reduced Senosiain rate and the other HOCO<sup>\*</sup> chemistry added by Ploeger based on its ability to adequately predict SCWO C1 data.

#### 5.2.4.2 Selecting the “Best” H<sub>2</sub>O<sub>2</sub> + OH Rate

An attempt was made in this study to have the Ploeger-revised Sullivan model predict select data from the Savage '98 methane SCWO study and the Sullivan '03 methylphosphonic acid (MPA) SCWO study. Although the best HOCO<sup>\*</sup> chemistry still seemed to be the adjusted Senoisian rate, an additional problem with the revised model was identified. The new rate for reaction (R8)



contributed to predict an over-oxidation of methane SCWO and MPA SCWO even though it was part of the excellent prediction for CO SCWO. This disagreement may have more to do with the significant increase in the complexity of the mechanisms and real world chemistry of methane and MPA versus CO than anything else, but it warrants a closer look at different rates used for Reaction (R8) in various SCWO DCKM.

Figure 5.5 is an Arrhenius-type plot of rate constant versus inverse temperature from 400 – 700°C for several different rates for Reaction R8. Note that the rate chosen by Ploeger when revising the Sullivan model is the fastest rate (same rate used in Rice and Croiset (2001)), particularly at higher temperatures, while the original Sullivan model employs one of the slower, more temperature-independent rates of all the models. The rate in the Sullivan model is from the most recent source (Kappel, Luther *et al.*, 2002) but that source simply reconfirms the lower temperature results of an earlier study (Hippler, Neunaber *et al.*, 1995) and that rate constant expression is a unique, non-Arrhenius combination of two different rate constant expressions:

$$k / \text{cm}^3 \text{mol}^{-1} \text{s}^{-1} = 1.7 \times 10^{18} \exp(-14800 \text{K} / T) + 2.0 \times 10^{12} \exp(-215 \text{K} / T) \quad (5-4)$$

The rate chosen by Ploeger is the second most recent (Marinov, 1995) and it too has a unique, non-Arrhenius expression for its rate constant as seen in Table 5-4. At the very least, the rates for Reaction (R8) should be examined more closely, but for our purposes in this methane SCW POX study, we decided to retain the Marinov rate which gave us the best agreement with the CO SCWO data.

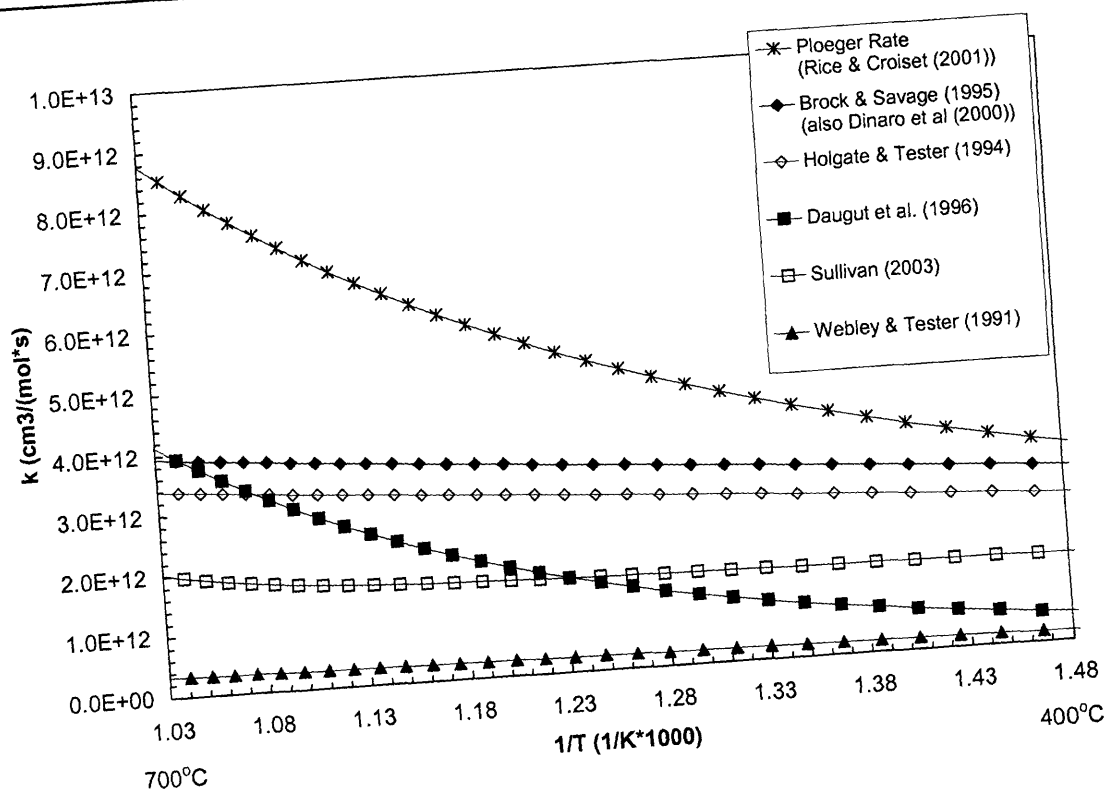


**Figure 5.5 Comparison of  $\text{H}_2\text{O}_2 + \text{OH}^\bullet$  rate constants found in various SCWO Detailed Chemical Kinetic Models (DCKMs). Rate chosen by Ploeger is one taken from the DCKM of Rice & Croiset (2001).**

#### 5.2.4.3 Model Assessment Conclusions

In this brief assessment of the Ploeger-revised Sullivan model, it was determined that adjustments had to be to the new treatment of  $\text{HOCO}^\bullet$  chemistry. All other changes to the Sullivan model, like the new rate for Reaction (R8) and the new thermochemical parameters and reactions for methyl peroxy species, seem to result in adequate predictions of SCWO C1 data, although a closer examination is warranted. The sensitivity of the adjusted model to specific species thermo parameters was not explored and the new model was not examined over a broad range of temperatures. In spite of these shortcomings, the adjusted model was deemed sufficiently accurate for a modeling analysis of SCW methane POX.

### 5.3 A DETAILED CHEMICAL KINETIC MODELING ANALYSIS OF METHANE POX IN SCW

Recall that the main objective of this modeling study was to examine methane POX in SCW and identify those conditions which would maximize methanol selectivity at reasonable conversions. Three major steps were undertaken to complete this evaluation. First, the ability of the model to predict SCW methane POX experimental data was analyzed. Second, based on those experimental conditions, a detailed reaction pathway was identified. Third, a wide range of conditions were explored to arrive at the most promising SCW environment for methane POX to methanol.

#### 5.3.1 Model Prediction of SCW methane POX experimental data

Of the previous SCW methane POX studies found in table 5.1, the experimental conditions and results of Lee and Foster (1996) were chosen as our modeling comparison. Three of the earlier studies included heterogeneous catalysis which is not modeled in the current DCKM, and two of the earlier studies were batch or semi-batch studies that may have had issues related to mixing and sampling. The most recent study of Sato *et al.* (2004) was conducted under conditions very similar to those of Lee and Foster, but only Lee and Foster provided tabulated kinetic data.

Figure 5.6 compares Lee and Foster SCW methane POX data at 400°C, 250 bar with DCKM model predictions. In this figure, major species selectivity, defined as moles of species generated as a percentage of moles of methane consumed, is plotted versus time. Two clear observations can immediately be made: the model predicts higher methanol and lower CO<sub>2</sub>

selectivities than experimentally observed and there is a considerable amount of scatter in the experimental data. Although there is scatter in the data, the trends in major species selectivity are still quite different than model predictions and the Lee and Foster methanol selectivity trend is in general agreement with the more recent experimental data of Sato and co-workers.

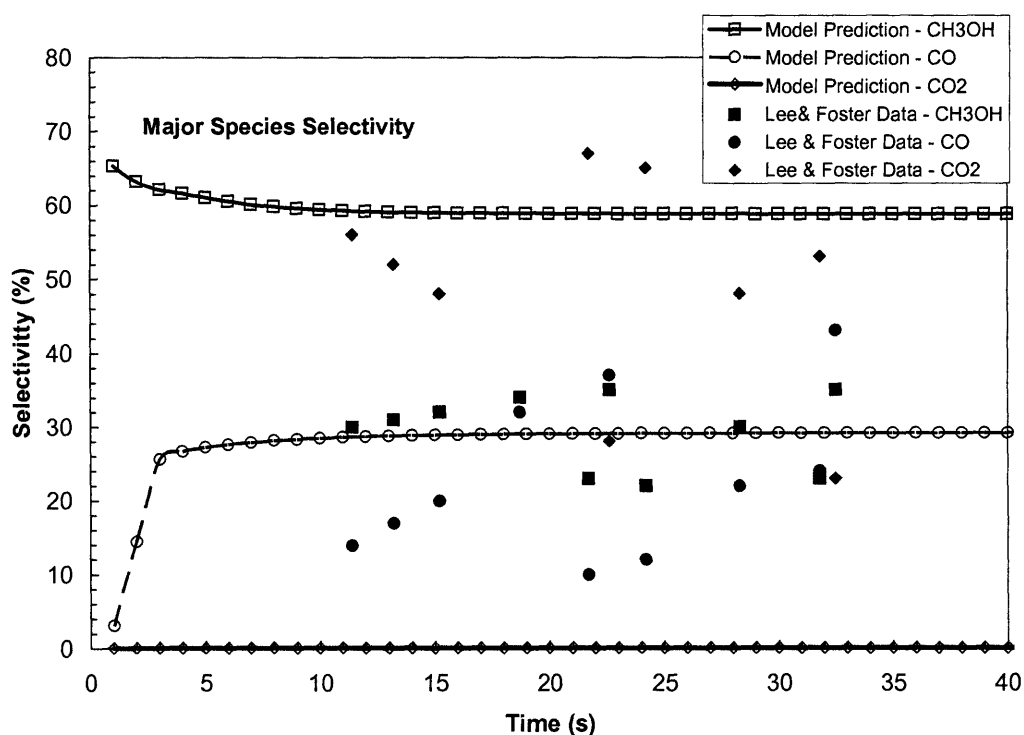


**Figure 5.6 Major Species Selectivity Comparison of Methane SCW POX Data with DCKM Predictions.** Experimental conditions are 400°C, 250 bar,  $[\text{CH}_4]_0 = 0.384\text{M}$ ,  $[\text{O}_2]_0 = 0.012\text{M}$ . Lee and Foster data are points, Ploeger-adjusted Sullivan model predictions are lines. (Lee and Foster (1996)).

There are several reasons that may explain the disagreement of the model predictions with the data. As mentioned earlier, detailed chemical kinetic models developed for SCWO may not adequately reflect some real-world reactor conditions like the influence of reactor walls, solvent effects of supercritical water, and the non-ideality of this dense fluid media. Reactor



walls may serve as either a catalytic surface, promoting further oxidation, or as a sink that may prematurely quench free radicals important in oxidation mechanisms. Supercritical water solvents may help to accelerate certain reactions by preferentially solvating important transition states, or they may inhibit overall reaction rates through cage effects which may slow diffusion of reactants. Of particular concern with conditions similar to those of Lee and Foster is the proper treatment of non-ideal effects. Lee and Foster conducted experiments at temperatures close to the critical temperature of water ( $T_c = 374^\circ\text{C}$ ) and methane and oxygen initial concentrations were not dilute ( $[\text{CH}_4]_0 \sim 4 \text{ mole } \%$ ,  $[\text{O}_2]_0 \sim 0.1 \text{ mol}\%$ ).

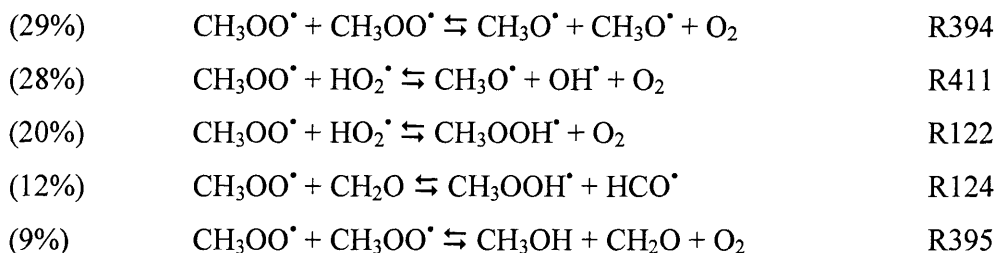
With an understanding of the shortcomings of this particular detailed chemical kinetic model, it was decided to proceed with the model in its current state for several reasons, among them are:

- Initial versions of this model were similarly poor at predicting SCW methane POX selectivity data even with other literature parameter values for various species like methyl peroxy,  $\text{HOCO}^\bullet$ ,  $\text{H}_2/\text{O}_2$  chemistry.
- In nearly all cases, these models seem to predict the “best case scenario” in terms of methanol selectivity and methane conversion, and the trends were consistent with experimental data.

### 5.3.2 Reaction Path Analysis

The dominant pathways from methane to methanol are shown in Figure 5.7. This figure is essentially a summary of this rate of production (ROP), or flux analysis for carbon chemistry at the intermediate conditions stated earlier. The reaction network depicted in this figure results from identifying all major consumption pathways for all major species based on the peak flux for each consumption reaction. Each arrow corresponds to an important elementary reaction in our

mechanism, and the percentage values near each arrow give a relative contribution for that reaction's role in total consumption of the reactant species. For example, under these conditions, methyl peroxy radical,  $\text{CH}_3\text{OO}^\bullet$  is consumed by five major pathways;



where the percentages on the left correspond to the relative contribution of that reaction to the overall consumption of  $\text{CH}_3\text{OO}^\bullet$  and the reaction numbers correspond with the numbers found in the mechanism in Appendix B.

The reaction network in Figure 5.7 suggests several important conclusions. In this particular model, the methyl peroxy species,  $\text{CH}_3\text{OO}^\bullet$  and  $\text{CH}_3\text{OOH}^\bullet$ , seem to play a more important role than previous models. For example, when Sato *et al.* (2004) applied Savage's model (Savage, Rovira *et al.*, 2000) to their SCW methane POX data, the major path from  $\text{CH}_3^\bullet$  was not through the methyl peroxy species but was directly to methoxy,  $\text{CH}_3\text{O}^\bullet$ , corresponding to R65 in our model:



The emphasis on methoxy in this model is not surprising given the conditions of low temperature and limited oxygen, but three of the five major degradation pathways for  $\text{CH}_3\text{OO}^\bullet$  are new or adjusted reactions by Ploeger to the original Sullivan model. The importance of these methyl peroxy pathways in this POX mechanism certainly warrants further investigation.

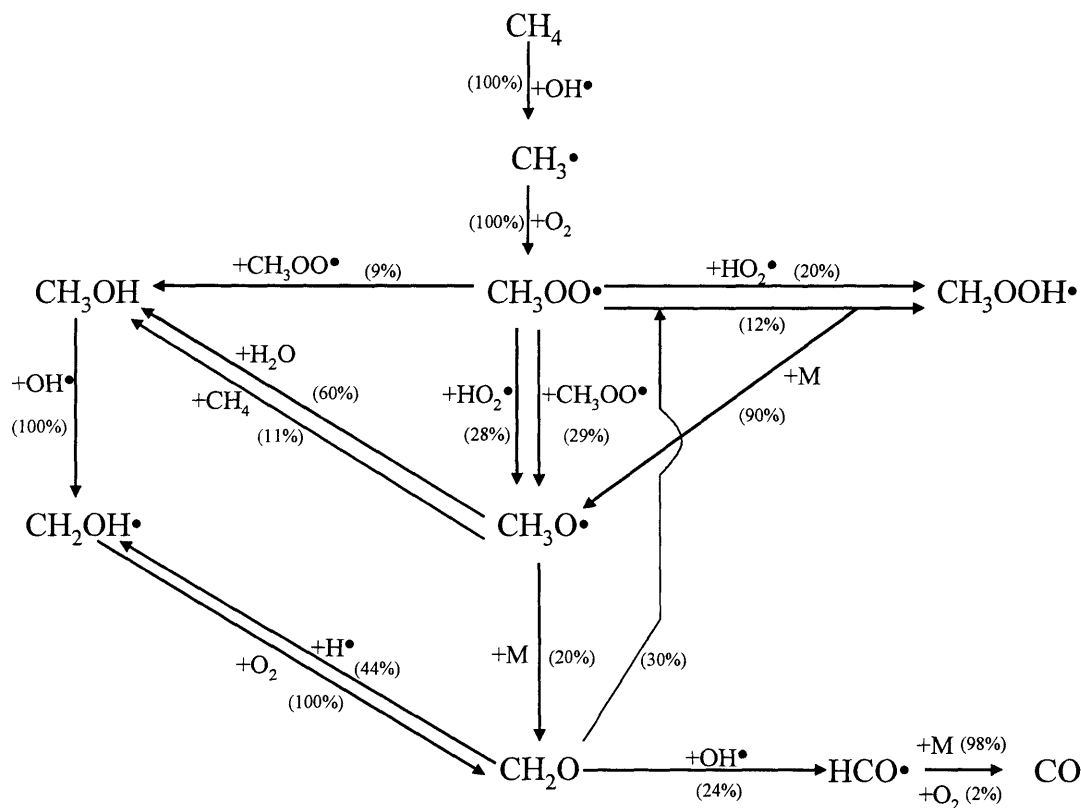
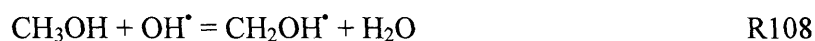


**Figure 5.7 Dominant Pathways from Methane to Methanol in SCW. Conditions:  $T=400^{\circ}\text{C}$ ,  $P=250\text{bar}$ ,  $[\text{CH}_4]_0 = 0.3\text{M}$ ,  $[\text{O}_2]_0 = 0.009\text{M}$ .** Each arrow corresponds to an important elementary reaction in our mechanism, and the percentage values near each arrow give a relative contribution for that reaction's role in total consumption of the reactant species.

This reaction path analysis also reveals the major formation and decomposition pathways for methanol, the partial oxidation product of interest. Under these experimental conditions, methanol is formed and consumed by one major reaction each:



Methanol certainly appears doomed in this model since the reaction which makes it, also forms a reactant,  $\text{OH}^*$ , which destroys methanol. Also, the overall rate of the consumption reaction, R108, is anywhere from three to five orders of magnitude faster than the formation reaction, R109; which explains the typical POX experimental observation – methanol reacts away faster than you can make it. Figure 5.8 displays a comparison of rate constants for methanol formation and degradation reactions. Although the formation reaction (-R109) has a higher activation energy, resulting in a faster rate at higher temperatures, the decomposition reaction is still three orders of magnitude faster than the formation reaction. Therefore, temperature should not affect methanol selectivity if all other conditions of pressure and initial concentrations remain the same.

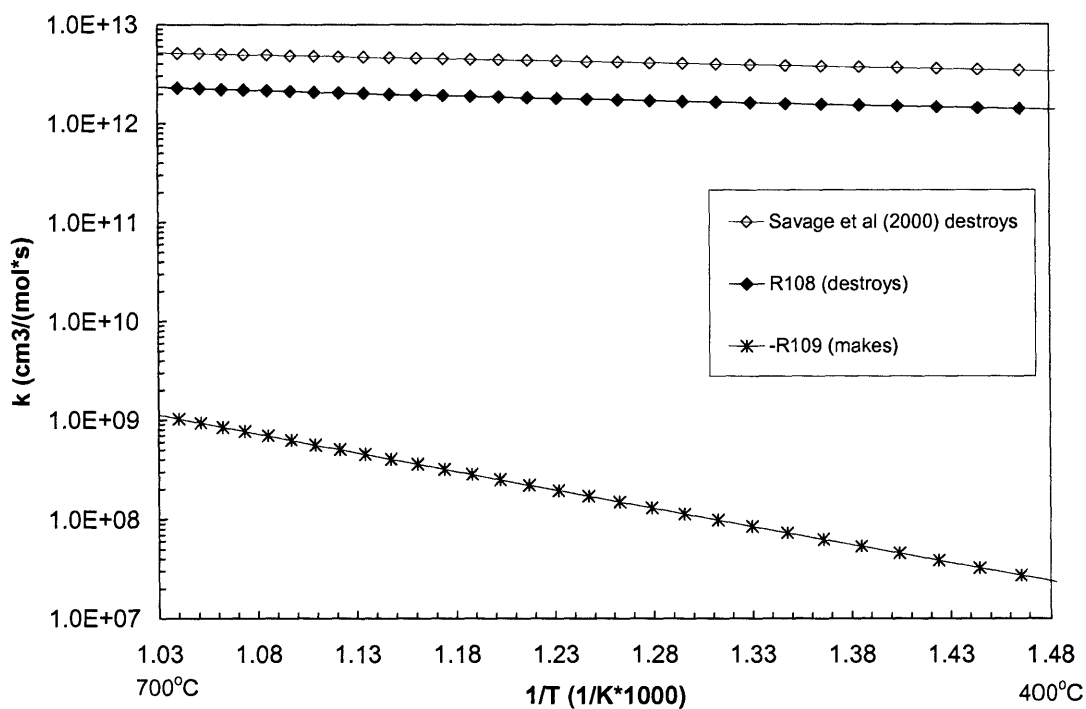


**Figure 5.8 Comparison of Methanol Formation and Decomposition Rate Constants.** Rate Constant used in Savage et al (2000) model displayed for comparison.

An additional conclusion from this pathway analysis is the possible influence water may have on methanol selectivity. Since water appears in both reactions –R109 (as a reactant) and R108 (as a product), it is reasonable to assume that increased water concentrations or increased water densities may shift equilibrium conditions to higher methanol yields. It is difficult to draw other conclusions from the pathway depicted in Figure 5.7 since this pathway was generated from a fixed set of initial conditions of reactant concentrations, temperature and pressure. In the next section, a wide range of initial conditions are explored with the DCKM to help identify the most promising conditions for methanol production.

### 5.3.3 Model Predictions over a Range of Conditions

#### 5.3.3.1 Effect of O<sub>2</sub> Concentration

Oxygen concentration was chosen as the first parameter to vary. For this set of model calculations, pressure was set at 245 bar, initial methane concentration was set at 1 mM, temperatures from 350°C – 600°C were explored and initial oxygen to methane ratios,  $[O_2]_0/[CH_4]_0$ , were varied between 0.1 – 50. Figure 5.9 is an example of the methanol selectivity versus time charts generated via successive model calculations. From this chart, one can see that varying the  $[O_2]_0/[CH_4]_0$  ratio does not drastically change predicted maximum methanol selectivity, but the highest selectivity achieved was 0.83 for  $[O_2]_0/[CH_4]_0 = 1$ . Although this selectivity result is relatively high, it only corresponds to a methane conversion of 0.41%, far off from a goal of about 15% or more conversion. Also interesting to note in Figure 5.9 is that maximum methanol selectivity is achieved fairly early in a reaction residence time and at about the same time for every oxygen to methane ratio. This observation suggests that kinetics leading to methanol formation are not measurably dependent on oxygen concentration in contrast to what has been observed for rate dependence on temperature, pressure and methane concentration.

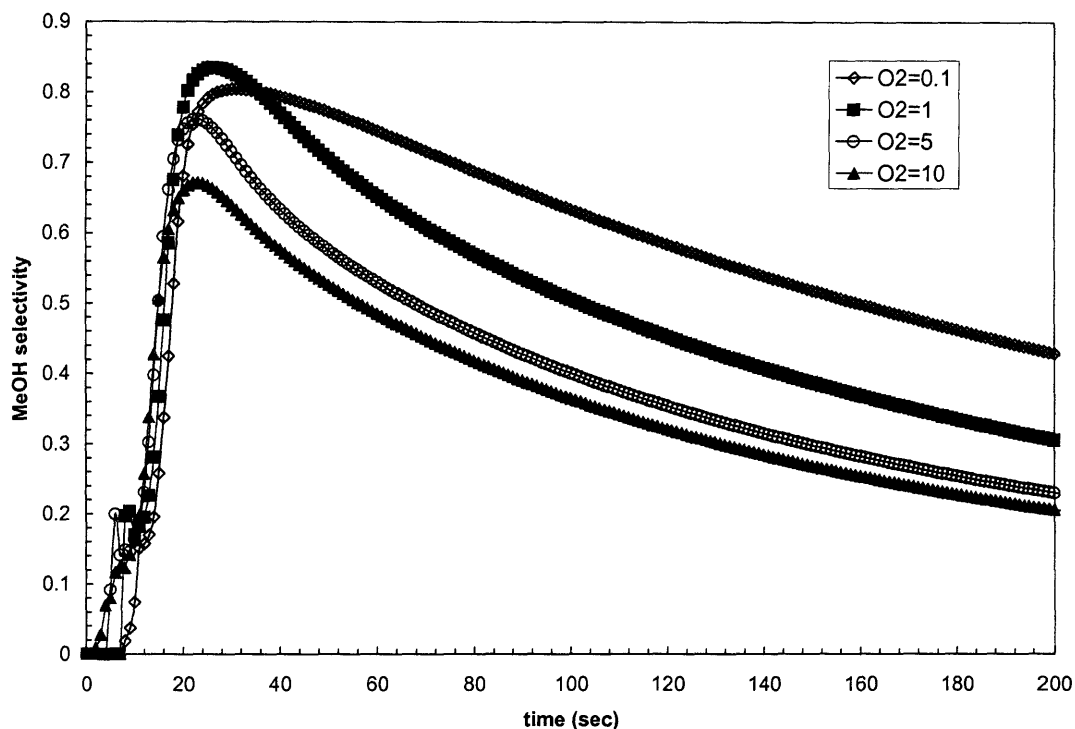


**Figure 5.9** Methanol selectivity versus time for different initial oxygen/methane ratios-  
varying oxygen.  $P = 245$  bar,  $[\text{CH}_4]_0 = 1$  mM,  $T = 400^\circ\text{C}$ .

### 5.3.3.2 Effect of $\text{CH}_4$ Concentration

A set of model calculations was performed by varying methane concentration while fixing all other parameters. For these calculations, pressure was set at 245 bar, initial oxygen concentration was set at 1 mM, temperatures from  $350^\circ\text{C}$  –  $600^\circ\text{C}$  were explored and initial methane to oxygen ratios,  $[\text{CH}_4]_0/[\text{O}_2]_0$ , were varied between 0.1 – 50, corresponding to  $[\text{O}_2]_0/[\text{CH}_4]_0$  ratios between 10 – 0.02. Figure 5.10 is an example of the methanol selectivity versus time charts generated via successive model calculations. There appears to be two major differences between this chart reflecting methane concentration variation and Figure 5.9

reflecting oxygen variation. As one can see in Figure 5.10, methane concentration variation seems to significantly affect both the value of maximum methanol selectivity and the time that that maximum occurs. The highest maximum methanol selectivity achieved in the fastest time when the methane to oxygen ratio was 50, and the lowest maximum methanol selectivity developed in the slowest time when the methane to oxygen ratio was the least, at a value of 0.1. However, in both cases, methane conversion was still low, achieving only 2.6% conversion shortly after the highest selectivity was achieved.

Figure 5.10 portrays an interesting methanol selectivity trace over time at high methane concentrations and low temperatures. As we saw earlier in Figure 5.6, at low temperatures, high methane concentrations and low oxygen concentrations, once the oxygen is consumed, the methanol formed appears to be stable over time at a fairly high selectivity. Although difficult to conclude due to scatter, the Lee & Foster methanol selectivity data in Figure 5.6 seem to support this modeling observation. An industrial POX process may have difficulty extracting methanol at just the right time corresponding with a narrow peak selectivity, but if methanol selectivity remains high as in Figure 5.10, then “perfect timing” is not as critical.

#### 5.3.3.3 *Effect of Temperature*

Two sets of modeling calculations were performed where temperature was varied between 400 – 600°C while pressure was held at 245 bar. One set was based on a high methanol selectivity from the oxygen concentration variation study corresponding with  $[O_2]_o/[CH_4]_o = 0.1$ . The other set was based on a high methanol selectivity from the methane concentration variation study corresponding with  $[CH_4]_o/[O_2]_o = 50$ . In both cases, maximum methanol selectivity occurred at the lowest temperature. For example, the maximum methanol selectivity for  $[O_2]_o/[CH_4]_o = 0.1$  went from 0.83 at 400°C decreasing almost linearly to 0.42 at 600°C.

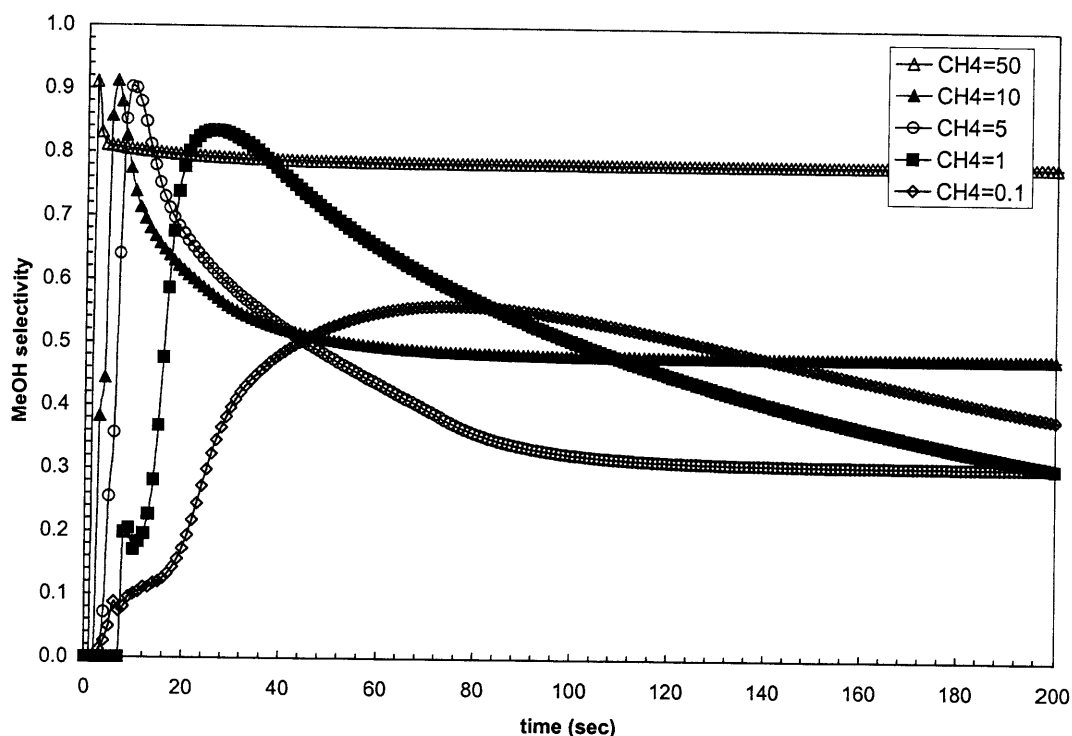
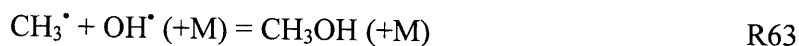
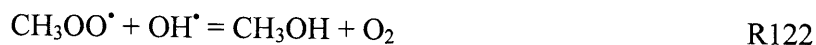


**Figure 5.10** Methanol selectivity versus time for different initial methane/oxygen ratios – varying methane.  $P = 245$  bar,  $[O_2]_0 = 1$  mM,  $T = 400^\circ\text{C}$ .

A closer look at methanol fluxes in the reaction network provides an explanation for this temperature-dependent observation. Recalling that at lower temperatures, the main reaction responsible for producing methanol is the reverse of Reaction #109:



At higher temperatures, however, the reverse of this reaction is favored and it now plays a significant role in destroying methanol. The production of methanol is then left up to relatively minor reactions which cannot compete with both reactions 109 and 108 consuming methanol.





### 5.3.3.4 Effect of Pressure

One set of modeling calculations was performed where pressure was varied between 100 – 600 bar while temperature was held at 400°C, methane initial concentration set to 1 mM and  $[O_2]_0/[CH_4]_0 = 0.1$ . Figure 5.11 portrays maximum methanol selectivity achieved at each pressure. It is clear from this figure that maximum methanol selectivity is highest at higher pressures. However, plotted on a secondary x-axis in Figure 5.11 are methane conversion values corresponding with maximum methanol selectivity versus pressure. There is a trade-off where high methanol selectivity is achieved only at minuscule methane conversion values. It is likely that high pressure, or high water density, enhances reactions that produce methanol as we predicted with water being a reactant in both Reaction #s R108 and R109. However, it appears that pressure also increases the rate of destruction of methanol as well as increases the selectivity of carbon to carbon monoxide at the expense of methanol.

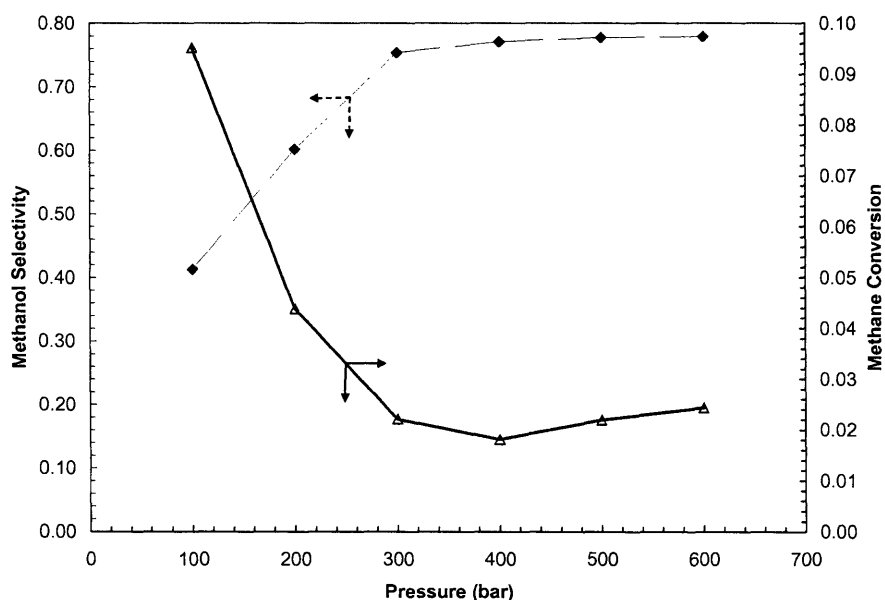


**Figure 5.11 Maximum methanol selectivity and methane conversion versus pressure.** Methane conversion is value at same time as highest methanol selectivity.  $T = 400^\circ\text{C}$ ,  $[CH_4]_0 = 1 \text{ mM}$ ,  $[O_2]_0 = 0.1 \text{ mM}$ .

## 5.4 CONCLUSIONS

A Detailed C1 Chemical Kinetic Model (DCKM) was refined and analyzed to support an examination of the effects of experimental conditions on methanol selectivity and methane conversion for the partial oxidation of methane in supercritical water (SCW POX). Although a deliberate sensitivity analysis has yet to be performed on this model, a detailed study of several key reactions and rates from literature were chosen which result in good agreement of model predictions with reliable C1 SCWO experimental data. SCW methane POX predictions from the refined model were then compared with POX experimental data. Disagreements between the model and the data were discussed along with a detailed critique of experimental issues associated with all previous SCW methane POX experimental studies. A reaction path analysis was developed from the DCKM which helped to elucidate the fate of methane and methanol in this environment and to identify a set of promising conditions to maximize methanol selectivity.

Upon detailed analysis of both experimental and modeling results, the maximum methanol selectivity of about 80 % and maximum methane conversion of about 1 % occurs at low temperatures ( $T < 400^{\circ}\text{C}$ ), medium to high pressure ( $P > 300$  bar), high methane concentration ( $[\text{CH}_4]_0 > 50\text{mM}$ ) and medium to high methane to oxygen ratios ( $[\text{CH}_4]_0/[\text{O}_2]_0 > 10$ ). The experimental results may have achieved less than the maximum possible methanol selectivity due to issues such as inadequate mixing and wall effects. The modeling results may also be under-predicting methanol selectivity due to improper modeling of non-ideal effects and solvent effects. However, the current model predictions and experimental results both substantiate our concern that SCW methane POX may fall short of the goal of greater than 70 % methanol selectivity and 15% methane conversion. Nevertheless, other sets of experimental conditions that may show more promise have not been fully explored experimentally. In

particular, the use of stable, selective catalysts, or inert wall material, or partial oxidation in the presence of hydrothermal flames have not been thoroughly analyzed here. We recommend that such work be pursued in future studies.

## 5.5 REFERENCES

- Aki, S. N. K. K. and M. A. Abraham (1994). "Catalytic partial oxidation of methane in supercritical water." *Journal of Supercritical Fluids* 7(4): 259-263.
- Akiya, N. and P. E. Savage (1998). "Role of Water in Formic Acid Decomposition." *AIChE J.* 44(2): 405-415.
- Alkam, M. K., V. M. Pai, et al. (1996). "Methanol and Hydrogen Oxidation Kinetics in Water at Supercritical States." *Combustion and Flame* 106: 110-130.
- Baulch, D. L., C. J. Cobos, et al. (1992). "Evaluated Kinetic Data for Combustion Modeling." *J. Phys. Chem. Ref. Data* 21: 411-429.
- Brock, E. E. (1997). "Detailed chemical kinetic modeling of the supercritical water oxidation of simple hydrocarbons." (DA9721951): 61.
- Brock, E. E., Y. Oshima, et al. (1996). "Kinetics and Mechanism of Methanol Oxidation in Supercritical Water." *J. Phys. Chem.* 100: 15834-15842.
- Broll, D., A. Kramer, et al. (2002). "Heterogeneously catalyzed partial oxidation of methane in supercritical water." *Chemie Ingenieur Technik* 74(6): 795-800.
- Broll, D., A. Kramer, et al. (2001). "Heterogeneously Catalyzed Partial Oxidation in Supercritical Water." *Chem. Eng. Technol.* 24(2): 142-146.
- Burcat, A. (2005). *Ideal Gas Thermodynamic Data in Polynomial form for Combustion and Air Pollution Use.* 2005.
- Christoforakos, M. and E. U. Franck (1986). "An equation of state for binary fluid mixtures to high temperatures and pressures." *Ber. Bunsenges. Phys. Chem.* 90: 780.
- Dagaut, P., J. C. Boettner, et al. (1990). "Ethylene pyrolysis and oxidation: a kinetic modeling study." *Int. J. Chem. Kinet.* 22(6): 641-664.

- Dagaut, P., B. D. de Marcillac, et al. (1995). "Chemical kinetic modeling of the supercritical water oxidation of simple fuels: H<sub>2</sub>, CO and CH<sub>4</sub>." *J. Chim. Phys. Phys.-Chim. Biol.* **92**(5): 1124-41.
- DiNaro, J., J. Howard, et al. (2000). "Elementary reaction mechanism for benzene oxidation in supercritical water." *J Phys Chem A* **104**(45): 10576-10586.
- Dixon, C. N. and M. A. Abraham (1992). "Conversion of Methane to Methanol by Catalytic Supercritical Water Oxidation." *The Journal of Supercritical Fluids* **5**: 269-273.
- Duncan, T. and C. Miller (2000). "The HCO<sub>2</sub> Potential Energy Surface: Stationary Point Energetics and the HOCO Heat of Formation." *J. Chem. Phys.* **113**(3): 5138-5140.
- Foulds, G. A. and B. F. Gray (1995). "Homogeneous gas-phase partial oxidation of methane to methanol and formaldehyde." *Fuel Processing Technology* **42**: 129-150.
- Fulle, D., H. Hamann, et al. (1996). "High pressure range of addition reactions of HO. II. Temperature and pressure dependence of the reaction HO + CO = HOCO = H + CO<sub>2</sub>." *J. Phys. Chem* **105**(3): 983-1000.
- Gardiner, W. C. J., D. B. Olson, et al. (1978). "Thermochemical Properties of HOCO and HOCO+ formed from OH+CO." *Chemical Physics Letters* **53**(1): 134-137.
- Gesser, H. D., N. R. Hunter, et al. (1985). "The Direct Conversion of Methane to Methanol by Controlled Oxidation." *Chemical Reviews* **85**(4): 235 - 244.
- Haar, L., J. S. Gallagher, et al. (1984). NBS/MRC Steam Tables. New York, Hemisphere Publishing Corp.
- Hall, T. J., J. S. J. Hargreaves, et al. (1995). "Catalytic synthesis of methanol and formaldehyde by partial oxidation of methane." *Fuel Processing Technology* **42**: 151-178.
- Held, T. J. and F. L. Dryer (1998). "A comprehensive mechanism for methanol oxidation." *International Journal of Chemical Kinetics* **30**(11): 805-830.
- Hipler, H., H. Neunaber, et al. (1995). "Shock wave studies of the reactions HO+H<sub>2</sub>O<sub>2</sub>=H<sub>2</sub>O+HO<sub>2</sub> and HO+HO<sub>2</sub>=H<sub>2</sub>O+O<sub>2</sub> between 930 and 1680 K." *J Chem Phys* **103**: 3510.
- Hirth, T. and E. U. Franck (1993). "Oxidation and Hydrothermolysis of Hydrocarbons in Supercritical Water at High Pressures." *Ber. Bunsenges. Phys. Chem.* **97**(9): 1091-1098.
- Holgate, H. R. (1993). "Oxidation Chemistry and Kinetics in Supercritical Water: Hydrogen, Carbon Monoxide, and Glucose." thesis, Chemical Engineering, Massachusetts Institute of Technology, Cambridge, MA.

- Holgate, H. R. and J. W. Tester (1994a). "Oxidation of hydrogen and carbon monoxide in sub- and supercritical water: reaction kinetics, pathways, and water-density effects. 1. experimental results." *J. Phys. Chem.* **98**(3): 800-809.
- Holgate, H. R. and J. W. Tester (1994b). "Oxidation of hydrogen and carbon monoxide in sub- and supercritical water: reaction kinetics, pathways, and water-density effects. 2. elementary reaction rate modeling." *J. Phys. Chem.* **98**(3): 810-822.
- Hughes, K. J., T. Turanyi, et al. (2001). "Development and testing of a comprehensive chemical mechanism for the oxidation of methane." *International Journal of Chemical Kinetics* **33**(9): 513-538.
- Janoschek, R. and M. J. Rossi (2002). "Thermochemical Properties of Free Radicals from G3MP2B3 Calculations." *Int. J. Chem. Kinet.* **34**: 550-560.
- Kaiser, E. W., C. K. Westbrook, et al. (1986). "Acetaldehyde Oxidation in the Negative Temperature Coefficient Regime: Experimental and Modeling Results." *International Journal of Chemical Kinetics* **18**: 655-688.
- Kappel, C. K., K. Luther, et al. (2002). "Shock wave study of the unimolecular dissociation of H<sub>2</sub>O<sub>2</sub> in its falloff range and of its secondary reactions." *Phys Chem Chem Phys* **4**: 4392-4398.
- Larson, C., P. Stewart, et al. (1988). "Pressure and Temperature Dependence of Reactions Proceeding Via a Bound Complex. An Approach for Combustion and Atmospheric Chemistry Modelers. Application to HO + CO → [HOCO] → H + CO<sub>2</sub>." *Int. J. Chem. Kinet.* **20**: 27-40.
- Lee, J. H. and N. R. Foster (1996). "Direct Partial Oxidation of Methane to Methanol in Supercritical Water." *The Journal of Supercritical Fluids* **9**: 99-105.
- Marinov, N. M. (1999). "A Detailed Chemical Kinetic Model for High Temperature Ethanol Oxidation." *International Journal of Chemical Kinetics* **31**: 183-220.
- Marinov, N. M. W., C. K.; Pitz, W. J. (1995). "Detailed and global chemical kinetics model for hydrogen." *Transport Phenomena in Combustion, Proceedings of the International Symposium on Transport Phenomena in Combustion, 8th*, San Francisco.
- Meeks, E., H. K. Moffat, et al. (1996). AURORA: A Fortran Program for Modeling Well Stirred Plasma and Thermal Reactors with Gas and Surface Reactions, Sandia National Laboratories.
- Melius, C. F., N. E. Bergan, et al. (1990). "Effects of water on combustion kinetics at high pressure". *Twenty-Third Symposium (International) on Combustion*, Orleans, France.

- Nozaki, T. H., Akinori; Okazaki, Ken. (2004). "Partial oxidation of methane using a microscale non-equilibrium plasma reactor." *Catalysis Today* **98**(4): 607-616.
- Ploeger, J. (2006). "Co-oxidation in SCW:MPA-Ethanol and Ammonia-Ethanol Model Systems." PhD thesis, Chemical Engineering, MIT, Cambridge, MA.
- Ploeger, J. M., B. P.A., et al. (2005). "Modeling Oxidation and Hydrolysis Reactions in Supercritical Water -- Free Radical Elementary Reaction Networks and their Applications." *Combust. Sci. Technol.*
- Rice, S. and E. Croiset (2001). "Oxidation of simple alcohols in supercritical water III. formation of intermediates from ethanol." *Ind. Eng. Chem. Res.* **40**: 86-93.
- Ruscic, B. and M. Litorja (2000). "Photoionization of HOCO Revisited: A New Upper Limit to the Adiabatic Ionization Energy and Lower Limit to the Enthalpy of Formation." *Chemical Physics Letters* **316**: 45-50.
- Sato, T., M. Watanabe, et al. (2003). "Analysis of the density effects on partial oxidation of methane in supercritical water." *The Journal of Supercritical Fluids* **00**: 1-9.
- Savage, P. E., R. Li, et al. (1994). "Methane to Methanol in Supercritical Water." *The Journal of Supercritical Fluids* **7**(2): 135-144.
- Savage, P. E., J. Rovira, et al. (2000). "Oxidation kinetics for methane/methanol mixtures in supercritical water." *The Journal of Supercritical Fluids* **17**: 155-170.
- Savage, P. E., J. Yu, et al. (1998). "Kinetics and mechanism of methane oxidation in supercritical water." *The Journal of Supercritical Fluids* **12**: 141-153.
- Schmitt, R. G., P. B. Butler, et al. (1993). CHEMKIN Real Gas. University of Iowa.
- Senosiain, J. P., C. B. Musgrave, et al. (2003). "Temperature and pressure dependence of the reaction of OH and CO: Master Equation Modeling on a high-level potential energy surface." *International Journal of Chemical Kinetics* **35**: 464-474.
- Steinfeld, J. I., J. S. Francisco, et al. (1999). Chemical Kinetics and Dynamics. Upper Saddle River, NJ, Prentice-Hall, Inc.
- Sullivan, P. (2003). "Oxidation Kinetics of Methylphosphonic Acid in Supercritical Water: Experimental Measurements and Model Development." thesis, Department of Chemical Engineering, MIT, Cambridge, MA.
- Tsang, W. and R. F. Hampson (1986). "Chemical Kinetic Database for Combustion Chemistry. Part I. Methane and Related Compounds." *Journal of Physical Chemistry Reference Data* **15**: 1087.

- 
- Ung, A. Y. M. and R. A. Back (1964). "Photolysis of water vapor and reactions of hydroxyl radicals." *Can J Chem Rev De Chim* **42**(4): 753-763.
- Vogel, F., J. L. DiNaro Blanchard, et al. (2005). "Critical Review of Kinetic Data for the Oxidation of Methanol in Supercritical Water." *Journal of Supercritical Fluids* **34**: 249-286.
- Warnatz, J. (1984). Rate coefficients in the C/H/O system. *Combustion Chemistry*. W. C. J. Gardiner. New York, Springer-Verlag: 197-360.
- Webley, P. A. (1989). "Fundamental Oxidation Kinetics of Simple Compounds in Supercritical Water." thesis, Department of Chemical Engineering, MIT, Cambridge, MA.
- Webley, P. A. and J. W. Tester (1991). "Fundamental Kinetics of Methane Oxidation in Supercritical Water." *Energy and Fuels* **5**(3): 411-419.
- Yetter, R. A., F. L. Dryer, et al. (1991). "A comprehensive reaction mechanism for carbon monoxide/hydrogen/oxygen kinetics." *Combust. Sci. Technol.* **79**: 129-140.
- Yu, H. G., J. T. Muckerman, et al. (2001). "A theoretical study of the potential energy surface for the reaction  $\text{OH} + \text{CO} = \text{H} + \text{CO}_2$ ." *J Chem Phys Lett* **349**: 547-554.
- Zhang, Q., D. He, et al. (2002). "Comparatively high yield methanol production from gas phase partial oxidation of methane." *Applied Catalysis A: General* **224**: 201-207.

## 6 Model Maillard Reaction under Hydrothermal Conditions

### 6.1 MOTIVATION AND INTRODUCTION

Recall from Chapter 1 that there are many advantages to employing hydrothermal environments in the conversion of waste biomass to fuels and other useful products. Numerous research studies have explored the gasification and conversion of wet waste biomass in sub and supercritical water achieving encouraging results. However, some studies have uncovered conditions which lead to the formation of undesirable side products. For example, feed stocks high in carbohydrates and proteins have formed undesirable nitrogenous polymer side products which reduce yields of saleable products and clog components of hydrothermal systems (Adams, 2004). The objective of this study is to examine reactions of a model carbohydrate and amino acid system at hydrothermal conditions. We will determine reaction kinetics and global pathways and possibly identify a set of parameters that may reduce the yields of undesired polymeric products. Work on this project is part of a collaboration with other research group members, including Andrew Peterson and Sam Maurer and Dr. K.C. Swallow, a visiting professor from Merrimack College. Although the final objectives of this project will not be achieved for several months, the initial results are presented here to summarize my contributions in the project's initial phases.

#### 6.1.1 *The Maillard Reaction*

The problematic reaction described above is generally called a Maillard reaction, named after L.C. Maillard who began the first series of studies on reactions between sugars and amino acids in 1912 (Vallentyne, 1964). This reaction is extremely well-known in the food processing industry and is responsible for several common sights and smells such as the browning of bread



or the flavor of coffee. Maillard reactions involving various combinations of reducing sugars and amino compounds have been studied extensively and are thought to proceed through three basic phases of a reaction scheme first proposed by (Hodge, 1953) and reproduced in Figure 6-1.

In the first phase, the carbonyl group of a reducing sugar combines with a free amino group of an amino acid in a condensation reaction to form an n-substituted glycosylamine. This intermediate is unstable and rearranges into an “Amadori” compound. In the second phase the Amadori compounds can react one of three ways. One way is through the loss of two more water molecules to form reductones and dehydroreductones which can further degrade to aldehydes and aldols. A second path is through various fission products like acetol, diacetyl and pyruvaldehyde which can also further degrade to intermediate products. The third path forms a Schiff’s base of hydroxymethyl furfural (HMF) or furfural through the loss of three water molecules. In the third phase, all intermediate products can then react further with amino acids to form the brown nitrogenous polymers and copolymers know as melonoidins.

### *6.1.2 Influencing the Maillard Reaction*

The wealth of Maillard reaction research has identified the effects of certain parameters on the rate of formation and yields of melanoidin products. Although most of these studies are focused on temperatures less than 250°C and lower pressures, they may provide some insight into which parameters are most important under hydrothermal conditions.

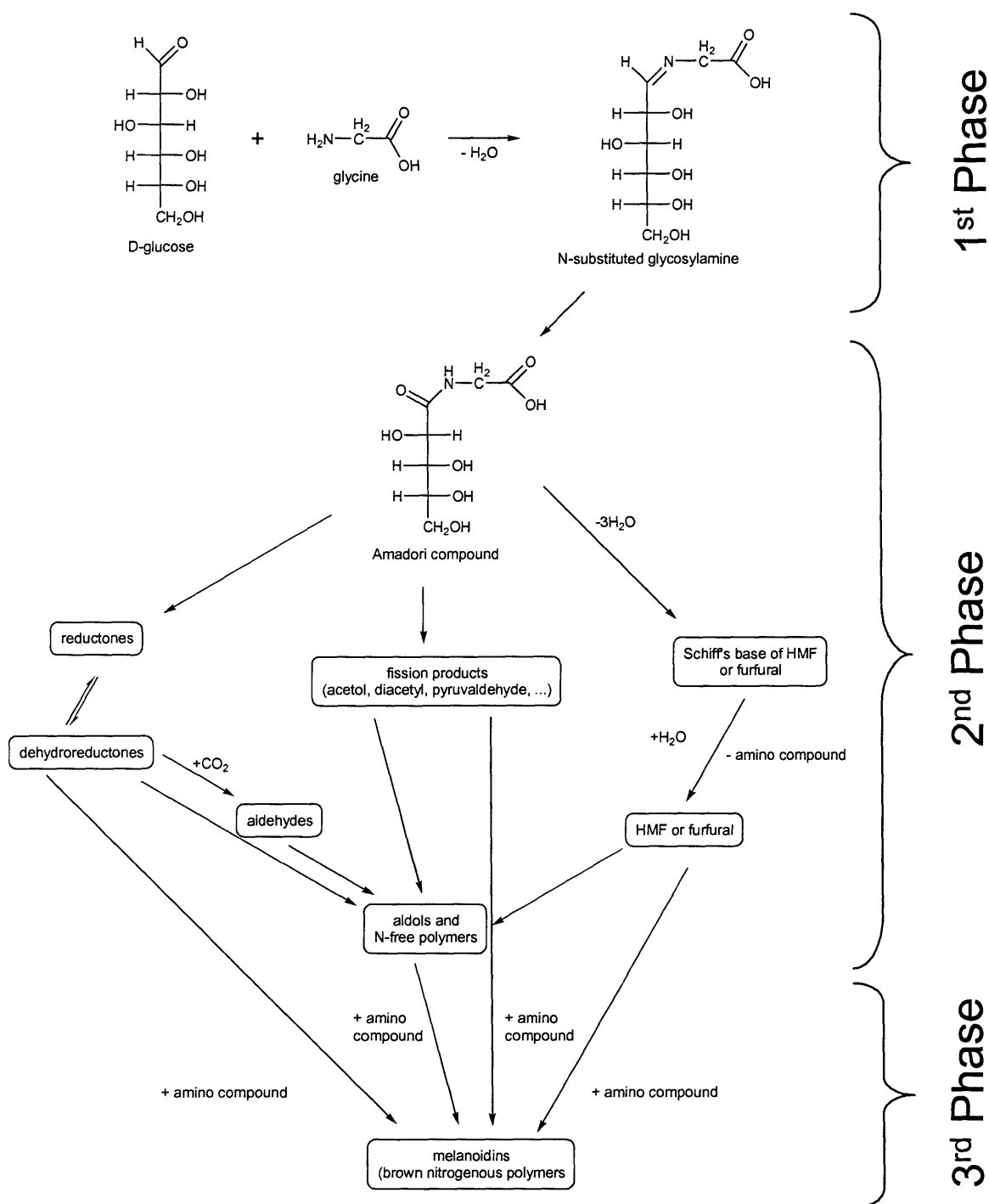


Figure 6.1. Mechanism of Maillard reaction commonly cited from Hodge (1953).

- **Temperature and time:** Studies have shown that increases in temperature and/or time generally result in higher melanoidin yields (Scaman, 2005).
- **System composition:** Typically, pentoses are more reactive than hexoses and basic amino acids are more reactive than aliphatic amino acids. Also, the more dilute one component is, the more slowly the Maillard reaction progresses. For example, with an initial glucose-glycine ratio of 10:1 progressed more slowly than with an initial ratio of 1:1 (Scaman, 2005; Vallentyne, 1964).
- **Water concentration:** The mechanism in Figure 6-1 shows the overall production of water during the Maillard reaction so it is logical to assume that higher water concentrations would hinder the production of melanoidins. However, very few studies of Maillard reactions under hydrothermal conditions can be found in the literature (Scaman, 2005).
- **pH:** Although there are conflicting reports on the effects of pH, it is generally thought that lower pH inhibits Maillard reactions because of the presence of the less reactive protonated form of the amino group and the less reactive closed form of the sugar (Martins, 2003; Scaman, 2005).
- **Pressure:** Conflicting reports exist for the effects of pressure at high pH, but most reports agree that higher pressures inhibit the Maillard reaction at lower pHs (Bristow and Isaacs, 1999; Hill, Isaacs *et al.*, 1999; Hill, Ledward *et al.*, 1996; Moreno, Molina *et al.*, 2003).

## 6.2 PREVIOUS GLUCOSE-GLYCINE STUDIES

Although the glucose-glycine model Maillard reaction system chosen for this study has been examined extensively under typical food processing conditions (see, for example, Tehrani, Kersiene *et al.*, 2002; Manzocco and Maltini, 1999; Leong and Wedzicha, 1999), little is known about the effects of a hydrothermal environment on these mixtures. Glucose and glycine have been studied separately at hydrothermal conditions but only one study exists on the model mixture of glucose and glycine under hydrothermal conditions. A review of that study and an

overview of previous glucose and glycine single compound hydrothermal studies are presented here.

### 6.2.1 Glycine in sub and supercritical water

Few studies have been performed with glycine as a model compound under hydrothermal conditions, but most studies agree that it is highly refractory in sub-critical water. Vallentyne (1964) studied the thermal stability of several amino acid solutions in unknown pressure conditions. He reported a 0.37-life of 2-3 hours for a 0.01M glycine solution at 252°C. (Alargov, Deguchi *et al.*, 2002) examined hydrothermal glycine reactions from 250 - 400°C and 150 - 400 bar by injecting a room-temperature glycine solution into sub and supercritical water and analyzing the quenched effluent after approximately 10 seconds of reaction time. Significant conversion was only seen at 300°C and above. This study focused on the formation of glycine oligomers and measured significant quantities of diglycine and diketopiperazine (glycine anhydride) at higher temperatures and lower pressures.

Islam, Kaneko *et al.* (2003) confirmed the findings of Alargov with a separate study in a flow reactor at 250 bar, 200 - 400°C, two minutes residence time, an initial glycine concentration of 0.1M. Di-, tri- and tetraglycine were formed along with diketopiperazine at 200 - 350°C but not at supercritical water conditions at 400°C. Unlike Alargov, Islam reported diketopiperazine yields to decrease with temperature, but the residence times of the two studies were drastically different. It is possible that the longer residence times of Islam's experiments allowed the further degradation of these glycine oligomers.

Sato, Quitain *et al.* (2004) studied the decomposition of five different amino acids in high temperature high pressure water, and postulated the fate of glycine based on its formation and subsequent degradation in this study and data from an earlier study published in a Japanese

journal (Sato, Daimon *et al.*, 2002). They found that glycine can hydrothermally degrade through three possible routes: decarboxylation forming methyl amine and CO<sub>2</sub>, deamination and reaction with water to form glycolic acid or deamination and reaction with oxygen to form formic acid and CO<sub>2</sub>. They also published Arrhenius parameters for glycine decomposition at 300 bar from 260 – 340°C, but no rate data were provided, making it impossible to evaluate the quality of their results.

$$k_{\text{glycine}} (kJ, mol, s) = 3.51 \times 10^{13} \exp(-166 / RT) \quad (6-1)$$

### 6.2.2 Glucose in sub and supercritical water

Hydrolysis of glucose has been the subject of many experimental studies for over a century and all confirm the rapid degradation of glucose under hydrothermal conditions. Kruse, Krupka *et al.* (2005) list 39 references alone that cover glucose-related hydrothermal research in the past 15 years. An overall degradation network for glucose under hydrothermal conditions is presented in Figure 6-2, compiled from some of the more recent studies. The earlier glucose hydrolysis work focused on sub-critical conditions in the temperature range of 100 – 250°C reporting 5-hydroxymethylfurfural (5-HMF) as the major degradation product at those conditions. 5-HMF would then hydrolyze further to levulinic acid and formic acid or polymerize to a colored sugar solution (Wolf from, Schuetz *et al.*, 1948; Singh, 1948; Newth, 1951; Mednick, 1962).

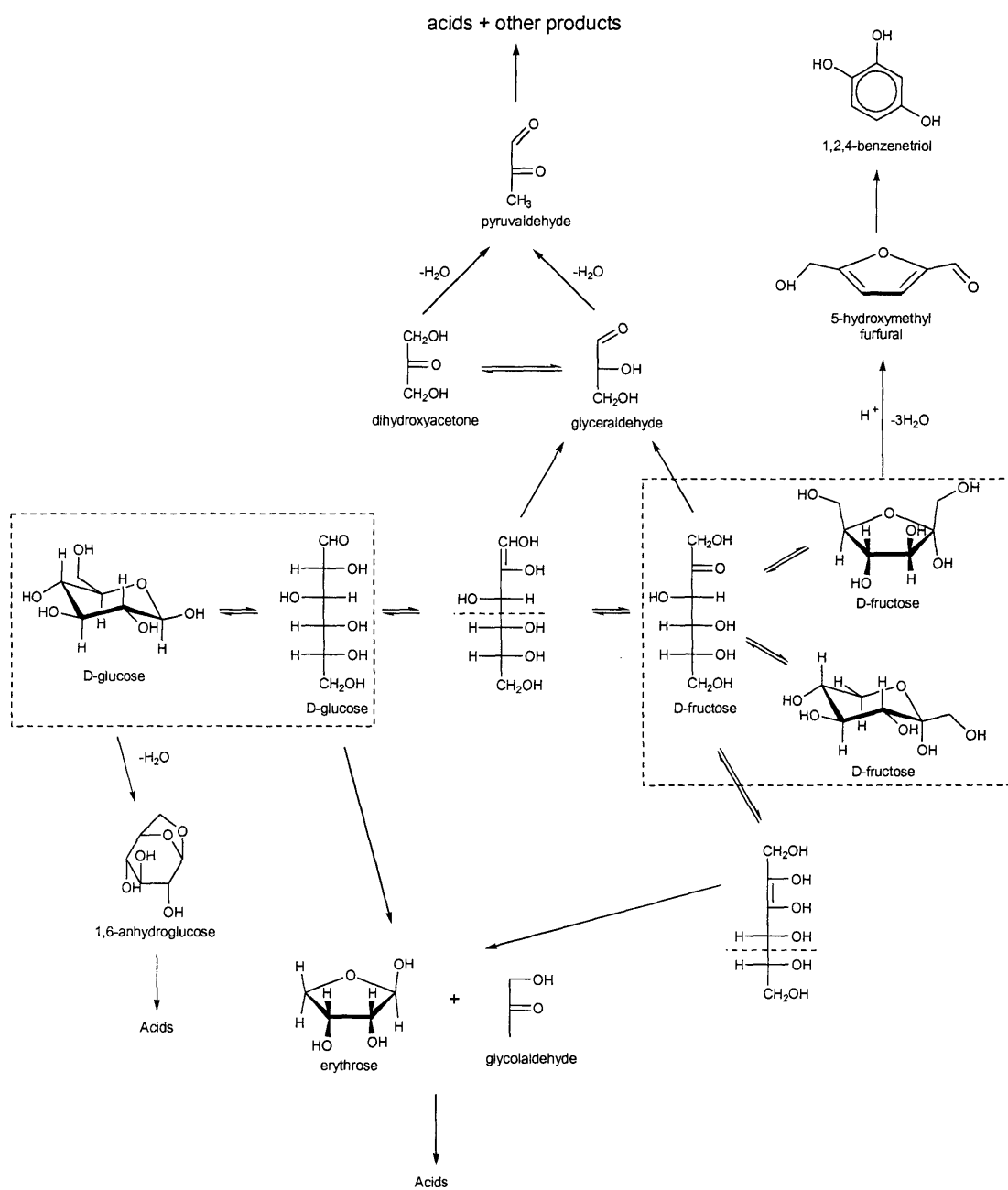


**Figure 6.2. Reaction network for glucose destruction.** Adapted from (Kabyemela, Adschiri et al. (1997)), Antal et al (1990), and Srokol et al (2004).

The first studies of glucose hydrolysis in supercritical water were conducted at MIT in the 1970s (Amin, Reid *et al.*, 1975). Reports from these early studies showed the glucose hydrolysis product spectra changing from char and liquid organics below the critical temperature of water to gases, little char and liquid furans and furfurals above the critical point (Amin, Reid *et al.*, 1975; Modell, 1985; Woerner, 1976). Researchers in Antal's group at the University of Hawaii have extensively studied the hydrolysis of glucose and related sugars over a wide range of sub and supercritical water conditions. In their work on the sub-critical hydrolysis of fructose, sucrose and xylose, they found the major degradation products to be 5-HMF and furfurals with smaller amounts of formic acid, lactic acid, levulinic acid, pyruvaldehyde and glyceraldehyde being formed (Antal, Mok *et al.*, 1990; Antal and Mok, 1988; Antal, Leesomboon *et al.*, 1991). Holgate and Meyers, also from MIT, studied short time glucose hydrolysis and oxidation in supercritical water and identified similar hydrolysis products in addition to finding significant quantities of acetic acid and acetaldehyde at lower supercritical temperatures (Holgate, Meyer *et al.*, 1995). Three more recent studies, which cite these earlier works, provide an adequate description of the current knowledge of glucose hydrothermal degradation.

Kabyemela, Adschiri *et al.* (1999) published a thorough account of their work on the decomposition of glucose and fructose at 300 – 400°C, 250 – 400 bar and very short residence times of 0.02 to 2 seconds, identifying major products and pathways and developing kinetic expressions for macroscopic pathways. Glucose destruction was drastic; they reported approximately 55% conversion after 2 seconds at 300°C and 90% conversion after 1 second at 350°C. A list of observed decomposition products from this and other studies is provided in Table 6-1. However, a concern with this study is that although they reported short residence times, they do not discuss relative mixing length after the cold sugar solution meets the pre-

heated sub and supercritical water. Their results may have been affected by pre-mature degradation of the sugar during the short but drastic heat-up period and/or pyrolysis rather than hydrolysis degradation due to inadequate mixing.

**Table 6.1. Glucose degradation products observed in various studies.** Studies and their conditions are given at the bottom of the table.

<i>Compound</i>	<i>Study</i>
acetaldehyde	[d, c]
acetic acid	[a-d]
acetone	[d]
acetylacetone (2,5-hexanedione)	[c]
2-acetylfuran	[c]
acrylic acid (propenoic acid)	[d, c]
1,6-anhydroglucose	[a, b]
1,2,4-benzenetriol	[d]
cellobiose	[b]
dihydroxyacetone	[d, a]
erythrose	[a]
formic acid	[d-b]
fructose	[a, b]
2-furaldehyde (furfural)	[d, c]
glyceraldehyde	[d, a]
glycolaldehyde	[d, a]
glycolic acid	[d]
5-hydroxymethylfurfural	[a-d]
lactic acid	[d, c]
levulinic acid	[b]
5-methylfurfural	[c]
pyruvaldehyde	[d, a]
solid precipitate ("humic solid")	[b]
<b>gaseous products</b>	<b>[b]</b>

(a) (Kabyemela): 300-400°C, 250-400 bar, 0.02-2 sec.

(b) (Xiang): 200-230°C, unreported pressure (sealed in ampoules), 0.5-30 min, with weak H<sub>2</sub>SO<sub>4</sub>.

(c) (Holgate): 425-600°C, 246 bar, 6 sec.

(d) (Srokol): 340°C, 275 bar, 120 sec.

Srokol, Bouche *et al.* (2004) studied the hydrothermal treatment of several dilute (50mM) monosaccharides at 340°C, 275 bar and 25-204 seconds residence in a tubular flow reactor. They observed 5-HMF and glycolaldehyde as the major products in the degradation of four



different sugars, but fructose formed mostly 5-HMF while glucose formed mostly glycolaldehyde. This implies that while glucose and fructose can isomerize, their different degradation products prevent them from being in equilibrium at these conditions. This study includes the effects of acid and base additions on the product spectra, and the results of separate experiments studying the subsequent degradation of intermediate products of glucose. 5-HMF and glycolaldehyde appear under both acid and base conditions which might be attributed to the high  $K_w$  of water at sub-critical conditions, but certain pathways, like the path to HMF, appear to be suppressed under basic conditions. The reaction pathway work of this study significantly contributed to the generation of Figure 6-2.

Xiang, Lee *et al.* (2004) studied the kinetics of glucose decomposition in dilute-acid mixtures at 180-230°C in sealed glass ampoule reactors at unspecified pressures. At 200°C, glucose conversion was measured to be approximately 15% after 5 minutes and approximately 55% after 30 minutes in solutions with an ambient pH of 1.8. Also at 200°C, lower ambient pH solutions seemed to increase glucose destruction with the highest conversion being approximately 68% after 30 minutes at a pH of 1.5. Degradation products identified in this study are in general agreement with previous studies and are included in Table 6-1.

### 6.2.3 Glucose and Glycine Mixtures in sub and supercritical water

Inoue and co-workers published the only study in the literature on the hydrothermal treatment of model glucose and glycine mixtures (Inoue, Noguchi *et al.*, 2004; Minowa, Inoue *et al.*, 2002). They reacted mixed solutions of 10 mM glucose and 10 mM glycine in a 100 mL autoclave which was purged and pressurized with nitrogen gas to 30 bar and equipped with a magnetic stirrer. The autoclave was then gradually heated in an electric furnace to 150 – 350°C and rapidly cooled after reaching the designated temperature. One long residence time experiment was performed where cooling was delayed for one hour after reaching 350°C. The products were then separated into four different phases for analysis: gas, aqueous, oil (acetone solubles) and solid residue.

This preliminary study reported only limited findings. The yields of oil and diethyl ether extracts increased with temperature. Pyrazines and pyridines were identified as the primary nitrogen-containing compounds in the oil and aqueous phases. The authors postulated that these compounds were derived from the decomposition of melanoidin polymers, but their limited data and proposed mechanism can also support a theory that these compounds are melanoidin precursors. Although one can certainly learn from their detailed analysis of reaction products, the results of the Inoue *et al.* study are difficult to interpret given a lack of information on reaction pressures, temperature profiles, reactant exit concentrations and estimates of error.

---

### **6.3 INITIAL EXPERIMENTAL RESULTS FROM GLUCOSE/GLYCINE**

#### **DEGRADATION STUDIES**

Initial scoping experiments using tubular batch cells in a fluidized sand bath resulted in high conversions and difficulties with product recovery. Follow-up experiments were conducted on our high pressure CSTR, fully described earlier in Section 3.2. Although the CSTR system proved to be appropriate to study the more refractory compound glycine, experiments with glucose and glucose-glycine mixtures resulted in near complete conversion even at the shortest reactor hold-up times. In order to examine much shorter residence times and partial conversion conditions, a short plug-flow reactor (PFR) was installed which bypassed the CSTR, connecting the cross which mixed the preheated water and cold organic solution to the tank heat exchanger. The PFR was a 316 SS tube, ¼" O.D. (6.35 mm) x 1/8" I.D. (3.18mm) x 1.5m long, which resulted in a 7 second residence time at a liquid flow rate of 100 mL/min. Reynolds numbers in the PFR were calculated to be in the range of 2000 – 9000 at our conditions. Unfortunately, a temperature drop (~5- 10°C) was observed from the inlet to the outlet of the PFR that was not resolved until after the experiments of this study and should be considered when analyzing this preliminary data. A total of 36 experiments were performed to investigate glucose and glycine separately and glucose-glycine mixtures. A summary of the reaction conditions and conversion results is provided in Table 6-2.

**Table 6.2. Results obtained in preliminary experiments on glucose and glycine.** CSTR experiments had residence times of 3-67 min while PFR experiments had 10 sec residence times. Initial concentrations for glycine and glucose ranged from 100 – 2000 ppm.

<i>Reactant</i>	<i>Conditions</i>	<i>Conversion</i>
Glycine	250°C, 55 bar, 4-12 min, pH 2,5	0-5%
	250°C, 55 bar, 67 min, pH 5	0-5%
	300°C, 110 bar, 6 min, pH 5	33%
Glucose	250°C, 55 bar, 6 min, pH 5	86%
	100-300°C, 55 bar, 7 sec, pH 5	0-86%
Glucose + Glycine	250°C, 55 bar, 6 min, pH 2,5	98-100% of both
	100-300°C, 55 bar, 7 sec, pH 5	0-100% of both

In our study, several issues with the reactor system were experienced and may have impacted our results. As discussed in Section 3.2, we have identified shortcomings with the present CSTR design that involve possible mixing issues and phase separation issues. These issues may help explain the fact that our carbon balance for glycine experiments was consistently high (~101-113%). Another possible explanation for high carbon balance is the possibility of glycine precipitating out of the concentrated feed solutions in the small dead volumes of the syringe pump feed system which may have added glycine to the next feed solution loaded into the syringe pump.

When the PFR bypass was installed, we measured sporadic concentrations in the effluent which may have resulted from improper mixing at the mixing cross or inconsistent flow of the syringe pump or complications with a check valve. These sporadic readings were not seen in the CSTR experiments, presumably due to improved mixing in the larger volume CSTR following the mixing tee. The slow flow of the concentrated organic feed mixing with the pre-heated water feed may result in improper and sporadic mixing initially that does not have time to be resolved

in the short PFR before the heat exchanger. Improvements to the current mixing cross or alternate mixing cross designs should be explored for future experiments.

For glucose and glucose-glycine experiments at our conditions, it is possible to form solid and even additional liquid phases that present phase separation issues and difficulties achieving steady state conditions. We installed a series of 0.5  $\mu\text{m}$  filters in a filter bank downstream of the heat exchanger, but during the course of an experiment, the pressure drop across that bank increases as solids build-up. We have not seen the formation of a second liquid or oil phase, but we have seen the effluent drastically change color which makes it difficult to observe phase splitting. If a second liquid phase is forming, it may be small, difficult to detect and possibly accumulating in a dead zone of our system. Naturally any of these issues will complicate our results. Nonetheless, this set of initial experiments helped to identify the experimental operating conditions and analytical protocols necessary for a more detailed analysis of this model Maillard system in hydrothermal media.

### *6.3.1 Initial degradation results: Glycine*

Glycine alone was found to be unreactive in water at 250°C since greater than 95% of the glycine fed into the system was recovered. Our experiments covered residence times ranging from 3 to 10 minutes and initial glycine concentrations ranging from 100 to 2000 ppm. Although we found a consistent trend towards slightly more destruction at pH 2 than at pH 5, the highest conversion measured at 250°C was only 8%. Increasing the residence time by an order of magnitude, to 67 minutes, showed no significant increase in glycine destruction. Raising the temperature from 250°C to 300°C increased destruction from <5% to approximately 33%. These results are consistent with those of Vallentyne but slower than those of Sato as previously

discussed in Section 6.2.1. However, Sato's experiments were at a higher pressure (300 bar) and difficult to further analyze due to a lack of information provided.

### 6.3.2 Initial degradation results: Glucose

Glucose was much more reactive than glycine, with approximately 85-90% conversion after six minutes in the CSTR at 250°C. As expected, when glucose was studied in the PFR bypass at temperatures from 50 – 250°C at seven seconds residence time, lower conversions were observed. Glucose destruction was still high at 250°C ( $X \sim 60\%$ ), but at lower temperatures we achieved much lower conversions (e.g.,  $X \sim 35\%$  at 200°C and  $X \sim 6\%$  at 150°C).

Figure 6-3 plots the results of assumed first order Arrhenius behavior from our scoping experiments with glucose in the PFR and CSTR system (diamonds and triangles in that figure, respectively). The data from related studies by other groups are also plotted for comparison. Although all sets of data appear to conflict, there may be reasonable explanations for the discrepancies. For example, the Xiang data are from long time batch studies in glass ampoules with unknown pressures, phase behavior and mixing behavior. The Kabyemela data are from extremely short time flow experiments in metal reactors at higher pressures (250-400 bar). Our preliminary results seem to indicate faster glucose degradation in our system than observed/reported in previous studies and a smaller global activation energy. Possible explanations for these discrepancies include the PFR and CSTR issues mentioned earlier as well as possible pressure effects and reactor wall material effects. Other explanations may include a proper assessment of errors and uncertainties from these other studies that are not currently reported. It is clear from the comparison of data in Figure 6-3 that hydrothermal glucose degradation is a complex process that must be carefully characterized in order to arrive at meaningful results.

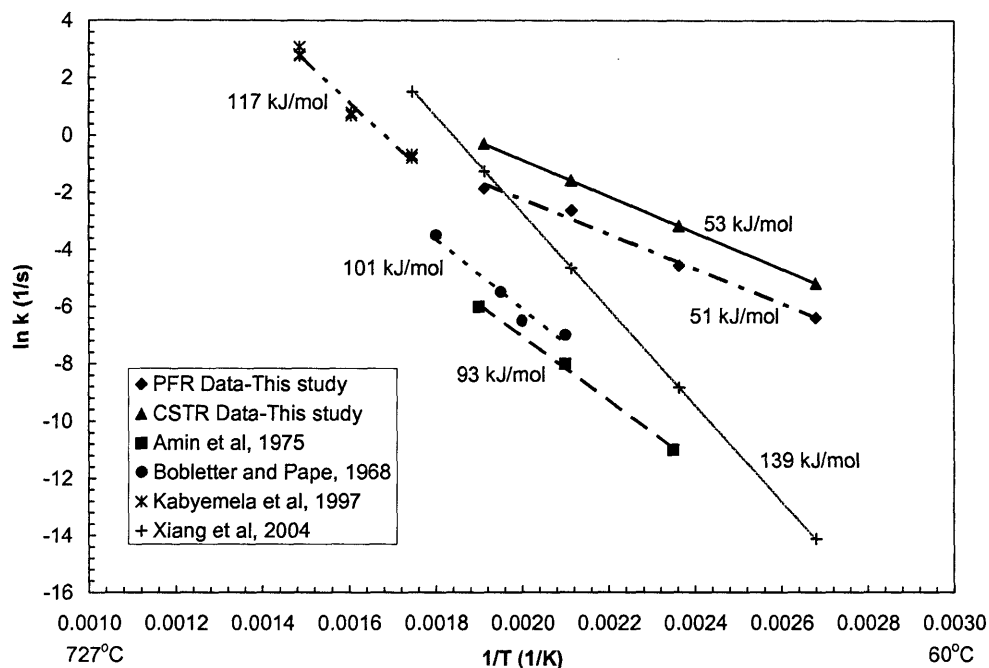


**Figure 6.3. Assumed First Order Arrhenius Plot of Glucose Degradation Data.** Values for activation energies displayed next to linear fits. PFR and CSTR data from this study. Data from Amin et al, Bobleter and Pape, and Kabyemela et al from Kabyemela *et al.*, 1997. Xiang *et al* data from Xiang *et al*, 2004.

### 6.3.3 Kinetics of degradation: Glucose and Glycine Mixtures

Mixtures of glucose and glycine react much more readily than either component alone. Before the tubular flow reactor bypass was built, experiments were conducted with a glucose-glycine mixed feed in the CSTR at 250°C and 6 minutes residence time. Both glucose and glycine were nearly non-detectable in the outlet streams for those experiments indicating complete conversion. We recently conducted our first set of experiments with a glucose-glycine mixture fed to our short residence-time tubular flow reactor, but we have been unable to analyze those results due to HPLC failures. However, the HPLC chromatograms of the products from

---

those experiments follow a similar trend to the glucose short time degradation results – little conversion and formation of degradation products below 200°C.

## 6.4 PRODUCT IDENTIFICATION

### 6.4.1 Analytical Techniques

The complex chemistry involved in this study presents several challenging analytical problems. Despite months of work, we have made only limited progress in developing proper techniques for product identification and quantification. Nevertheless, this limited progress has provided significant insight into the outline of degradation pathways for this model Maillard system. The suite of analytical methods employed in this study include two different HPLC methods, an assay method for spectrophotometric determine of glucose, the use of pH and ammonia electrodes, total organic carbon (TOC) analysis of the liquid phase, elemental (carbon, hydrogen, nitrogen (CHN)) analysis of the solid phase, and multiple GC methods for both gas and liquid phase analysis. Although we were prepared to analyze the gas phase in this study, we never observed sufficient gas flow to adequately quantify gas phase products.

The reactants, glycine and glucose, are separated and quantified by one HPLC method using both refractive index and ultra-violet detection. This method is based on a similar method for sugar detection found in the literature (Karkacier, Erbas *et al.*, 2003), and was chosen for its versatility and speed in separating and detecting both glucose and glycine without complicated pre-column derivatization. Other methods were explored including electrochemical detection with a pulsed amperometric detector and spectrophotometric methods with assays, but those methods achieved poor results due to complications with the mixtures or loss of sensitivity



to one or both reactants. The glucose-glycine HPLC method uses a DIONEX isocratic pump (model IP25) flowing a 75:25 mixed solvent of low UV acetonitrile:water at 1.0 mL/min. The column is an Alltech Alltima Amino 100A, 5  $\mu$  column, 250mm x 4.6mm (P/N 88217) preceded by an Alltech Alltima Amino 5  $\mu$  guard column cartridge (P/N 96085). The column is contained in a Timberline column heater set at 30°C. The eluents first flow through a Rainin Dynamax UV/visible detector (Model UV-D II) set at 190 nm then a Varian Refractive Index (RI) Detector (Model Star 9040). The UV detector is more sensitive for glycine where as the RI detector is more sensitive to glucose. A Rainin Dynamax autosampler (model AI-200)) handled all standards and samples injecting a full-loop (20  $\mu$ L sample loop) onto the column and washing in between injections with 250  $\mu$ L of the same degassed 75: 25 acetonitrile:water mobile phase. This method lacks some sensitivity to glucose, so the glucose concentrations of several samples were separately confirmed with a standard enzymatic technique similar to the one employed by Holgate (1993) (SIGMA P/N GAHK-20).

Although this HPLC method was convenient for separation and quantification of reactants, it did a poor job of separating degradation products with most compounds not being retained by the column. Therefore, a separate HPLC method was developed for product identification and quantification based on similar method found in Holgate (1993). A Beckman System GOLD HPLC system was used for this method which consisted of two solvent delivery modules (Models 116 and 126) and a UV Diode Array detector (Model 168). A 0.01N H<sub>2</sub>SO<sub>4</sub> mobile phase was delivered at 0.7 mL/min to an Interaction Ionguard column and an Interaction ORH-801 organic acid column contained in a Timberline column heater set at 60°C. Detection was by absorption at 210 nm for organic acids and 290 nm for compounds containing isolated carbonyl groups and other chromophores. Samples were injected by a Rheodyne two-position

---

zero-volume valve with a 20  $\mu\text{L}$  sample loop (P/N 7161). Peak identification was accomplished by comparison of sample peak retention times with those of standard solutions of pure compounds. Calibrations for identified products were not yet performed, but all injected standards were nominally 100 ppm which provided a rough concentration to area count ratio for semi-quantitative analysis. Table 6-3 contains a complete list of all compounds tested by this HPLC UV method. It includes compounds previously found in glucose degradation studies (see Table 6-1) and other compounds thought to be possible intermediates in the combined degradation of glucose-glycine.

Other analytical methods used in this study include pH and ammonia selective electrodes (Hach P/N 51910 and Orion P/N 9512BN respectively). GC methods described previously in Section 3.5.1 were also employed for gas phase analysis, but gas products were not quantified due to insufficient gas flow for all experiments. GC analysis was also performed on select liquid phase samples following the GC method described in section 3.5.1, but few peaks were observed or identified using this method. Total organic carbon (TOC) analysis of the liquid phase and elemental (carbon, hydrogen, nitrogen (CHN)) analysis of the solid phase were also performed with the help of Professor Gschwend's lab at MIT. Unfortunately the results from the TOC analysis were disappointing. All but one sample, including prepared standards gave higher TOC readings than anticipated. The high readings for the standards,  $\sim 10\%$  higher than anticipated, may have been due to a systematic problem with the instrument, but the high readings for our samples ( $\sim 20\%$  higher than anticipated) may have been due to residual organic in our lab DI water. Our lab DI water was tested separately and found to have  $\sim 2.4$  ppm TOC. Factoring in this level of background contamination gave more reasonable results for our samples which had to be diluted ten to fifty times to fall within the calibrated range of 0 – 20 ppm.

**Table 6.3. Summary of Compounds Tested as Possible Liquid Phase Products.** Retention times correspond to an Interaction ORH-801 organic acid column heated to 60°C, 0.01N H<sub>2</sub>SO<sub>4</sub> mobile phase, 0.7 mL/min flow rate.

<i>Compound</i>	<i>RT, min</i>	<i>λ, nm</i>	<i>Glucose Experiments</i>	<i>Glucose-Glycine Experiments</i>	<i>Comments</i>
<i>Glucose degradation products from Table 6-1</i>					
acetaldehyde	11.60	290			
acetic acid	9.69	210	√	√	
acetone	13.95	290			
acetonylacetone (2,5-hexanedione)	15.27	210,290			2 <sup>nd</sup> peak @ 32.67
2-acetylfuran	34.90	210			
acrylic acid (propenoic acid)	11.39	210	√	√	2 <sup>nd</sup> peak @ 13.10
1,6-anhydroglucose	ND	210,290			
1,2,4-benzenetriol	16.72			√	Many peaks
cellobiose	ND				Small peak @ 12
dihydroxyacetone	8.66	210	√		
erythrose	ND				
formic acid	8.75	210	√		
fructose	ND				Small peaks 6.4, 8.2
2-furaldehyde (furfural)	28.90	210,290		√	
glyceraldehyde	11.37	210,290			Small peak @7.3
glycolaldehyde	7.97	210,290			
glycolic acid	7.84	210	√		
5-hydroxymethylfurfural	19.71	210,290	√	√	
lactic acid	8.15	210	√	√	
levulinic acid	10.30	210,290	√	√	
5-methylfurfural	42.75	210		√	
pyruvaldehyde	7.82	210,290	√		Many peaks
<i>Other products</i>					
glycine	3.51	210		√	Solvent peak
formaldehyde	ND				
glycine anhydride	12.05	210		√	
propionaldehyde	14.37	290			
gluconic acid	5.43	210	√		
propionic acid	11.30	210			peak 13 min
succinic acid	7.44	210	√		
hydroxyacetone	10.93	210,290	√		Small peaks @ 210
oxalic acid	3.57	210			Solvent peak
crotonic acid	16.23	210			
glutaric acid	8.62	210			

RT = retention time on ORH-801 column; λ = UV wavelength for detection;

ND = not detectable at either 210 or 290 nm

As a result of these issues, our TOC findings were only semi-quantitative in nature, but still revealed interesting information about the fate of carbon in this reactive environment. Table 6-4 lists TOC results from four different samples and the corresponding experimental conditions of those samples. As expected, the glycine experiment that resulted in limited conversion retained all of its carbon in the aqueous phase. However, all other samples showed significant loss of carbon from the liquid phase including the short time PFR experiments with glucose and glucose-glycine mixtures. The CHN analysis of solids removed from the 0.5  $\mu\text{m}$  filter elements revealed some carbon in the solid phase which provided qualitative support for the loss of carbon from the aqueous phase. Further analysis is required to determine if the carbon missing from the aqueous phase can be accounted for in the solid samples or if we should be looking for a second liquid or oil phase.

**Table 6.4. Semi-quantitative results of TOC and CHN analysis for select glucose, glycine and glucose-glycine experiments.**

<i>Reactant</i>	<i>Conditions</i>	<i>Conversion</i>	<i>~% TOC in Effluent</i>	<i>C/H/N of solid</i>
Glycine	250°C, 55 bar, 6.3 min, pH 5	0-5%	107%	N/A
Glucose	250°C, 55 bar, 7 sec, pH 5	86%	89%	3% N, 19% C, 6% H
Glucose + Glycine	250°C, 55 bar, 6.3 min, pH 2,5	98-100% of both	15%	[pH2]2% N, 14% C, 4% H
				[pH2]2% N, 26% C, 4% H
	300°C, 55 bar, 7 sec, pH 5	95-100% of both	63%	No sample

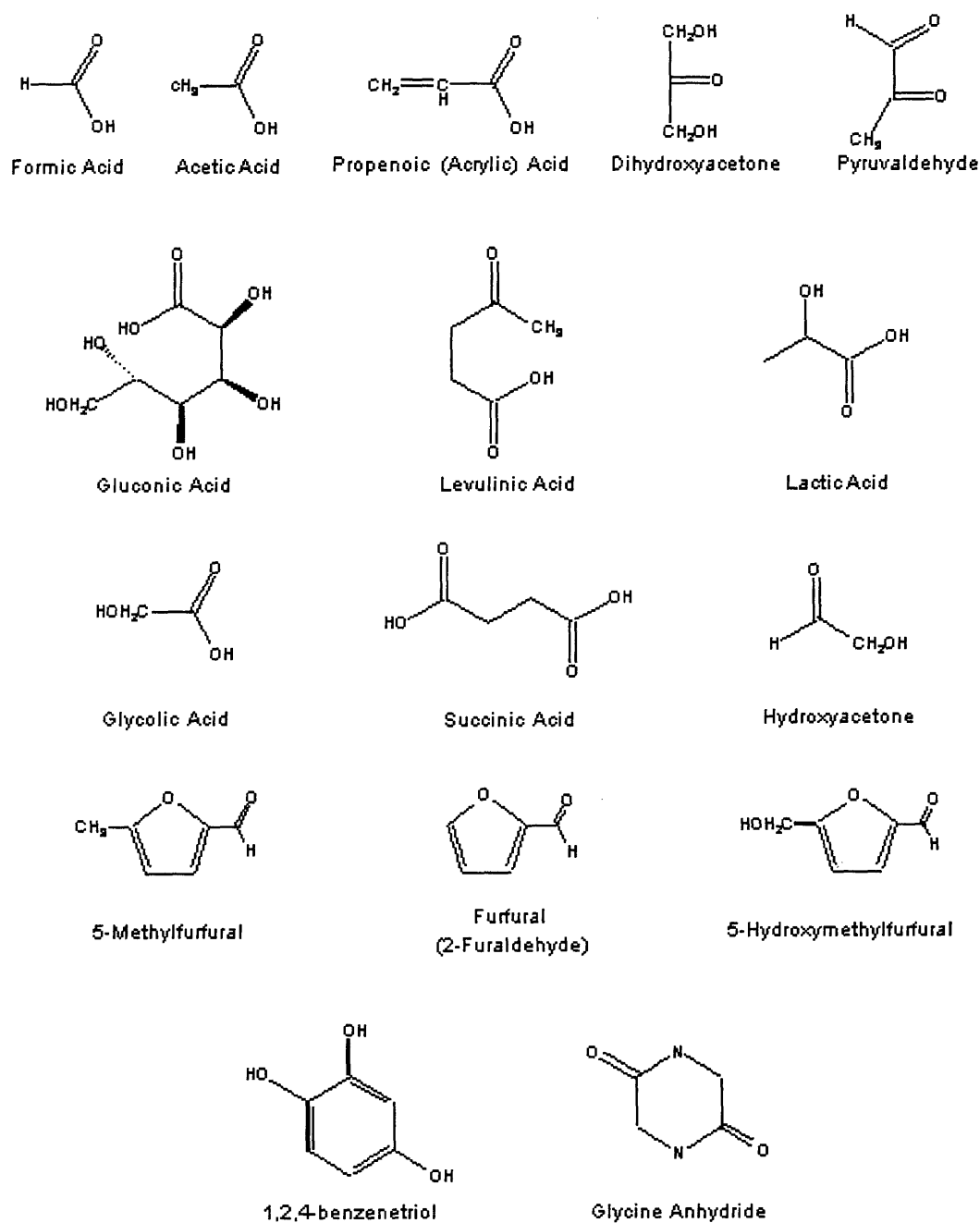


**Figure 6.4** Compounds Identified in Liquid Effluent of Glucose and Glycine Hydrothermal Experiments

The following sections present preliminary results of product identification for glycine degradation, glucose degradation and glucose-glycine degradation separately. Figure 6-4 contains chemical structures of several identified products. Peak detection was accomplished primarily by retention time (RT) matching and UV absorption at two different wavelengths,  $\lambda = 210$  nm and 290 nm. Analysis at these two wavelengths enabled some discrimination between peaks by functional group, and allowed identification of compounds that only absorb at one or the other wavelength. For example, carboxylic acids have the maximum absorbance at about 210 nm while saturated aldehydes and ketones have their maximum absorbance at around 290 nm. Detection by UV absorption has the disadvantage of limited sensitivity for compounds without double bonds or chromophores, like methanol or glucose in its cyclic, hemiacetal form. Despite the shortcomings of this peak identification method, these preliminary results offer significant insight into degradation pathways of these model compounds and their mixtures.

#### 6.4.2 Product Identification: Glycine

HPLC with UV and RI detection and GC analyses revealed only one degradation product of glycine, glycine anhydride, a ring-shaped dimer of glycine. Figure 6-5 displays the typical HPLC chromatogram of a glycine effluent showing only glycine anhydride at relatively low absorbance. Identification of this product was confirmed by retention time matching with 3 different chromatography methods. In agreement with our observed low glycine conversions, the corresponding concentration of glycine anhydride was low; approximately one mole of glycine anhydride formed per 1000 moles of glycine fed. Glycine anhydride concentrations did increase with increased conversion of glycine at higher temperatures and longer residence times, but decreased at lower pHs. Glycine effluents were examined for other possible degradation products like CO<sub>2</sub>, formic acid and glycolic acid, and they were not found. We were unable to

test for methyl amine. Additionally, a small amount of ammonia was detected in the reactor effluent using an ammonia-selective electrode. These product results agree with those found by Alargov et al (2001) and Islam et al (2003) but not with Sato et al (2004) who did not report the presence of glycine anhydride.

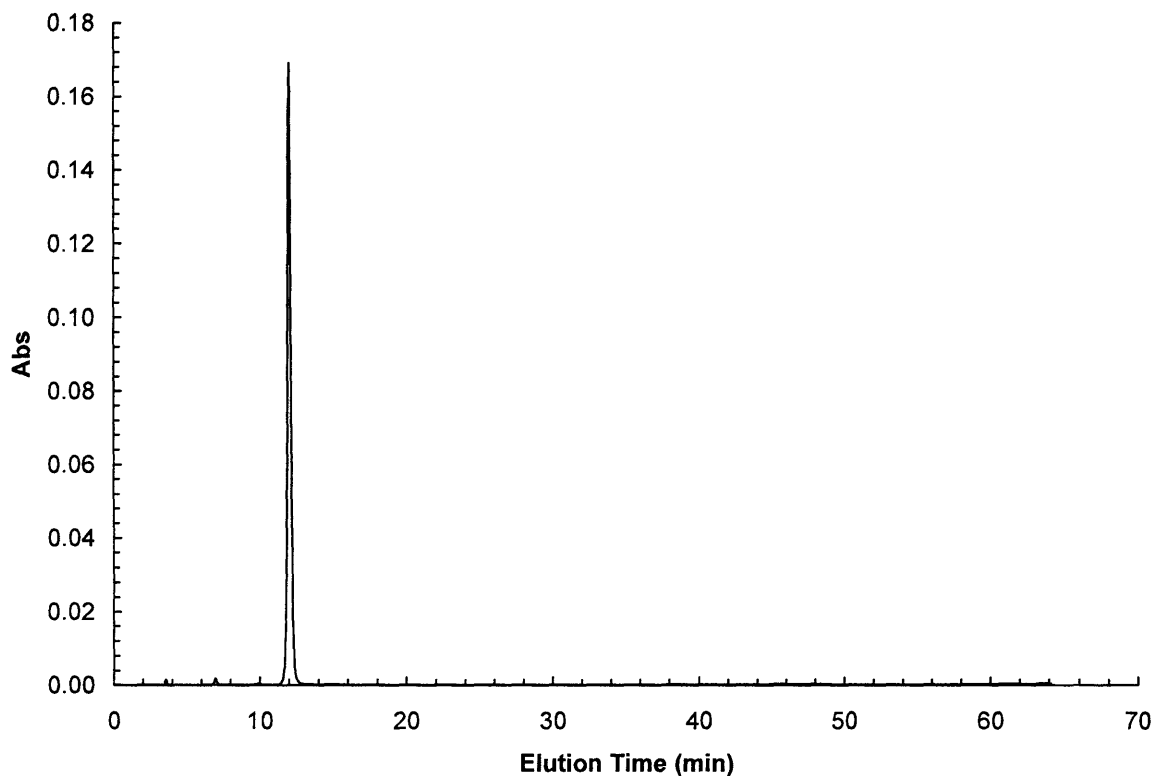


**Figure 6.5. HPLC Chromatogram of Glycine Degradation products. T=250C, P=800psig, 1000ppm glycine, 12.6 min residence time, pH = 2.0. UV detection at 210 nm.**

### 6.4.3 Product Identification: Glucose

Figures 6-6 and 6-7 depict the glucose degradation products at long residence times and short residence times respectively. Figure 6-6 corresponds to a 6.3 minute residence time run in the CSTR at 250°C while Figure 6-7 corresponds to a 10 second residence time at three different temperatures to show the evolution of various products as temperature is increased. Two interesting observations can be quickly made in comparing these two figures; the drastic evolution of products when temperature is increased and the disparity in types of products in the short time effluent versus the long time effluent. Figure 6-7 clearly shows that the effluent from the short time experiment at 150°C does not contain any appreciable products that absorb at 210 nm which makes perfect sense since the corresponding conversion for this experiment was measured to be 6%. The effluent from the 200°C experiment begins to show the slight evolution of a few compounds while the effluent from the 250°C experiment, one where conversion was measured to be 60%, shows several sizeable peaks including a peak that corresponds to 5-hydroxymethylfurfural (5-HMF), a very common glucose hydrothermal degradation product. Some of these peaks were tentatively identified as gluconic acid, pyruvicaldehyde, formic acid and acetic acid, but they may also correspond with compounds we have not yet tested.

The effluent from the long time CSTR experiment has only one compound in common with the short time PFR experiment, that is 5-HMF. Some of the peaks were tentatively identified as succinic acid, glycolic acid, lactic acid, levulinic acid, hydroxyacetone and propenoic acid. Like the results from the short time experiment, these products are mostly low molecular weight acids which correspond with the end of the glucose degradation network discussed previously and presented in Figure 6-2. The fact that we did not see intermediate compounds like glyceraldehyde, glycolaldehyde, dihydroxyacetone and 1,6-anhydroglucose



leads one to believe that glucose destruction rapidly proceeds through the first wave of decomposition intermediates in less than 10 seconds. The identification of pyruvaldehyde in the high temperature short time run, which is a second wave intermediate product found in Figure 6-2, confirms that the first wave of products appear to be unstable and rapidly decompose to products of subsequent stages. Another interesting observation is that species concentrations and corresponding peak sizes appear to be relatively similar for both short and long time effluents. For example, the 5-HMF peak at short time is roughly 3.7 ppm while at long time its roughly 5.2 ppm. In all cases, the peaks appear small and may correspond with low concentrations of all identified species, further complicating the task of closing the carbon balance.

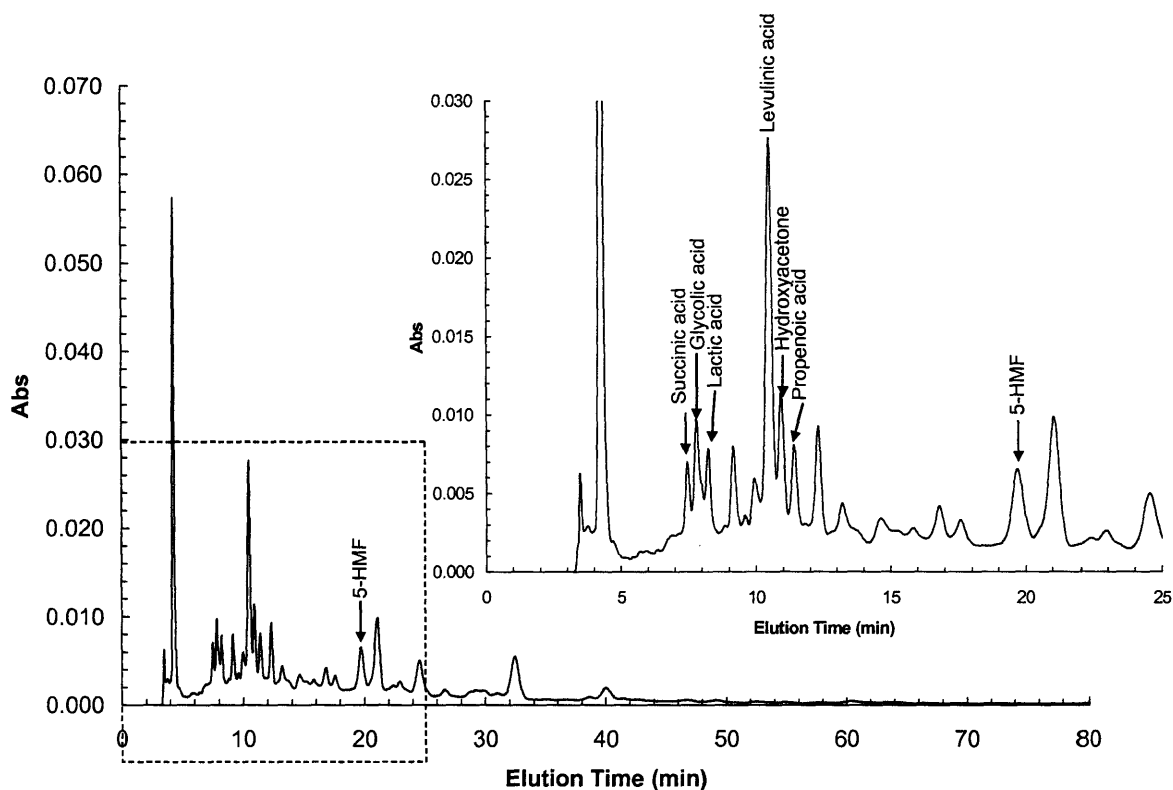


**Figure 6.6. HPLC Chromatogram of Glucose Degradation products. T=250°C, P=800 psig (55 bar), 1000 ppm glucose, 6.3 min residence time in the CSTR reactor system, pH = 5.0. UV detection at 210 nm.**

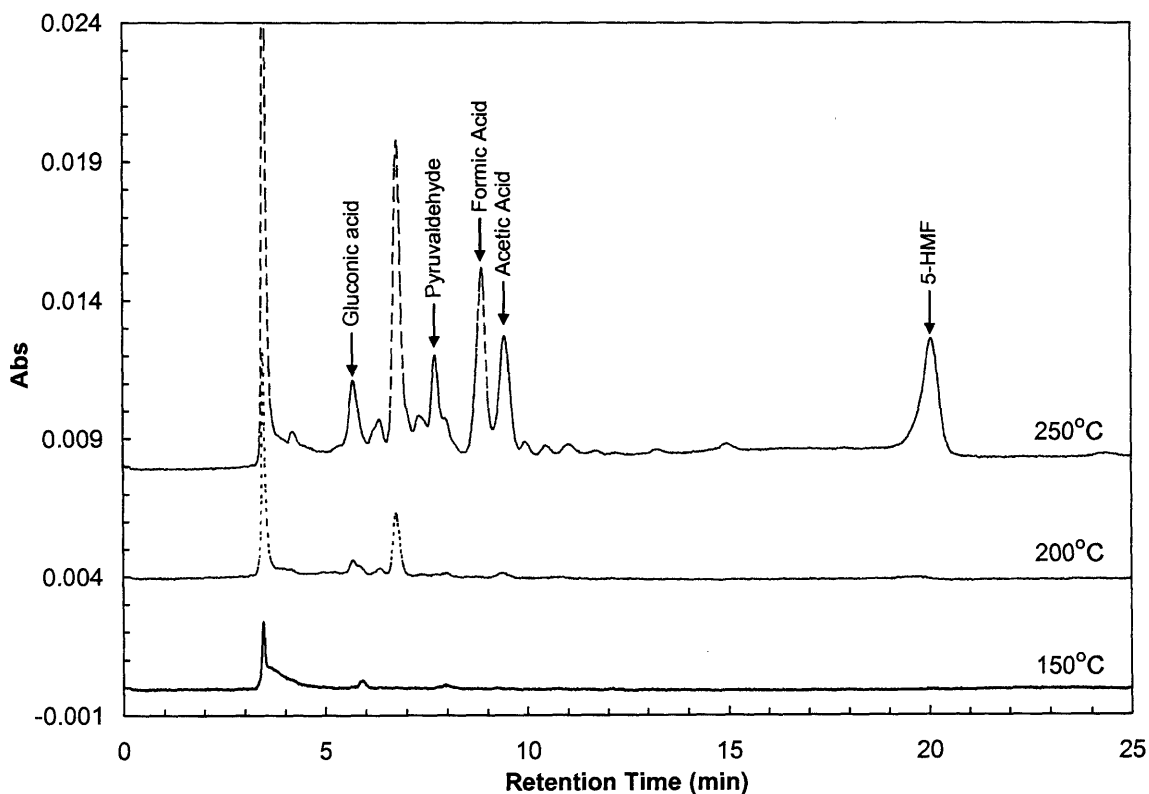


**Figure 6.7. HPLC Chromatogram of Glucose Degradation products. T=150-250°C, P=800 psig (55 bar), 1000 ppm glucose, 7 sec residence time in the PFR reactor system, pH = 5.0. UV detection at 210 nm.**

#### 6.4.4 Product Identification: Glucose-Glycine Mixtures

The discussion of product identification in the aqueous phase effluent of the glucose-glycine experiments is presented by comparing several chromatograms, but first, it is important to mention that the effluent color changes under various conditions. At high temperatures, hydrothermal degradation of glucose alone produced a brown-colored effluent which is in agreement with some of the earlier studies mentioned in Section 6.2.2. At longer residence times and both low and medium pH, glucose-glycine mixtures produced a darker brown effluent that

also had an “burnt-bread” like odor corresponding with Maillard-type melanoidin products. At shorter times in the PFR, glucose-glycine mixtures did not discolor and only a faint smell of melanoidins evolved at the highest temperature. These simple observations of sight and smell confirmed the presence of Maillard-type products at longer times and higher temperatures, and confirmed that the degradation of glucose alone will discolor the effluent.

Figures 6-8 and 6-9 present the first comparison of chromatograms from glucose-glycine effluents at pH2 versus pH5. Figure 6-8 displays the results from UV absorption at 210 nm while Figure 6-9 displays the results from 290 nm absorption. Like the long time results of glucose degradation, these chromatograms depict many peaks corresponding to many compounds of relatively small concentration, even smaller than glucose products seen in Figure 6-6 (peak height of ~0.03 for glucose products versus ~0.003 for glucose-glycine products). Also like glucose effluents, the peaks that did match tested standards were identified low molecular weight acids as the bulk of the products. The major difference in the pH2 effluent versus the pH5 effluent is the presence of small amounts of furfural-type compounds typical of low pH degradation of glucose; 5-HMF, furfural, 5-methylfurfural and the subsequent degradation product, 1,2,4-trihydroxybenzene. The increased presence of these furfural-type compounds may indicate that glucose is degrading more quickly before it has a chance to combine with glycine and travel down one of several Maillard pathways.

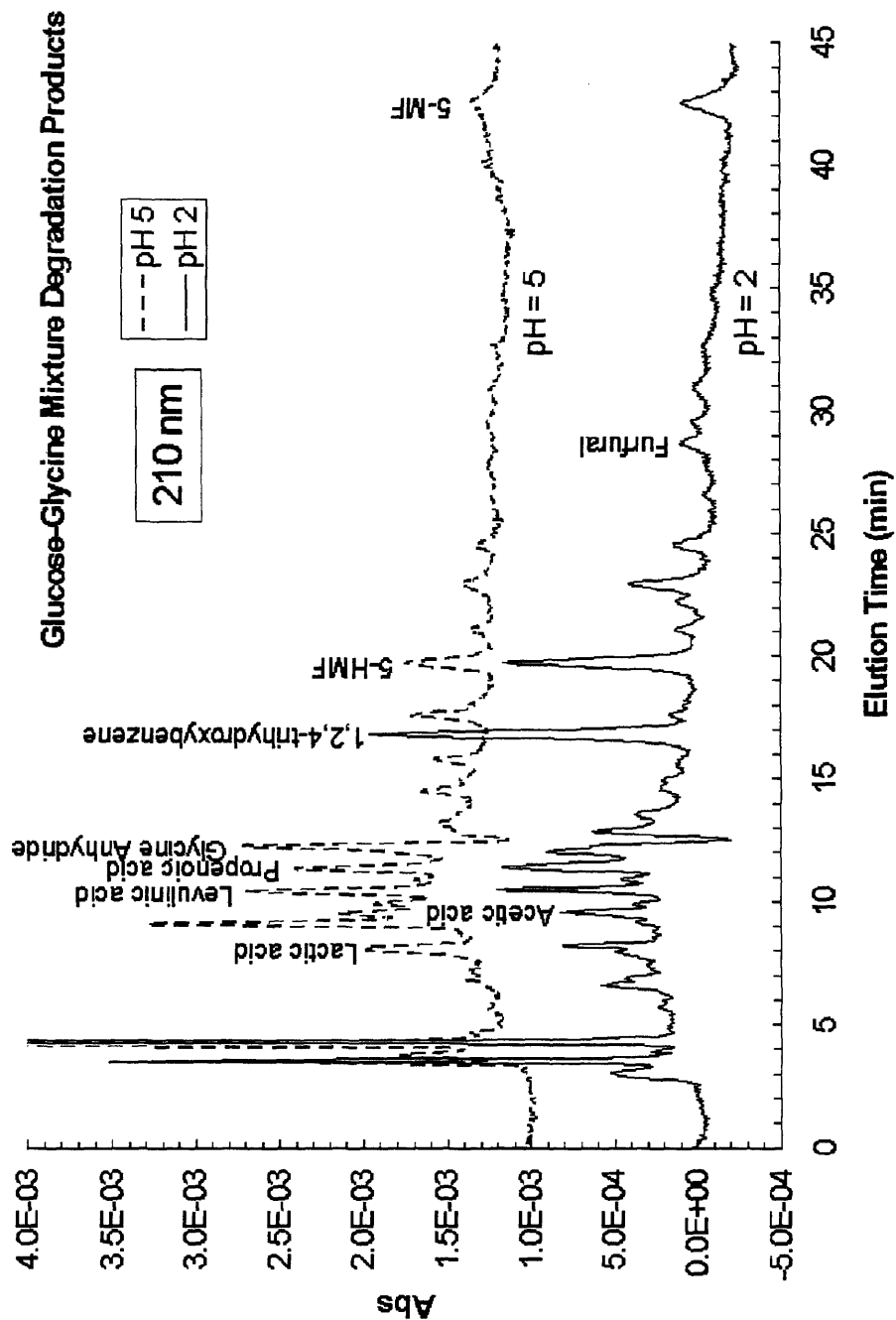


Figure 6-8. HPLC Chromatogram of Glucose-Glycine Degradation products. T=250°C, P=800 psig (55 bar), 1000 ppm glucose, 500 ppm glycine, 6.3 min residence time in the CSTR reactor system, pH =2.0 and 5.0. UV detection at 210 nm.

Figure 6.8. HPLC Chromatogram of Glucose-Glycine Degradation products. T=250°C, P=800 psig (55 bar), 1000 ppm glucose, 500 ppm glycine, 6.3 min residence time in the CSTR reactor system, pH =2.0 and 5.0. UV detection at 210 nm.

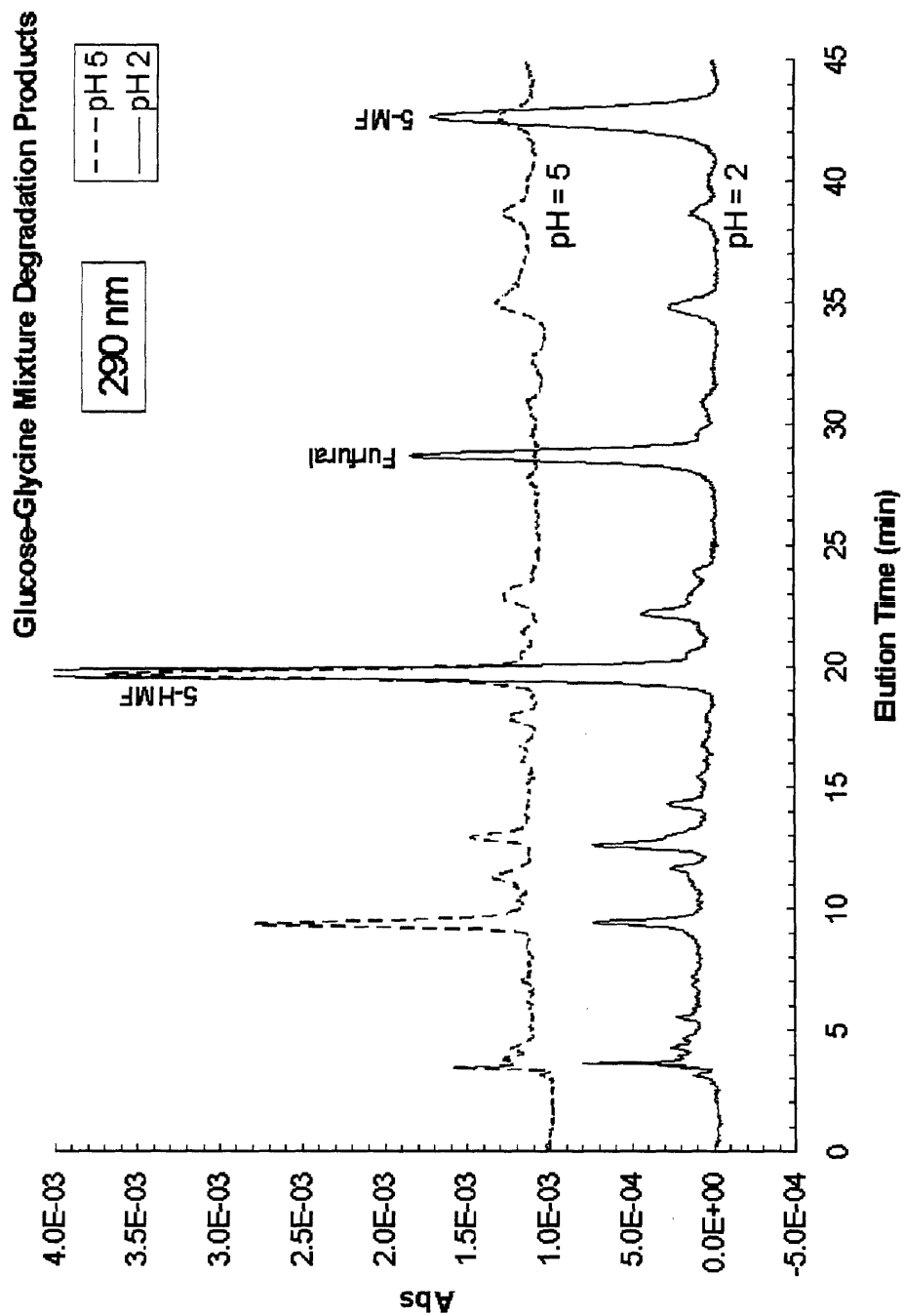


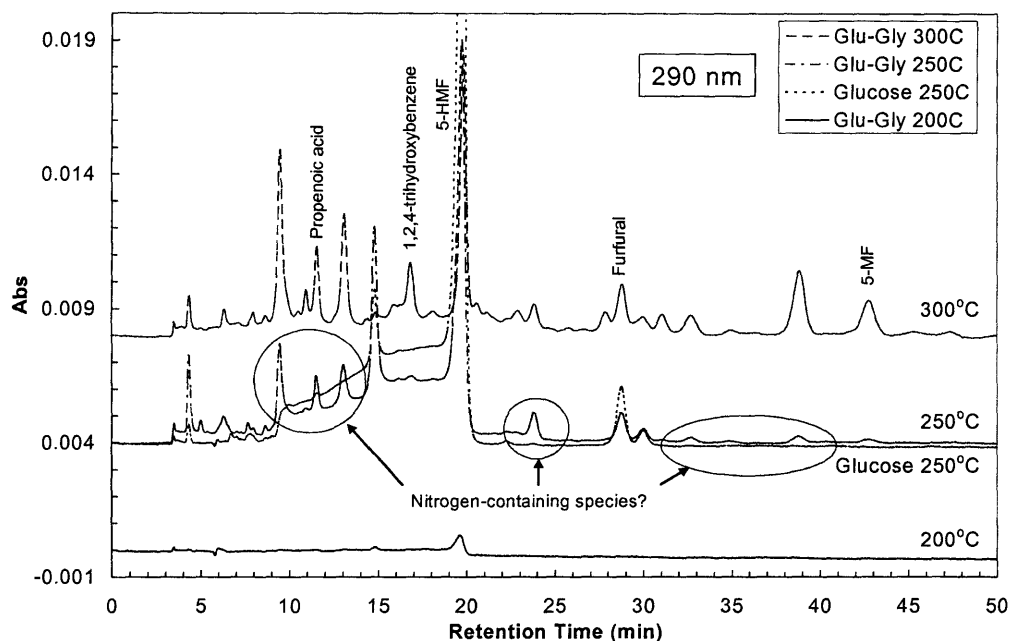
Figure 6-9. HPLC Chromatogram of Glucose-Glycine Degradation products. T=250°C, P=800 psig (55 bar), 1000 ppm glucose, 500 ppm glycine, 6.3 min residence time in the CSTR reactor system, pH =2.0 and 5.0. UV detection at 290 nm.

Figure 6.9. HPLC Chromatogram of Glucose-Glycine Degradation products. T=250°C, P=800 psig (55 bar), 1000 ppm glucose, 500 ppm glycine, 6.3 min residence time in the CSTR reactor system, pH =2.0 and 5.0. UV detection at 290 nm.

---

The comparison of glucose-glycine short-time experiments at different temperatures is presented in Figures 6-10 (absorption at 290 nm) and 6-11 (absorption at 210 nm). A glucose effluent 290 nm chromatogram is included in Figure 6.10 for comparison. Like the short time experimental results for glucose, these effluent chromatograms evolve from no peaks at low temperature to numerous small peaks at higher temperatures. Note the similarities between the 250°C chromatogram in Figure 6-7 and the 250°C chromatogram in Figure 6-11. Note too that these effluent chromatograms also show rapid decomposition to small acids and furfural-type compounds indicating rapid progression down decomposition pathways in less than 10 seconds.

Figures 6-10 and 6-11 tell an interesting story of 5-HMF production and decomposition. In Figure 6-11, the amount of 5-HMF grows with temperature until the reaction temperature reaches 250°C, then at 300°C, the peak is smaller apparently giving way to developing other later eluting furfural-type compounds like furfural itself and 5-MF. The comparison of the chromatograms for glucose and glucose-glycine effluents in Figure 6-10 shows that roughly four peaks are similar, 5-HMF and furfural being two of them, but several peaks are part of the glucose-glycine chromatogram but not part of the glucose chromatogram. These peaks may correspond to carbon-nitrogen compounds of a Maillard reaction network that have not yet been tested or they may correspond with other glucose-type degradation products that simply appear faster in the more reactive glucose-glycine mixtures. Additional testing is warranted to identify compounds that are unique to the glucose-glycine mixture.



**Figure 6.10** HPLC Chromatogram of Glucose-Glycine Degradation products. T=200-300°C, P=800 psig (55 bar), 1000 ppm glucose, 500 ppm glycine, 7 sec residence time in the PFR reactor system, pH = 5.0. UV detection at 290 nm. Glucose degradation shown for comparison.

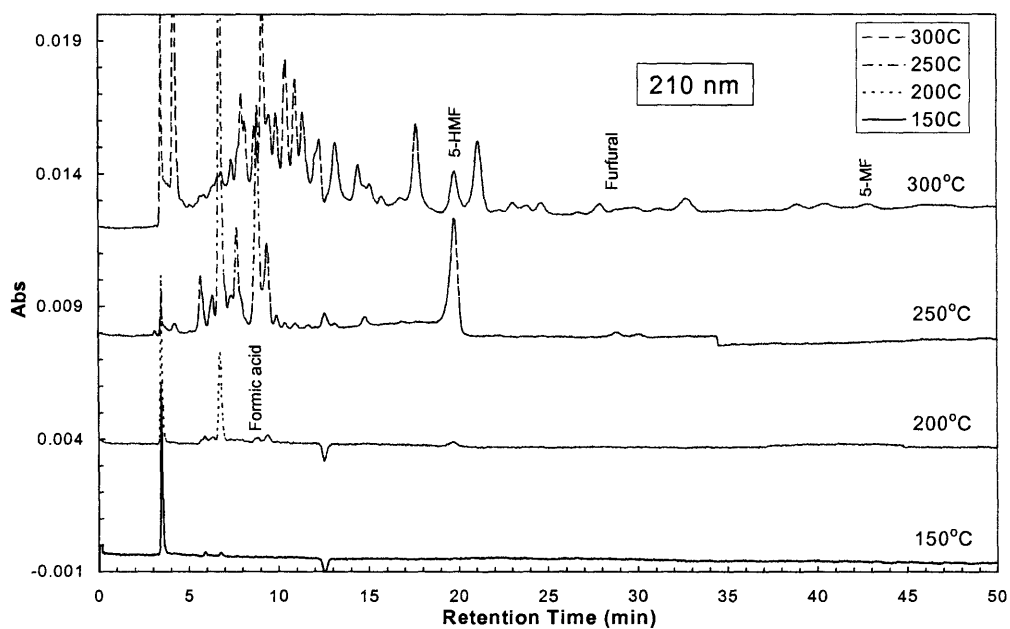


**Figure 6.11** HPLC Chromatogram of Glucose-Glycine Degradation products. T=200-300°C, P=800 psig (55 bar), 1000 ppm glucose, 500 ppm glycine, 7 sec residence time in PFR reactor system, pH = 5.0. UV detection at 210 nm.

## 6.5 SUMMARY AND RECOMMENDATIONS

Although it has been difficult to achieve fully quantitative results in the initial stages of this challenging study, we have made significant progress that will significantly enhance future work. Despite varying pH, time and temperature, we did not observe significant changes in the Maillard mechanism at play, but product chromatograms did show possible development of alternate pathways particularly with furfural-type compounds. Below is a summarized list of our accomplishments to date followed by specific recommendations for future tasks in this study.

- **Analytical protocols:** We have developed several analytical chemistry methods to properly characterize solid and liquid products. Follow-up tasks include refining these methods to improve accuracy and expanding these methods to confirm product identification through GC or LC-MS or other redundant analytical means. Also, future analysis should include routinely monitoring absorbance at 297 nm (early Maillard reaction products) and 420 nm (late Maillard reaction products similar to a glucose-glycine study by (Manzocco and Maltini (1999))).
- **Individual degradation studies of glucose and glycine:** Glycine was found to be refractory under the hydrothermal conditions studied while glucose was quite reactive even at residence times less than 10 seconds. Follow-up tasks include more short time glucose degradation runs to completely characterize the effects of pH and pressure/density before exploring those parameters in the glucose-glycine mixture studies. To support these and other follow-up tasks, it is necessary to refine the design of the current mixing cross and plug flow reactor system and verify improved mixing and proper phase separation before conducting the next set of experiments.



- **Degradation studies of glucose-glycine mixtures:** The degradation of glucose-glycine mixtures was studied at long and short times at pH 2 and pH 5 and over a range of temperatures. Near complete conversion of both reactants was observed in almost all conditions. Some liquid phase products were identified and analyzed, but TOC and CHN analysis showed that significant carbon may still be missing. Follow-up tasks should include more experiments using a well designed, short time flow reactor while varying pH and pressure as potential Maillard-inhibiting parameters. Also, analysis of the effluent should be expanded to include identification and quantification of other Maillard-type intermediate products like Amadori rearrangement products and other furfurals.

## 6.6 REFERENCES

- Adams, T. (2004). Problems with hydrothermal treatment of carbohydrate feed streams. A. Peterson. Cambridge, MA.
- Alargov, D. K., S. Deguchi, et al. (2002). "Reaction Behaviors of Glycine under Super- and Subcritical Water Conditions." *Origins of Life and Evolution of the Biosphere* **32**(1): 1-12.
- Amin, S., R. C. Reid, et al. (1975). Reforming and decomposition of glucose in an aqueous phase. Intersociety Conference on Environmental Systems, San Francisco, CA., ASME Paper #75-ENAs-21.
- Antal, M. J., T. Leesomboon, et al. (1991). "Kinetic-Studies of the Reactions of Ketoses and Aldoses in Water at High-Temperature .3. Mechanism of Formation of 2-Furaldehyde from D-Xylose." *Carbohydrate Research* **217**: 71-85.
- Antal, M. J. and W. S. L. Mok (1988). A study of the acid-catalyzed dehydration of fructose in near-critical water. Research in Thermochemical Biomass Conversion. A. V. Bridgewater and J. L. Kuester. New York, Elsevier.
- Antal, M. J., W. S. L. Mok, et al. (1990). "Kinetic-Studies of the Reactions of Ketoses and Aldoses in Water at High-Temperature .1. Mechanism of Formation of 5-

- (Hydroxymethyl)-2-Furaldehyde from D-Fructose and Sucrose." *Carbohydrate Research* **199**(1): 91-109.
- Bristow, M. and N. S. Isaacs (1999). "The effect of high pressure on the formation of volatile products in a model Maillard reaction." *Journal of the Chemical Society-Perkin Transactions 2*(10): 2213-2218.
- Hill, V., N. S. Isaacs, et al. (1999). "Effect of high hydrostatic pressure on the volatile components of a glucose-lysine model system." *Journal of Agricultural and Food Chemistry* **47**: 3675-3681.
- Hill, V., D. A. Ledward, et al. (1996). "Influence of high hydrostatic pressure and pH on the rate of Maillard browning in a glucose-lysine system." *Journal of Agricultural and Food Chemistry* **44**: 594-598.
- Hodge, J. E. (1953). "Dehydrated foods, chemistry of browning reactions in model systems." *Journal of Agricultural and Food Chemistry* **1**(15): 928-943.
- Holgate, H. R., J. C. Meyer, et al. (1995). "Glucose Hydrolysis and Oxidation in Supercritical Water." *Aiche Journal* **41**(3): 637-648.
- Inoue, S., M. Noguchi, et al. (2004). "Organic compounds formed by thermochemical degradation of glucose-glycine melanoidins using hot compressed water." *Journal of Chemical Engineering of Japan* **37**(7): 915-919.
- Islam, M. N., T. Kaneko, et al. (2003). "Reaction of amino acids in a Supercritical water-flow reactor simulating submarine hydrothermal systems." *Bulletin of the Chemical Society of Japan* **76**(6): 1171-1178.
- Kabyemela, B. M., T. Adschiri, et al. (1997). "Kinetics of glucose epimerization and decomposition in subcritical and supercritical water." *Industrial & Engineering Chemistry Research* **36**(5): 1552-1558.
- Kabyemela, B. M., T. Adschiri, et al. (1999). "Glucose and fructose decomposition in subcritical and supercritical water: Detailed reaction pathway, mechanisms, and kinetics." *Industrial & Engineering Chemistry Research* **38**(8): 2888-2895.
- Karkacier, M., M. Erbas, et al. (2003). "Comparison of Different Extraction and Detection Methods for Sugars Using Amino-Bonded Phase HPLC." *Journal of Chromatographic Science* **41**: 331-333.
- Kruse, A., A. Krupka, et al. (2005). "Influence of proteins on the hydrothermal gasification and liquefaction of biomass: 1. Comparison of different feedstocks." *Industrial and Engineering Chemical Research* **44**(9): 3013-3020.

- Leong, L. P. and B. L. Wedzicha (1999). "A critical appraisal of the kinetic model for the Maillard browning of glucose and glycine." *Food Chemistry* **68**(1): 21-28.
- Manzocco, L. and E. Maltini (1999). "Physical changes induced by the Maillard reaction in a glucose-glycine solution." *Food Research International* **32**: 299-304.
- Martins, S. I. (2003). Unravelling the Maillard reaction network by multiresponse kinetic modelling, Wageningen University, The Netherlands: 170.
- Mednick, M. L. (1962). "The acid-base-catalyzed conversion of aldohexose into 5-(hydroxymethyl)-2-furfural." *J. Org. Chem.* **27**: 398-403.
- Minowa, T., S. Inoue, et al. (2002). Hydrothermal reaction of biomass model compounds. Proceedings of Bioenergy 2002, Boise, ID, USA.
- Modell, M. (1985). Gasification and liquefaction of forest products in supercritical water. Fundamentals of Thermochemical Biomass Conversion. R. P. Overend, T. A. Milne and L. K. Mudge. New York, Elsevier Applied Science: 95-119.
- Moreno, F. J., E. Molina, et al. (2003). "High-pressure effects on Maillard reaction between glucose and lysine." *Journal of Agricultural and Food Chemistry* **51**(394-400).
- Newth, F. H. (1951). "The formation of furan compounds from hexoses." *Adv. Carbohydr. Chem.* **6**: 83-106.
- Sato, N., H. Daimon, et al. (2002). "Decomposition of glycine in high temperature high pressure water." *Kagaku Kogaku Ronbunshu* **28**(1): 113-117.
- Sato, N., A. T. Quitain, et al. (2004). "Reaction kinetics of amino acid decomposition in high-temperature and high-pressure water." *Industrial & Engineering Chemistry Research* **43**(13): 3217-3222.
- Scaman, C. (2005). Maillard Reaction. **2005**.
- Singh, B., G. R. Dean, et al. (1948). "The role of 5-(hydroxymethyl)-2-furfural in the discoloration of sugar solutions." *J. Am. Chem. Soc.* **70**: 517-522.
- Srokol, Z., A. G. Bouche, et al. (2004). "Hydrothermal upgrading of biomass to biofuel; studies on some monosaccharide model compounds." *Carbohydrate Research* **339**(10): 1717-1726.
- Tehrani, K. A., M. Kersiene, et al. (2002). "Thermal degradation studies of glucose/glycine melanoidins." *Journal of Agricultural and Food Chemistry* **50**: 4062-4068.

- 
- Vallentyne, J. R. (1964). "Biogeochemistry of organic matter - II Thermal reaction kinetics and transformation products of amino compounds." *Geochimica et Cosmochimica Acta* **28**(2): 157-188.
- Woerner, G. A. (1976). "Thermal decomposition and reforming of glucose and wood at the critical conditions of water." Masters thesis, Chemical Engineering, MIT, Cambridge, MA.
- Wolfson, M. L., R. D. Schuetz, et al. (1948). "Chemical Interactions of amino compounds and sugars. III. The conversion of D-glucose to 5-(hydroxymethyl)-2-furaldehyde." *J. Am. Chem. Soc.* **70**: 514-517.
- Xiang, Q., Y. Y. Lee, et al. (2004). "Kinetics of glucose decomposition during dilute-acid hydrolysis of lignocellulosic biomass." *Applied Biochemistry and Biotechnology* **113-16**: 1127-1138.

---

## 7 Summary and Conclusions

Model reactants under hydrothermal conditions were examined to improve our understanding of chemical transformations in this high temperature and pressure environment. Results have a direct impact on present and future hydrothermal fuel conversion research for a range of fossil-based and bio-mass based feed stocks. Four different experimental reactor systems were developed and employed in this study. The performance of each system was thoroughly analyzed with solutions recommended to resolve identified shortcomings. Methane was chosen as one model compound and two different approaches were taken to examine its conversion in supercritical water. Catalytic reformation of methane was studied experimentally while partial oxidation of methane was studied through the application of a detailed chemical kinetic model that was modified and refined specifically for this study. Glucose and glycine were also chosen as model compounds to study related conversion pathways experimentally under hydrothermal conditions for biomass-based feed stocks. The primary conclusions obtained in this work are described below:

### 7.1 CATALYTIC REFORMATION OF METHANE

An experimental study of the catalytic reformation of methane in SCW was completed that explored the use of carefully chosen catalysts under a variety of conditions and measured the conversion of methane and yields of various products. Eight metal catalysts were selected based on a thorough review of previous catalysis experiments in hydrothermal conditions and those thought to be active for methane reforming. The range of conditions studied included 350 – 630°C, 150 – 400 bar, 0.01 – 2 wt% methane, 10 seconds to 72 minutes residence time, and with and without catalyst present. Four different experimental reactor designs were employed; a

---

PBR, a CSTR and two different batch reactor designs. A variety of techniques for reducing the metal catalysts and keeping them active in SCW were examined.

Despite the range of conditions studied here, significant conversion of methane was never achieved. The most encouraging result was the relatively low yield of CO<sub>2</sub> (2.19% of the product gas volume) in the experiments employing the 1% Ru/TiO<sub>2</sub> catalyst pellets. A thorough analysis of each catalyst before and after exposure to SCW revealed significant degradation which helped to explain the observed low methane conversions. Based on this analysis and our experimental results, the most promising catalyst identified was 1% Ru/TiO<sub>2</sub>. Similarly, the most promising active metal was ruthenium, and the most promising supports were titania (rutile) with some promise for zirconia and activated carbon. Although active for steam reforming and other hydrothermal catalyst applications, the nickel and platinum catalysts examined in this study showed signs of rapid degradation and deactivation and yielded little conversion of methane.

Experiments with alkali salts in SCW revealed the importance of corrosion in the evolution of hydrogen from this media. Comparable amounts of hydrogen were produced from argon-alkali-SCW mixtures and from methane-argon-alkali-SCW mixtures suggesting that a significant amount of hydrogen in SCW reaction effluents can be attributed to oxidation of metal reactor material and not from hydrocarbon sources. Additional SCW alkali salt experiments in the same Hastelloy C-276 reactor revealed an increasing activation of methane, further emphasizing the likely importance of progressive corrosion. Comparable experiments in a gold-plated reactor still showed evidence of hydrogen generation from metal oxidation, but did not show evidence of corrosion. In the Hastelloy C-276 reactor, corrosion was confirmed by the

presence of metal particulates and measurable amounts of dissolved nickel and chromium from the reactor metal alloy in the effluent.

## 7.2 SCW POX OF METHANE – AN ELEMENTARY REACTION MODELING STUDY

A C1 detailed chemical kinetic model (DCKM) was refined and analyzed to support an examination of the effects of experimental conditions on methanol selectivity and methane conversion for the partial oxidation of methane in supercritical water (SCW POX). Although a deliberate sensitivity analysis was not performed on this model, a detailed study of several key reactions and rates from literature were chosen which resulted in good agreement of model predictions with reliable C1 SCWO experimental data. SCW methane POX predictions from the refined model were then compared with POX experimental data. Disagreements between the model and the data were discussed along with a detailed critique of experimental issues associated with all previous SCW methane POX experimental studies. A reaction path analysis was developed from the DCKM which helped to elucidate the fate of methane and methanol in this environment and to identify a set of promising conditions to maximize methanol selectivity.

Upon detailed analysis of both experimental and modeling results, the maximum methanol selectivity of about 80 % and maximum methane conversion of about 2 % occurs at low temperatures ( $\sim 400^{\circ}\text{C}$ ), medium to high pressure ( $P > 300$  bar), and high methane concentration ( $[\text{CH}_4]_0 > 50\text{mM}$ ) with fuel-rich conditions at medium to high methane to oxygen ratios of  $[\text{CH}_4]_0/[\text{O}_2]_0 > 10$ . The experimental results may have achieved less than the maximum possible methanol selectivity due to issues such as inadequate mixing and wall effects. The modeling results may also be under-predicting methanol selectivity due to inadequate inclusion of non-ideal PVTN effects and solvent effects. However, the agreement of current model

predictions and experimental results substantiates our concern that SCW methane POX may fall short of the goal of greater than 70 % methanol selectivity and 15% methane conversion.

Nevertheless, other sets of experimental conditions that may show more promise have not been fully explored experimentally. In particular, the use of stable, selective catalysts, or inert wall material, or partial oxidation in the presence of hydrothermal flames have not been thoroughly analyzed here, and may improve the limited success discovered in this study.

### 7.3 MODEL MAILLARD REACTION UNDER HYDROTHERMAL CONDITIONS

Glucose, glycine and glucose-glycine mixtures were studied as a model Maillard reaction system in a hydrothermal environment to explore a range of conditions that might alter the formation of undesired Maillard-type polymeric products. Initial experiments were performed to study the individual hydrothermal degradation pathways of glycine and glucose and how those pathways change when these model compounds are mixed. Despite varying pH, time and temperature, we did not observe significant changes in the Maillard mechanism at play, but product chromatograms did show possible development of alternate pathways particularly with furfural-type compounds. Below is a summarized list of our accomplishments to date.

- **Analytical protocols:** We have developed several analytical chemistry methods to properly characterize solid and liquid products. Liquid analysis included two different HPLC methods incorporating three different detectors, a glucose assay method, TOC analysis, and GC-FID analysis. A CHN elemental analyzer was used to characterize the solid products.
- **Individual degradation studies of glucose and glycine:** Glycine was found to be largely refractory in our hydrothermal conditions from 50 to 300°C at 55 – 110 bar and 4 – 67 minutes residence time while glucose was quite reactive. Glycine conversions ranged



---

from 0 – 33% over these conditions while glucose conversion was as high as 35% after just 7.3 seconds residence time at 200°C and 55 bar. A range of temperatures and much shorter residence times were explored and a small set of conditions was identified to examine partial conversion of glucose.

- ***Degradation studies of glucose-glycine mixtures:*** The degradation of glucose-glycine mixtures was studied at times of 10 seconds and 6 minutes at pH 2 and pH 5 and over a range of temperatures from 100 – 300°C. Near complete conversion of both reactants was observed in almost all conditions. Several liquid phase products were identified and analyzed, but TOC and CHN analysis showed that significant reacted carbon is still unaccounted for.

---

## 8 Recommendations

Several issues were identified in the course of this research. Analysis of those issues has enabled us to develop a detailed listing of critical tasks that could be pursued in future research to improve experimental results and theoretical understanding. The principal recommended tasks are presented here:

### 8.1 EXPERIMENTAL SYSTEM IMPROVEMENTS:

The extensive experimental work of thesis has identified several issues that should be addressed to improve our ability to examine model compounds in the extreme temperatures and pressures of hydrothermal environments. The specific recommendations for each experimental system appear below:

#### *8.1.1 PFR System:*

- ***Gaseous Reactant Feed:*** More accurate feed delivery of gaseous reactants can be achieved by two separate approaches. First, a new delivery system involving a gas booster, micrometering valve and flow meter should be pursued. With this new system, we will be able to deliver a wider range of pure gas concentrations that are measured rather than calculated, increasing our confidence in feed concentration values. The gas saturator feed system can remain as an alternative feed delivery of low concentrations, but a more elaborate calibration of feed flow rates as a function of pump settings, saturator pressures, and system pressures should be examined to improve feed conversion values and carbon balance closures.
- ***DOH operation:*** Our experiments suffered through several issues with failures of the direct ohmic heating (DOH) preheating system. Most of the failures involved leaks

which may have resulted from too much current passing through the DOH tubing. This issue was compounded when a loss of pressure from the leak caused the DOH to overheat and on one occasion, a 40 amp fuse was blown in the power control box. To alleviate this problem, we made sure to attach the DOH leads to 1/16" fittings with more metal mass than the previous technique of trying to connect the leads to the thin-walled tubing. Also, future experimentalists using the PFR system should consider redesigning the power control to the DOH where more careful selection of fuses may prevent serious tube or circuit damage.

- ***Catalyst deactivation prior to experiment:*** As discussed in Section 3.1.3, the PFR system was altered to reduce the catalyst in the packed bed reactor during heat-up and prior to any experiment by flowing a H<sub>2</sub>-He stream over it. However, the present design could not prevent exposure of the reduced catalyst to hydrothermal conditions (sub- and supercritical water) as feed streams were changed over and the system was pressurized. This design shortcoming may have caused significant catalyst deactivation prior to the start of any experiment. To minimize this problem, the PFR system should be altered in one of two ways:
  - 1) Build a high pressure gaseous feed system that will allow the simultaneous feed of a high concentration reducing gas, keeping the metal catalyst active while the system achieves specific hydrothermal conditions.
  - 2) Allow the simultaneous flow of an appropriate labile feed (e.g., methanol or hexane) that will itself crack or reform, producing sufficient quantities of hydrogen which should keep the catalyst active during pressurization and heat-up.

---

Both suggestions should help to keep a catalyst active at the start of a SCW experiment, but care must be taken to properly differentiate products of co-fed reducing streams from products of the reaction of interest.

### 8.1.2 CSTR System:

- **Residence Time Distribution:** A quantitative residence time distribution (RTD) study was never performed on the CSTR system. Although Marrone's and Vogel's early work using the CSTR suggested that nearly well-stirred conditions can be achieved in this reactor (Marrone, 1998), the best way to be sure of this fact is if the signature ideal mixing exponential decay profile is observed in RTD experimental measurements. An RTD analysis is critical for future kinetic studies using the CSTR.
- **Temperature Gradient at Supercritical Water Conditions:** With the help of the newly installed temperature data acquisition system, a significant temperature gradient in the reactor itself was identified and examined (See Section 3.3.3 for a more detailed discussion). A representative from Autoclave Engineers finally suggested installing more powerful additional cartridge heaters in the main nut at the top of the reactor to actively heat the cooler section. Time did not allow us to follow through with this suggestion, but the next CSTR experimentalist should explore the idea to help alleviate the current non-isothermal conditions at SCW conditions.
- **Potential multi-phase flow conditions:** In the current design, a pure organic feed is delivered by a syringe pump directly into the reactor, which, under most circumstances, immediately turns into a single phase reacting medium. However, the quenched reactor effluent may form multiple liquid and solid phases which are not handled very well in the current CSTR system. One instance of these complications was observed

when feeding hexane as a reducing agent during some catalyst experiments. Unreacted hexane and other insoluble organics caused erratic flow, poor separation, and possible pooling in some dead-volume zones of the reactor system. The current CSTR should be modified to properly separate multiple liquid effluents and reduce possible pooling sites for these multi-phase effluents.

### 8.1.3 Batch Direct Inject System:

As we discussed in Sections 3.3 and 3.4, two different batch reactor designs were used in this study. A tube batch reactor design was first explored but it was abandoned after several issues were not resolved. Although it may be worthwhile to re-address those issues and improve that original design, the recommendations below only apply to refining our second batch design which seems to have fewer issues and more versatility:

- **Failure of high pressure fittings:** Although not as catastrophic as the tube batch reactor failures, the reactors made from HIP fittings also suffered from leaks. Leaks were mostly found after 1/16" (1.59 mm) compression fittings but occasionally the larger 9/16" (14.28 mm) fittings would leak through weep holes in cross or tee fittings. Failures of 1/16" (1.59 mm) fittings were difficult to repair by retightening, but larger 9/16" (14.28 mm) fittings were easily repaired by re-tightening or removing, sanding the sealing surface and re-tightening. A few SS316 cross fittings also seized, but the use of an anti-seize compound (Swagelok Silver Goop) eliminated that problem. Leaks associated with failed fittings were most likely caused by severe temperature and pressure cycling upon injection of cold water into the hot reactor or upon quenching by rapid expansion. Although it would be difficult to avoid some degree of cycling to achieve well-defined

conditions, compression fittings should be avoided in problem areas like inlet and outlet fittings and in some cases welding the smaller fittings in place should be considered.

- ***Incomplete recovery of the gas effluent:*** Particularly during metal catalyst experiments with the smaller volume batch cell, complete recovery of the gas effluent was difficult. At times, the failure to recover all the gas could be traced to possible leaks in the system, but even with controlled tests under hot conditions, it was difficult to recover all of an inert gas like argon. Cold tests were generally successful, and detailed troubleshooting eliminated possible issues like pressure drop across catalyst beds and leaks past the outlet and vacuum valves. Control tests pointed to two possible major contributors to low gas recovery: small, difficult-to-detect leaks past the pressure relief valve and improper condensing and gas-liquid separation of the reactor effluent during quenching. After removing the pressure relief valve and installed a crude cold trap to collect condensed water, recovery of gas products vastly improved. Nevertheless, a more detailed series of tests should be performed to optimize the gas sampling procedure.

## 8.2 CATALYTIC REFORMATION OF METHANE IN SCW

The SCW catalyst studies performed in this research have identified the most promising combinations of active metals and supports for SCW reforming of methane and other hydrocarbons. Recommended future research focuses on a closer examination of the most promising catalysts including a detailed kinetic experimental study and studies on long-term catalyst stability.

- ***Further studies with Ru-TiO<sub>2</sub>:*** Ruthenium on titania was the most promising catalyst identified. It is a clear choice for a future study on the kinetics of SCW reformation of

---

methane in a well-defined packed bed system. That study should also examine the long term stability of this catalyst in both sub- and supercritical water and look at the reformation of mixed feeds like natural gas simulants or heavier hydrocarbons co-fed with methane.

- ***Further studies with nickel catalysts:*** Although the nickel catalysts explored in this research performed poorly, most of the issues may have been related to the type of support used and the reducing techniques employed. Nickel may still be an attractive active metal for SCW reformation of methane if we use more stable supports without unstable binders or promoters and we include additives that will reduce sintering of the nickel. Raney-nickel catalysts have been successful in the gasification of biomass at lower temperatures and it would be worthwhile to study the stability and activity of this catalyst under SCW reforming conditions.
- ***Future studies co-feeding methane with other hydrocarbons:*** Methane alone may be too refractory to convert in SCW, but the conversion of natural sources of methane may prove to be more promising, including mixtures of other hydrocarbons not only in natural gas compositions but in gas streams associated with production from oil fields. These heavier hydrocarbons are more labile and are likely to reform more easily producing *in situ* hydrogen which will help keep stable SCW catalysts active. With the right composition and operating conditions ( $T$ ,  $P$ , and  $\tau$ ), one might achieve attractive conversions of gaseous mixtures to hydrogen-rich streams or other desirable products.
- ***Further alkali salt studies:*** Additional alkali salt studies should be pursued to identify the role, if any, that the alkali salt plays in SCW reformation of methane. It is clear from our experiments that alkali salts induce a corrosion related pathway, but the use of a gold

plated reactor should help eliminate this pathway and focus on any possible homogenous catalysis involving the alkali salt in this environment. Using  $CD_4$  or  $D_2O$  in lieu of  $CH_4$  and  $H_2O$  might also be an effective way of identifying the true source of hydrogen evolution in this complex environment. Experiments with  $CO$  instead of  $CH_4$  may also help to validate and understand the observations of Kruse and Dinjus who claim that alkali salts catalyze the water gas shift reaction in hydrothermal environments.

- **Multi-component mineral catalysts:** The choice of a multi-component mineral catalyst is not as obvious. In his somewhat controversial 1999 book, *The Deep Hot Biosphere*, Thomas Gold documented and summarized several interesting theories which sparked our interests. Gold proposed that abiogenic methane, as it traveled through high temperature and high pressure regions deep in the earth, was oxidized by oxygen contained in the lattice of multicomponent minerals or by other oxidative species like sulfates (Gold, 1999). If this abiogenic theory can adequately explain  $CH_4$  and  $CO_2$  production from deep wells from non-sedimentary rock reservoirs, then a similar process might work in a supercritical water environment whose conditions are fairly close to those found below the earth's surface. Multicomponent minerals also appear to play a large role in the interesting chemistry of hydrothermal vents whose conditions also approach those of SCW.

### **8.3 SCW POX OF METHANE – AN ELEMENTARY REACTION MODELING STUDY**

The SCW POX of methane modeling study identified several areas to improve our mechanistic modeling efforts in SCW as well as a set of promising conditions to more closely



examine POX of methane in SCW. The principal recommendations for each of those areas are included below:

### 8.3.1 C1 SCW DCKM:

- **Sensitivity analysis:** A thorough sensitivity analysis should be performed on the current refined detailed chemical kinetic model (DCKM) to identify the most sensitive thermodynamic and kinetic parameters of this model. The parameters with the highest sensitivities should then be more closely examined to determine the most reasonable values in supercritical water. For example, from this study, HOCO chemistry and H<sub>2</sub>O<sub>2</sub> chemistry appear to significantly impact model predictions and should be more closely scrutinized.
- **HOCO chemistry:** Incorporation of the latest rate constant values from the literature for HOCO chemistry resulted in model predictions becoming worse, which emphasizes the need to more closely examine the behavior of this sub-system in SCW. One task that may help resolve the existing shortcoming is to explore the effect of water solvation on the transition state theory rate constants using *ab initio* calculations. *Ab initio* calculations of transition state energies at different dielectric strengths could determine if the transition state barriers are affected by the changes occurring in the solvent media.
- **Extensive model predictions of previous SCWO data:** The ultimate goal of a SCW C1 mechanism is to have it accurately predict reaction rates and products over a wide range of SCWO conditions for several model compounds with validated experimental data. Therefore, future refinements of the current C1 mechanism should be followed by assessments of how well the resulting model predicts experimental results for different model compounds like CO, CH<sub>4</sub>, MPA, ethanol, methanol, acetic acid, etc. Naturally, we

must consider the effects of different experimental reactor systems and operating conditions, but the ultimate goal of a universally applicable model is to robustly predict kinetics results with acceptable accuracy.

### 8.3.2 Future SCW POX of Methane Experiments:

- **Validate model predictions of SCW POX of methane:** Although our refined C1 model did not predict acceptable methanol selectivities and methane conversions, it would be prudent to pursue a few experiments under well-defined conditions to validate those predictions. Conditions corresponding to the highest conversions and selectivities should be selected for these scoping runs. The most promising conditions for these experiments are low temperatures ( $\sim 400^\circ\text{C}$ ), medium to high pressure ( $P > 300$  bar), high methane concentration ( $[\text{CH}_4]_0 > 50\text{mM}$ ) and medium to high methane to oxygen ratios ( $[\text{CH}_4]_0/[\text{O}_2]_0 > 10$ ).
- **POX with stable catalysts:** The catalyst work in this study identified a stable catalyst that has not been explored in any SCW partial oxidation tests with methane. Ruthenium on titania should be stable even under oxidation conditions in SCW and may prove to be promising under the right set of partial oxidation conditions.
- **SCW POX of methane in hydrothermal flames:** Hydrothermal flames have proven to be quite effective in completely oxidizing simulated waste streams in the presence of excess oxygen (Wellig, 2003). The extremely short residence times and high temperatures of hydrothermal flame systems may provide the right conditions for partial oxidation of methane in a fuel-rich environment. It may be possible to flow a methane-rich SCW stream rapidly through the high, localized temperatures of a hydrothermal flame in order

to quickly convert methane to intermediate products which are then immediately quenched as they flow to the cooler regions of the reactor beyond the flame.

#### 8.4 MODEL MAILLARD REACTION CHEMISTRY UNDER HYDROTHERMAL CONDITIONS

Significant progress has been made in our model Maillard reaction study, but a bulk of the work lies ahead. The following recommendations are critical to the success of this project and are subdivided into these categories: analytical protocols, pure model compound studies, and mixture studies:

- **Analytical protocols:** Several analytical protocols are in place now but follow-up tasks include refining these methods to improve accuracy and expanding these methods to close material balances and confirm product identification through GC-MS or LC-MS or other redundant analytical means. Pulsed amperometry detection (PAD) could be an alternate analytical method to simultaneously detect sugars and amino acids and their degradation products.
- **Pure model compound degradation studies of glucose and glycine:** Follow-up tasks may include more short time glucose degradation studies to completely characterize the effects of pH and pressure before exploring those parameters in the glucose-glycine mixture studies. To support these and other follow-up tasks, it is necessary to refine the design of the current mixing cross and plug flow reactor system and verify that improved mixing and proper phase separation is achievable before conducting the next set of experiments. A cooled nozzle injection of the feed could be an alternative to help eliminate premature degradation before the reactor (see Lachance, 1995).

- 
- *Glucose-glycine mixture degradation studies*: Follow-up tasks should include more experiments using a well designed, short time flow reactor while varying pH and pressure as potential Maillard-inhibiting parameters. Also, analysis of the effluent should be expanded to include identification and quantification of other Maillard-type intermediate products like Amadori rearrangement products and other furfurals.

## 8.5 REFERENCES

Gold, T. (1999). Deep Hot Biosphere. New York, Spring-Verley.

Lachance, R. P. (1995). "Oxidation and Hydrolysis Reactions in Supercritical Water: Chlorinated Hydrocarbons and Organosulfur Compounds." Masters thesis, Chemical Engineering, MIT, Cambridge, MA.

Marrone, P. A. (1998). "Hydrolysis and Oxidation of Model Organic Compounds in Sub-and Supercritical Water: Reactor Design, Kinetics Measurements, and Modeling." PhD thesis, Chemical Engineering, Massachusetts Institute of Technology, Cambridge, MA.

Wellig, B. (2003). "Transpiring Wall Reactor for Supercritical Water Oxidation." thesis, Swiss Federal Institute of Technology ETH, Zurich.

## A Appendix A

The contents of this appendix are the NASA polynomial coefficients used in the thermochemical text file to support kinetic modeling. The format of this file conforms to the format for thermochemical parameter input to CHEMKIN software (see documentation for CHEMKIN software version 3.7 or higher). This file was originally created by Sullivan (2003) and recently modified by Ploeger. It is included here for completeness.

```

THERMO
  300.000 1000.000 5000.000
! NASA Polynomial format for CHEMKIN-II

O          L 1/900  1          G  200.000  3500.000  1000.000  1
  2.54363697E+00-2.73162486E-05-4.19029520E-09  4.95481845E-12-4.79553694E-16  2
  2.92260120E+04  4.92229457E+00  3.16826710E+00-3.27931884E-03  6.64306396E-06  3
-6.12806624E-09  2.11265971E-12  2.91222592E+04  2.05193346E+00  4
O2         TPIS890  2          G  200.000  3500.000  1000.000  1
  3.66096083E+00  6.56365523E-04-1.41149485E-07  2.05797658E-11-1.29913248E-15  2
-1.21597725E+03  3.41536184E+00  3.78245636E+00-2.99673415E-03  9.84730200E-06  3
-9.68129508E-09  3.24372836E-12-1.06394356E+03  3.65767573E+00  4
H          L 7/88H  1          G  200.000  3500.000  1000.000  1
  0.25000000E+01  0.00000000E+00  0.00000000E+00  0.00000000E+00  0.00000000E+00  2
  0.25473660E+05-0.44668285E+00  0.25000000E+01  0.00000000E+00  0.00000000E+00  3
  0.00000000E+00  0.00000000E+00  0.25473660E+05-0.44668285E+00  4
H2         TPIS78H  2          G  200.000  3500.000  1000.000  1
  0.29328305E+01  0.82659802E-03-0.14640057E-06  0.15409851E-10-0.68879615E-15  2
-0.81305582E+03-0.10243164E+01  0.23443029E+01  0.79804248E-02-0.19477917E-04  3
  0.20156967E-07-0.73760289E-11-0.91792413E+03  0.68300218E+00  4
OH         S 9/010  1H  1          G  200.000  6000.000  1000.000  1
  2.83853033E+00  1.10741289E-03-2.94000209E-07  4.20698729E-11-2.42289890E-15  2
  3.69780808E+03  5.84494652E+00  3.99198424E+00-2.40106655E-03  4.61664033E-06  3
-3.87916306E-09  1.36319502E-12  2.61399147E+03-1.03998477E-01  4
H2O        L 8/89H  2O  1          G  200.000  3500.000  1000.000  1
  0.26770389E+01  0.29731816E-02-0.77376889E-06  0.94433514E-10-0.42689991E-14  2
-0.29885894E+05  0.68825500E+01  0.41986352E+01-0.20364017E-02  0.65203416E-05  3
-0.54879269E-08  0.17719680E-11-0.30293726E+05-0.84900901E+00  4
HO2        L 5/89H  1O  2          G  200.000  3500.000  1000.000  1
  4.17226590E+00  1.88120980E-03-3.46292970E-07  1.94685160E-11  1.76091530E-16  2
  6.18188510E+01  2.95779740E+00  4.30178800E+00-4.74902010E-03  2.11579530E-05  3
-2.42759610E-08  9.29206700E-12  2.94808760E+02  3.71670100E+00  4
H2O2       L 7/88H  2O  2          G  200.000  3500.000  1000.000  1
  4.57333537E+00  4.04984070E-03-1.29479479E-06  1.97281710E-10-1.13402846E-14  2
-1.80548121E+04  7.04278488E-01  4.27611269E+00-5.42822417E-04  1.67335701E-05  3
-2.15770813E-08  8.62454363E-12-1.77055536E+04  3.43505074E+00  4
CH2        L S/93C  1H  2          G  200.000  3500.000  1000.000  1
  3.14631886E+00  3.03671259E-03-9.96474439E-07  1.50483580E-10-8.57335515E-15  2
  4.60412605E+04  4.72341711E+00  3.71757846E+00  1.27391260E-03  2.17347251E-06  3
-3.48858500E-09  1.65208866E-12  4.58723866E+04  1.75297945E+00  4
CH2(S)     L S/93C  1H  2          G  200.000  3500.000  1000.000  1
  3.13501686E+00  2.89593926E-03-8.16668090E-07  1.13572697E-10-6.36262835E-15  2
  5.05040504E+04  4.06030621E+00  4.19331325E+00-2.33105184E-03  8.15676451E-06  3
-6.62985981E-09  1.93233199E-12  5.03662246E+04-7.46734310E-01  4
CH3        L11/89C  1H  3          G  200.000  3500.000  1000.000  1
  0.29781206E+01  0.57978520E-02-0.19755800E-05  0.30729790E-09-0.17917416E-13  2
  0.16509513E+05  0.47224799E+01  0.36571797E+01  0.21265979E-02  0.54583883E-05  3
-0.66181003E-08  0.24657074E-11  0.16422716E+05  0.16735354E+01  4
CH4        ANHARMONIC J 5/61C  1H  4          G  300.000  5000.000  1000.  1
  0.16354256E+01  0.10084431E-01-0.33692369E-05  0.53497280E-09-0.31552817E-13  2

```

```

-0.10005603E+05 0.99936953E+01 0.51498792E+01-0.13671008E-01 0.49180130E-04 3
-0.48474403E-07 0.16669441E-10-0.10246648E+05-0.46413244E+01 4
CO TPIS79C 10 1 G 200.000 3500.000 1000.000 1
0.30484859E+01 0.13517281E-02-0.48579405E-06 0.78853644E-10-0.46980746E-14 2
-0.14266117E+05 0.60170977E+01 0.35795335E+01-0.61035369E-03 0.10168143E-05 3
0.90700586E-09-0.90442449E-12-0.14344086E+05 0.35084093E+01 4
CO2 L 7/88C 10 2 G 200.000 3500.000 1000.000 1
0.46365111E+01 0.27414569E-02-0.99589759E-06 0.16038666E-09-0.91619857E-14 2
-0.49024904E+05-0.19348955E+01 0.23568130E+01 0.89841299E-02-0.71220632E-05 3
0.24573008E-08-0.14288548E-12-0.48371971E+05 0.99009035E+01 4
HCO L12/89H 1C 10 1 G 200.000 3500.000 1000.000 1
3.92001542E+00 2.52279324E-03-6.71004164E-07 1.05615948E-10-7.43798261E-15 2
3.65342928E+03 3.58077056E+00 4.23754610E+00-3.32075257E-03 1.40030264E-05 3
-1.34239995E-08 4.37416208E-12 3.87241185E+03 3.30834869E+00 4
CH2O L 8/88H 2C 10 1 G 200.000 3500.000 1000.000 1
0.31694807E+01 0.61932742E-02-0.22505981E-05 0.36598245E-09-0.22015410E-13 2
-0.14478425E+05 0.60423533E+01 0.47937036E+01-0.99081518E-02 0.37321459E-04 3
-0.37927902E-07 0.13177015E-10-0.14308955E+05 0.60288702E+00 4
CH2OH T12/00C 1H 30 1 G 200.000 6000.000 1000. 1
5.09312037E+00 5.94758550E-03-2.06496524E-06 3.23006703E-10-1.88125052E-14 2
-4.05813228E+03-1.84690613E+00 4.47832317E+00-1.35069687E-03 2.78483707E-05 3
-3.64867397E-08 1.47906775E-11-3.52476728E+03 3.30911984E+00 4
CH3O 121686C 1H 30 1 G 300.00 3000.00 1000.000 1
4.75779238E+00 7.44142474E-03-2.69705176E-06 4.38090504E-10-2.63537098E-14 2
3.90139164E+02-1.96680028E+00 3.71180502E+00-2.80463306E-03 3.76550971E-05 3
-4.73072089E-08 1.86588420E-11 1.30772484E+03 6.57240864E+00 4
CH3OH L 8/88C 1H 40 1 G 200.000 3500.000 1000.000 1
3.52726795E+00 1.03178783E-02-3.62892944E-06 5.77448016E-10-3.42182632E-14 2
-2.60028834E+04 5.16758693E+00 5.65851051E+00-1.62983419E-02 6.91938156E-05 3
-7.58372926E-08 2.80427550E-11-2.56119736E+04-8.97330508E-01 4
CH3OO 7/13/98 thermC 1H 30 2 G 300.000 5000.000 1385.000 1
2.15300459E+00 1.55773677E-02-5.74102807E-06-6.94911845E-10 6.69196639E-13 2
-1.99000926E+02 1.62015564E+01 2.15300459E+00 1.55773677E-02-5.74102807E-06 3
-6.94911845E-10 6.69196639E-13-1.99000926E+02 1.62015564E+01 4
CH3OOH 7/13/98 thermC 1H 40 2 G 300.000 5000.000 1390.000 1
6.86907934E+00 1.00840883E-02-3.66515947E-06 5.96302681E-10-3.58894156E-14 2
-1.98402231E+04-1.24951986E+01 3.72654981E+00 7.51851847E-03 2.35970425E-05 3
-3.52694507E-08 1.42757614E-11-1.83982011E+04 9.02539433E+00 4
! based on equilibrium off of Kaiser
CH2OOH C 1H 30 2 G 300.00 3000.00 1000.00 1
3.51989885E+00 7.15385362E-03 2.16933412E-05-3.36606869E-08 1.38669884E-11 2
1.52813709E+04 7.08512448E+00 3.51989885E+00 7.15385362E-03 2.16933412E-05 3
-3.36606869E-08 1.38669884E-11 1.52813709E+04 7.08512448E+00 4
PO(OH)2CH3 7/13/98 C 1H 50 3P 1G 300.000 3000.000 1000.000 1
9.84725826E+00 2.10808647E-02-1.36739458E-05 4.84864350E-09-7.33936794E-13 2
-1.13205511E+05-2.16293017E+01 8.37905032E-01 5.85742531E-02-7.21777141E-05 3
4.53472462E-08-1.12117954E-11-1.11744352E+05 2.07858918E+01 4
PO(OH)3 3/03/03 H 30 4P 1 G 300.000 3000.000 1000.000 1
9.42033906E+00 1.31692785E-02-8.61258014E-06 3.23165452E-09-5.24241023E-13 2
-1.40065199E+05-1.66980449E+01 2.73667804E+00 3.93100460E-02-4.63936258E-05 3
2.69583061E-08-5.92566778E-12-1.38945136E+05 1.50683536E+01 4
PO(OH)2CH2 C 1H 40 3P 1G 300.000 3000.000 1000.000 1
1.16138837E+01 1.40002390E-02-8.91593733E-06 3.26893197E-09-5.24240643E-13 2
-8.70343624E+04-2.81188409E+01 3.07807026E-02 6.60892282E-02-9.75991409E-05 3
7.08710034E-08-1.99494207E-11-8.52373109E+04 2.57283389E+01 4
PO2(OH)CH3 C 1H 40 3P 1G 300.000 3000.000 1000.000 1
6.51516939E+00 2.73492204E-02-2.10839230E-05 8.39484564E-09-1.36302661E-12 2
-7.88184298E+04-4.74501822E+00 2.29261843E+00 4.28724596E-02-4.14221064E-05 3
1.92482516E-08-3.17784255E-12-7.80905103E+04 1.54962180E+01 4
PO(OH)3CH3 C 1O 4H 6P 1G 300.00 3000.000 1000.0 1
1.30873885E+01 2.24461012E-02-1.14316008E-05 2.98468023E-09-3.14544948E-13 2
-1.11605314E+05-3.62110216E+01-3.92468414E-01 8.06024511E-02-1.06913030E-04 3
7.35106297E-08-2.00357721E-11-1.09458090E+05 2.69107154E+01 4
PO2OH P 10 3H 1 G 300.0 3000.0 1000.0 1
5.67905593E+00 1.08259533E-02-7.75177861E-06 2.83323253E-09-4.19393061E-13 2
-8.68882466E+04-1.75594000E+00 1.42381098E+00 2.77276365E-02-3.31095460E-05 3
1.98361633E-08-4.71072235E-12-8.61784712E+04 1.84342970E+01 4
PO(OH)2CH2OO C 1O 5H 4P 1G 300.000 3000.0 1000.0 1
4.43040609E+00 5.67444342E-02-6.36569013E-05 3.52993185E-09-7.48532904E-12 2
-1.03228621E+05 7.89846275E+00 3.25521872E+00 6.45651796E-02-8.23879245E-05 3
5.44392007E-08-1.45407875E-11-1.03094860E+05 1.29398012E+01 4

```

PO(OH)2CH2OOH	C	10	5H	5P	1G	300.00	3000.0	1000.00	1	
3.26219010E+00	6.91897876E-02	-8.38525235E-05	4.95520397E-08	-1.12463567E-11					2	
-1.20713583E+05	1.33745794E+01	2.28746584E+00	7.56825541E-02	-9.94159052E-05					3	
6.54664549E-08	-1.71162831E-11	-1.20602736E+05	1.75550640E+01						4	
PO(OH)2CH2O	C	10	4H	4P	1G	300.000	3000.000	1000.00	1	
1.10926375E+01	2.07922872E-02	-1.39675263E-05	4.96048460E-09	-7.33937401E-13					2	
-9.99869671E+04	-2.42085836E+01	2.83218996E+00	5.38952733E-02	-6.34893083E-05					3	
3.76132573E-08	-8.70624074E-12	-9.86189802E+04	1.49138159E+01						4	
PO2(OH)CH2OOH	C	10	5H	4P	1G	300.0	3000.000	1000.00	1	
4.01003832E+00	5.81239648E-02	-6.40557216E-05	3.45248828E-08	-7.25496689E-12					2	
-8.69694317E+04	1.11292719E+01	3.71806018E+00	6.01366669E-02	-6.90241933E-05					3	
3.97313680E-08	-9.21421495E-12	-8.69373063E+04	1.23714587E+01						4	
PO(OH)2	H	20	3P	1	G	300.0	3000.000	1000.00	1	
7.54982463E+00	9.91728389E-03	-7.35020380E-06	3.03593563E-09	-5.24240567E-13					2	
-8.16599646E+04	-8.22793809E+00	1.82257988E+00	3.43642126E-02	-4.66713244E-05					3	
3.12467003E-08	-8.13326726E-12	-8.07439210E+04	1.86276111E+01						4	
PO(OH)2CH2OH	C	1H	5O	4P	1G	300.00	3000.000	1000.00	1	
1.27187433E+01	2.07705309E-02	-1.40510541E-05	5.26570859E-09	-8.38785439E-13					2	
-1.29287960E+05	-3.28801523E+01	2.80822090E+00	6.15341139E-02	-7.68463060E-05					3	
4.81229071E-08	-1.17527605E-11	-1.27670045E+05	1.38651726E+01						4	
PO(OH)2CHO	C	1H	3O	4P	1G	300.00	3000.000	1000.00	1	
1.06502620E+01	1.61911301E-02	-1.03460707E-05	3.57648891E-09	-5.24241099E-13					2	
-1.14595214E+05	-2.07273864E+01	2.59200792E+00	5.30297621E-02	-7.44884765E-05					3	
5.37852606E-08	-1.53720085E-11	-1.13355760E+05	1.66377504E+01						4	
PO(OH)2CO	C	1H	2O	4P	1G	300.00	3000.000	1000.00	1	
1.23281332E+01	9.01316791E-03	-5.03061443E-06	1.55175240E-09	-2.09696227E-13					2	
-9.73062543E+04	-2.77189124E+01	5.12225197E+00	4.19805046E-02	-6.28371535E-05					3	
4.73096510E-08	-1.39237922E-11	-9.61965621E+04	5.69952451E+00						4	
PO(OH)2CHOH	C	1H	4O	4P	1G	300.00	3000.00	1000.00	1	
1.34871295E+01	1.85071454E-02	-1.50929000E-05	6.56349848E-09	-1.15333046E-12					2	
-1.10790368E+05	-3.64380864E+01	-5.33135886E-01	7.60144514E-02	-1.03476160E-04					3	
6.67761069E-08	-1.64683408E-11	-1.08497636E+05	2.97229393E+01						4	
PO2(OH)CH2OH	C	1H	4O	4P	1G	300.00	3000.00	1000.00	1	
8.47469084E+00	2.64522897E-02	-1.77930928E-05	6.33516387E-09	-9.43634388E-13					2	
-8.57625138E+04	-1.29940429E+01	2.04067938E+00	5.11671354E-02	-5.25984646E-05					3	
2.73776690E-08	-5.46027000E-12	-8.46749052E+04	1.76648106E+01						4	
PO2CH3	C	1H	3O	2P	1G	300.00	3000.00	1000.00	1	
3.21259514E+00	2.09074227E-02	-1.35554757E-05	4.53410347E-09	-6.29089516E-13					2	
-6.13771779E+04	1.18667043E+01	2.47382300E+00	2.15478143E-02	-9.68518624E-06					3	
-2.36684421E-09	2.50128469E-12	-6.12074649E+04	1.57675760E+01						4	
POOHCH2	C	1H	3O	2P	1G	300.00	3000.00	1000.00	1	
7.14016089E+00	1.41703485E-02	-8.20786563E-06	2.49072709E-09	-3.14544606E-13					2	
-4.83043278E+04	-8.77977600E+00	3.74705251E-01	4.33724673E-02	-5.60372752E-05					3	
3.76467543E-08	-1.00778124E-11	-4.72276644E+04	2.28942777E+01						4	
POOH	P	1H	1O	2	G	300.00	3000.00	1000.00	1	
4.80131563E+00	7.33342808E-03	-5.29308588E-06	2.01541515E-09	-3.14544568E-13					2	
-5.76141537E+04	2.07604083E+00	1.70132210E+00	1.99998025E-02	-2.46737757E-05					3	
1.51485972E-08	-3.63309976E-12	-5.71061398E+04	1.67136479E+01						4	
HOCO	GARDAbInit	C	1H	1O	2	G	300.00	5000.000	1000.00	1
3.64368663E+00	1.95698371E-03	1.87464682E-05	-2.82107863E-08	1.20915122E-11					2	
-2.30778108E+04	8.17760558E+00	4.46368155E+00	6.10666447E-03	-2.99481425E-06					3	
7.13091393E-10	-6.68293438E-14	-2.35240745E+04	2.63104239E+00						4	
H4PO4	H	4O	4P	1	G	300.00	3000.00	1000.00	1	
1.28584730E+01	1.14809490E-02	-6.20037210E-06	2.05269450E-09	-3.14544570E-13					2	
-1.13822810E+05	-3.55326590E+01	-5.48322880E-01	7.13482970E-02	-1.08054770E-04					3	
8.00355370E-08	-2.29045600E-11	-1.11730460E+05	2.68858140E+01						4	
HCOOH	therm C	1H	2O	2	g	300.000	5000.000	1376.000	1	
6.68733013E+00	5.14289368E-03	-1.82238513E-06	2.89719163E-10	-1.70892199E-14					2	
-4.83995400E+04	-1.13104798E+01	1.43548185E+00	1.63363016E-02	-1.06257421E-05					3	
3.32132977E-09	-4.02176103E-13	-4.64616504E+04	1.72885798E+01						4	
C2H6	121686C	2H	6	g	0300.00	4000.00	1000.00		1	
0.04825938E+02	0.01384043E+00	-0.04557259E-04	0.06724967E-08	-0.03598161E-12					2	
-0.01271779E+06	-0.05239507E+02	0.01462539E+02	0.01549467E+00	0.05780507E-04					3	
-0.01257832E-06	0.04586267E-10	-0.01123918E+06	0.01443229E+03						4	
C2H5	12387C	2H	5	g	0300.00	5000.00	1000.00		1	
0.07190480E+02	0.06484077E-01	-0.06428065E-05	-0.02347879E-08	0.03880877E-12					2	
0.01067455E+06	-0.01478089E+03	0.02690702E+02	0.08719133E-01	0.04419839E-04					3	
0.09338703E-08	-0.03927773E-10	0.01287040E+06	0.01213820E+03						4	
C2H4	121286C	2H	4	g	0300.00	5000.00	1000.00		1	
0.03528419E+02	0.01148518E+00	-0.04418385E-04	0.07844601E-08	-0.05266848E-12					2	
0.04428289E+05	0.02230389E+02	-0.08614880E+01	0.02796163E+00	-0.03388677E-03					3	

0.02785152e-06-0.09737879e-10 0.05573046e+05 0.02421149e+03	4
C2H3 12787C 2H 3 g 0300.00 5000.00 1000.00	1
0.05933468e+02 0.04017746e-01-0.03966740e-05-0.01441267e-08 0.02378644e-12	2
0.03185435e+06-0.08530313e+02 0.02459276e+02 0.07371476e-01 0.02109873e-04	3
-0.01321642e-07-0.01184784e-10 0.03335225e+06 0.01155620e+03	4
C2H2 121386C 2H 2 g 0300.00 5000.00 1000.00	1
0.04436770e+02 0.05376039e-01-0.01912817e-04 0.03286379e-08-0.02156710e-12	2
0.02566766e+06-0.02800338e+02 0.02013562e+02 0.01519045e+00-0.01616319e-03	3
0.09078992e-07-0.01912746e-10 0.02612444e+06 0.08805378e+02	4
C2H 81193C 2H 1 g 0300.00 4000.00 1000.00	1
0.03986367e+02 0.03143123e-01-0.01267243e-04 0.02924363e-08-0.02716320e-12	2
0.06655884e+06 0.01191063e+02 0.02737704e+02 0.08048446e-01-0.09244310e-04	3
0.06525259e-07-0.01939580e-10 0.06683813e+06 0.07300220e+02	4
C2H5OH 3/12/95 tHermC 2H 60 1 g 300.000 5000.000 1391.000	1
7.95264841e+00 1.31574144e-02-4.43693359e-06 6.82201160e-10-3.93096335e-14	2
-3.23602958e+04-1.76537972e+01 4.23149045e-01 2.92858167e-02-1.73845099e-05	3
4.79006785e-09-6.74917252e-13-2.95683054e+04 2.33538763e+01	4
C2H4OH 3/12/95 tHermC 2H 50 1 g 0300.00 5000.00 1391.00	1
7.52241939e+00 1.10492715e-02-3.72576465e-06 5.72827397e-10-3.30061759e-14	2
-7.29333590e+03-1.24958732e+01 1.17714711e+00 2.48115685e-02-1.50299503e-05	3
4.79006785e-09-6.40994211e-13-4.95369043e+03 2.20081586e+01	4
CH3CHOH 3/12/95 tHermC 2H 50 1 g 0300.00 5000.00 1553.00	1
7.26631179e+00 1.09588926e-02-3.63662803e-06 5.53659830e-10-3.17012322e-14	2
-8.64310684e+03-1.06794104e+01 1.83974631e+00 1.87789371e-02-4.60544253e-06	3
-2.13116990e-09 9.43772653e-13-6.29595195e+03 2.01446141e+01	4
CH3CH2O MARNOC 2H 50 1 G 300.00 5000.000 1000.00	1
-2.42878712E-01 2.96327850E-02-1.89310518E-05 5.40213140E-09-3.60236273E-13	2
-3.15027589E+03 2.46552716E+01-2.42878712E-01 2.96327850E-02-1.89310518E-05	3
5.40213140E-09-3.60236273E-13-3.15027589E+03 2.46552716E+01	4
C2H5O 3/12/95 tHermC 2H 50 1 g 300.000 5000.000 1389.000	1
7.87339772e+00 1.13072907e-02-3.84421421e-06 5.94414105e-10-3.43894538e-14	2
-6.07274953e+03-1.73416790e+01 4.94420708e-01 2.71774434e-02-1.65909010e-05	3
5.15204200e-09-6.48496915e-13-3.35252925e+03 2.28079378e+01	4
CH2CHO 110393O 1H 3C 2 g 0300.00 5000.00 1000.00	1
0.05975670e+02 0.08130591e-01-0.02743624e-04 0.04070304e-08-0.02176017e-12	2
0.04903218e+04-0.05045251e+02 0.03409062e+02 0.01073857e+00 0.01891492e-04	3
-0.07158583e-07 0.02867385e-10 0.01521477e+05 0.09558290e+02	4
HOC2H4OO 2/14/95 tHermC 2H 50 3 g 300.000 5000.000 1392.000	1
1.07432659e+01 1.30957787e-02-4.45370088e-06 6.88548738e-10-3.98230113e-14	2
-2.55911274e+04-2.33254953e+01 4.11839445e+00 2.72240632e-02-1.60824430e-05	3
5.17033408e-09-7.31610168e-13-2.30857785e+04 1.28482112e+01	4
CH3CO 120186C 2H 30 1 g 0300.00 5000.00 1000.00	1
0.05612279e+02 0.08449886e-01-0.02854147e-04 0.04238376e-08-0.02268404e-12	2
-0.05187863e+05-0.03274949e+02 0.03125278e+02 0.09778220e-01 0.04521448e-04	3
-0.09009462e-07 0.03193718e-10-0.04108508e+05 0.01122885e+03	4
CH2CO 121686C 2H 20 1 g 0300.00 5000.00 1000.00	1
0.06038817e+02 0.05804840e-01-0.01920954e-04 0.02794485e-08-0.01458868e-12	2
-0.08583402e+05-0.07657581e+02 0.02974971e+02 0.01211871e+00-0.02345046e-04	3
-0.06466685e-07 0.03905649e-10-0.07632637e+05 0.08673553e+02	4
HCCO 32387H 1C 20 1 g 0300.00 4000.00 1000.00	1
0.06758073e+02 0.02000400e-01-0.02027607e-05-0.01041132e-08 0.01965165e-12	2
0.01901513e+06-0.09071262e+02 0.05047965e+02 0.04453478e-01 0.02268283e-05	3
-0.01482095e-07 0.02250742e-11 0.01965892e+06 0.04818439e+01	4
CH3CHO 120186C 2O 1H 4 g 0300.00 5000.00 1000.00	1
0.05868650e+02 0.01079424e+00-0.03645530e-04 0.05412912e-08-0.02896844e-12	2
-0.02264569e+06-0.06012946e+02 0.02505695e+02 0.01336991e+00 0.04671953e-04	3
-0.01128140e-06 0.04263566e-10-0.02124589e+06 0.01335089e+03	4
CH3CO2 8/ 9/99 tHermC 2H 30 2 g 300.000 5000.000 1395.000	1
8.54059736e+00 8.32951214e-03-2.84722010e-06 4.41927196e-10-2.56373394e-14	2
-2.97290678e+04-2.10778361e+01 1.37440768e+00 2.49115604e-02-1.74308894e-05	3
6.24799508e-09-9.09516835e-13-2.72330150e+04 1.74510638e+01	4
CH3CO3 6/26/95 tHermC 2H 30 3 g 300.000 5000.000 1396.000	1
1.15641474e+01 8.02672958e-03-2.77497463e-06 4.34069277e-10-2.53202435e-14	2
-1.93142188e+04-3.13182392e+01 2.61619505e+00 2.94830898e-02-2.23952554e-05	3
8.56474251e-09-1.31255496e-12-1.62923875e+04 1.64911398e+01	4
CH3CO3H 6/26/95 tHermC 2H 40 3 g 300.000 5000.000 1391.000	1
1.25060485e+01 9.47789695e-03-3.30402246e-06 5.19630793e-10-3.04233568e-14	2
-4.59856703e+04-3.79195947e+01 2.24135876e+00 3.37963514e-02-2.53887482e-05	3
9.67583587e-09-1.49266157e-12-4.24677831e+04 1.70668133e+01	4
! This compound from Burcat	
C2O RUS 79C 2O 1 G 200.000 6000.000 1000.	1



```

0.51512722E+01 0.23726722E-02-0.76135971E-06 0.11706415E-09-0.70257804E-14 2
0.33241888E+05-0.22183135E+01 0.28648610E+01 0.11990216E-01-0.18362448E-04 3
0.15769739E-07-0.53897452E-11 0.33749932E+05 0.88867772E+01 4
CHOCHO      MARNOVC  20  2H  2  G  300.00  5000.000  1000.00  1
4.22077963E+00 4.40953711E-02 3.11033052E-05 9.85174145E-09-1.17496347E-12 2
-3.15371998E+04-4.34926405E+00 4.22077963E+00 4.40953711E-02 3.11033052E-05 3
9.85174145E-09-1.17496347E-12-3.15371998E+04-4.34926405E+00 4
! BURCAT AGAIN, HCCOH HCCO WITH AN EXTRA 15TH PARAMETER
HCCOH      T 4/93C  2H  2O  1  OG  200.000  6000.000  1000.  1
0.63660255E+01 0.55038729E-02-0.18851901E-05 0.29446414E-09-0.17218598E-13 2
0.89184965E+04-0.82504705E+01 0.19654173E+01 0.25585205E-01-0.38773334E-04 3
0.31566335E-07-0.10081670E-10 0.97694090E+04 0.12602749E+02 4
HCCO      T 6/94C  2H  1O  1  OG  200.000  6000.000  1000.  1
0.58469006E+01 0.36405960E-02-0.12959007E-05 0.20796919E-09-0.12400022E-13 2
0.19248496E+05-0.52916533E+01 0.23350118E+01 0.17010083E-01-0.22018867E-04 3
0.15406447E-07-0.43455097E-11 0.20050299E+05 0.11976729E+02 4
CH2(OH)2   CBS-Q C  1O  2H  4  G  300.00  5000.000  1000.00  1
7.59775110E-01 2.42691498E-02-1.60168806E-05 5.29445902E-09-6.46618088E-13 2
-4.82047072E+04 2.03640037E+01 7.59775110E-01 2.42691498E-02-1.60168806E-05 3
5.29445902E-09-6.46618088E-13-4.82047072E+04 2.03640037E+01 4
!Burcat
C3H6      L 4/85C  3H  6  0  OG  300.000  5000.000  1000.  1
0.67213974E 01 0.14931757E-01-0.49652353E-05 0.72510753E-09-0.38001476E-13 2
-0.92453149E 03-0.12155617E 02 0.14575157E 01 0.21142263E-01 0.40468012E-05 3
-0.16319003E-07 0.70475153E-11 0.10740208E 04 0.17399460E 02 0.24557265E 04 4
nC3H7     N-L 9/84C  3H  7  0  OG  300.000  5000.000  1000.  1
0.77026987E 01 0.16044203E-01-0.52833220E-05 0.76298590E-09-0.39392284E-13 2
0.82984336E 04-0.15480180E 02 0.10515518E 01 0.25991980E-01 0.23800540E-05 3
-0.19609569E-07 0.93732470E-11 0.10631863E 05 0.21122559E 02 0.12087447E 05 4
iC3H7     I-L 9/84C  3H  7  0  OG  300.000  5000.000  1000.  1
0.65294638E 01 0.17193288E-01-0.57153220E-05 0.83408080E-09-0.43663532E-13 2
0.77179102E 04-0.91399021E 01 0.14461584E 01 0.20988975E-01 0.77172672E-05 3
-0.18481391E-07 0.71269024E-11 0.98206094E 04 0.20108200E 02 0.11221480E 05 4
C3H8      L 4/85C  3H  8  0  OG  300.000  5000.000  1000.  1
0.75341368E 01 0.18872239E-01-0.62718491E-05 0.91475649E-09-0.47838069E-13 2
-0.16467516E 05-0.17892349E 02 0.93355381E 00 0.26424579E-01 0.61059727E-05 3
-0.21977499E-07 0.95149253E-11-0.13958520E 05 0.19201691E 02-0.12489986E 05 4
iC4H8     T 6/83C  4H  8  0  OG  300.000  5000.  1000.  1
0.20535841E+01 0.34350507E-01-0.15883197E-04 0.33089662E-08-0.25361045E-12 2
-0.21397231E+04 0.15556360E+02 0.11811380E+01 0.30853380E-01 0.50865247E-05 3
-0.24654888E-07 0.11110193E-10-0.17904004E+04 0.21075639E+02-0.06494670E+03 4
tC4H9     L 1/93C  4H  9  0  OG  200.000  6000.000  1000.  1
6.63074656E+00 2.59353745E-02-9.37163111E-06 1.51845890E-09-9.11190863E-14 2
2.00861323E+03-9.20581440E+00 6.87327133E+00-1.85146306E-02 1.30560116E-04 3
-1.50832755E-07 5.65358282E-11 4.10958938E+03 2.30016604E-01 6.21804532E+03 4
iC4H9     P10/84C  4H  9  0  OG  200.000  6000.000  1000.  1
9.43040607E+00 2.34271349E-02-8.53599182E-06 1.39748355E-09-8.44057456E-14 2
2.14214862E+03-2.42207994E+01 3.54885235E+00 1.78747638E-02 5.00782825E-05 3
-7.94475071E-08 3.35802354E-11 4.74011588E+03 1.11849382E+01 6.89397210E+03 4
iC4H10    I-L 4/85C  4H  10  0  OG  300.000  5000.000  1000.  1
0.10854125E 02 0.23317061E-01-0.77685427E-05 0.11348074E-08-0.59397203E-13 2
-0.21728570E 05-0.35915939E 02 0.54559016E 00 0.37825324E-01 0.56197796E-05 3
-0.30570963E-07 0.14058456E-10-0.18034047E 05 0.21129608E 02-0.16193704E 05 4

!Not using thermo
(CH3)3CCH(CH3)2  C  7H  16  0  OG  300.000  5000.000  1000.  1
0.10854125E 02 0.23317061E-01-0.77685427E-05 0.11348074E-08-0.59397203E-13 2
-0.21728570E 05-0.35915939E 02 0.54559016E 00 0.37825324E-01 0.56197796E-05 3
-0.30570963E-07 0.14058456E-10-0.18034047E 05 0.21129608E 02-0.16193704E 05 4
END

```

## B Appendix B

The contents of this appendix are the reactions and associated rate parameters used in the mechanism text file to support kinetic modeling. Specifically, the text below is an excerpt of a CHEMKIN “chem.out” file after running CHEMKIN using the mechanism for this study (for formatting questions, refer to the documentation for CHEMKIN software version 3.7 or higher). This file was originally created by Sullivan (2003) and recently modified by Ploeger. The only modification made for this study was the reduction by one order of magnitude of the pre-exponential factor of Reaction # 426. The entire text file is included here for completeness.

REACTIONS CONSIDERED	(k = A T**b exp(-E/RT))		
	A	b	E
1. (CH3)3CCH(CH3)2=>iC3H7+tC4H9	2.88E+16	0.0	72930.0
2. iC3H7+tC4H9=>(CH3)3CCH(CH3)2	4.12E+15	-1.1	0.0
3. iC3H7+tC4H9=C3H8+iC4H8	2.11E+14	-0.7	0.0
4. iC3H7+OH=C3H6+H2O	2.41E+13	0.0	0.0
5. nC3H7+OH=C3H6+H2O	2.41E+13	0.0	0.0
6. iC3H7+HO2=C3H6+H2O2	2.41E+13	0.0	0.0
7. nC3H7+HO2=C3H6+H2O2	2.41E+13	0.0	0.0
8. iC3H7+HCO=C3H8+CO	1.21E+14	0.0	0.0
9. nC3H7+HCO=C3H8+CO	1.21E+14	0.0	0.0
10. iC3H7+CH2O=C3H8+HCO	1.08E+11	0.0	6955.0
11. nC3H7+CH2O=C3H8+HCO	3.01E+03	2.9	5862.0
12. C3H8=C2H5+CH3	7.90E+22	-1.8	88694.0
13. C3H8+OH=nC3H7+H2O	3.97E+02	2.8	-310.0
14. C3H8+OH=iC3H7+H2O	1.01E+03	2.8	-310.0
15. C3H8+HO2=nC3H7+H2O2	2.95E+11	0.0	14944.0
16. C3H8+HO2=iC3H7+H2O2	9.64E+10	0.0	12578.0
17. tC4H9+O2=>iC4H8+HO2	4.82E+11	0.0	0.0
18. tC4H9+OH=>iC4H8+H2O	1.81E+13	0.0	0.0
19. iC4H10+OH=tC4H9+H2O	5.75E+10	0.5	63.6
20. iC4H10+OH=iC4H9+H2O	2.29E+10	1.5	775.0
21. iC4H10+HO2=tC4H9+H2O2	3.01E+04	2.5	15499.0
22. iC4H10+HO2=iC4H9+H2O2	3.61E+04	2.5	10531.0
23. iC4H10+O2=tC4H9+HO2	4.03E+13	0.0	50927.0
24. iC4H10+O2=iC4H9+HO2	3.97E+13	0.0	43992.0
25. iC4H10=iC3H7+CH3	1.10E+26	-2.6	90333.0
26. H2+O=OH+H	5.12E+04	2.7	6278.0
27. H2O+H=H2+OH	4.52E+08	1.6	18423.0
28. O2+H=HO2	2.07E+18	-1.7	890.0
29. O2+H=OH+O	9.76E+13	0.0	14845.0
30. H2O2+H=HO2+H2	1.69E+12	0.0	3755.0
31. H2O2+H=OH+H2O	1.02E+13	0.0	3578.0
32. H2O2+O=OH+HO2	6.62E+11	0.0	3975.0
33. H2O2+OH=H2O+HO2	2.40E+00	4.0	-2162.0
34. OH+OH=H2O2	2.96E+28	-5.3	2980.0
35. H+H+M=H2+M	1.87E+18	-1.0	0.0
O2	Enhanced by	4.000E-01	
CO	Enhanced by	7.500E-01	
CO2	Enhanced by	1.500E+00	
H2O	Enhanced by	6.500E+00	
CH4	Enhanced by	3.000E+00	
H2	Enhanced by	0.000E+00	

36.	H+H+H2=H2+H2		9.79E+16	-0.6	0.0
37.	H+O+M=OH+M		1.18E+19	-1.0	0.0
	O2	Enhanced by	4.000E-01		
	CO	Enhanced by	7.500E-01		
	CO2	Enhanced by	1.500E+00		
	H2O	Enhanced by	6.500E+00		
	CH4	Enhanced by	3.000E+00		
	H2	Enhanced by	0.000E+00		
38.	H+OH+M=H2O+M		5.53E+22	-2.0	0.0
	O2	Enhanced by	4.000E-01		
	CO	Enhanced by	7.500E-01		
	CO2	Enhanced by	1.500E+00		
	H2O	Enhanced by	6.500E+00		
	CH4	Enhanced by	3.000E+00		
	H2	Enhanced by	0.000E+00		
39.	H+HO2=H2+O2		4.28E+13	0.0	1410.0
40.	H+HO2=OH+OH		1.69E+14	0.0	875.0
41.	H+HO2=H2O+O		3.01E+13	0.0	1721.0
42.	O+O+M=O2+M		5.40E+13	0.0	-1788.0
	O2	Enhanced by	4.000E-01		
	CO	Enhanced by	7.500E-01		
	CO2	Enhanced by	1.500E+00		
	H2O	Enhanced by	6.500E+00		
	CH4	Enhanced by	3.000E+00		
	H2	Enhanced by	0.000E+00		
43.	O+HO2=O2+OH		3.19E+13	0.0	0.0
44.	OH+OH=O+H2O		1.51E+09	1.1	100.0
45.	OH+HO2=H2O+O2		1.91E+16	-1.0	0.0
46.	HO2+HO2=H2O2+O2		4.22E+14	0.0	11984.0
	Declared duplicate reaction...				
47.	HO2+HO2=H2O2+O2		1.32E+11	0.0	-1630.0
	Declared duplicate reaction...				
48.	CH4+O2=CH3+HO2		3.97E+13	0.0	56892.0
49.	CH4+H=CH3+H2		1.32E+04	3.0	8038.0
50.	CH4+CH2=CH3+CH3		4.30E+12	0.0	10038.0
51.	CH4+CH2(S)=CH3+CH3		7.00E+13	0.0	0.0
52.	CH4+O=CH3+OH		7.23E+08	1.6	8485.0
53.	CH4+OH=CH3+H2O		1.57E+07	1.8	2782.0
54.	CH4+HO2=CH3+H2O2		9.03E+12	0.0	24720.0
55.	CH4+CH3OO=CH3OOH+CH3		1.81E+11	0.0	18481.0
56.	O2+CH3=CH2O+OH		3.31E+11	0.0	8944.0
57.	O2+CH3=CH3O+O		1.32E+14	0.0	31398.0
58.	CH3+O2(+M)<=>CH3OO(+M)		7.83E+08	1.2	0.0
	Low pressure limit:		0.15500E+27	-0.33000E+01	0.00000E+00
	TROE centering:		0.33600E+00	0.23900E+03	0.10000E+06
	O2	Enhanced by	4.000E-01		
	CO	Enhanced by	7.500E-01		
	CO2	Enhanced by	1.500E+00		
	H2O	Enhanced by	6.500E+00		
	CH4	Enhanced by	3.000E+00		
	H2	Enhanced by	0.000E+00		
59.	H+CH3(+M)=CH4(+M)		2.11E+14	0.0	0.0
	O2	Enhanced by	4.000E-01		
	CO	Enhanced by	7.500E-01		
	CO2	Enhanced by	1.500E+00		
	H2O	Enhanced by	6.500E+00		
	CH4	Enhanced by	3.000E+00		
	H2	Enhanced by	0.000E+00		
	Low pressure limit:		0.17600E+25	-0.18000E+01	0.00000E+00
	TROE centering:		0.37000E+00	0.33150E+04	0.61000E+02
60.	H2+CH2(S)=CH3+H		7.23E+13	0.0	0.0
61.	CH3+O=CH2O+H		8.43E+13	0.0	0.0
62.	CH3+O<=>CH3O		7.97E+16	-2.1	625.0
63.	CH3+OH(+M)=CH3OH(+M)		2.79E+18	-1.4	1330.0
	Low pressure limit:		0.40000E+37	-0.59200E+01	0.31400E+04
	TROE centering:		0.41200E+00	0.19500E+03	0.59000E+04
64.	CH2(S)+H2O(+M)=CH3OH(+M)		4.80E+18	-1.2	1145.0
	Low pressure limit:		0.18800E+39	-0.63600E+01	0.50400E+04
	TROE centering:		0.60270E+00	0.20800E+03	0.39220E+04
65.	CH3+HO2=CH3O+OH		1.80E+13	0.0	0.0
66.	CH3+HO2=CH2O+H2O		1.11E+05	1.9	-2460.0

67.	CH <sub>3</sub> +HCO=CH <sub>4</sub> +CO	1.20E+14	0.0	0.0
68.	CH <sub>2</sub> O+CH <sub>3</sub> =CH <sub>4</sub> +HCO	7.83E-08	6.1	1970.0
69.	CH <sub>3</sub> +CH <sub>3</sub> O<=>CH <sub>4</sub> +CH <sub>2</sub> O	2.41E+13	0.0	0.0
70.	CH <sub>3</sub> +CH <sub>2</sub> OH<=>CH <sub>4</sub> +CH <sub>2</sub> O	2.41E+12	0.0	0.0
71.	CH <sub>3</sub> +CH <sub>3</sub> OO<=>CH <sub>3</sub> O+CH <sub>3</sub> O	2.41E+13	0.0	0.0
72.	CH <sub>3</sub> OH+CH <sub>3</sub> <=>CH <sub>4</sub> +CH <sub>2</sub> OH	3.19E+01	3.2	7172.0
73.	CH <sub>3</sub> OH+CH <sub>3</sub> <=>CH <sub>4</sub> +CH <sub>3</sub> O	1.44E+01	3.1	6935.0
74.	CH <sub>2</sub> +H=CH <sub>3</sub>	2.16E+13	0.3	0.0
75.	O <sub>2</sub> +CH <sub>3</sub> O=CH <sub>2</sub> O+HO <sub>2</sub>	2.17E+10	0.0	1750.0
76.	O <sub>2</sub> +CH <sub>2</sub> OH=CH <sub>2</sub> O+HO <sub>2</sub>	1.57E+15	-1.0	0.0
	Declared duplicate reaction...			
77.	O <sub>2</sub> +CH <sub>2</sub> OH=CH <sub>2</sub> O+HO <sub>2</sub>	7.23E+13	0.0	3578.0
	Declared duplicate reaction...			
78.	H+CH <sub>3</sub> O=CH <sub>2</sub> O+H <sub>2</sub>	1.81E+13	0.0	0.0
79.	H+CH <sub>2</sub> OH=CH <sub>2</sub> O+H <sub>2</sub>	3.08E+13	0.0	0.0
80.	OH+CH <sub>3</sub> O=CH <sub>2</sub> O+H <sub>2</sub> O	1.81E+13	0.0	0.0
81.	OH+CH <sub>2</sub> OH=CH <sub>2</sub> O+H <sub>2</sub> O	2.41E+13	0.0	0.0
82.	CH <sub>3</sub> OOH<=>CH <sub>3</sub> O+OH	6.00E+14	0.0	42330.0
83.	O+CH <sub>3</sub> O=CH <sub>2</sub> O+OH	1.81E+12	0.0	0.0
84.	O+CH <sub>2</sub> OH=CH <sub>2</sub> O+OH	9.03E+13	0.0	0.0
85.	CH <sub>3</sub> O+HO <sub>2</sub> <=>CH <sub>2</sub> O+H <sub>2</sub> O <sub>2</sub>	3.01E+11	0.0	0.0
86.	CH <sub>2</sub> OH+HO <sub>2</sub> <=>CH <sub>2</sub> O+H <sub>2</sub> O <sub>2</sub>	1.21E+13	0.0	0.0
87.	2CH <sub>3</sub> O<=>CH <sub>2</sub> O+CH <sub>3</sub> OH	6.03E+13	0.0	0.0
88.	CH <sub>3</sub> O+CH <sub>2</sub> OH<=>CH <sub>3</sub> OH+CH <sub>2</sub> O	2.41E+13	0.0	0.0
89.	CH <sub>2</sub> OH+CH <sub>2</sub> OH<=>CH <sub>3</sub> OH+CH <sub>2</sub> O	4.82E+12	0.0	0.0
90.	CH <sub>3</sub> O+CH <sub>3</sub> OH<=>CH <sub>3</sub> OH+CH <sub>2</sub> OH	3.01E+11	0.0	4074.0
91.	CH <sub>3</sub> O+CH <sub>2</sub> <=>CH <sub>3</sub> +CH <sub>2</sub> O	1.81E+13	0.0	0.0
92.	CH <sub>3</sub> O+CH <sub>2</sub> (S)<=>CH <sub>3</sub> +CH <sub>2</sub> O	1.81E+13	0.0	0.0
93.	CH <sub>2</sub> +CH <sub>2</sub> OH<=>CH <sub>3</sub> +CH <sub>2</sub> O	1.21E+12	0.0	0.0
94.	CH <sub>3</sub> O+CH <sub>2</sub> O<=>CH <sub>3</sub> OH+HCO	1.02E+11	0.0	2981.0
95.	CH <sub>2</sub> OH+CH <sub>2</sub> O<=>CH <sub>3</sub> OH+HCO	5.49E+03	2.8	5862.0
96.	CH <sub>3</sub> O+HCO<=>CH <sub>3</sub> OH+CO	9.04E+13	0.0	0.0
97.	CH <sub>2</sub> OH+HCO<=>CH <sub>3</sub> OH+CO	1.21E+14	0.0	0.0
98.	CH <sub>2</sub> OH+HCO<=>CH <sub>2</sub> O+CH <sub>2</sub> O	1.81E+14	0.0	0.0
99.	CH <sub>3</sub> O+CO=CH <sub>3</sub> +CO <sub>2</sub>	6.81E-18	9.2	-2840.0
100.	CH <sub>3</sub> O+CH <sub>3</sub> OO<=>CH <sub>2</sub> O+CH <sub>3</sub> OOH	3.01E+11	0.0	0.0
101.	CH <sub>2</sub> OH+CH <sub>3</sub> OO=CH <sub>2</sub> O+CH <sub>3</sub> O+OH	1.21E+13	0.0	0.0
102.	CH <sub>3</sub> O(+M)=CH <sub>2</sub> O+H(+M)	6.80E+13	0.0	26171.0
	Low pressure limit:	0.51700E+24	-0.24000E+01	0.24307E+05
	TROE centering:	0.80200E+01	0.12580E+04	0.10220E+04 0.45400E+03
	O <sub>2</sub>	Enhanced by	4.000E-01	
	CO	Enhanced by	7.500E-01	
	CO <sub>2</sub>	Enhanced by	1.500E+00	
	H <sub>2</sub> O	Enhanced by	6.500E+00	
	CH <sub>4</sub>	Enhanced by	3.000E+00	
	H <sub>2</sub>	Enhanced by	0.000E+00	
103.	CH <sub>2</sub> OH(+M)=CH <sub>2</sub> O+H(+M)	7.00E+14	0.0	29637.0
	Low pressure limit:	0.12600E+17	0.00000E+00	0.30020E+05
	O <sub>2</sub>	Enhanced by	4.000E-01	
	CO	Enhanced by	7.500E-01	
	CO <sub>2</sub>	Enhanced by	1.500E+00	
	H <sub>2</sub> O	Enhanced by	6.500E+00	
	CH <sub>4</sub>	Enhanced by	3.000E+00	
	H <sub>2</sub>	Enhanced by	0.000E+00	
104.	CH <sub>3</sub> OH+H<=>CH <sub>2</sub> OH+H <sub>2</sub>	1.44E+13	0.0	6095.0
105.	CH <sub>3</sub> OH+H<=>CH <sub>3</sub> O+H <sub>2</sub>	3.60E+12	0.0	6095.0
106.	CH <sub>3</sub> OH+O<=>CH <sub>2</sub> OH+OH	3.88E+05	2.5	3080.0
107.	CH <sub>3</sub> OH+O<=>CH <sub>3</sub> O+OH	1.00E+13	0.0	4684.0
108.	CH <sub>3</sub> OH+OH<=>CH <sub>2</sub> OH+H <sub>2</sub> O	7.10E+06	1.8	-596.0
109.	CH <sub>3</sub> OH+OH<=>CH <sub>3</sub> O+H <sub>2</sub> O	1.00E+06	2.1	496.7
110.	CH <sub>3</sub> OH+O <sub>2</sub> <=>CH <sub>2</sub> OH+HO <sub>2</sub>	2.05E+13	0.0	4490.0
111.	CH <sub>3</sub> OH+HO <sub>2</sub> <=>CH <sub>2</sub> OH+H <sub>2</sub> O <sub>2</sub>	3.98E+13	0.0	19400.0
112.	CH <sub>3</sub> OH+CH <sub>2</sub> <=>CH <sub>2</sub> OH+CH <sub>3</sub>	3.19E+01	3.2	7172.0
113.	CH <sub>3</sub> OH+CH <sub>2</sub> <=>CH <sub>3</sub> O+CH <sub>3</sub>	1.44E+01	3.1	6935.0
114.	CH <sub>3</sub> OH+CH <sub>2</sub> (S)<=>CH <sub>2</sub> OH+CH <sub>3</sub>	1.51E+12	0.0	0.0
115.	CH <sub>3</sub> OH+CH <sub>3</sub> OO<=>CH <sub>2</sub> OH+CH <sub>3</sub> OOH	1.81E+11	0.0	13712.0
116.	CH <sub>3</sub> OH(+M)<=>CH <sub>2</sub> OH+H(+M)	2.69E+16	-0.1	98940.0
	Low pressure limit:	0.23400E+41	-0.63300E+01	0.10310E+06
	TROE centering:	0.77300E+00	0.69300E+03	0.53330E+04 0.10000E+06
117.	H+CH <sub>3</sub> O(+M)<=>CH <sub>3</sub> OH(+M)	2.43E+12	0.5	50.0
	Low pressure limit:	0.46600E+42	-0.74400E+01	0.14080E+05

	TROE centering:	0.70000E+00	0.10000E+03	0.90000E+05	0.10000E+05		
	H2	Enhanced by	2.000E+00				
	H2O	Enhanced by	6.000E+00				
	CH4	Enhanced by	2.000E+00				
	CO	Enhanced by	1.500E+00				
	CO2	Enhanced by	2.000E+00				
118.	CH3OO+H2=CH3OOH+H			3.01E+13	0.0	26032.0	
119.	CH3OO+H=CH3O+OH			9.64E+13	0.0	0.0	
120.	CH3OO+O=CH3O+O2			3.61E+13	0.0	0.0	
121.	CH3OO+OH=CH3OH+O2			6.03E+13	0.0	0.0	
122.	CH3OO+HO2=CH3OOH+O2			2.29E+11	0.0	-1550.0	
123.	CH3OO+H2O2=CH3OOH+HO2			2.41E+12	0.0	9936.0	
124.	CH2O+CH3OO<=>CH3OOH+HCO			1.99E+12	0.0	11665.0	
125.	CH3OO+HCO<=>CH3OOH+CO			3.01E+13	0.0	0.0	
126.	CH2+CH3OO<=>CH2O+CH3O			1.81E+13	0.0	0.0	
127.	CH3OOH+H=CH3O+H2O			7.27E+10	0.0	1860.0	
128.	CH3OOH+OH=CH3OO+H2O			7.23E+11	0.0	-258.0	
129.	CH3OOH=CH2O+H2O			3.09E-02	4.5	39758.0	
130.	H+CH2 (S)=CH2+H			2.00E+14	0.0	0.0	
131.	CH2+O=CO+H+H			7.20E+13	0.0	0.0	
132.	CH2+O=CO+H2			4.80E+13	0.0	0.0	
133.	O+CH2<=>H+HCO			8.00E+13	0.0	0.0	
134.	CH2 (S)+O<=>H2+CO			1.50E+13	0.0	0.0	
135.	CH2 (S)+O<=>CO+H+H			1.50E+13	0.0	0.0	
136.	CH2+OH=CH2O+H			1.81E+13	0.0	0.0	
137.	OH+CH2 (S)<=>H+CH2O			3.00E+13	0.0	0.0	
138.	O2+CH2=CO2+H2			5.43E+12	0.0	1491.0	
139.	O2+CH2=CO2+H+H			5.43E+12	0.0	1491.0	
140.	O2+CH2=CO+OH+H			8.15E+12	0.0	1491.0	
141.	O2+CH2=CO+H2O			1.48E+12	0.0	1491.0	
142.	O2+CH2=CH2O+O			4.20E+12	0.0	1491.0	
143.	CH2+O2=HCO+OH			4.30E+10	0.0	-500.0	
144.	O2+CH2 (S)=CO+OH+H			3.13E+13	0.0	0.0	
145.	CH2 (S)+O2<=>CO+H2O			1.20E+13	0.0	0.0	
146.	HO2+CH2<=>OH+CH2O			2.00E+13	0.0	0.0	
147.	HO2+CH2 (S)<=>OH+CH2O			3.02E+13	0.0	0.0	
148.	CH2 (S)+H2O2<=>CH3+HO2			3.01E+13	0.0	0.0	
149.	CO2+CH2=CH2O+CO			2.35E+10	0.0	0.0	
150.	CH2 (S)+CO2<=>CO+CH2O			1.40E+13	0.0	0.0	
151.	CH2 (S)+CH2O<=>CH3+HCO			1.20E+12	0.0	0.0	
152.	CH2+HCO=CH3+CO			1.81E+13	0.0	0.0	
153.	CH2 (S)+HCO<=>CH3+CO			1.81E+13	0.0	0.0	
154.	CH2 (S)+M=CH2+M			1.51E+13	0.0	0.0	
	O2	Enhanced by	4.000E-01				
	CO	Enhanced by	7.500E-01				
	CO2	Enhanced by	1.500E+00				
	H2O	Enhanced by	6.500E+00				
	CH4	Enhanced by	4.800E-01				
155.	CH2O+H=HCO+H2			1.26E+08	1.6	2165.0	
156.	CH2O+O=HCO+OH			4.16E+11	0.6	2763.0	
157.	CH2O+OH=HCO+H2O			3.43E+09	1.2	-447.0	
158.	O2+CH2O=HCO+HO2			6.02E+13	0.0	40657.0	
159.	CH2O+HO2=H2O2+HCO			3.01E+12	0.0	13076.0	
160.	H+HCO (+M)<=>CH2O (+M)			1.09E+12	0.5	-260.0	
	Low pressure limit:	0.24700E+25	-0.25700E+01	0.42500E+03			
	TROE centering:	0.78240E+00	0.27100E+03	0.27550E+04	0.65700E+04		
	H2	Enhanced by	2.000E+00				
	H2O	Enhanced by	6.000E+00				
	CH4	Enhanced by	2.000E+00				
	CO	Enhanced by	1.500E+00				
	CO2	Enhanced by	2.000E+00				
161.	H2+CO (+M)<=>CH2O (+M)			4.30E+07	1.5	79600.0	
	Low pressure limit:	0.50700E+28	-0.34200E+01	0.84350E+05			
	TROE centering:	0.93200E+00	0.19700E+03	0.15400E+04	0.10300E+05		
	H2	Enhanced by	2.000E+00				
	H2O	Enhanced by	6.000E+00				
	CH4	Enhanced by	2.000E+00				
	CO	Enhanced by	1.500E+00				
	CO2	Enhanced by	2.000E+00				
162.	H+HCO=CO+H2			9.03E+13	0.0	0.0	
163.	O+HCO=CO+OH			3.01E+13	0.0	0.0	

164.	O+HCO=CO2+H	3.01E+13	0.0	0.0
165.	O2+HCO=HO2+CO	3.01E+12	0.0	0.0
166.	OH+HCO=H2O+CO	1.02E+14	0.0	0.0
167.	HCO+HCO=CH2O+CO	3.01E+13	0.0	0.0
168.	HCO=H+CO	4.50E+13	0.0	21500.0
169.	O2+CO=CO2+O	1.26E+13	0.0	47060.0
170.	O+CO(+M)<=>CO2(+M)	1.80E+10	0.0	2385.0
	Low pressure limit: 0.60200E+15 0.00000E+00 0.30000E+04			
	H2 Enhanced by	2.000E+00		
	O2 Enhanced by	6.000E+00		
	H2O Enhanced by	6.000E+00		
	CH4 Enhanced by	2.000E+00		
	CO Enhanced by	1.500E+00		
	CO2 Enhanced by	3.500E+00		
171.	CO+HO2=CO2+OH	1.51E+14	0.0	23666.0
172.	PO(OH)2CH3<=>PO2CH3+H2O	2.20E+12	0.0	41900.0
173.	PO(OH)2CH3<=>PO2OH+CH4	6.40E+11	0.4	64100.0
174.	PO(OH)2CH3<=>POOHCH2+H2O	2.56E+09	1.3	73000.0
175.	PO(OH)2CH3<=>POOH+CH3OH	5.09E+11	0.7	105130.0
176.	PO2CH3+OH<=>PO2OH+CH3	1.00E+12	0.0	2000.0
177.	PO(OH)2CH3+OH<=>PO(OH)2CH2+H2O	1.04E+06	2.4	-1137.0
178.	PO(OH)2CH3+OH<=>PO2(OH)CH3+H2O	2.13E+04	2.4	198.0
179.	PO(OH)2CH3+OH<=>PO(OH)3CH3	5.32E+03	2.0	836.6
180.	PO(OH)2CH2+H=PO(OH)2CH3	1.00E+14	0.0	0.0
181.	PO2(OH)CH3+H=PO(OH)2CH3	1.00E+14	0.0	0.0
182.	PO(OH)2CH3+H=PO(OH)2CH2+H2	2.80E+07	2.0	7700.0
183.	PO(OH)2CH3+O=PO(OH)2CH2+OH	2.20E+06	2.4	5500.0
184.	PO(OH)2CH3+CH3=PO(OH)2CH2+CH4	6.51E+11	0.0	11600.0
185.	PO(OH)2CH3+CH3O=PO(OH)2CH2+CH3OH	1.58E+11	0.0	7000.0
186.	PO(OH)2CH2+HO2=PO(OH)2CH3+O2	1.50E+11	0.0	0.0
187.	PO(OH)2CH3+CH3OO=PO(OH)2CH2+CH3OOH	6.06E+12	0.0	20430.0
188.	PO(OH)2CH2OO+PO(OH)2CH3 <=>PO(OH)2CH2OOH+PO(OH)2CH2	6.06E+12	0.0	20430.0
189.	PO(OH)2CH3+HO2=PO(OH)2CH2+H2O2	4.02E+12	0.0	19400.0
190.	PO(OH)3CH3=PO(OH)3+CH3	7.35E+11	0.1	2932.0
191.	PO(OH)2CH2+O2<=>PO(OH)2CH2OO	2.94E+13	-0.4	0.0
192.	PO(OH)2CH2+CH3OO<=>PO(OH)2CH2O+CH3O	1.90E+12	0.0	-1200.0
193.	PO(OH)2CH2+PO(OH)2CH2OO <=>PO(OH)2CH2O+PO(OH)2CH2O	1.90E+12	0.0	-1200.0
194.	PO(OH)2CH2+HO2<=>PO(OH)2CH2O+OH	3.00E+13	0.0	0.0
195.	PO(OH)2CH2+O2=PO(OH)2CH2O+O	1.00E+13	-0.2	27902.0
196.	PO(OH)2CH2O<=>PO(OH)2+CH2O	1.10E+13	0.0	16700.0
197.	PO(OH)2CH2O+O2=PO(OH)2CHO+HO2	3.60E+10	0.0	1090.0
198.	PO(OH)2CH2O+CO=PO(OH)2CH2+CO2	4.68E+02	3.2	5380.0
199.	PO(OH)2CH2O+OH=PO(OH)2CHO+H2O	1.00E+13	0.0	0.0
200.	PO(OH)2CH2OH=PO(OH)2+CH2OH	5.94E+23	-1.7	91163.0
201.	PO(OH)2CH2OH=PO(OH)2CH2+OH	1.25E+23	-1.5	96005.0
202.	PO(OH)2CH2OH=PO(OH)2CHO+H2	7.24E+11	0.1	91010.0
203.	PO(OH)2CH2OH+HO2=PO(OH)2CH2O+H2O2	2.50E+12	0.0	24000.0
204.	PO(OH)2CH2OH+OH=PO(OH)2CH2O+H2O	7.46E+11	0.3	1634.0
205.	PO(OH)2CH2OH+H=PO(OH)2CH2O+H2	1.50E+07	1.6	3038.0
206.	PO(OH)2CH2OH+O=PO(OH)2CH2O+OH	1.58E+07	2.0	4448.0
207.	PO(OH)2CH2OH+CH3=PO(OH)2CH2O+CH4	1.45E+02	3.0	7649.0
208.	PO(OH)2CH2OH+HO2=PO(OH)2CHOH+H2O2	8.20E+03	2.5	10750.0
209.	PO(OH)2CH2OH+OH=PO(OH)2CHOH+H2O	4.64E+11	0.1	0.0
210.	PO(OH)2CH2OH+H=PO(OH)2CHOH+H2	2.58E+07	1.6	2827.0
211.	PO(OH)2CH2OH+O=PO(OH)2CHOH+OH	1.88E+07	1.9	1824.0
212.	PO(OH)2CH2OH+CH3=PO(OH)2CHOH+CH4	7.28E+02	3.0	7948.0
213.	PO(OH)2CH2OH+PO(OH)2CH2 =PO(OH)2CHOH+PO(OH)2CH3	5.00E+10	0.0	10400.0
214.	PO(OH)2CH2OH+O2=PO(OH)2CHOH+HO2	1.50E+13	0.0	50150.0
215.	PO(OH)2CHOH+O2=PO(OH)2CHO+HO2 Declared duplicate reaction...	8.43E+15	-1.2	0.0
216.	PO(OH)2CHOH+O2=PO(OH)2CHO+HO2 Declared duplicate reaction...	4.82E+14	0.0	5017.0
217.	PO(OH)2CHOH+O=PO(OH)2CHO+OH	1.00E+14	0.0	0.0
218.	PO(OH)2CHOH+HO2=PO(OH)2CHO+H2O2	4.00E+13	0.0	0.0
219.	PO(OH)2CHOH+OH=PO(OH)2CHO+H2O	5.00E+12	0.0	0.0
220.	PO(OH)2CHO=PO(OH)2+HCO	2.61E+15	0.1	80550.0
221.	PO(OH)2CHO+HO2=PO(OH)2CO+H2O2	3.01E+12	0.0	11930.0
222.	PO(OH)2CHO+OH=PO(OH)2CO+H2O	2.34E+10	0.7	-1113.0

223.	PO(OH)2CHO+H=PO(OH)2CO+H2	1.34E+13	0.0	3300.0
224.	PO(OH)2CHO+O=PO(OH)2CO+OH	5.94E+12	0.0	1868.0
225.	PO(OH)2CHO+CH3=PO(OH)2CO+CH4	2.61E+06	1.8	5911.0
226.	PO(OH)2CHO+O2=PO(OH)2CO+HO2	3.01E+13	0.0	39150.0
227.	PO(OH)2CHO+CH3OO=PO(OH)2CO+CH3OOH	3.01E+12	0.0	11930.0
228.	PO(OH)2CH2OO=PO(OH)2CHO+OH	1.32E+09	1.4	41590.0
229.	PO(OH)2CO=PO(OH)2+CO	3.00E+12	0.0	16720.0
230.	PO(OH)2CO+O=PO(OH)2+CO2	2.00E+13	0.0	0.0
231.	PO(OH)2CO+CH3OO=PO(OH)2+CO2+CH3O	2.40E+13	0.0	0.0
232.	PO(OH)2CO+PO(OH)2CH2OO =PO(OH)2+CO2+PO(OH)2CH2O	2.40E+13	0.0	0.0
233.	PO(OH)2CH2OO+HO2<=>PO(OH)2CH2OOH+O2	1.62E+11	0.0	-1987.0
234.	PO(OH)2CH2OO+H2O2<=>PO(OH)2CH2OOH+HO2	2.40E+12	0.0	9935.0
235.	PO(OH)2CH2OO+CH3<=>PO(OH)2CH2O+CH3O	3.80E+12	0.0	-1200.0
236.	PO(OH)2CH2OO+CH3OO<=>PO(OH)2CH2O+CH3O+O2	1.00E+11	0.0	0.0
237.	PO(OH)2CH2OO+PO(OH)2CH2OO <=>PO(OH)2CH2O+PO(OH)2CH2O+O2	3.23E+10	0.0	248.0
238.	PO(OH)2CH2OO+PO(OH)2CH2OO =PO(OH)2CHO+PO(OH)2CH2OH+O2	1.64E+10	0.0	248.0
239.	PO(OH)2CH2OO+CH4=PO(OH)2CH2OOH+CH3	1.81E+11	0.0	18480.0
240.	PO(OH)2CH2OO+CH2O=PO(OH)2CH2OOH+HCO	1.99E+12	0.0	11660.0
241.	PO(OH)2CH2OO+H2=PO(OH)2CH2OOH+H	3.00E+13	0.0	26030.0
242.	PO(OH)2CH2OO+H=PO(OH)2CH2O+OH	9.64E+13	0.0	0.0
243.	PO(OH)2CH2OO+HCO=PO(OH)2CH2O+H+CO2	3.01E+13	0.0	0.0
244.	PO(OH)2CH2OO+CH3O=PO(OH)2CH2OOH+CH2O	3.00E+11	0.0	0.0
245.	PO(OH)2CH2OO+CH2OH=PO(OH)2CH2OOH+CH2O	1.21E+13	0.0	0.0
246.	PO(OH)2CH2OO+CH3OH=PO(OH)2CH2OOH+CH2OH	1.81E+11	0.0	13712.0
247.	PO(OH)2CH2OO+O=PO(OH)2CH2O+O2	3.61E+13	0.0	0.0
248.	PO(OH)2CH2OO+CH2=PO(OH)2CH2O+CH2O	1.81E+13	0.0	0.0
249.	PO(OH)2CH2OO<=>PO2(OH)CH2OOH	1.00E+10	0.0	35250.0
250.	PO(OH)2CH2O<=>PO2(OH)CH2OH	1.00E+10	0.0	32100.0
251.	PO2(OH)CH2OH=PO2OH+CH2OH	3.50E+13	0.0	7910.0
252.	PO(OH)2CH2OOH<=>PO(OH)2CH2O+OH	6.31E+14	0.0	42300.0
253.	PO(OH)2CH2OOH+OH=PO(OH)2CH2OO+H2O	7.23E+11	0.0	-258.0
254.	PO(OH)2CH2OOH+H=PO(OH)2CH2O+H2O	7.27E+10	0.0	1860.0
255.	PO2(OH)CH2OOH=PO2OH+CH2O+OH	3.50E+13	0.0	7910.0
256.	PO(OH)2CH2OOH+OH=PO2(OH)CH2OOH+H2O	2.13E+04	2.4	198.0
257.	PO2(OH)CH3<=>PO2OH+CH3	1.10E+13	0.0	16700.0
258.	PO(OH)3=PO2OH+H2O	2.09E+07	1.5	42118.0
259.	PO2OH+H<=>PO(OH)2	3.20E+08	1.6	6190.0
260.	PO(OH)2+H<=>PO2OH+H2	4.00E+13	0.0	0.0
261.	PO(OH)3=PO(OH)2+OH	3.63E+15	0.0	120000.0
262.	PO(OH)3+H<=>PO(OH)2+H2O	3.09E+06	2.6	37721.0
263.	PO(OH)2+O2=PO2OH+HO2	1.30E+02	2.4	419.5
264.	PO(OH)3+H=H4PO4	4.94E+06	2.1	21771.0
265.	H4PO4=PO(OH)2+H2O	1.58E+09	0.9	26893.0
266.	C2H5OH(+M)=CH2OH+CH3(+M)	5.94E+23	-1.7	91163.0
	Low pressure limit: 0.28800E+86 -0.18900E+02	0.10991E+06		
	TROE centering: 0.50000E+00 0.20000E+03	0.89000E+03	0.46000E+04	
	H2O	Enhanced by 5.000E+00		
	H2	Enhanced by 2.000E+00		
	CO2	Enhanced by 3.000E+00		
	CO	Enhanced by 2.000E+00		
267.	C2H5OH(+M)=C2H5+OH(+M)	1.25E+23	-1.5	96005.0
	Low pressure limit: 0.32500E+86 -0.18810E+02	0.11493E+06		
	TROE centering: 0.50000E+00 0.30000E+03	0.90000E+03	0.50000E+04	
	H2O	Enhanced by 5.000E+00		
	H2	Enhanced by 2.000E+00		
	CO2	Enhanced by 3.000E+00		
	CO	Enhanced by 2.000E+00		
268.	C2H5OH(+M)=C2H4+H2O(+M)	2.79E+13	0.1	66136.0
	Low pressure limit: 0.25700E+84 -0.18850E+02	0.86452E+05		
	TROE centering: 0.70000E+00 0.35000E+03	0.80000E+03	0.38000E+04	
	H2O	Enhanced by 5.000E+00		
269.	C2H5OH(+M)=CH3CHO+H2(+M)	7.24E+11	0.1	91007.0
	Low pressure limit: 0.44600E+88 -0.19420E+02	0.11559E+06		
	TROE centering: 0.90000E+00 0.90000E+03	0.11000E+04	0.35000E+04	
	H2O	Enhanced by 5.000E+00		
270.	C2H5OH+OH=C2H4OH+H2O	1.74E+11	0.3	600.0
271.	C2H5OH+OH=CH3CHOH+H2O	4.64E+11	0.1	0.0
272.	C2H5OH+OH=CH3CH2O+H2O	7.46E+11	0.3	1634.0

273.	$C_2H_5OH+H=C_2H_4OH+H_2$	1.23E+07	1.8	5098.0
274.	$C_2H_5OH+H=CH_3CHOH+H_2$	2.58E+07	1.6	2827.0
275.	$C_2H_5OH+H=CH_3CH_2O+H_2$	1.50E+07	1.6	3038.0
276.	$C_2H_5OH+O=C_2H_4OH+OH$	9.41E+07	1.7	5459.0
277.	$C_2H_5OH+O=CH_3CHOH+OH$	1.88E+07	1.9	1824.0
278.	$C_2H_5OH+O=CH_3CH_2O+OH$	1.58E+07	2.0	4448.0
279.	$C_2H_5OH+CH_3=C_2H_4OH+CH_4$	2.19E+02	3.2	9622.0
280.	$C_2H_5OH+CH_3=CH_3CHOH+CH_4$	7.28E+02	3.0	7948.0
281.	$C_2H_5OH+CH_3=CH_3CH_2O+CH_4$	1.45E+02	3.0	7649.0
282.	$C_2H_5OH+HO_2=C_2H_4OH+H_2O_2$	1.23E+04	2.5	15750.0
283.	$C_2H_5OH+HO_2=CH_3CHOH+H_2O_2$	8.20E+03	2.5	10750.0
284.	$C_2H_5OH+HO_2=CH_3CH_2O+H_2O_2$	2.50E+12	0.0	24000.0
285.	$CH_3CH_2O+M=CH_3CHO+H+M$	1.16E+35	-5.9	25274.0
286.	$CH_3CH_2O+M=CH_3+CH_2O+M$	1.35E+38	-7.0	23800.0
287.	$CH_3CH_2O+CO=C_2H_5+CO_2$	4.68E+02	3.2	5380.0
288.	$CH_3CH_2O+O_2=CH_3CHO+HO_2$	4.00E+10	0.0	1100.0
289.	$CH_3CH_2O+H=CH_3+CH_2OH$	3.00E+13	0.0	0.0
290.	$CH_3CH_2O+H=C_2H_4+H_2O$	3.00E+13	0.0	0.0
291.	$CH_3CH_2O+OH=CH_3CHO+H_2O$	1.00E+13	0.0	0.0
292.	$CH_3CHOH+O_2=CH_3CHO+HO_2$	4.82E+14	0.0	5017.0
	Declared duplicate reaction...			
293.	$CH_3CHOH+O_2=CH_3CHO+HO_2$	8.43E+15	-1.2	0.0
	Declared duplicate reaction...			
294.	$CH_3CHOH+O=CH_3CHO+OH$	1.00E+14	0.0	0.0
295.	$CH_3CHOH+H=CH_3+CH_2OH$	3.00E+13	0.0	0.0
296.	$CH_3CHOH+H=C_2H_4+H_2O$	3.00E+13	0.0	0.0
297.	$CH_3CHOH+HO_2=CH_3CHO+OH+OH$	4.00E+13	0.0	0.0
298.	$CH_3CHOH+OH=CH_3CHO+H_2O$	5.00E+12	0.0	0.0
299.	$CH_3CHOH+M=CH_3CHO+H+M$	1.00E+14	0.0	25000.0
300.	$CH_3CHO+OH=CH_3CO+H_2O$	3.00E+12	-0.1	-978.5
301.	$CH_3CHO+OH=CH_2CHO+H_2O$	1.11E+11	0.5	402.5
302.	$CH_3CHO+O=CH_3CO+OH$	1.77E+18	-1.9	2975.0
303.	$CH_3CHO+O=CH_2CHO+OH$	3.72E+13	-0.2	3556.0
304.	$CH_3CHO+H=CH_3CO+H_2$	4.66E+13	-0.3	2988.0
305.	$CH_3CHO+H=CH_2CHO+H_2$	1.85E+12	0.4	5359.0
306.	$CH_3CHO+CH_3=CH_3CO+CH_4$	3.90E-07	5.8	2200.0
307.	$CH_3CHO+CH_3=CH_2CHO+CH_4$	2.45E+01	3.1	5727.0
308.	$CH_3CHO+HO_2=CH_3CO+H_2O_2$	2.40E+19	-2.2	14030.0
309.	$CH_3CHO+HO_2=CH_2CHO+H_2O_2$	2.32E+11	0.4	14864.0
310.	$CH_3CHO+O_2=CH_3CO+HO_2$	1.00E+14	0.0	42200.0
311.	$CH_2CHO+H=CH_3+HCO$	5.00E+13	0.0	0.0
312.	$CH_2CHO+H=CH_2CO+H_2$	2.00E+13	0.0	0.0
313.	$CH_2CHO+O=CH_2O+HCO$	1.00E+14	0.0	0.0
314.	$CH_2CHO+OH=CH_2CO+H_2O$	3.00E+13	0.0	0.0
315.	$CH_2CHO+O_2=CH_2O+CO+OH$	3.00E+10	0.0	0.0
316.	$CH_2CHO+CH_3=C_2H_5+CO+H$	4.90E+14	-0.5	0.0
317.	$CH_2CHO+HO_2=CH_2O+HCO+OH$	7.00E+12	0.0	0.0
318.	$CH_2CHO+HO_2=CH_3CHO+O_2$	3.00E+12	0.0	0.0
319.	$CH_2CHO=CH_3+CO$	1.17E+43	-9.8	43756.0
320.	$CH_2CHO=CH_2CO+H$	1.81E+43	-9.6	45868.0
321.	$C_2H_6+CH_3=C_2H_5+CH_4$	5.50E-01	4.0	8300.0
322.	$C_2H_6+H=C_2H_5+H_2$	5.40E+02	3.5	5210.0
323.	$C_2H_6+O=C_2H_5+OH$	3.00E+07	2.0	5115.0
324.	$C_2H_6+OH=C_2H_5+H_2O$	7.23E+06	2.0	864.0
325.	$C_2H_5+H=C_2H_4+H_2$	1.25E+14	0.0	8000.0
326.	$C_2H_5+H=CH_3+CH_3$	3.00E+13	0.0	0.0
327.	$C_2H_5+H=C_2H_6$	3.00E+13	0.0	0.0
328.	$C_2H_5+OH=C_2H_4+H_2O$	4.00E+13	0.0	0.0
329.	$C_2H_5+O=CH_3+CH_2O$	1.00E+14	0.0	0.0
330.	$C_2H_5+HO_2=C_2H_6+O_2$	3.00E+12	0.0	0.0
331.	$C_2H_5+HO_2=CH_3+CH_2O+OH$	3.00E+13	0.0	0.0
332.	$C_2H_5+O_2=C_2H_4+HO_2$	2.89E+28	-5.4	7585.0
333.	$C_2H_5+O_2=CH_3CHO+OH$	4.90E+11	-0.5	8357.0
334.	$C_2H_4+OH=C_2H_4OH$	1.29E+12	0.0	-817.0
335.	$C_2H_4OH+O_2=HOC_2H_4OO$	1.00E+12	0.0	-1100.0
336.	$HOC_2H_4OO=CH_2O+CH_2O+OH$	6.00E+10	0.0	24500.0
337.	$C_2H_4+H=C_2H_3+H_2$	3.36E-07	6.0	1692.0
338.	$C_2H_4+OH=C_2H_3+H_2O$	2.02E+13	0.0	5936.0
339.	$C_2H_4+O=CH_3+HCO$	1.02E+07	1.9	179.0
340.	$C_2H_4+O=CH_2CHO+H$	3.39E+06	1.9	179.0
341.	$C_2H_4+CH_3=C_2H_3+CH_4$	6.62E+00	3.7	9500.0



342.	C2H4+H(+M)=C2H5(+M)	1.08E+12	0.5	1822.0
	Low pressure limit:	0.11100E+35	-0.50000E+01	0.44480E+04
	TROE centering:	0.10000E+01	0.10000E-14	0.95000E+02 0.20000E+03
	H2O	Enhanced by	5.000E+00	
	H2	Enhanced by	2.000E+00	
	CO2	Enhanced by	3.000E+00	
	CO	Enhanced by	2.000E+00	
343.	C2H4(+M)=C2H2+H2(+M)	1.80E+14	0.0	87000.0
	Low pressure limit:	0.15000E+16	0.00000E+00	0.55443E+05
344.	C2H3+H(+M)=C2H4(+M)	6.10E+12	0.3	280.0
	Low pressure limit:	0.98000E+30	-0.38600E+01	0.33200E+04
	TROE centering:	0.78200E+00	0.20800E+03	0.26630E+04 0.60950E+04
	H2O	Enhanced by	5.000E+00	
345.	C2H3+H=C2H2+H2	9.00E+13	0.0	0.0
346.	C2H3+O=CH2CO+H	3.00E+13	0.0	0.0
347.	C2H3+O2=CH2O+HCO	1.70E+29	-5.3	6500.0
348.	C2H3+O2=CH2CHO+O	5.50E+14	-0.6	5260.0
349.	C2H3+O2=C2H2+HO2	2.12E-06	6.0	9484.0
350.	C2H3+OH=C2H2+H2O	2.00E+13	0.0	0.0
351.	C2H3+C2H=C2H2+C2H2	3.00E+13	0.0	0.0
352.	C2H3+CH3=C2H2+CH4	2.00E+13	0.0	0.0
353.	C2H2+OH=C2H+H2O	3.37E+07	2.0	14000.0
354.	C2H2+OH=HCCOH+H	5.04E+05	2.3	13500.0
355.	C2H2+OH=CH2CO+H	2.18E-04	4.5	-1000.0
	Declared duplicate reaction...			
356.	C2H2+OH=CH2CO+H	2.00E+11	0.0	0.0
	Declared duplicate reaction...			
357.	C2H2+OH=CH3+CO	4.83E-04	4.0	-2000.0
358.	HCCOH+H=CH2CO+H	1.00E+13	0.0	0.0
359.	C2H2+O=CH2+CO	6.12E+06	2.0	1900.0
360.	C2H2+O=HCCO+H	1.43E+07	2.0	1900.0
361.	C2H2+O=C2H+OH	3.16E+15	-0.6	15000.0
362.	C2H2+CH3=C2H+CH4	1.81E+11	0.0	17289.0
363.	C2H2+O2=HCCO+OH	4.00E+07	1.5	30100.0
364.	C2H2+M=C2H+H+M	4.20E+16	0.0	107000.0
365.	C2H2+H(+M)=C2H3(+M)	3.11E+11	0.6	2589.0
	Low pressure limit:	0.22500E+41	-0.72690E+01	0.65770E+04
	TROE centering:	0.10000E+01	0.10000E-14	0.67500E+03 0.10000E+16
	H2O	Enhanced by	5.000E+00	
	H2	Enhanced by	2.000E+00	
	CO2	Enhanced by	3.000E+00	
	CO	Enhanced by	2.000E+00	
366.	CHOCHO(+M)=CH2O+CO(+M)	4.27E+12	0.0	50600.0
	Low pressure limit:	0.89100E+17	0.00000E+00	0.49200E+05
367.	CHOCHO=CO+CO+H2	4.07E+42	-8.5	69278.0
368.	CHOCHO+OH=HCO+CO+H2O	1.00E+13	0.0	0.0
369.	CHOCHO+O=HCO+CO+OH	7.24E+12	0.0	1970.0
370.	CHOCHO+H=CH2O+HCO	1.00E+12	0.0	0.0
371.	CHOCHO+HO2=HCO+CO+H2O2	1.70E+12	0.0	10700.0
372.	CHOCHO+CH3=HCO+CO+CH4	1.74E+12	0.0	8440.0
373.	CHOCHO+O2=HCO+CO+HO2	1.00E+14	0.0	37000.0
374.	CH3CO(+M)=CH3+CO(+M)	3.00E+12	0.0	16722.0
	Low pressure limit:	0.12000E+16	0.00000E+00	0.12518E+05
375.	CH2CO+O=CO2+CH2	1.75E+12	0.0	1350.0
376.	CH2CO+H=CH3+CO	2.71E+04	2.8	714.0
377.	CH2CO+H=HCCO+H2	2.00E+14	0.0	8000.0
378.	CH2CO+O=HCCO+OH	1.00E+13	0.0	8000.0
379.	CH2CO+OH=HCCO+H2O	1.00E+13	0.0	2000.0
380.	CH2CO+OH=CH2OH+CO	3.73E+12	0.0	-1013.0
381.	CH2CO(+M)=CH2+CO(+M)	3.00E+14	0.0	70980.0
	Low pressure limit:	0.36000E+16	0.00000E+00	0.59270E+05
382.	C2H+H2=C2H2+H	4.09E+05	2.4	864.3
383.	C2H+OH=HCCO+H	2.00E+13	0.0	0.0
384.	C2H+O2=CO+CO+H	9.04E+12	0.0	-457.0
385.	HCCO+H=CH2(S)+CO	1.00E+14	0.0	0.0
386.	HCCO+O=H+CO+CO	8.00E+13	0.0	0.0
387.	HCCO+O2=HCO+CO+O	2.50E+08	1.0	0.0
388.	HCCO+O2=CO2+HCO	2.40E+11	0.0	-854.0
389.	HCCO+HCCO=C2H2+CO+CO	1.00E+13	0.0	0.0
390.	HCCO+OH=C2O+H2O	3.00E+13	0.0	0.0
391.	C2O+O=CO+CO	5.00E+13	0.0	0.0

392.	C2O+OH=CO+CO+H	2.00E+13	0.0	0.0
393.	C2O+O2=CO+CO+O	2.00E+13	0.0	0.0
394.	CH3OO+CH3OO=CH3O+CH3O+O2	5.48E+10	0.0	-835.0
395.	CH3OO+CH3OO=CH3OH+CH2O+O2	2.19E+09	0.0	-3580.0
396.	CH3CO3+CH3CHO=>CH3CO3H+CH3CO	1.20E+11	0.0	4900.0
397.	CH3CO3H+CH3CO=>CH3CO3+CH3CHO	1.99E+10	0.0	10000.0
398.	CH3CHO+CH3O=>CH3CO+CH3OH	1.15E+11	0.0	1280.0
399.	CH3CO+CH3OH=>CH3CHO+CH3O	3.02E+11	0.0	18160.0
400.	CH3CHO+CH3OO=>CH3CO+CH3OOH	3.55E+09	0.0	5050.0
401.	CH3CO+CH3OOH=>CH3CHO+CH3OO	5.02E+09	0.0	10100.0
402.	CH3CO+O2=>CH3CO3	1.00E+10	0.0	-2700.0
403.	CH3CO3=>CH3CO+O2	2.88E+16	-1.0	37300.0
404.	CH3CO3+HO2=>CH3CO3H+O2	1.00E+12	0.0	0.0
405.	CH3CO3H+O2=>CH3CO3+HO2	3.98E+15	0.0	40000.0
406.	CH3CO3H=>CH3+CO2+OH	2.00E+14	0.0	40150.0
407.	CH3CO3+CH3OO=>CH3CO2+CH3O+O2	1.81E+12	0.0	0.0
408.	CH3CO3+HO2=>CH3CO2+OH+O2	1.00E+12	0.0	0.0
409.	CH3CO3+CH3CO3=>CH3CO2+CH3CO2+O2	4.78E+12	0.0	0.0
410.	CH3CO2(+M)=>CH3+CO2(+M)	3.00E+12	0.0	16722.0
	Low pressure limit:	0.12000E+16	0.00000E+00	0.12518E+05
411.	CH3OO+HO2=>CH3O+OH+O2	1.00E+12	0.0	0.0
412.	CH3OOH+OH=>CH2OOH+H2O	2.51E+13	0.0	1000.0
413.	CH2OOH+H2O=>CH3OOH+OH	3.01E+13	0.0	32800.0
414.	CH3OOH+CH3O=>CH3OO+CH3OH	7.07E+11	0.0	4000.0
415.	CH3OO+CH3OH=>CH3OOH+CH3O	3.01E+13	0.0	32800.0
416.	CH3OOH+CH3O=>CH2OOH+CH3OH	7.07E+11	0.0	4000.0
417.	CH2OOH+CH3OH=>CH3OOH+CH3O	3.01E+13	0.0	32800.0
418.	HCOOH+HO2=HOCO+H2O2	2.40E+19	-2.2	14030.0
419.	HCOOH+OH=HOCO+H2O	1.85E+07	1.5	-962.0
420.	HCOOH+H=HOCO+H2	6.06E+13	-0.3	2988.0
421.	HCOOH+CH3=HOCO+CH4	3.90E-07	5.8	2200.0
422.	HOCO+O2=CO2+HO2	8.73E+11	0.0	0.0
423.	HOCO+HO2=CO2+H2O2	1.00E+12	0.0	0.0
424.	HOCO+CH3OO=CO2+CH3OOH	1.00E+12	0.0	0.0
425.	CO+OH(+M)=HOCO(+M)	1.20E+07	1.8	-236.0
	Low pressure limit:	0.72400E+26	-0.38500E+01	0.15500E+04
	TROE centering:	0.60000E+00	0.10000E-14	0.10000E+16
426.	OH+CO(+M)=>H+CO2(+M)	9.54E+03	2.0	-1484.0
	High pressure limit:	0.38000-137	0.51930E+02	-0.75965E+05
	TROE centering:	0.60000E+00	0.10000E-14	0.10000E+16

NOTE: A units mole-cm-sec-K, E units cal/mole

## C Appendix C – Experimental Data

This appendix documents the experimental conditions and data from the study on catalytic reformation of methane in SCW. Certain SCW methane reforming experiments using various reducing techniques in the CSTR and PBR are omitted from these tables because steady state conditions were never achieved. Data from the hydrothermal model Maillard study will be published upon completion of the project in Andrew Peterson's doctoral thesis. Additional details can be found in the laboratory notebooks kept on file at MIT, Bldg 66-053.

### C.1 CATALYTIC REFORMATION OF METHANE IN SCW: CSTR

#### EXPERIMENTS

**Table C.1 Experimental Data for CSTR Experiments: SCW Reforming of Methane.**

Additional experiments using various reducing methods are omitted because steady state conditions were never achieved.

Run #	Catalyst	Temp (°C)	Pressure (psig)	$\tau$ (sec)	[CH <sub>4</sub> ] <sub>0</sub> (mM)	X (CH <sub>4</sub> ) (%)	[CO <sub>2</sub> ] (mM)	[H <sub>2</sub> ] (mM)
CH4-CSTR1	None	505	3737	128	1.11	-6.91	0.00	0.00
CH4-CSTR2	None	409	3560	197	1.47	6.34	0.00	0.03
CH4-CSTR3	Ni pellets	412	3690	210	1.63	11.49	0.00	0.03
CH4-CSTR4	Ni pellets	411	3433	183	1.53	2.20	0.00	0.01
CH4-CSTR5	Ni wire	412	3457	188	1.47	-2.66	0.00	0.01
CH4-CSTR6	Ni wire	520	3699	197	1.15	2.32	0.00	0.03
CH4-CSTR7	Ni wire	593	3573	209	1.05	-0.30	0.01	0.09
CH4-CSTR8	Ni wire	518	3787	204	2.23	1.66	0.00	0.02
CH4-CSTR9	Ni wire	518	2077	248	1.09	17.98	0.00	0.03
CH4-CSTR10	KATALCO 57-7	410	3776	238	2.14	4.37	0.03	0.01
CH4-CSTR11	KATALCO 57-7	500	3741	212	1.22	-1.08	0.00	0.01
CH4-CSTR12	KATALCO 57-7	487	1978	98	0.58	7.24	0.00	0.00
CH4-CSTR13	C11-PR	409	3465	196	1.68	2.10	0.00	0.01
CH4-CSTR14	C11-PR	497	3682	210	1.11	-0.15	0.00	0.02

## C.2 CATALYTIC REFORMATION OF METHANE IN SCW: BATCH TUBE

### EXPERIMENTS

**Table C.2 Experimental Data for Tube Batch Experiments: SCW Reforming of Methane.** Additional control experiments and experiments with possible leaks are omitted. (a) calculated pressure – pressure was not measured due to installation of a high temperature valve

Run #	Catalyst	Sand Bath Temp (°C)	Max Pressure (psig)	$\tau$ (HR:MIN)	[CH <sub>4</sub> ] <sub>o</sub> (psig)	[H <sub>2</sub> ] (vol $\mu$ L)	CO <sub>2</sub> (vol $\mu$ L)
TUBE-BATCH1	5% Pt/Al <sub>2</sub> O <sub>3</sub> powder	550	5300	1:17	32	3.0	0
TUBE-BATCH2	5% Pt/ Al <sub>2</sub> O <sub>3</sub> powder	550	2500	0:43	150	2.3	0
TUBE-BATCH3	1.1 wt% NaOH	600	3550 (a)	0:30	30	14.6	0
TUBE-BATCH4	no catalyst	600	3550 (a)	0:39	30	4.6	0
TUBE-BATCH5	KATALCO 57-7	600	4960	0:38	30	0	0
TUBE-BATCH6	C-11PR	600	5570	0:37	35	4.7	0
TUBE-BATCH7	5% Pt/ Al <sub>2</sub> O <sub>3</sub> powder	550	4250	1:12	33	3.7	0
TUBE-BATCH8	0.5% Pt/1/8" Al <sub>2</sub> O <sub>3</sub> pellets	600	5900	0:37	33	4.2	0.18
TUBE-BATCH9	0.5% Pt/1/8" Al <sub>2</sub> O <sub>3</sub> pellets	600	3550 (a)	0:33	32	5.3	0.07
TUBE-BATCH10	0.5% Pt/1/8" Al <sub>2</sub> O <sub>3</sub> pellets	600	3550 (a)	0:32	80	13.2	0.34
TUBE-BATCH11	0.5% Pt/1/8" Al <sub>2</sub> O <sub>3</sub> pellets	600	4450	0:34	110	2.7	0.38
TUBE-BATCH12	1.0% Pt/ZrO <sub>2</sub>	600	810	0:35	110	0	0

### C.3 CATALYTIC REFORMATION OF METHANE IN SCW: DIRECT INJECT

#### BATCH EXPERIMENTS WITH METAL CATALYSTS

**Table C.3 Experimental Data for Direct Inject Batch Experiments: SCW Reforming of Methane with Metal Catalysts.** Additional control experiments and experiments with possible leaks are omitted.

Run #	Catalyst	Temp (°C)	Max Pressure (psig)	$\tau$ (MIN)	[CH <sub>4</sub> ] <sub>0</sub> (psig)	H <sub>2</sub> (vol %)	CO <sub>2</sub> (vol %)
DI-BATCH1	Ru TiO <sub>2</sub>	600	4200	10.00	66.00	55.40	2.19
DI-BATCH2	Ru TiO <sub>2</sub>	600	4022	10.00	62.20	65.30	2.13
DI-BATCH3	Pt C	600	3607	20.00	70.5	97.20	0.89
DI-BATCH4	Pt-CeO-ZrO <sub>2</sub>	600	3724	10.00	73.1	98.30	trace
DI-BATCH5	Pt-CeO-ZrO <sub>2</sub>	600	4100	10.00	9.3	99.70	0

## C.4 CATALYTIC REFORMATION OF METHANE IN SCW: DIRECT INJECT BATCH EXPERIMENTS WITH ALKALI SALTS

**Table C.4 Experimental Data for Direct Inject Batch Experiments: SCW Reforming of Methane with Alkali Salts.**

Run #	Salt	Temp (°C)	Max Pressure (psig)	$\tau$ (MIN)	[CH <sub>4</sub> ] <sub>o</sub> (psig)	H <sub>2</sub> (vol %)	CO <sub>2</sub> (vol %)
DI-BATCH6	no salt	600	4090	~30	31.3	1.18	0
DI-BATCH7	1wt % KOH	600	4190	15	300 Ar	3.90	0
DI-BATCH8	1wt% KOH	600	4070	15	30.2	3.03	0
DI-BATCH9	1wt % NaOH	600	4270	15	300 Ar	2.21	0
DI-BATCH10	1wt% NaOH	600	4290	15	30.2	3.79	trace
DI-BATCH11	1wt% K <sub>2</sub> CO <sub>3</sub>	600	4130	15	310 Ar	2.86	0
DI-BATCH12	1wt% K <sub>2</sub> CO <sub>3</sub>	600	4360	15	31.3	2.99	trace
DI-BATCH13	1wt % KOH	600	4465	15	310 Ar	2.92	0
DI-BATCH14	1wt% KOH	600	4465	15	31.3	6.06	0
DI-BATCH15	1wt% KOH	600	4490	15	31.3	8.26	0.15%
DI-BATCH16	1wt % KOH	600	4413	15	310 Ar	4.04	0
DI-BATCH17 (gold cell)	1wt % KOH	600	4309	15	300 Ar	2.91	0
DI-BATCH18 (gold cell)	1wt% KOH	600	4699	15	30.2	2.19	0

## D Appendix D – Catalyst Analysis Data

The contents of this appendix are the catalyst analysis data from all metal catalysts employed in this study.

### D.1 XRD RESULTS

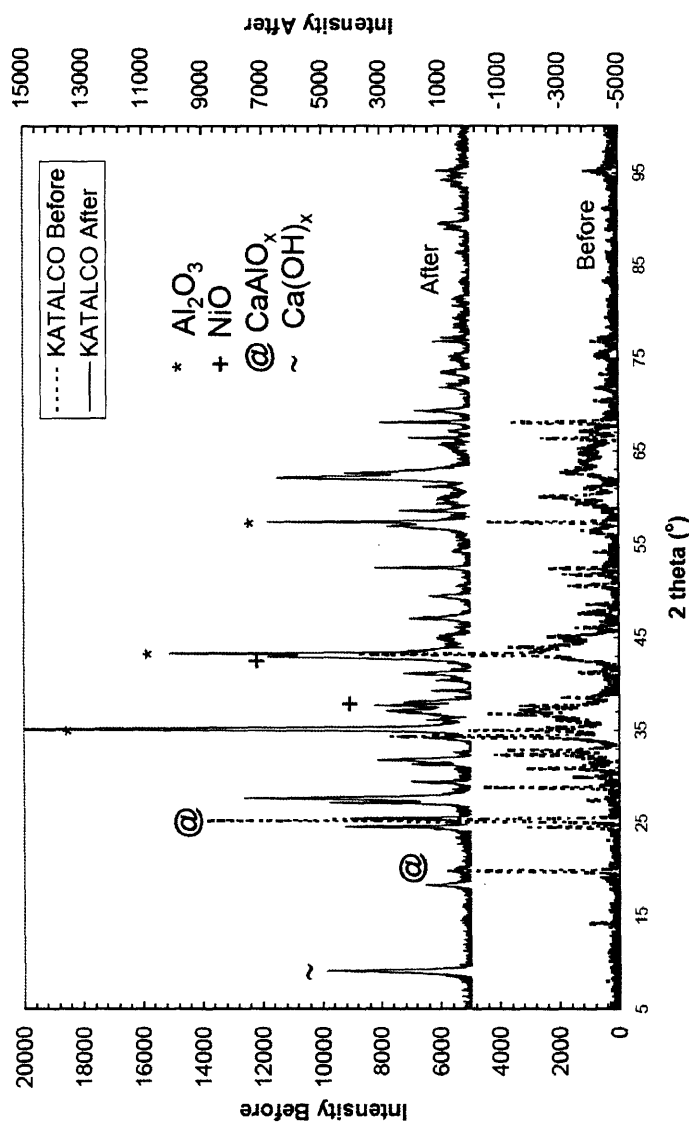


Figure D.1 XRD Results of KATALCO 57-7 pellets before and after exposure to SCW

Figure D.1 XRD Results of KATALCO 57-7 pellets before and after exposure to SCW (11 hrs, 400-500°C, 245 bar).

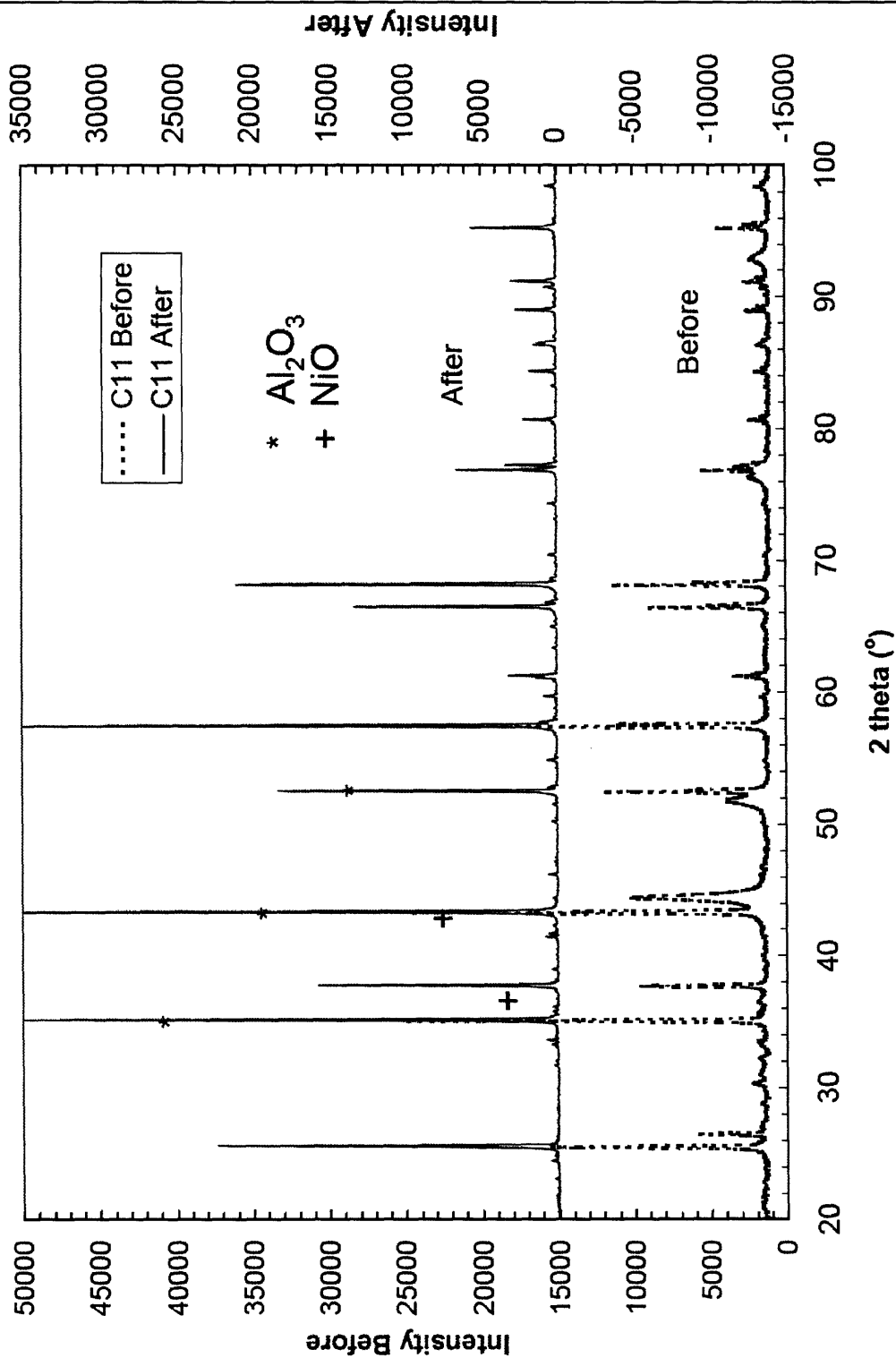


Figure D.2 XRD Results of C11-PR pellets before and after exposure to SCW

Figure D.2 XRD Results of C11-PR pellets before and after exposure to SCW (37.5 hrs, 400-500°C, 245 bar; shorter exposure time saw similar results).



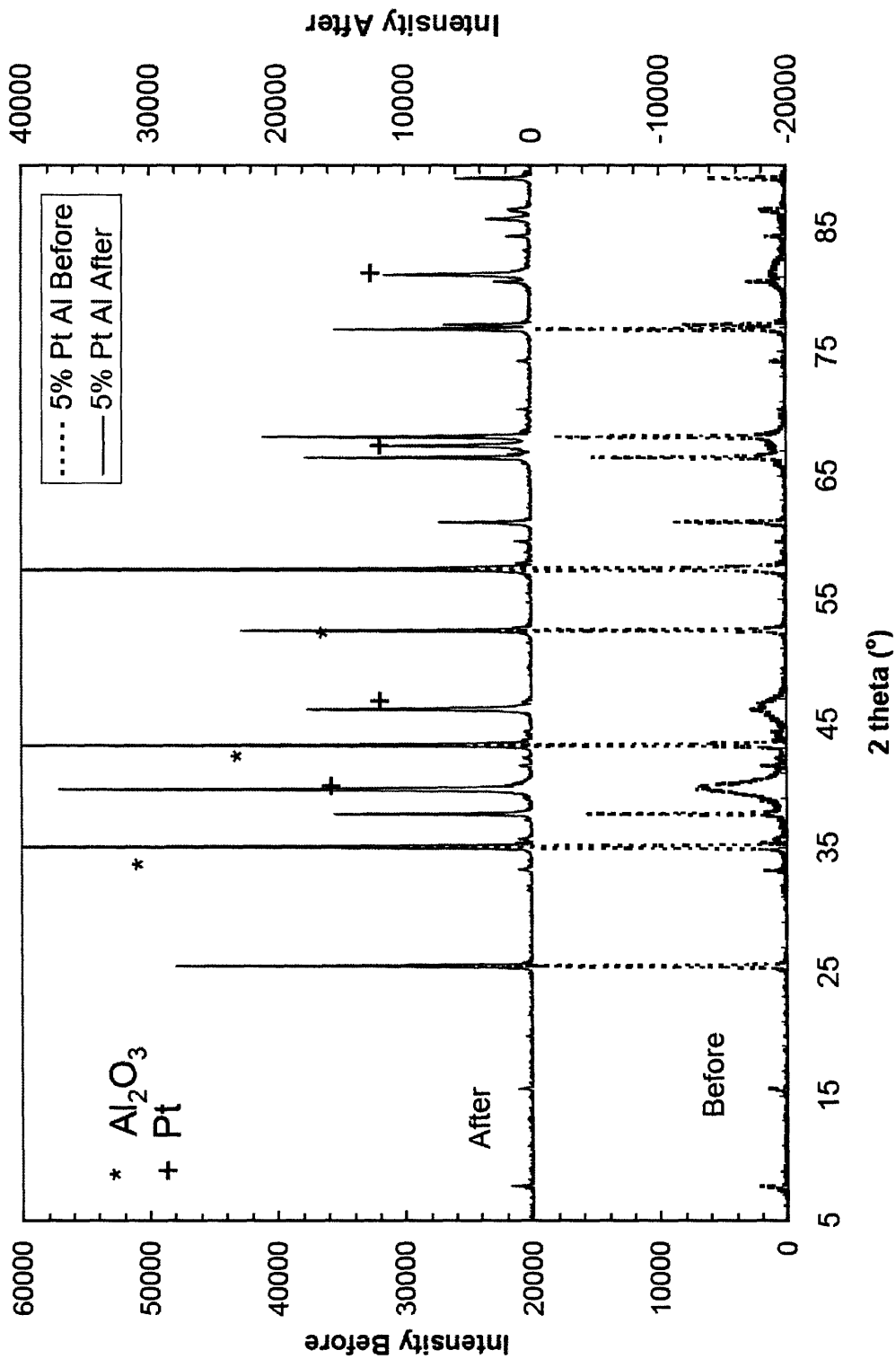


Figure D.3 XRD Results of 5% Pt/Al<sub>2</sub>O<sub>3</sub> powder before and after exposure to SCW

Figure D.3 XRD Results of 5% Pt/Al<sub>2</sub>O<sub>3</sub> powder before and after exposure to SCW (1.3 hrs, 550°C, 370 bar).

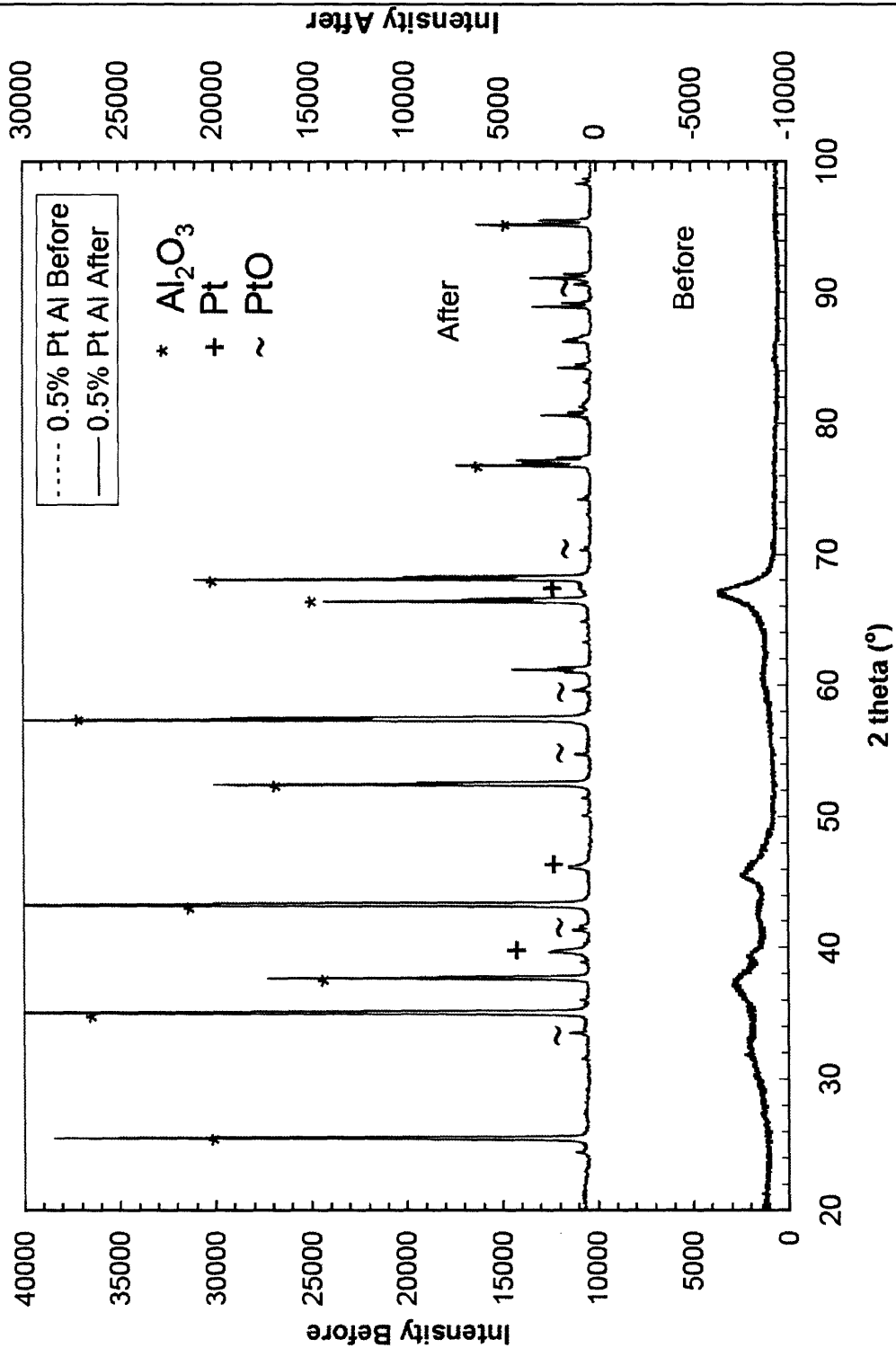
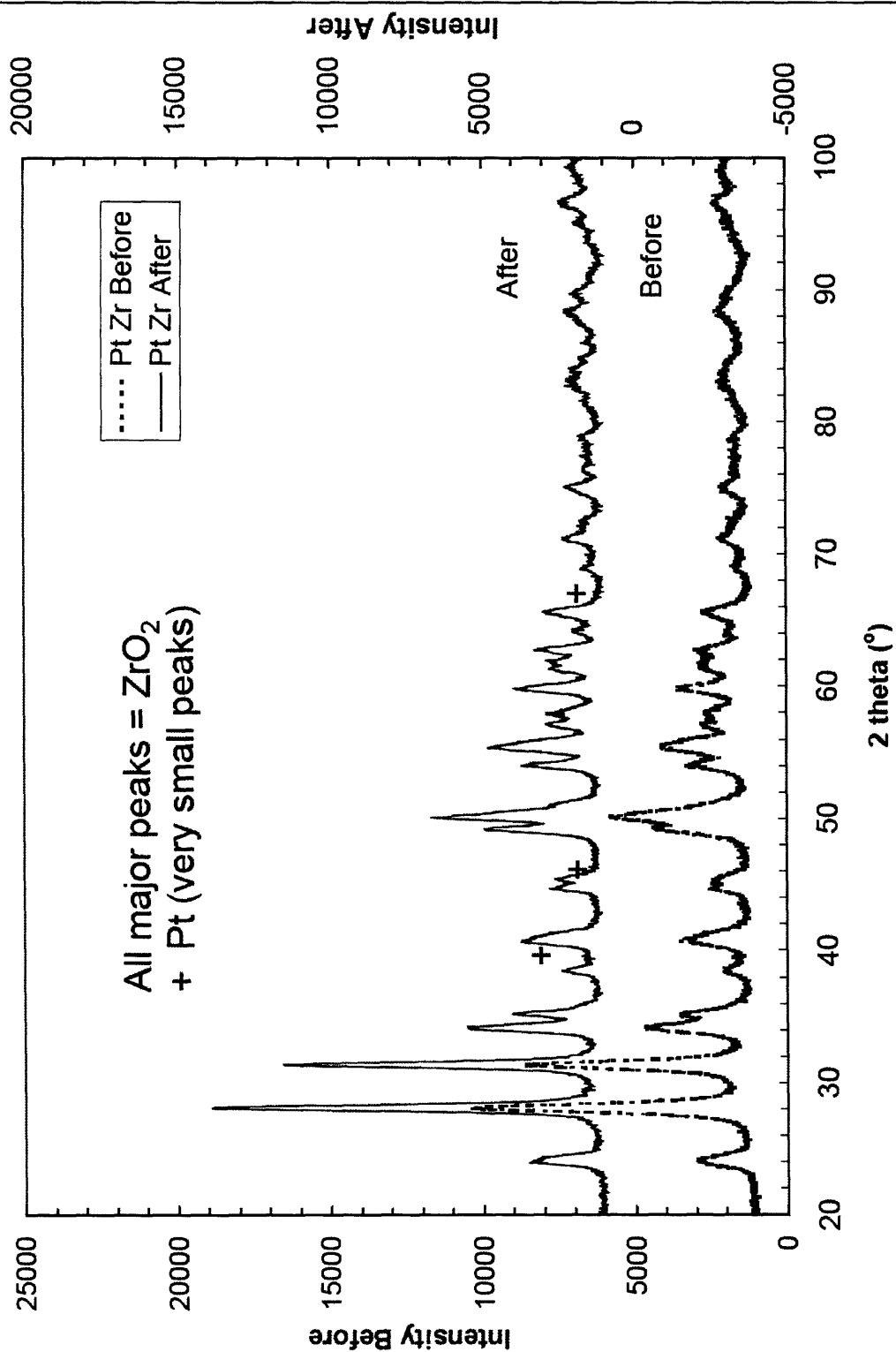
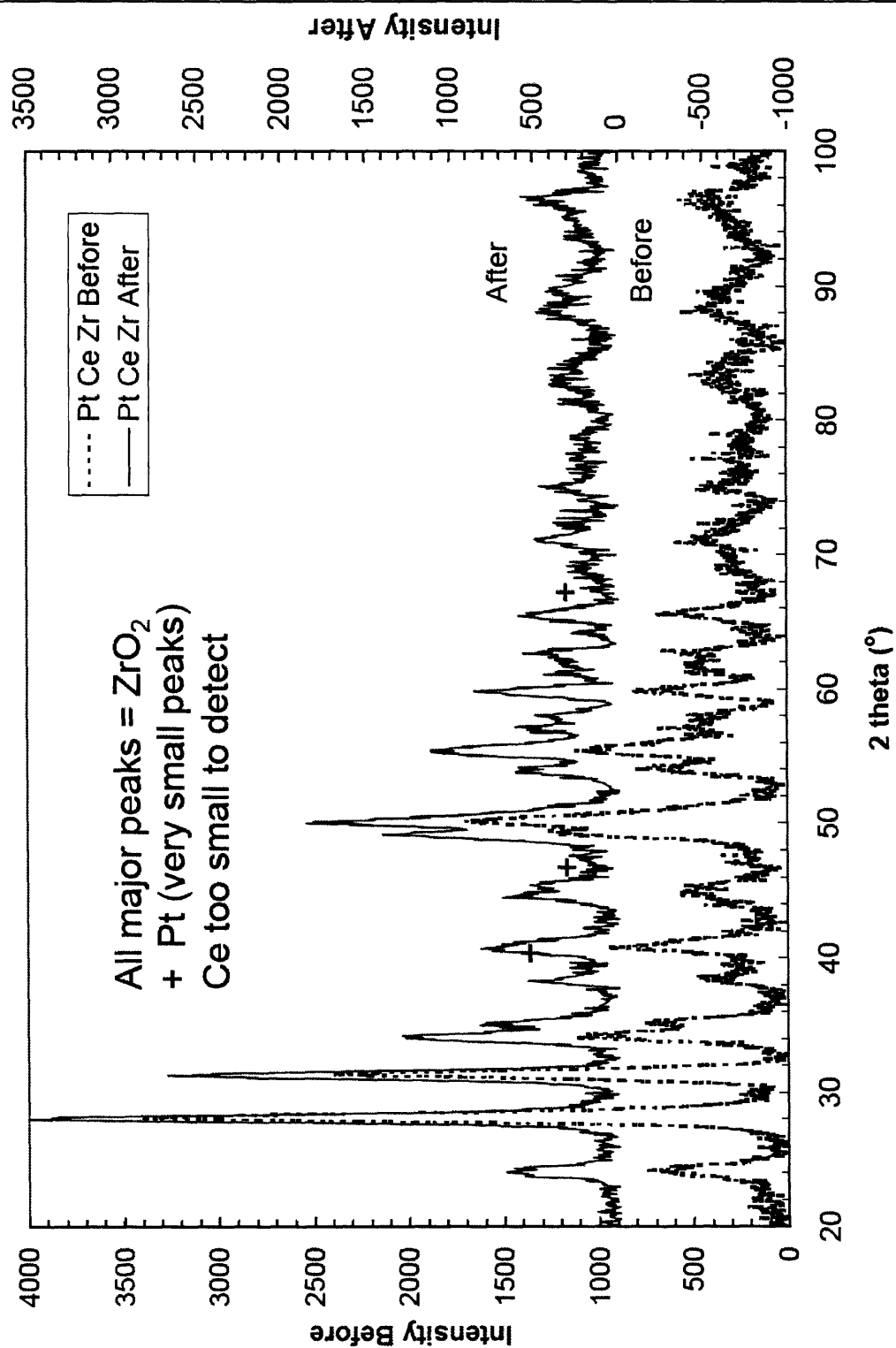


Figure D.4 XRD Results of 0.5% Pt/Al<sub>2</sub>O<sub>3</sub> pellets before and after exposure to SCW

Figure D.4 XRD Results of 0.5% Pt/Al<sub>2</sub>O<sub>3</sub> pellets before and after exposure to SCW (0.5 hrs, 600°C, 420 bar).

Figure D.5 XRD Results of 1% Pt/ZrO<sub>2</sub> powder before and after exposure to SCWFigure D.5 XRD Results of 1% Pt/ZrO<sub>2</sub> powder before and after exposure to SCW (0.5 hrs, 600°C, 245 bar).

Figure D.6 XRD Results of 1% Pt/5% CeO/ZrO<sub>2</sub> powder before and after exposure to SCWFigure D.6 XRD Results of 1% Pt/5% CeO/ ZrO<sub>2</sub> powder before and after exposure to SCW (2.3 hrs, 600°C, 270 bar).

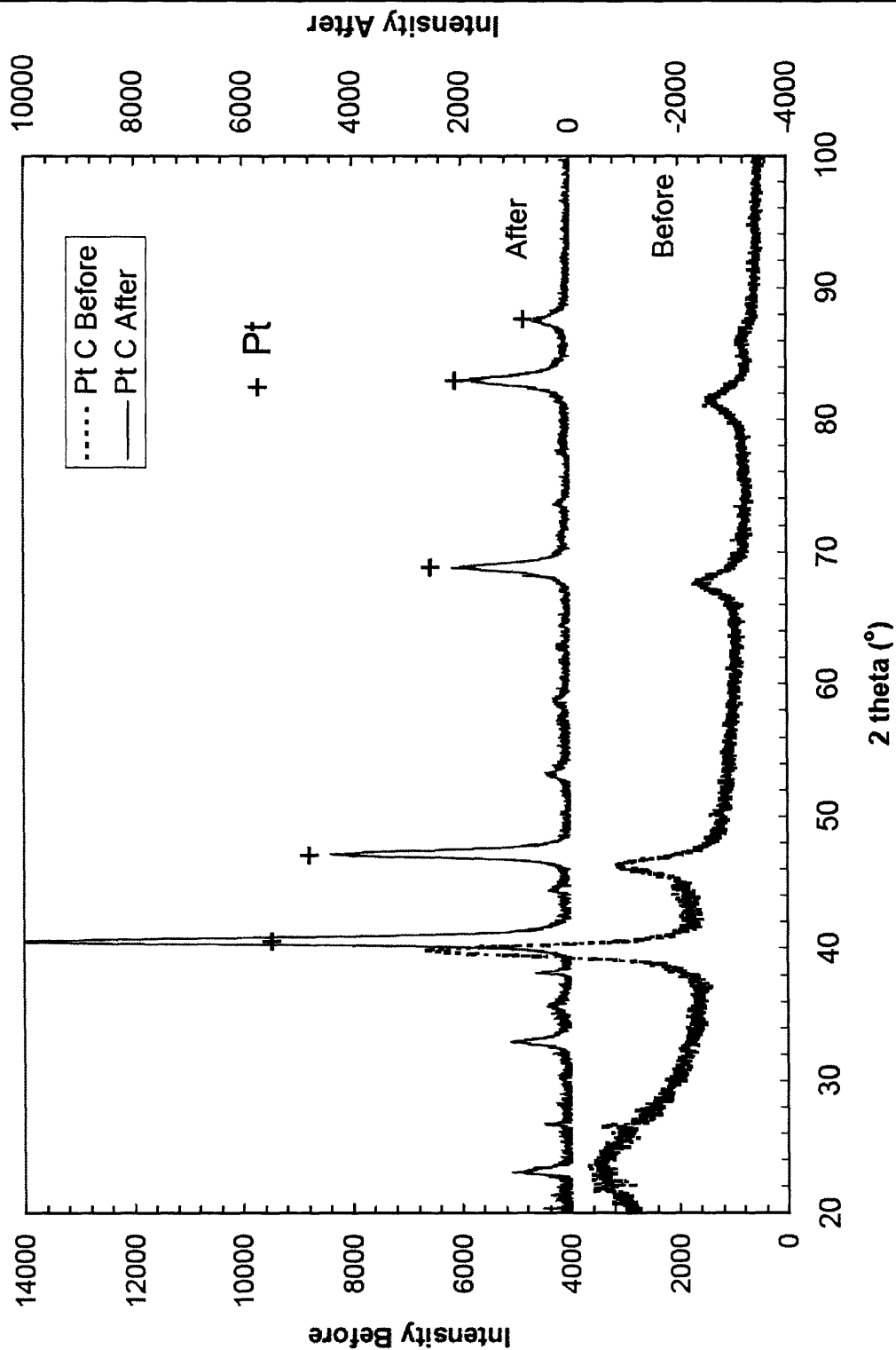


Figure D.7 XRD Results of 10% Pt/activated carbon powder before and after exposure to SCW

Figure D.7 XRD Results of 10% Pt/activated carbon powder before and after exposure to SCW (0.5 hrs, 600°C, 265 bar).

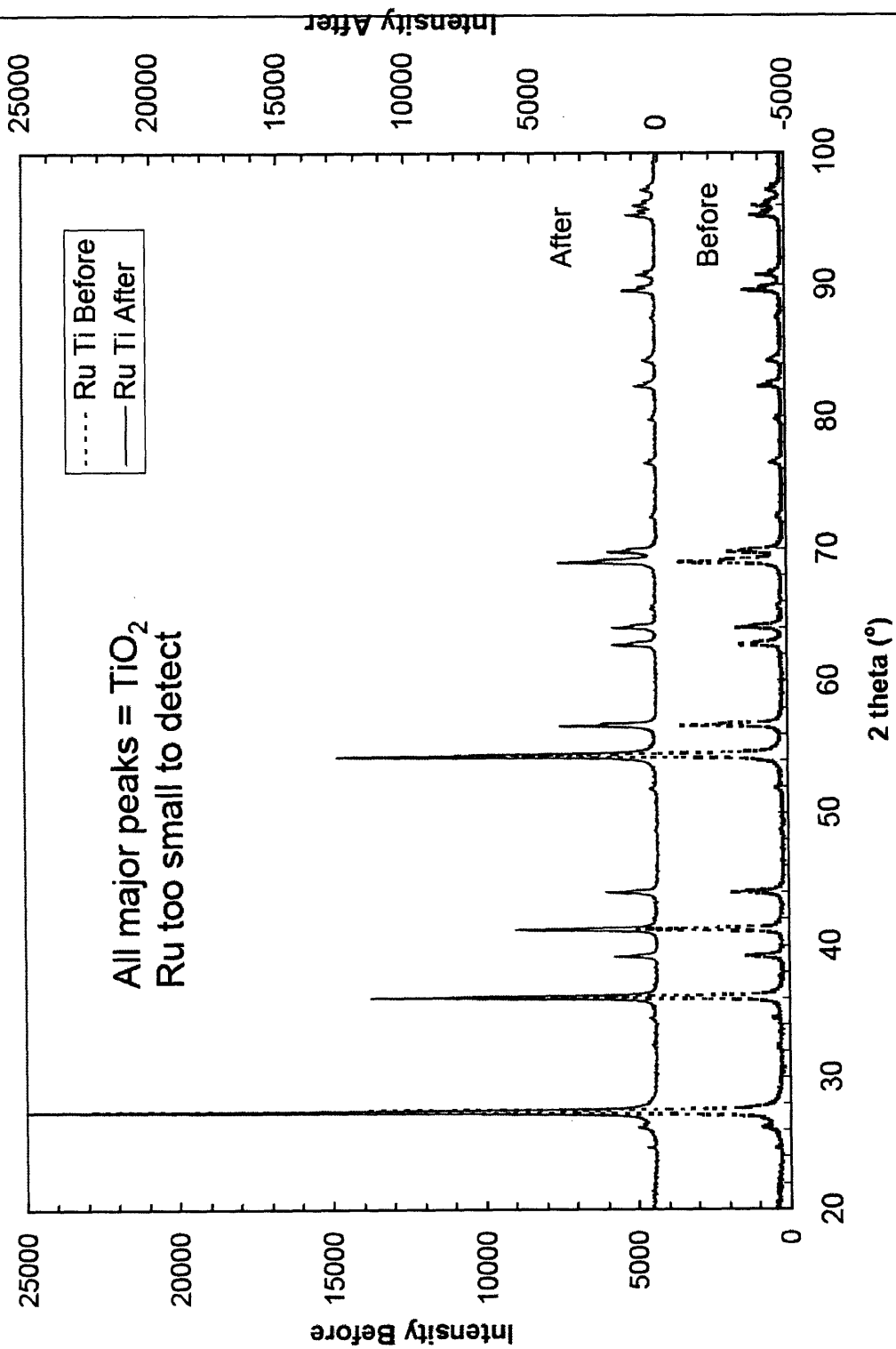


Figure D.8 XRD Results of 1% Ru/TiO<sub>2</sub> pellets before and after exposure to SCW

Figure D.8 XRD Results of 1% Ru/TiO<sub>2</sub> pellets before and after exposure to SCW (0.7 hrs, 600°C, 300 bar).

## D.2 XPS RESULTS

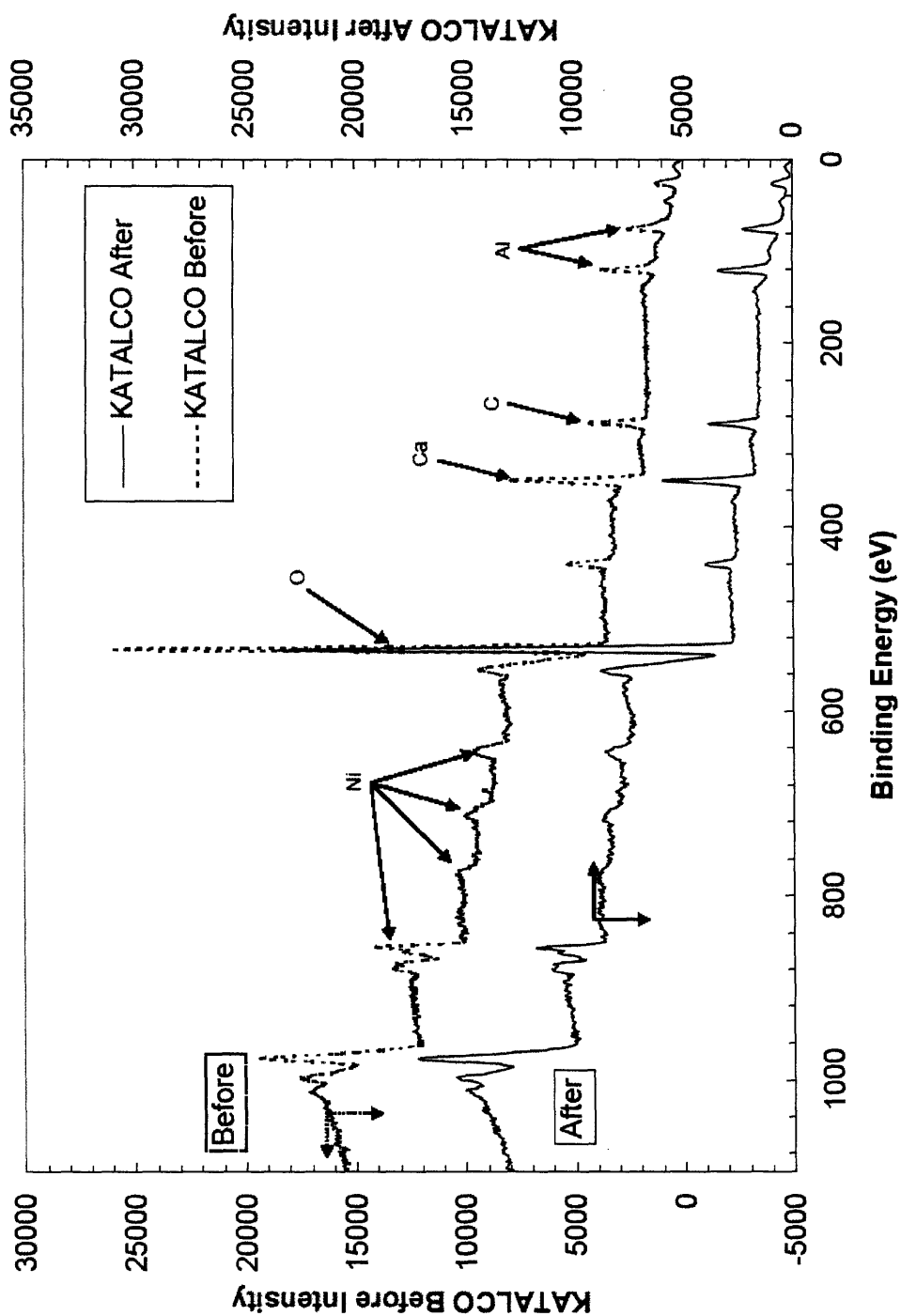


Figure D.9 XPS Results of KATALCO 57-7 pellets before and after exposure to SCW

Figure D.9 XPS Results of KATALCO 57-7 pellets before and after exposure to SCW (11 hrs, 400-500°C, 245 bar).

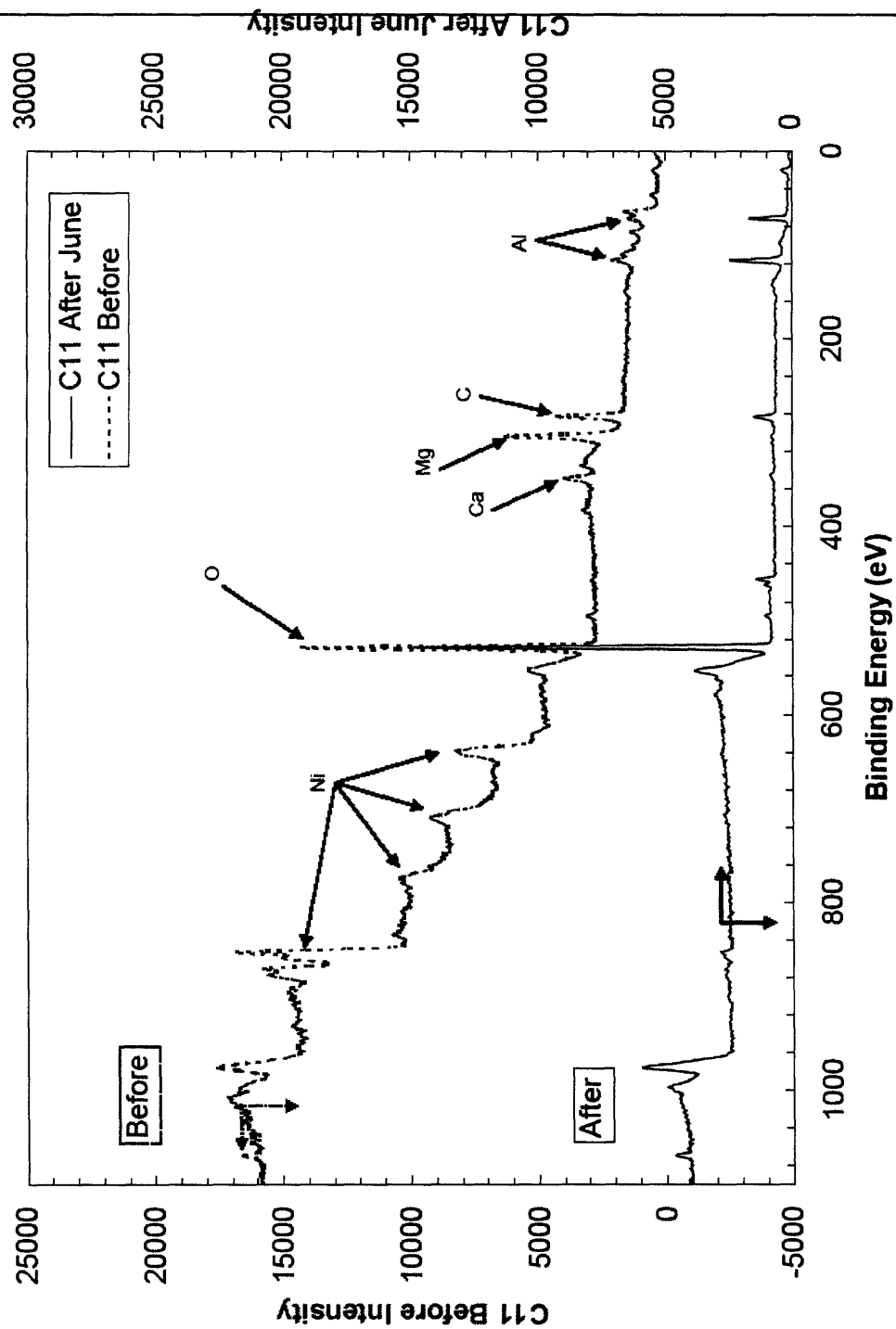


Figure D.10 XPS Results of C11-PR pellets before and after exposure to SCW

Figure D.10 XPS Results of C11-PR pellets before and after exposure to SCW (37.5 hrs, 400-500°C, 245 bar; shorter exposure time saw similar results).



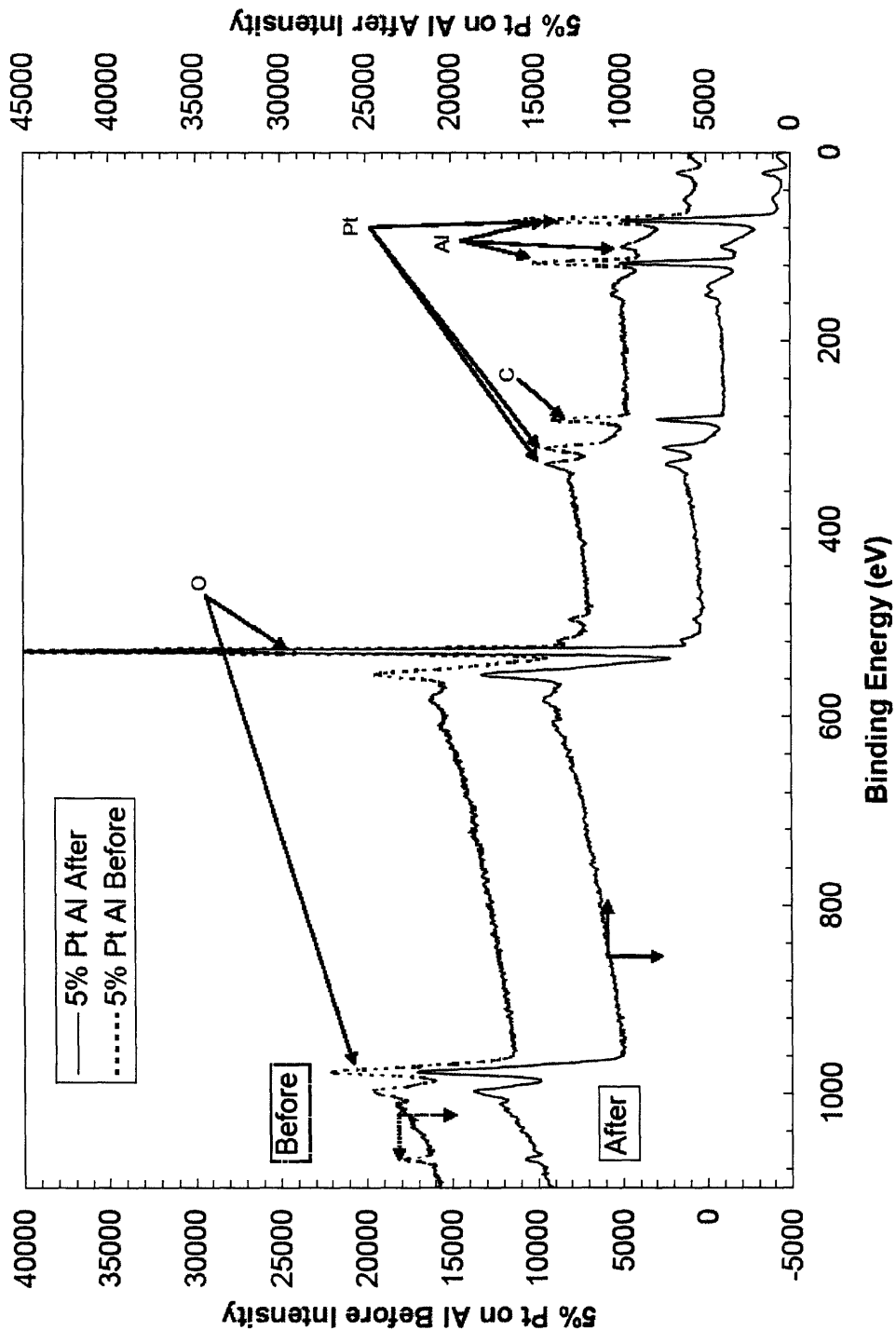


Figure D.11 XPS Results of 5% Pt/Al<sub>2</sub>O<sub>3</sub> powder before and after exposure to SCW

Figure D.11 XPS Results of 5% Pt/Al<sub>2</sub>O<sub>3</sub> powder before and after exposure to SCW (1.3 hrs, 550°C, 370 bar).

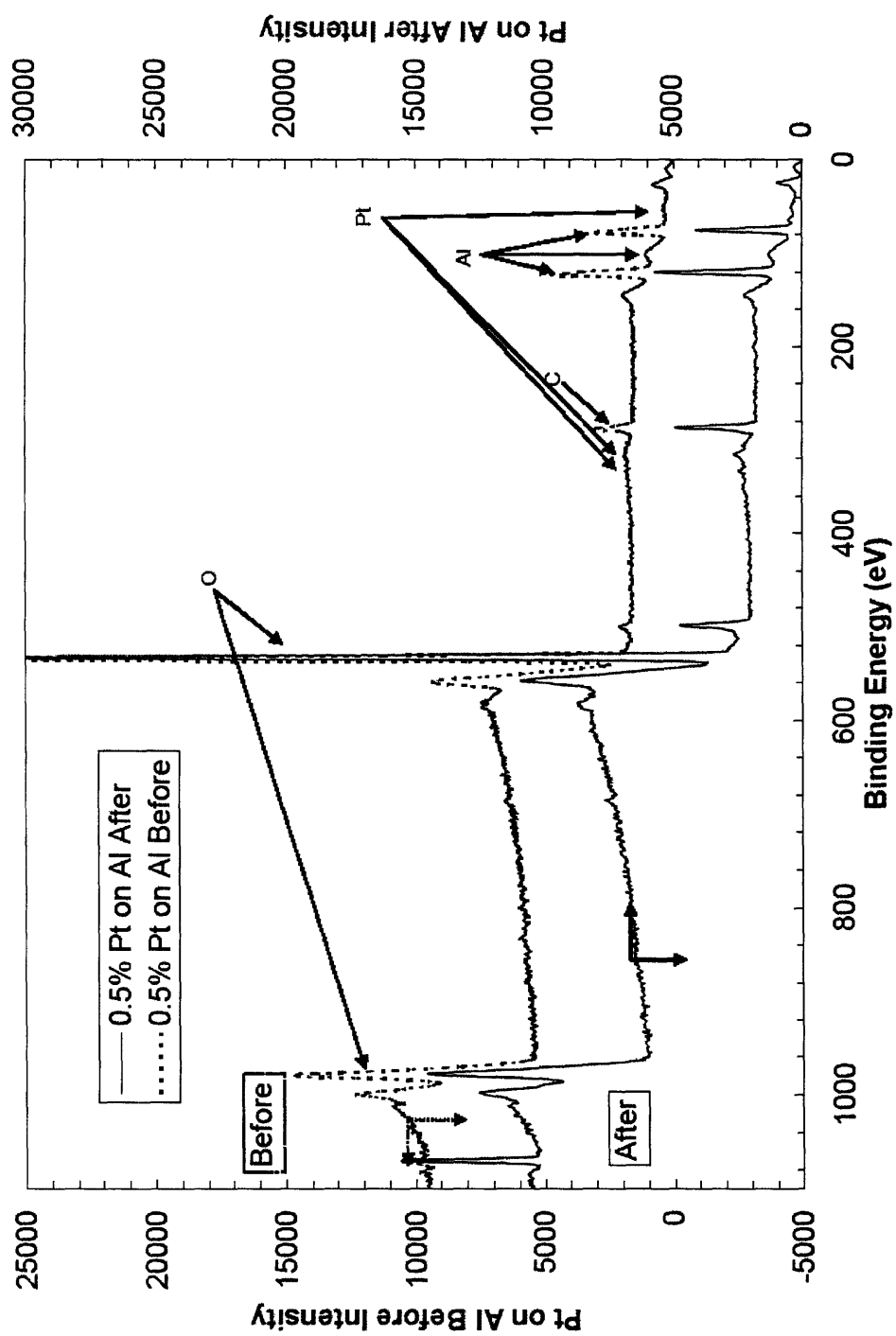


Figure D.12 XPS Results of 0.5% Pt/Al<sub>2</sub>O<sub>3</sub> pellets before and after exposure to SCW

Figure D.12 XPS Results of 0.5% Pt/Al<sub>2</sub>O<sub>3</sub> pellets before and after exposure to SCW (0.5 hrs, 600°C, 420 bar) .

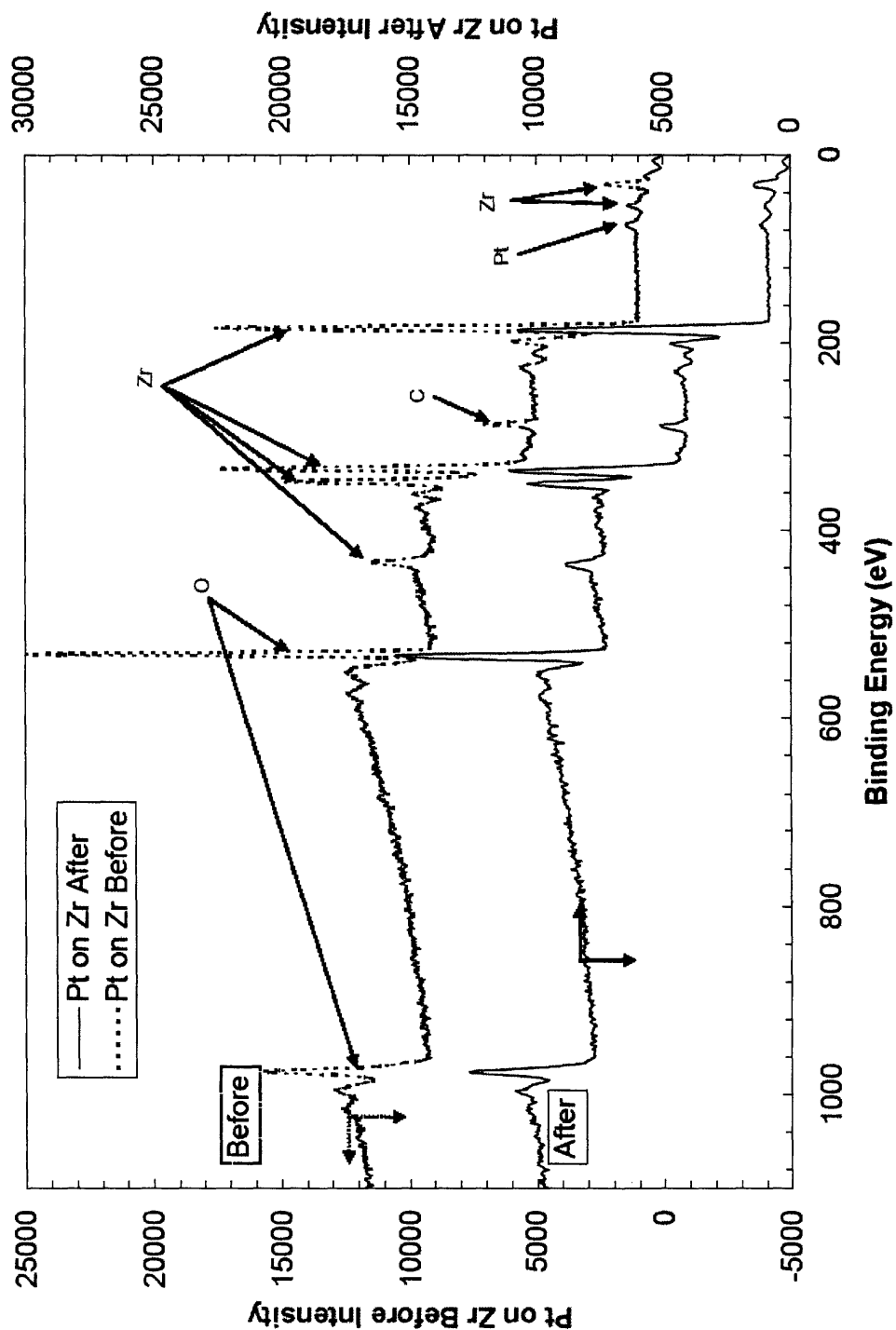


Figure D.13 XPS Results of 1% Pt/ZrO<sub>2</sub> powder before and after exposure to SCW

Figure D.13 XPS Results of 1% Pt/ZrO<sub>2</sub> powder before and after exposure to SCW (0.5 hrs, 600°C, 245 bar).

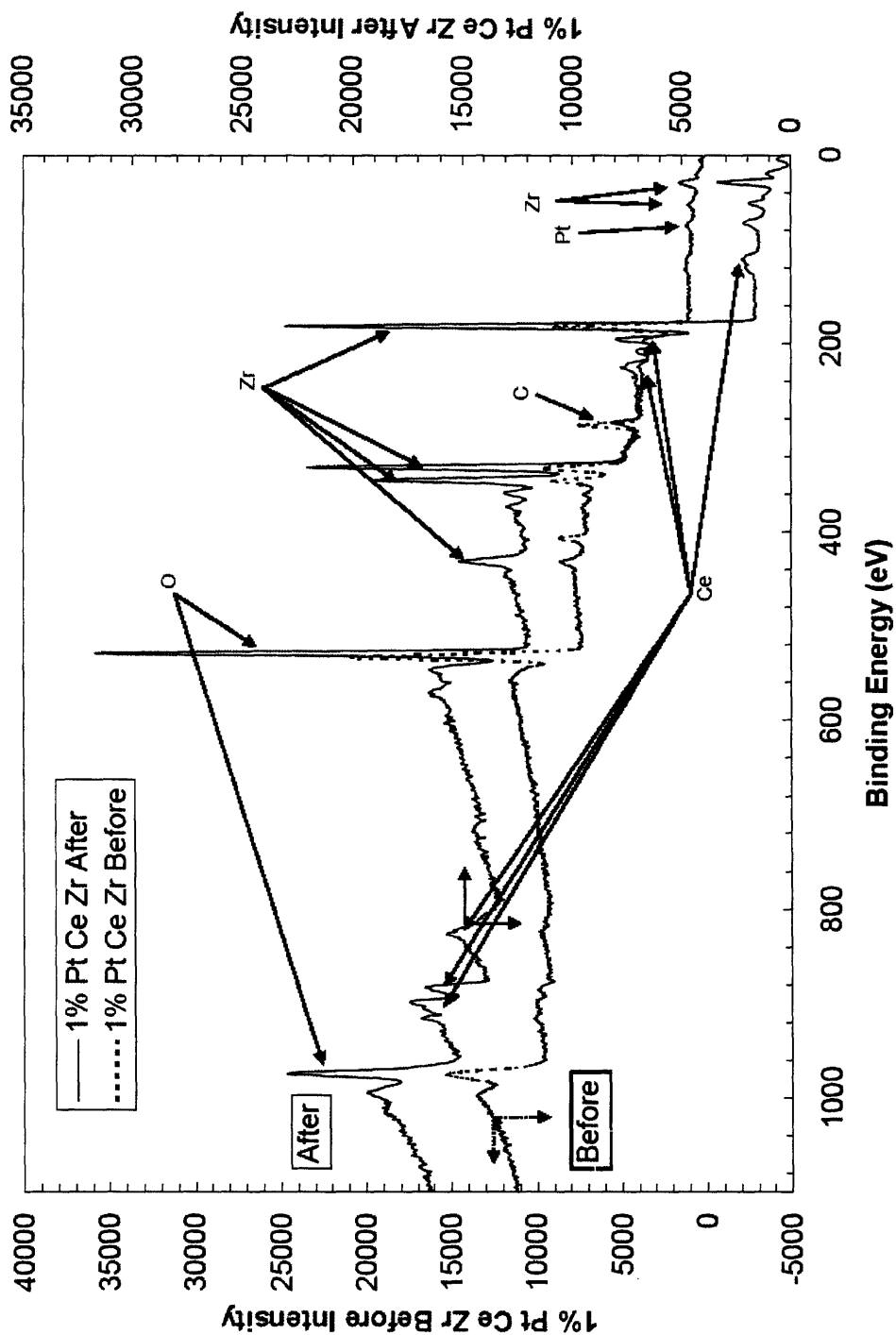


Figure D.14 XPS Results of 1% Pt/5% CeO/ZrO<sub>2</sub> powder before and after exposure to SCW

Figure D.14 XPS Results of 1% Pt/5% CeO/ ZrO<sub>2</sub> powder before and after exposure to SCW (2.3 hrs, 600°C, 270 bar).

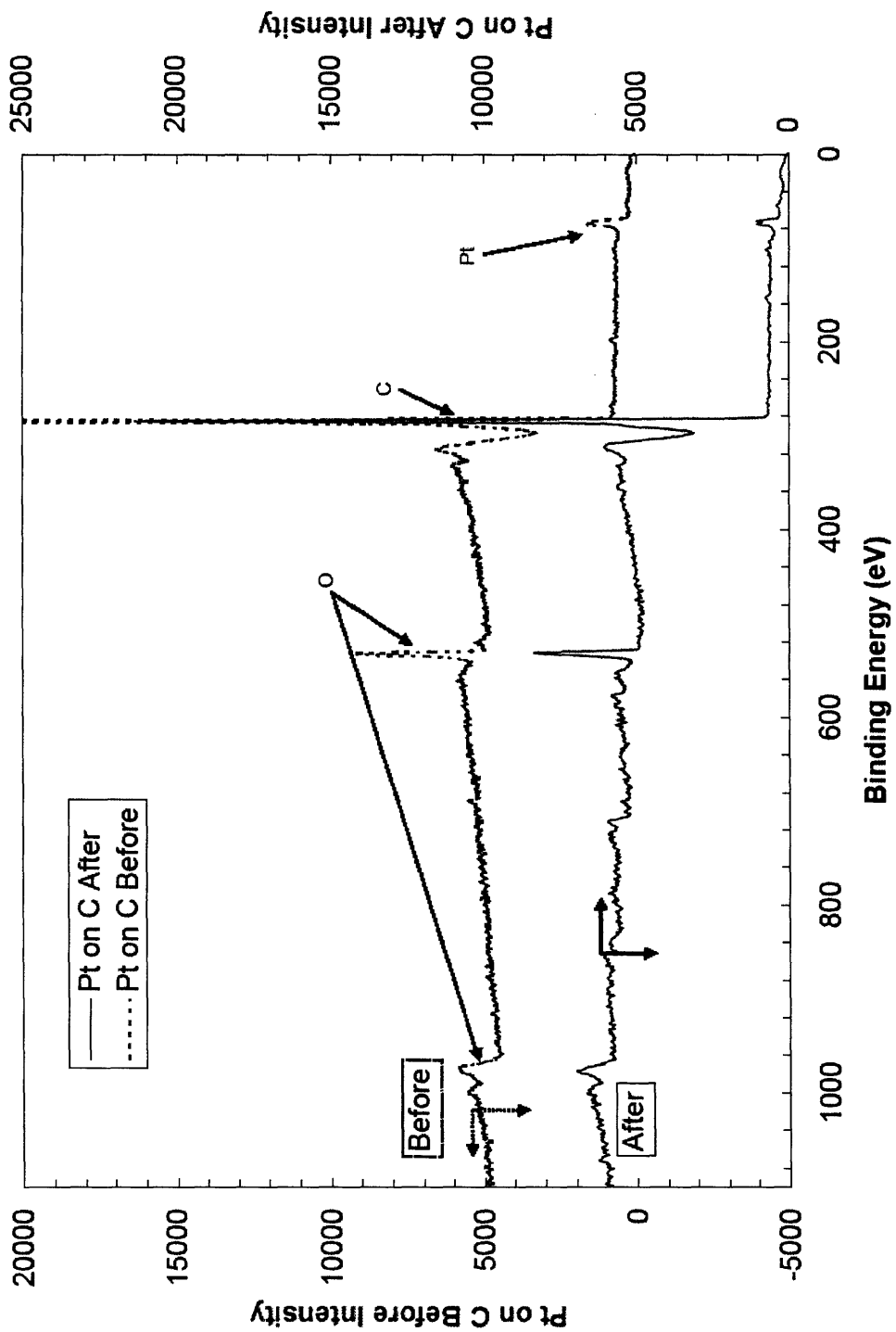


Figure D.15 XPS Results of 10% Pt/activated carbon powder before and after exposure to SCW

Figure D.15 XPS Results of 10% Pt/activated carbon powder before and after exposure to SCW (0.5 hrs, 600°C, 265 bar).

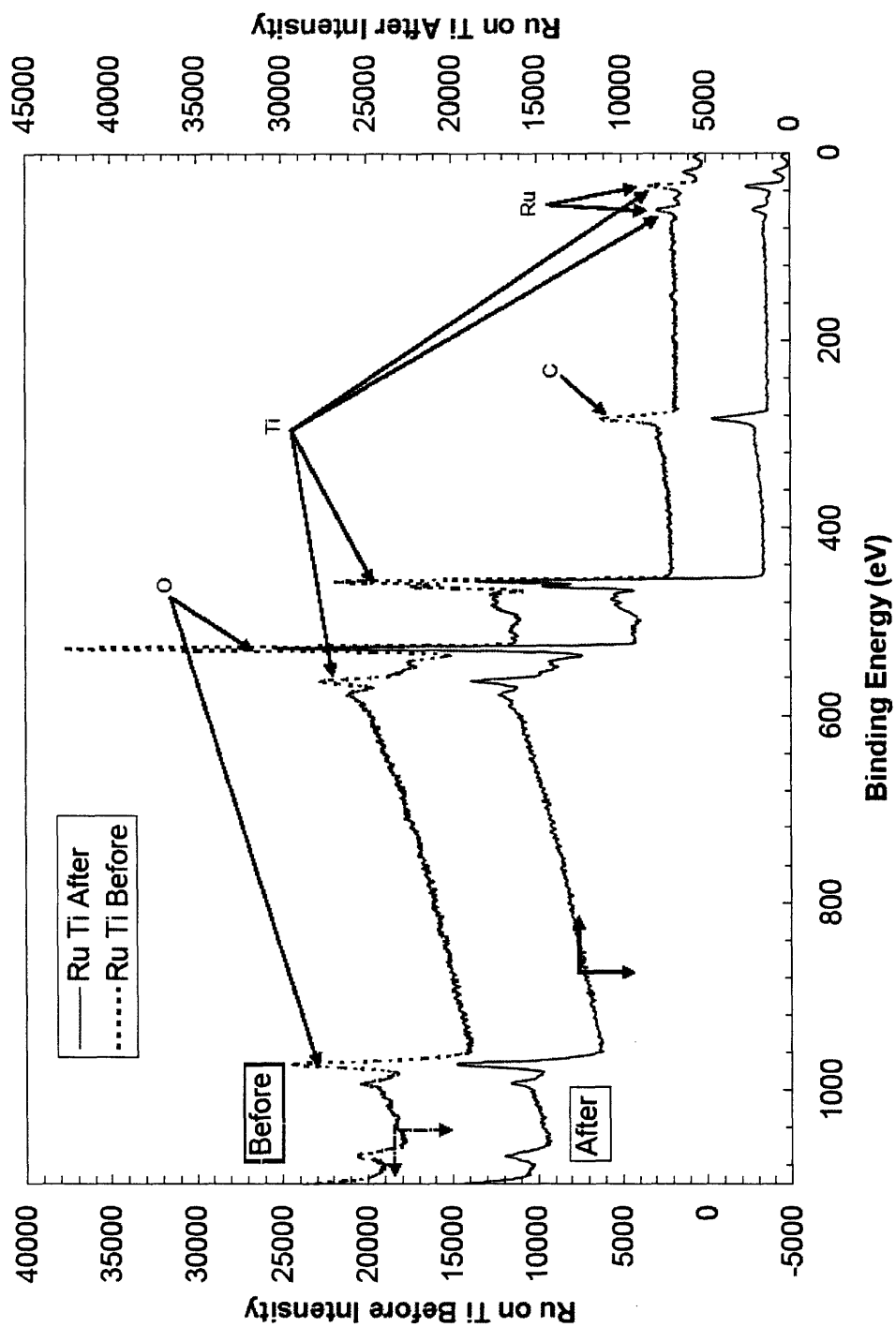


Figure D.16 XPS Results of 1% Ru/TiO<sub>2</sub> pellets before and after exposure to SCW

Figure D.16 XPS Results of 1% Ru/TiO<sub>2</sub> pellets before and after exposure to SCW (0.7 hrs, 600°C, 300 bar).

### D.3 BET SURFACE AREA MEASUREMENTS

**Table D.1 BET Results for all Metal Catalysts.**

Catalyst	Surface Area Before (m <sup>2</sup> /g)	Surface Area After (m <sup>2</sup> /g)
KATALCO (18 wt% NiO on CaO/Al <sub>2</sub> O <sub>3</sub> spt) (Johnson Mathey)	15.24 ± 0.03	13.33 ± 0.06
C-11PR (~ 50 wt% NiO on Al <sub>2</sub> O <sub>3</sub> spt, Si) (Shell catalyst)	7.94 ± 0.04	1.01 ± 0.04
5% Pt/ Al <sub>2</sub> O <sub>3</sub> powder (Alfa-Aesar)	0.70 ± 0.05	0.37 ± 0.03
0.5% Pt/ Al <sub>2</sub> O <sub>3</sub> pellets (Alfa-Aesar)	96.31 ± 0.23	1.73 ± 0.02
1% Pt/ZrO <sub>2</sub> (proprietary)	No sample left	No sample left
1 % Pt/5% CeO/ZrO <sub>2</sub> (proprietary)	No sample left	No sample left
10% Pt/Activated Carbon (Alfa-Aesar)	729 ± 14	795 ± 15
1 % Ru/TiO <sub>2</sub> (Degussa)	9.74 ± 0.04	7.58 ± 0.04